

TECNOLÓGICO NACIONAL DE MEXICO

3



Instituto Tecnológico de Tijuana

Centro de Graduados e Investigación en Química

“Diseño de nano-ablandadores magnéticos para mejorar la calidad del agua recuperada”

“Design of magnetic nano-softeners to improve reclaimed water quality”

Trabajo de tesis

Presentado por
Estephany Santiago Siliceo

Para obtener el grado de:
DOCTOR EN CIENCIAS EN QUÍMICA

Directora de tesis:

Dra. Mercedes Teresita Oropeza Guzmán

Codirectora de tesis:

Dra. Georgina Esther Pina Luis

Tijuana, B.C.

Octubre 2021



INSTITUTO TECNOLÓGICO DE MÉXICO / IT TIJUANA

DIVISIÓN DE ESTUDIOS DE POSGRADO E INVESTIGACIÓN

CARTA DE SESIÓN DE DERECHOS

En la ciudad de Tijuana, Baja California, el día **17** del mes de **Junio** del año **2021**, la C. **Estephany Santiago Siliceo** alumna del posgrado en Ciencias en Química, con número de control **D08270762**, manifiesta que es autor intelectual del presente trabajo de Tesis bajo la dirección de la **Dra. Mercedes Teresita Oropeza Guzmán** y la **Dra. Georgina Esther Pina Luis**, y ceden los derechos del trabajo titulado '**Diseño de nano-ablandadores magnéticos para mejorar la calidad del agua recuperada**' al Tecnológico Nacional de México / IT Tijuana para su difusión con fines académicos y de investigación.

Los usuarios de la información no deben reproducir el contenido textual, gráficas, código, formulas o datos del trabajo sin permiso expreso del autor o director del trabajo. Este debe ser obtenido escribiendo a cualquiera de las siguientes direcciones de correo electrónico estephansantiago@gmail.com y oropeza@tectijuana.mx. Si el permiso se otorga, el usuario deberá dar el agradecimiento correspondiente y citar la fuente del mismo.

ATENTAMENTE

Estephany Santiago Siliceo





Instituto Tecnológico de Tijuana

Tijuana, Baja California, 20/octubre/2021

Oficio No.

293/CG/2021 Asunto: Se autoriza
impresión de trabajo de tesis

GUADALUPE HERNÁNDEZ ESCOBEDO
JEFE DE LA DIVISIÓN DE ESTUDIOS DE POSGRADO E
INVESTIGACIÓN PRESENTE

Los que suscriben tienen a bien informar que el manuscrito de tesis titulado “Diseño de nano-ablandadores magnéticos para mejorar la calidad del agua recuperada”, presentado por la **C. Estephany Santiago Siliceo**, (con número de control D08270762), cumple con los requisitos de calidad y formato para tesis de Doctorado en Ciencias en Química. Por consiguiente, se aprueba y autoriza al interesado para que proceda a la impresión del mismo.

ATENTAMENTE

DRA. GEORGINA ESTHER PINA LUIS
Presidente

DRA. MERCEDES TERESITA OROPEZA GUZMÁN
Secretario del Jurado

DR. ANTONIO TIRADO GUÍZAR
Vocal del Jurado

DR. EDUARDO ALBERTO LÓPEZ MALDONADO
Vocal del Jurado

DR. JOSÉ MANUEL ROMO HERRERA
Vocal del Jurado

C.p. Oficina de Titulación
C.p. Expediente
C.p. Interesado GEPL/MTOG/ATG/EALM/JMRH



Dedicatorias personales

Primeramente, a Dios, a ti señor, justo juez, que me has sabido guiar y cuidar en este camino de vida que persigo. Gracias por que en esta vida puedo perseguir mi pasión, mi sueño y por ti señor he encontrado la fortaleza y sabiduría para no perderme en el camino.

A mis amados padres, los contadores Luis Mario y Norma Teresa, papis este logro es tanto mío como de ustedes, gracias por siempre estar para mí, por enseñarme a ser mujer de bien, trabajadora y valiente como ustedes. Gracias por su amor incondicional, por nunca cortarme las alas y ser mis cómplices incondicionales. Ustedes mis más grandes amores en la vida les debo todo lo que soy y seré. Los amo siempre.

A mis amados hermanos Moisés, Luisa María y Juan Pablo, espero poderles brindar un ejemplo de perseverancia, luchan por sus metas y sueños, nunca se rindan y persigan su pasión en la vida sin perder humildad. Gracias por su apoyo y amor, los amo con mi vida.

A mi abuelita Gloria, mujer fuerte y valiente, y mis abuelos Blanca y Agustín, que desde el cielo me guían y me protegen. Los amo mucho mis viejitos, gracias por enseñarme valores y amor a la familia.

A mi familia y amigos en Tuxtla y Tijuana. Gracias por siempre brindarme un consejo, una opinión, una ayuda, un abrazo y ánimos de seguir adelante. Gracias a todos ustedes que me han acompañado por este camino, siendo testigos de mi crecimiento y logros.

Finalmente, estas últimas líneas son para mí, Estephany, gracias por nunca rendirte, por no tirar la toalla. Ha sido un camino largo, difícil, muy solitario y lleno de dolor, pero lo has sabido superar todo con amor, amor propio, a Dios y a tus allegados, no pierdas nunca tu rumbo, humildad y pasión por la vida. Disfruta tus logros y ve por más que aquí empieza tu vida. Eres fuerte, eres mujer, eres vida. Vive y se feliz. Te amo.

Table of contents

| | |
|---|--------------------------------------|
| Autorización de impresión..... | ¡Error! Marcador no definido. |
| Dedicatorias personales | iv |
| Table of contents | v |
| Abbreviation list | xi |
| Figure's list..... | xiii |
| Table's list | xix |
| Agradecimientos..... | xxi |
| Reconocimientos institucionales | xxii |
| Vita, publications, field of interests..... | xxiii |
| Vita | xxiii |
| Publications | xxiii |
| Participation in symposiums/congress..... | xxiii |
| Doctoral Exchange | xxiv |
| Fields of interest | xxv |
| Resumen | xxvi |
| Abstract..... | xxvi |
| General introduction | 28 |
| General objective of the research | 29 |
| Chapter I | 30 |
| 1.1 Introduction | 31 |
| 1.2 Justification and objectives..... | 33 |
| 1.2.1 Justification..... | 33 |

| | |
|--|----|
| 1.2.2 Objectives | 33 |
| 1.3 Background..... | 34 |
| 1.3.1 Functional materials | 34 |
| 1.3.2 Functional nanomaterials..... | 34 |
| 1.3.3 Iron-oxide magnetic nanoparticles | 38 |
| 1.3.4 Synthesis of magnetic nanoparticles..... | 41 |
| 1.3.5 Surface modification and functionalization of magnetic nanoparticles | 43 |
| 1.3.6 Hypothesis | 47 |
| 1.4 Experimental and methods | 49 |
| 1.4.1 Materials and reagents..... | 49 |
| 1.4.2 Equipment..... | 49 |
| 1.4.3 Methodology..... | 49 |
| 1.5 Results and discussions | 51 |
| 1.6 Conclusions | 53 |
| 1.7 References | 54 |
| Chapter II..... | 57 |
| 2.1 Introduction | 58 |
| 2.2 Justification and objectives..... | 59 |
| 2.2.1 Justification..... | 59 |
| 2.2.2 General objective..... | 59 |
| 2.3 Background..... | 60 |
| 2.3.1 Characterization of nanomaterials..... | 60 |
| 2.3.2 Microscopy-based techniques..... | 62 |
| 2.3.3 Spectroscopy-based characterization techniques..... | 66 |

| | |
|--|-----|
| 2.3.4 Other characterization techniques | 67 |
| 2.3.6 Hypothesis | 74 |
| 2.4 Experimental and methods | 75 |
| 2.4.1 Equipment..... | 75 |
| 2.4.2 Methodology..... | 75 |
| 2.5 Results and discussions | 77 |
| 2.5.1 FT-IR analysis | 77 |
| 2.5.2 TGA analysis | 78 |
| 2.5.3 TEM characterization | 80 |
| 2.5.3 EDX characterization | 81 |
| 2.5.4 VSM measurements..... | 81 |
| 2.5.5 BET surface area measurements..... | 83 |
| 2.5.6 DLS measurements..... | 85 |
| 2.5.7 ζ -potential measurements | 86 |
| 2.6 Conclusions | 88 |
| 2.7 References | 89 |
| Chapter III..... | 97 |
| 3.1 Introduction | 98 |
| 3.2 Justification and objectives..... | 99 |
| 3.2.1 Justification..... | 99 |
| 3.2.2 General objective..... | 99 |
| 3.3 Background..... | 100 |
| 3.3.1 Water reuse and reclaimed water..... | 100 |
| 3.3.2 Reclaimed water (RW) application opportunities | 101 |

| | |
|--|-----|
| 3.3.3 RW quality..... | 103 |
| 3.3.4 RW composition in Tijuana, Baja California, México | 114 |
| 3.3.5 Hard water | 114 |
| 3.3.6 Hypothesis | 117 |
| 3.4 Experimental and methods | 119 |
| 3.4.1 Materials and reagents | 119 |
| 3.4.2 Equipment..... | 119 |
| 3.4.3 Methodology..... | 119 |
| 3.5 Results and discussions | 122 |
| 3.5.1 DLS and ζ -potential characterization of RW..... | 122 |
| 3.5.2 Alkalinity and hardness characterization of RW | 123 |
| 3.5.5 DLS comparison of RW and magnetic nanomaterials (MNP, MND, MCH, and MCCH)..... | 124 |
| 3.5.6 ζ -potential comparison of RW and magnetic nanomaterials (MNP, MND, MCH, and MCCH) | 125 |
| 3.6 Conclusions | 127 |
| 3.7 References | 128 |
| Chapter IV | 130 |
| 4.1 Introduction | 131 |
| 4.2 Justification and objectives..... | 132 |
| 4.2.1 Justification..... | 132 |
| 4.2.2 General Objective | 132 |
| 4.3 Background..... | 133 |
| 4.3.1 Wastewater treatment process | 133 |
| 4.3.2 RW treatment strategies..... | 135 |

| | |
|--|-----|
| 4.3.3 Advanced engineered treatment | 137 |
| 4.3.4 Opportunities for nanotechnology in water treatment..... | 148 |
| 4.3.5 Hypothesis: | 151 |
| 4.4 Experimental and methods | 152 |
| 4.4.1 Materials and reagents | 152 |
| 4.4.2 Equipment..... | 152 |
| 4.4.3 Methodology..... | 152 |
| 4.5 Results and discussions | 155 |
| 4.5.1 DLS and ζ -potential comparison of RW before and after treatment with magnetic nanomaterials (MNP, MND, MCH, and MCCH) | 155 |
| 4.5.2 Alkalinity and hardness removal from RW..... | 156 |
| 4.5.3 Transmittance comparison of RW before and after treatment with magnetic nano-softeners (MNP, MND, MCH, and MCCH) | 157 |
| 4.5.5 Gravimetric analysis of recovered nano-softeners | 158 |
| 4.5.6 FT-IR analysis of recovered nano-softeners..... | 158 |
| 4.5.7 Optical microscope images of recovered nano-softeners | 160 |
| 4.5.8 Comparison of RW treated with the different magnetic nano-softeners at different pH values | 161 |
| 4.6 Conclusions | 162 |
| 4.7 References | 163 |
| General conclusions..... | 166 |
| Annexes | 169 |
| 2.3.2.A Scanning electron microscopy | 169 |
| 2.3.2.A1 SEM for MNP characterization | 170 |
| 2.3.2.B Scanning Transmission Electron Microscopy (STEM) | 171 |

| | |
|---|-----|
| 2.3.2.B1 STEM for MNP characterization..... | 171 |
| 2.3.2.B2 Limitation of SEM and STEM technique | 172 |
| 2.3.2.1 Transmission electron microscopy | 173 |
| 2.3.2.2 Energy dispersive X-ray analysis (EDX) | 174 |
| 2.3.3.1 Fourier transform infrared spectroscopy (FT-IR)..... | 175 |
| 2.3.4.1 X-ray powder diffraction (XRD)..... | 176 |
| 2.3.5.1 Thermogravimetric analysis (TGA) | 180 |
| 2.3.5.2 Dynamic light scattering (DLS) | 182 |
| 2.3.5.3 Zeta Potential (ζ -potential) | 185 |
| 2.3.5.4 Brunauer-Emmett-Teller (BET) surface area analysis of nanoparticles | 187 |
| 2.3.5.5 Vibrating sample magnetometry (VSM) | 189 |
| 2.8.1 FT-IR of raw MNP and each of the modifier | 193 |
| 2.8.2 TGA of raw MNP and each of the modifier | 194 |
| 2.8.3A STEM/SEM characterization of MNP, MND, MCH and MCCH..... | 195 |
| 2.8.3B EDX tables for MNP, MND, MCH, and MCCH..... | 197 |
| 3.8.1 Urban reuse extensive water quality parameters | 199 |
| 3.8.2 Agricultural reuse extensive water quality parameters..... | 200 |
| ANNEX REFERENCES | 201 |

Abbreviation list

| | |
|--|---|
| α -Fe ₂ O ₃ | Hematite |
| γ -Fe ₂ O ₃ | Maghemite |
| ζ -potential | Zeta Potential |
| AOPs | Advanced Oxidation Processes |
| BET | Brunauer-Emmett-Teller |
| CH | Chitosan |
| CONAGUA | Consejo Nacional del Agua |
| DLS | Dynamic Light Scattering |
| EDX | Energy Dispersive X-ray Analysis |
| EPA | Environmental Protection Agency |
| FE-SEM | Field Emission Scanning Electron Microscope |
| FT-IR | Fourier Transform Infrared Spectroscopy |
| GAC | Granular Activated Carbon |
| IEP | Isoelectric Point |
| MCCH | Magnetic Carbamoyl Chitosan |
| MCH | Magnetic Chitosan |
| MND | Magnetic Nanodiamond |
| MNP | Magnetic Nanoparticle |
| MONPs | Metal Oxides Nanoparticles |
| ND | Nano Diamond |

| | |
|------|---|
| NF | Nano Filtration |
| PAC | Powdered Activated Carbon |
| RO | Reverse Osmosis |
| RW | Reclaimed Water |
| SEM | Scanning Electron Microscopy |
| SOC | Synthetic Organic Compunds |
| STEM | Scanning Transmission Electron Microscopy |
| TDS | Total Dissolved Solids |
| TGA | Thermogravimetric analysis |
| UV | Ultraviolet |
| VSM | Vibrating Sample Magnetometry |
| WHO | World health organization |
| WWTP | Wastewater Treatment Plant |
| XDR | X-ray powder Diffraction |

Figure's list

Chapter I

| | |
|--|----|
| Figure 1.1 Diagram of surface functionalization of nanoparticles. Left: original nanoparticle. Right: nanoparticle with surface functionalization. ¹⁵ | 36 |
| Figure 1.2 Basic nanomaterials classification: inorganic nanomaterials, organic nanomaterials, carbon-based materials. ³ | 37 |
| Figure 1.3 Alignment of the magnetic moment of individual atoms of iron. | 38 |
| Figure 1.4 Coercivity variation with particle diameter. ¹⁷ | 39 |
| Figure 1.5 Magnetization characteristics of ferromagnetic materials. ⁶ | 40 |
| Figure 1.6 The domains of ferromagnetic and superparamagnetic nanoparticles. ¹⁷ | 40 |
| Figure 1.7 Synthetic strategies and techniques used in nanotechnology, enlisting the typical processes or applications that a certain strategy or technique includes ⁴ | 41 |
| Figure 1.8 A comparison of the synthesis of superparamagnetic iron oxide nanoparticles by three different routes. ⁸ | 42 |
| Figure 1.9 (a) Particles stabilized by the electrostatic layer. (b) Particles stabilized by steric repulsion. ¹⁰ | 44 |
| Figure 1.10 Schematic illustration of different applications, structural transformations, and surface interactions of nanoscale iron oxide nanoparticles. ⁹ | 45 |
| Figure 1.11 MNP before (a) and after (b) being under the influence of a Nb magnet. | 51 |
| Figure 1.12 Schematic illustration of the formation of the nanoscavengers MND, MCH, and MCCH. | 52 |
| Figure 1.13 Working principle of the magnetic nanoscavengers. | 52 |

Chapter II

| | |
|---|----|
| Figure 2.1 Scheme of typical characterization techniques used with nanoparticles. ^{1,2} | 60 |
| Figure 2.2. TEM micrographs of the magnetite nanoparticles. ⁹ | 63 |
| Figure 2.3. TEM images of (a) Fe ₃ O ₄ , and (b) Fe ₃ O ₄ /Oleic Acid. ¹³ | 63 |
| Figure 2.4 SEM–EDX spectra of Fe ₃ O ₄ magnetic nanoparticle. ¹⁶ | 64 |

| | |
|---|----|
| Figure 2.5 EDX spectrum of the Fe-implanted ND. ¹⁷ | 65 |
| Figure 2.6 Spectra FT-IR of iron oxide magnetic nanoparticles. ¹⁸ | 66 |
| Figure 2.7 a) TGA curves of MNP coated with L-tyrosine (Tys), L-phenylalanine (PhA), L-arginine (Arg), glycine (Gly) and L-lysine (Lys). ²³ b) TGA of MNP and MNP functionalized with oxalic, succinic, glutamic acids, and L-arginine. ²⁵ | 68 |
| Figure 2.8 Particle concentration effects on the measurement of hydrodynamic diameter by DLS. ⁶ | 69 |
| Figure 2.9 Hydrodynamic size distributions of DMSA@MNPs, CS@MNPs, CSDMSA@ ... | 70 |
| Figure 2.10 ζ -potential of iron oxide particles at different pH levels. ³⁰ | 71 |
| Figure 2.11 ζ -potential measurements of (A) Fe ₃ O ₄ -CS, (B) Fe ₃ O ₄ -CSO, and (C) Fe ₃ O ₄ -silaneCOOH nanoparticles. ³² | 71 |
| Figure 2.12 Nitrogen sorption/desorption isotherm of cFe ₃ O ₄ (commercial) and nFe ₃ O ₄ (synthesized) magnetite samples. ³⁷ | 72 |
| Figure 2.13 Magnetization curves normalized per gram of sample (emu/g). ⁴¹ | 74 |
| Figure 2.14. FT-IR of MNP (black line), MND (grey line), MCH (yellow line), MCCH (orange line), and their principal functional groups. | 78 |
| Figure 2.15. TGA of MNP (black line), MND (grey line), MCH (yellow line), MCCH (orange line)..... | 79 |
| Figure 2.16. TEM micrographs of a) MNP, b) MND, c)MCH, and d) MCCH. Size distribution of e) MNP, f) MND, g) MCH, and h) MCCH..... | 80 |
| Figure 2.17. EDX spectra for MNP, MND, MCH, and MCCH. | 81 |
| Figure 2.18. Magnetization curves of MNP (black), MND (gray), MCH (yellow), and MCCH (orange)..... | 82 |
| Figure 2.19. Physisorption measurements and BET area of MNP, MDN, MCH and MCCH. | 84 |
| Figure 2.20. a) DLS of MNP (black line), MND (grey line), MCH (yellow line), MCCH (orange line).b) Zeta potential of MNP (black line), MND (grey line), MCH (yellow line), MCCH (orange line)..... | 85 |
| Figure 2.21. ζ -potential of MNP (black line), MND (grey line), MCH (yellow line), MCCH (orange line)..... | 87 |

Chapter III

| | |
|---|-----|
| Figure 3.1 Treatment technologies to achieve any desired level of water quality. ⁸ | 101 |
| Figure 3.2 Reclaimed water opportunities. ⁶ | 102 |
| Figure 3.3 Important parameters to characterize reclaimed water. ¹⁰ | 104 |
| Figure 3.4 Alkalinity and pH diagram. ²⁰ | 116 |
| Figure 3.5 DLS (black line) and ζ -potential (blue line) of the RW from the WWTP “La Morita”. The pH was adjusted using solutions of 0.001 M HCl and 0.001 M of NaOH. | 122 |
| Figure 3.6 Alkalinity (purple) and hardness (pink) measurements for RW from the WWTP “La Morita” at pH 7, 8, and 9 expressed as mg L ⁻¹ of CO ₃ | 123 |
| Figure 3.7 Comparison of the DLS measurements of RW (purple), MNP (black), MND (gray), MCH (yellow), and MCCH (orange) at pH of 7, 8, and 9. | 124 |
| Figure 3.8 RW at pH 7, 8 and 9. | 125 |
| Figure 3.9 Comparison of the Zeta Potential measurements of RW (purple), MNP (black), MND (gray), MCH (yellow), and MCCH (orange) at pH of 7, 8, and 9. | 125 |

Chapter IV

| | |
|--|-----|
| Figure 4.1 Wastewater treatment trains. (A) Preliminary treatment: screening of debris. Primary treatment: physical treatment. Secondary treatment: biological treatment via aerobic microbial degradation of organic matter. Secondary clarification: biological floc settles out as secondary sludge. Discharge: secondary effluent is discharged to the river. (B) Similar to treatment train (A) but with the addition of disinfection via chlorine gas and sand filtration to remove particulates before distribution for irrigation. (C) Advanced treatment: utilizes ultrafiltration to remove particulates and ultraviolet light for water disinfection before discharge for irrigation, groundwater recharge, or surface water. | 134 |
| Figure 4.2 Fit for Purpose - Treat the wastewater for potential uses (adapted from 2012 US EPA Guidelines for Water Reuse). ⁶ | 135 |
| Figure 4.3 Treatment processes commonly used in water reclamation. ⁷ | 137 |
| Figure 4.4 Surface functional groups and forces of attraction. | 139 |

| | |
|---|-----|
| Figure 4.5 Osmosis and reverse osmosis process diagram. ¹² | 140 |
| Figure 4.6 Separation process through reverse osmosis membrane. ⁸ | 141 |
| Figure 4.7 Schematic framework of functional cation exchange resin: (a) resin initially immersed in an aqueous solution containing B ⁺ cations and X ⁻ anions and (b) cation exchange resin in equilibrium with an aqueous solution of B ⁺ cations and X ⁻ anions. ⁸ | 143 |
| Figure 4.8 Scheme of the simplified process of magnetic nanoparticles used for heavy metal ions removal (HMR) in water treatment. ²³ | 150 |
| Figure 4.9 Comparison of measurements: a) and b) DLS and ζ-potential measurements, respectively, before RW treatment, nanoparticles are dispersed in deionized water, RW (purple), MNP (black), MND (gray), MCH (yellow), and MCCH (orange) at pH of 7, 8, and 9. C) and d) DLS and ζ-potential measurements, respectively, of untreated RW (purple) and RW treated with MNP (black), MND (gray), MCH (yellow), and MCCH (orange) at pH of 7, 8, and 9. | 155 |
| Figure 4.10 a) Comparison of the alkalinity removal of MNP (black), MND (gray), MCH (yellow), and MCCH (orange). b) Comparison of the hardness removal of MNP (black), MND (gray), MCH (yellow), and MCCH (orange). At pH of 7, 8, and 9, expressed as percentage in mg/L..... | 157 |
| Figure 4.11 FT-IR a) MNP (black line) before and after use at pH 7 (blue line), pH 8 (purple line) and pH 9 (wine line). b) MND (gray line) before and after use at pH 7 (blue line), pH 8 (purple line) and pH 9 (wine line). c) MCH (yellow line) before and after use at pH 7 (blue line), pH 8 (purple line) and pH 9 (wine line). d) MCCH (orange line) before and after use at pH 7 (blue line), pH 8 (purple line) and pH 9 (wine line)..... | 159 |
| Figure 4.12 Light microscope images of the nano-softeners after they were recovered from the RW treatment. The red line represents a 1 mm scale bar. | 160 |

Annexes

| | |
|--|-----|
| Figure A1. Outline of magnetic lens, beam path, and sample arrangement within a SEM. ¹ . | 169 |
| Figure A2. SEM image of raw magnetite nanoparticles. ⁶ | 170 |

| | |
|---|-----|
| Figure A3. High magnification BF/HAADF-STEM of individual particles of 32 nm Fe ₃ O ₄ . ¹¹ | 172 |
| Figure A4. A) Magnetite nanoparticles; B) magnetic chitosan nanoparticles. ¹⁵ | 172 |
| Figure A5. The optical electron beam diagram of TEM ¹⁷ | 173 |
| Figure A6. Schematic diagram of typical FT-IR spectrophotometer. ¹⁸ | 175 |
| Figure A7. X-ray diffraction set-up. ² | 177 |
| Figure A8. X-ray diffraction. ² | 177 |
| Figure A 9. XRD pattern of iron oxide nanoparticles. ²³ | 178 |
| Figure A10. (a) XRD pattern of iron oxide nanoparticles, (b) XRD pattern of chitosan coated iron oxidenanoparticles. ²⁴ | 179 |
| Figure A11. Schematic diagram of the TGA setup. ²⁸ | 181 |
| Figure A12. Scheme of a dynamic light scattering spectrometer. ³⁰ | 184 |
| Figure A13. Schematic representation of the ionic concentration and potential difference as a function of distance from the charged surface of a particle suspended in a dispersion medium. ³² | 185 |
| Figure A14. Isotherm plots with the volume of gas adsorbed onto the surface of the sample as pressure increases. ³³ | 188 |
| Figure A15. Schematic diagram of the essential features of a vibrating sample magnetometer. | 190 |
| Figure A16. Illustration of magnetization curves for ferromagnetic, paramagnetic, diamagnetic, and superparamagnetic materials. MS, MR, HC, and xi are the saturation magnetization, remanent magnetization, coercive field threshold, and the initial susceptibility of the material. ³⁵ | 191 |
| Figure A17. Representative M–H loops of (left) magnetic nanoparticles exhibiting hysteresis and (right) where no hysteresis is observed. ²² | 192 |
| Figure A18. FT-IR's of a) MNP (black line), ND (green line), and MND (grey line). b) MNP (black line), CH (wine line) and MCH (yellow line). c) MNP (black line), CCH (pink line), and MCCH (orange line). | 193 |



Figure A19. TGA's of a) MNP (black line), ND (green line), and MND (grey line). b) MNP (black line), CH (dark yellow line) and MCH (yellow line). c) MNP (black line), CCH (wine line), and MCCH (orange line)..... 194

Figure A20. a) SEM image of MNP powder and STEM images of dried drop of aqueous dispersion of b) MND, c) MCH, and d) MCH. 195

Figure A21. Size distribution of a) MCH, b) MNP, c)MCH, and d) MCCH. 196

Table's list

Chapter I

| | |
|--|----|
| Table 1.1 Nanomaterials: Examples, schematic, categories, and fabrication process. ^{3,12} | 35 |
| Table 1.2 Comparison of the most common chemical synthetic methods. ⁷ | 43 |
| Table 1.3 Different coating molecules/polymers for magnetic NPs to stabilize ferrofluids. ⁸ .. | 46 |

Chapter II

| | |
|---|----|
| Table 2.1 Parameters and physicochemical characterization techniques. | 61 |
|---|----|

Chapter III

| | |
|--|-----|
| Table 3.1 Main reclaimed wastewater uses and main related problems. ⁵ | 102 |
| Table 3.2 Microbiological criteria for different applications of wastewater reclamation. ¹ | 103 |
| Table 3.3 Interpretation of RW quality. ⁸ | 104 |
| Table 3.4 Water quality for urban reuse (not restricted). ⁹ | 105 |
| Table 3.5 Water quality for urban reuse (restricted). ⁹ | 105 |
| Table 3.6 Guidelines for interpretation of water quality for irrigation. ⁸ | 107 |
| Table 3.7 Water quality required for reuse in agriculture (non-commercially processed food crops). ⁹ | 108 |
| Table 3.8 Water quality required for reuse in agriculture (commercially processed food crops, surface irrigation of orchards and vineyards). ⁹ | 109 |
| Table 3.9 Water quality required for reuse in agriculture (for non-food crops, dairy pasture, feed, fiber, and seed crops) ⁹ | 109 |
| Table 3.10 Recommended limits of trace elements and dissolved solids for irrigation with treated water. ⁹ | 109 |
| Table 3.11 Water quality required in cooling water (recirculation systems). ⁹ | 110 |
| Table 3.12 Recommended boiler water limits. ⁸ | 111 |

| | |
|---|-----|
| Table 3.13 Water quality required for its reuse in the recharge of aquifers ⁹ | 113 |
| Table 3.14 Composition of reclaimed water, obtained from the wastewater plant treatment "La Morita" in Tijuana, Baja California, México..... | 114 |

Chapter IV

| | |
|---|-----|
| Table 4.1 RW technologies for secondary treatment of wastewater. ³ | 136 |
| Table 4.2 Disinfection technologies used for the RW systems. ³ | 136 |
| Table 4.3 Comparison of adsorption mechanisms between physical adsorption and chemisorption. ⁸ | 139 |
| Table 4.4 Reverse osmosis objectives and alternative processes. ⁸ | 142 |
| Table 4.5 Characteristics of ion exchange resins used in water treatment processes. ⁸ | 144 |
| Table 4.6 Advanced non-photochemical and photochemical oxidation processes. ¹⁷ | 146 |
| Table 4.7 Summary of different advanced oxidation processes (AOP) associated with wastewater and target compounds. ¹⁸ | 147 |
| Table 4.8 Transmittance of different types of water and Reclaimed Water treated with the different magnetite-base materials at pH 7..... | 158 |
| Table 4.9 Solids mass recovered after treating RW with magnetic nano-softeners (30 mg/L) | 158 |
| Table 4.10 Performances comparison of nano-softeners..... | 161 |

Annexes

| | |
|---|-----|
| Table A1. Description of particle system with different range of PDI value. ³⁰ | 184 |
| Table A2. EDX table for MNP | 197 |
| Table A3. EDX table for MND..... | 197 |
| Table A4. EDX table for MCH..... | 197 |
| Table A5. EDX table for MCCH. | 198 |
| Table A6. Water quality required for urban reuse, extended. ³⁸ | 199 |
| Table A 7. Water quality required for agricultural reuse, extended parameters. ³⁸ | 200 |

Agradecimientos

Agradezco profundamente a todos los doctores que me han guiado y participado en mi formación como doctora y han sabido alimentar mi curiosidad, que me han alentado a más y que me han retado mentalmente para ser una mejor persona y una buena investigadora.

Mil gracias a los doctores del Instituto de Ingeniería de la UABC, los doctores Benjamín Valdez Salas, Oscar Manuel Pérez Landeros y Navor Rosas-González, por su gran apoyo y asesoría durante mi estancia en dicha institución.

Mi gratitud a los doctores miembros de mi comité doctoral, los doctores Eduardo Alberto López Maldonado, Antonio Tirado Guízar, José Manuel Romo Herrera, que han sabido guiar este trabajo y a mi persona, aconsejándome y brindando su valioso punto de vista.

Agradezco a la Dra. Georgina Esther Pina Luis, por abrirme las puertas de su laboratorio y guiarme en el proceso de elección de asesor de este proyecto, por ser mi codirectora, una buena consejera, maestra y guía. Por su apoyo incondicional y por su gran labor en mi formación le doy mil gracias.

Y, por último, pero no menos importante, mis más grandes agradecimientos a mi asesora y directora de tesis, Dra. Mercedes Teresita Oropeza Guzmán, por haberme guiado en cada etapa del proyecto, por darme libertad creativa y la confianza para trabajar conmigo, por creer en mí y apoyarme incondicionalmente en cada idea. Gracias por ser mi segunda mamá, por darme el ejemplo de mujer e investigadora, he aprendido mucho de usted y espero seguirle aprendiendo y contando con su amistad. Sin duda, y sin afán de agraviar a nadie, la mejor asesora que me pudo haber tocado en este país. Que nuestros sueños y aspiraciones nunca se detengan. ¡Muchas gracias!

Reconocimientos institucionales

Este trabajo se realizó en los laboratorios de nanosensores y de investigación de tratamiento de aguas (LIDTA) del centro de graduados e investigación en química, pertenecientes al Tecnológico Nacional de México/ Instituto Tecnológico de Tijuana, bajo la dirección de la Dra. Mercedes Teresita Oropeza Guzmán y la codirección de la Dra. Georgina Esther Pina Luis.

Agradezco al Consejo Nacional de Ciencia y Tecnología (CONACyT) por brindarme la beca para poder realizar mis estudios de doctorado (becaria N° 633248), y por los fondos para esta investigación bajo el proyecto APN2016-2015.

Así mismo agradezco al Instituto de Ingeniería de la Universidad Autónoma de Baja California, por brindarme la oportunidad de realizar una estancia de investigación en sus instalaciones y por el apoyo brindado en las caracterizaciones.

I thank Qual Diamond Hi-Tech Corporation for their trust and support giving me their material (nanodiamonds) to be used in this work.

Also, I want to thank to doctors Eric Fullerton and Oscar Vazquez Mena, and the PhD student Jeffrey Brock, all of them from UC San Diego, for their help and collaboration in this thesis.

Finalmente, agradezco al Instituto Tecnológico de Tijuana, mi segunda casa, por recibirme y darme la oportunidad de formarme como maestra y doctora.

Vita, publications, field of interests

Vita

| | |
|---------------------------------|--|
| October 22 nd , 1990 | Born in Tuxtla Gutiérrez, Chiapas, México. |
| 2012 | B.S. in Chemical Engineering, Instituto Tecnológico de Tuxtla Gutiérrez. |
| 2016 | M.S. in Chemistry Sciences, Instituto Tecnológico de Tijuana, CONACyT fellow. |
| 2021 | Ph.D. in Chemistry Sciences, Instituto Tecnológico de Tijuana, CONACyT fellow. |

Publications

Estephany Santiago, Georgina Pina-Luis, Marisela Martinez-Quiroz, Oscar Perez-Landeros, Navor Rosas-González, Benjamin Valdez-Salas, and Mercedes T. Oropeza-Guzman. Eco-Friendly Magnetic Nanoscavengers as Emerging Materials for Improving Reclaimed Water Quality. *Adv Sustain Mater.* **2021**, 5, 2000236

Estephany Santiago, Sergio Perez-Sicairos, Georgina Pina-Luis, Oscar Perez-Landeros, Navor Rosas-González, Benjamin Valdez-Salas, Mercedes T. Oropeza-Guzmán. Magnetic chitosan physicochemical properties to improve treated water quality. *Revista Aristas.* **2021**, 16, 97-102

Participation in symposiums/congress

1. “Fluorescein electrochemistry on a gold electrode”. **XI International Symposium: Chemical Research at the Border Region**, November 14-16, 2018. Tijuana, Baja California, México. Estephany Santiago-Siliceo, Antonio Tirado-Guizar, Georgina E. Pina-Luis and Mercedes T. Oropeza-Guzmán.
2. “New nanotechnologies for water treatment: characterization of magnetic nanoscavengers”. **ACS Fall 2020 virtual meeting and expo “Moving chemistry from bench to the market”**. August 17-20, 2020. Online. Estephany Santiago, Mercedes T.

-
- Oropeza-Guzmán, Georgina E. Pina-Luis, Oscar M. Pérez-Landeros and Benjamín Valdez-Salas.
3. “Magnetic nanoscavengers: the new trend to improve water quality”. **Nano Scientific symposium: for a changing world**. October 14-15, 2020. Online. Estephany Santiago, Mercedes T. Oropeza-Guzmán, Georgina E. Pina-Luis, Marisela Martínez-Quiroz, Oscar M. Pérez-Landeros and Benjamín Valdez-Salas.
 4. “Magnetic nanoscavengers as nano-softeners: the new tool to improve water quality” **ACS Spring 2021 “Macromolecular chemistry: the second century”**. April 5-16, 2021. Online. Estephany Santiago, Mercedes T. Oropeza-Guzmán, Georgina E. Pina-Luis, Oscar M. Pérez-Landeros and Benjamín Valdez-Salas.
 5. “Magnetic chitosan physicochemical properties to improve treated water quality”. **Tijuana International Research Congress 2021 (CI2T)**. May 12-13, 2021. Estephany Santiago, Mercedes T. Oropeza-Guzmán, Georgina E. Pina-Luis, Oscar M. Pérez-Landeros and Benjamín Valdez-Salas.
 6. “Magnetic chitosan as nano-softener to improve groundwater quality”. **ACS Fall 2021 “Resilience of chemistry”**. August 22-26, 2021. Atlanta, Georgia, USA. Estephany Santiago, Alondra Deras-Vazquez, Navor Rosas-González, Georgina E. Pina-Luis, Mercedes T. Oropeza-Guzmán.
 7. “Physicochemistry of magnetic nanodiamonds”. **Encuentro virtual de química inorgánica 2021**. October 4-5, 2021. Online. Estephany Santiago; Oscar Vazquez-Mena; Eric Fullerton; Jeffrey Brock; Jeff Wu; Mercedes T. Oropeza-Guzmán.
 8. “Magnetic nanoscavengers and nanochemosensors: new technologies in water treatment”. **8vo. Encuentro estatal de jóvenes investigadores en Baja California 2021**. October 28-29, 2021. Online. Estephany Santiago; Mercedes T. Oropeza-Guzmán.

Doctoral Exchange

“Characterization of Magnetic nanoparticles”. **Instituto de Ingeniería, Universidad Autónoma de Baja California**. February 12-26, 2020. Mexicali, Baja California, México

Fields of interest

Synthesis and modification of nanomaterials and nanocomposites

Environmental chemistry

Nanosensors

Biopolymers

Drug delivery systems

Resumen

En el contexto del desarrollo de nuevas tecnologías para el tratamiento de agua, esta tesis presenta la concepción y desempeño de nanoablandadores magnéticos. Para tal fin, primeramente, se sintetizaron y funcionalizaron nanopartículas magnéticas (MNP) mediante co-precipitación química para producir tres diferentes nanoestructuras magnéticas: nanomagnetita-quitosano, nanomagnetita-nanodiamante y nanomagnetita-quitosano injertados con un ácido carbamoil benzoico. Estos nanomateriales magnéticos se caracterizaron por FT-IR, TGA, DLS, ζ -potencial, VSM y SEM/STEM, para demostrar su correcta funcionalización. Los nuevos materiales magnéticos fueron probados en agua recuperada de la planta de tratamiento de aguas residuales “La Morita” (Tijuana, B.C., México) para mejorar su calidad estética (alcalinidad y dureza) y comprobar su funcionalidad. Se prestó especial atención a los cambios en las propiedades del agua recuperada (RW, por sus siglas en inglés), que se producen por la interacción interfacial entre las especies iónicas y la superficie de los nanomateriales. La capacidad de los nanomateriales magnéticos para remover alcalinidad y dureza en RW se demostró a pH 7, 8 y 9 (mayores a 20% utilizando MCH a pH 7 y 8). Al mismo tiempo, se comprobó la posibilidad de recuperarlos para usos posteriores y reducir el costo de operación. Con todas estas características podemos clasificar los materiales preparados como nano-ablandadores sostenibles.

Abstract

In the context of developing new technologies for water treatment, this thesis presents the conception and performance of magnetic nano-softeners. To this end, firstly, magnetic nanoparticles (MNP) were synthesized and functionalized by chemical co-precipitation to produce three different magnetic nanostructures: nanomagnetite-chitosan, nanomagnetite-nanodiamond and nanomagnetite-chitosan grafted with a carbamoyl benzoic acid. These magnetic nanomaterials were characterized by FT-IR, TGA, DLS, ζ -potential, VSM and TEM, to prove their correct functionalization. The magnetic nano-softeners were tested on reclaimed water from the wastewater treatment plant “La Morita” (Tijuana, B.C., México) to improve their aesthetics quality (alkalinity and hardness) and verify their functionality. Special attention is

given to changes in reclaimed water (RW) properties, explaining them as the interfacial interaction between ionic species and nanomaterials surface. The ability of nano-softeners to remove alkalinity and hardness in RW is demonstrated at pH 7, 8 and 9 (greater than 20% using MCH at pH 7 and 8). At the same time, we prove the possibility of recovering them to further uses and reduce the operation cost. With all these characteristics we can classify the prepared materials as sustainable nano-softeners.

General introduction

Water shortage is a growing concern worldwide, therefore it is urgent to address this problem by recycling water. Reclaimed water (RW) is water that has been previously treated and its quality degree is directly related to the type of treatment achieved (primary, secondary, tertiary, advanced). The uses given to RW can be vast, but for some applications additional treatments (to the one given in the wastewater treatment plant) are needed.

Over the years nanotechnology has been more involved in water treatment. With the use of functionalized nanostructured materials scientists have been able to develop new water treatments techniques that target specific contaminants from water.

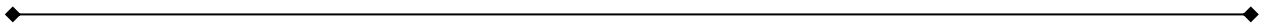
Among all the nanotechnologies available, iron-oxide magnetic nanoparticles (MNP) have attracted more attention due to their unique properties: inexpensive to produce, good stability, compatibility, magnetic separation, sufficient physical and chemical stability, biocompatibility and are environmentally safe.

MNP can remove/eliminate contaminants from water either by adsorption or photocatalysis. Adsorption is a well-known process with extensive applications to remove chemical pollutants from water, using MNP as adsorbents can help to eliminate various types of contaminants such as heavy metals, organic contaminants, dyes, ionic and anionic species, pharmaceutical products and pathogens. A combination of the superior adsorption performance and magnetic properties of MNP is a promising approach to treat RW.

In this thesis, we propose the synthesis and functionalization of magnetite nanoparticles to improve RW quality. We divide the content into four chapters. Firstly, we address the synthesis of these functional materials. Secondly, we characterize the obtained magnetic nanomaterials to prove their correct functionalization and possible performance on the water treatment. Thirdly, we characterize the problem water (RW). With this characterization, we will be able to measure the initial and final quality of the water in terms of its aesthetics (alkalinity and hardness). Finally, we achieve the RW treatment using the functionalized magnetic nanoparticles, where we compare the results obtained with each nano-softener to propose the most promising nanomaterial for water quality aesthetics improvement.

General objective of the research

Synthesize and functionalize hybrid and multifunctional MNP to obtain efficient versatile systems for the detection and removal of metal ions such as Ca^{2+} and Mg^{2+} present in reclaimed water.



Chapter I

Synthesis of functionalized magnetic nanoparticles

1.1 Introduction

Functional materials are a set of advanced materials and composites that can perform a certain “function” under a determined stimulus (thermal, electrical, mechanical, light, etc.).¹ Although some nanomaterials have excellent intrinsic properties, they generally do not have suitable properties for a few specific applications, thus nanomaterial functionalization becomes essential.²

Metal oxides nanoparticles are considered one of the most stable naturally occurring compounds due to their unique properties, unusual adsorptive capabilities and fast diffusivities, all these reasons make them to be counted among the widest used manufactured nanomaterials.^{3,4} Iron oxides: magnetite (Fe_3O_4), maghemite ($\gamma\text{-Fe}_2\text{O}_3$), and hematite ($\alpha\text{-Fe}_2\text{O}_3$) are the most prevailing types in the nature. They possess different physicochemical properties,^{5,6} in particular magnetite has been the most extensively studied due to the presence of the Fe^{2+} state showing an electron donor behavior.⁶

In the last decades, functional materials research has been focusing especially on the chemical methods to synthesize magnetic nanoparticles since they are efficient routes to shape-controlled, highly stable, and monodisperse magnetic nanoparticles. The most popular and used chemical methods include co-precipitation, thermal decomposition and/or reduction, microemulsion, and hydrothermal synthesis, all of them can produce high-quality magnetic nanoparticles. Among the above mentioned, the co-precipitation synthesis is the preferred route due to its simplicity and suitability. Another well appreciated characteristic is that it can be used on a large-scale production.^{7,8}

Magnetite nanoparticles tend to oxidize quickly under ambient conditions and lose their stability over a long period of time without agglomeration or precipitation.^{7,9} Then, it is necessary to develop efficient strategies to improve the chemical stability of magnetic nanoparticles and protect the particle against oxidation. In most of cases, the preparation strategies result in magnetic nanoparticles with a core–shell structure, where the coating methods can be divided into two major groups: coating with organic shells, including surfactant

and polymers, or coating with inorganic components, including silica, carbon, precious metals (Ag, Au) or oxides.^{7,8,10}

This protection will not only assure the magnetic nanoparticles against degradation but can also be used for further functionalization with specific components, and with the easy separation and controlled placement of these functionalized magnetic nanoparticles by means of an external magnetic field enables their application as magnetically controllable systems.⁷

1.2 Justification and objectives

1.2.1 Justification

Iron oxide magnetic nanoparticles are one of the most promising materials for a great diversity of science and engineering applications. As already mentioned, they can be synthesized by a broad range of techniques. Among all of them, co-precipitation is the fastest and simplest way to produce good quality magnetic nanoparticles with high reproducibility and escalation.

However, when the magnetite is modified it is a main issue to protect the magnetic core to avoid critical oxidation and damage its intrinsic properties. A specific modification to magnetite surface can be translated into an improvement but it also risks the magnetic properties.

1.2.2 Objectives

1.2.2.1 General objective:

Synthesize magnetic nanoparticles (MNP) and modify it with different organic molecules, to protect the magnetic core and functionalize them for further application in water treatment analysis.

1.2.2.2 Specific objectives:

- ❖ Synthesize raw MNP by co-precipitation method
- ❖ Use the biopolymer chitosan (CH) to modify MNP to obtain magnetic chitosan (MCH) by co-precipitation method
- ❖ Synthesize 4,4'-Biscarbonil(2-(naphthalen-1-methylcarbamoyl) benzoic acid to modify CH and obtain carbamoyl chitosan (CCH)
- ❖ Use the CCH previously synthesized to modify MNP and obtain magnetic carbamoyl chitosan (MCCH)
- ❖ Use nanodiamonds to modify MNP and obtain magnetic nanodiamond (MND)

1.3 Background

1.3.1 Functional materials

Functional materials are a fast-growing set of advanced materials and composites performing a certain “function” under a determined stimulus. This function is related to its properties such as shape, electrical conductivity, mechanical properties, color, etc., and the external stimulus can be thermal, electrical, mechanical, and light, among others.¹

Engineering and material sciences have progressively increased a distinction between structural materials and functional materials. In fact, it is much harder to distinguish a functional material accurately than it is to distinguish a structural material. However, the easiest way is to consider that comes when one structural material is related with load-bearing capacity and functional material is related with the response to a stimulus.¹¹

The group of functional materials mainly includes the following materials: dielectrics, pyroelectrics, piezoelectrics, ferroelectrics, ferroelectric relaxors, incipient ferroelectrics, semiconductors, ionic conductors, superconductors, electro-optics, and magnetic.







In the recent past, scientists were focused on the characterization of the bulk properties of functional materials, along with their description by theoretical models. Then science people developed and established considerable knowledge on the relationships between composition, microstructure, processing, and macroscopic properties for a wide variety of functional materials. Nowadays researchers are creating and producing materials to optimize them and to meet tomorrow’s needs. This “materials bulk” approach has changed to micro and nano scales speed on the published papers in the past decades.¹

1.3.2 Functional nanomaterials

Most of the materials and devices change their physical and functional properties, for example, surface to volume ratio, tunneling effect, catalytic properties, and aspect ratio increases significantly, with lowering the size (nanoscale).¹² Various techniques have been developed to control composition, size, shape and surface chemistry of different materials at the nano scale and tailor their properties for particular applications, making them functional for a specific purpose.¹³

Then it is necessary to know what a nanostructured material is. A nanostructured material is defined by its dimensionality: zero dimension (0D), one dimension (1D), two dimension (2D), three dimension (3D); and different varieties of anisotropic nanostructures depending upon the fabrication process. The 0D, 1D, and 2D systems have three, two, and one dimension below 100 nm (critical length), respectively. In the case of the 3D nanostructures, all three dimensions of the basic building blocks of the bulk structures are under 100 nm. Anisotropic nanostructures are the combination of the above-mentioned systems with different oblique angle and dimensionality. These systems present lower symmetry which in turn gives higher aspect ratio and functionality, but the main inconvenience with these structures is their fabrication process.¹² In Table 1.1 it can be observed the schematic representation, fabrication process, and some simple examples of the nanomaterials based on their dimensions.

Table 1.1 Nanomaterials: Examples, schematic, categories, and fabrication process.^{3,12}

| Dimension | Schematic | Fabrication process | Examples | Remarks |
|----------------|---|---|---|---|
| 0D |  | Chemical process | Quantum dots, Nanoparticles, nano-onions. | All three dimension < 100 nm |
| 1D |  | Chemical and vapor process | Nano rods, needles, tubes, nanoribbons, etc. | Two dimensions < 100 nm |
| 2D |  | Chemical and vapor process | Nanosheets, nanoplates, nanoprisms, nanodisks, nanowalls, etc. | One dimension <10 nm |
| 3D |  | Nanostructured composites | nanoflowers, nanocoils, nanopillars, nanoballs, dendritic-structures, dots in bulk matrix, etc. | All three dimension of building block <100 nm |
| Anisotropic 2D |  | Nanoimprint lithography | Self-assembly | 2D on oblique 2D |
| Anisotropic 3D |  | Oriented and oblique nanostructure growth | Multi-domains | High aspect ratio (1000), crystal size and geometry |

Although some nanomaterials have excellent intrinsic properties, they are not specific applications. Nanomaterial functionalization through surface engineering or interior modification is thus essential.²

Many functionalization techniques have been used to modify and functionalize the surface of nanoparticles. These methods include coating with a polymer, conjugation with target-specific agents, fluorescent probes, well-membrane penetration ligands, functionalization with a magnetic core, doping with luminescent lanthanide ion, small molecules, peptides, or antibodies.^{2,14} Figure 1.1 illustrates the surface modification of a nanoparticle, allowing to attach a variety of targeting molecules including drugs, antibodies, and nucleic acids.

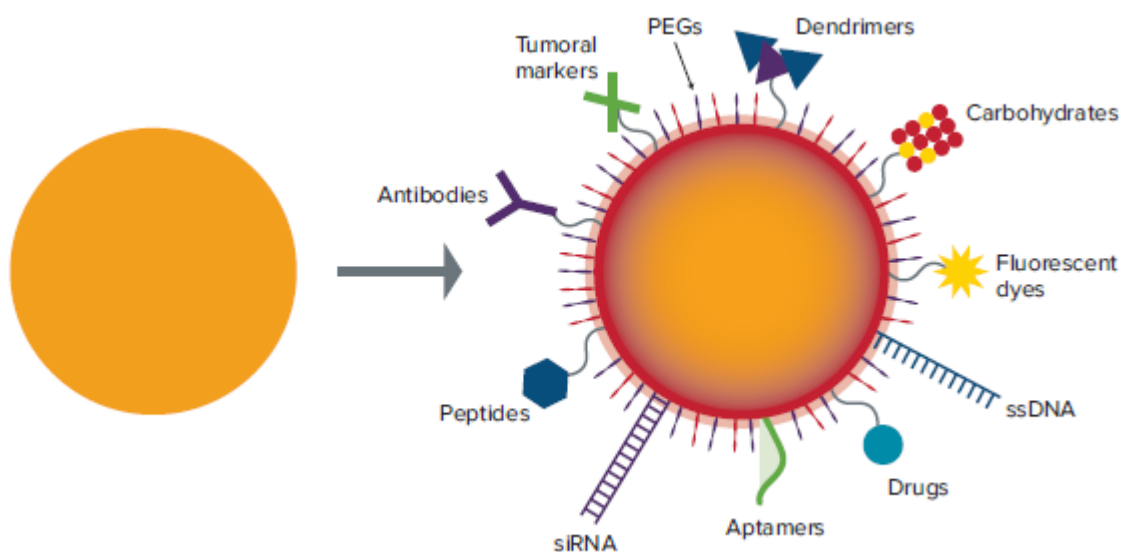


Figure 1.1 Diagram of surface functionalization of nanoparticles. Left: original nanoparticle. Right: nanoparticle with surface functionalization.¹⁵

Additionally, nanomaterials can be widely classified into two categories based on their chemistry: inorganic (non-carbon) and organic (hydrocarbon) nanomaterials. Metal-based NPs, metal oxide/hydroxide NPs, and transition metal chalcogenide NPs are inorganic nanomaterials. Carbon-based nanomaterials, such as graphene, carbon nanotubes, and fullerenes; are considered as a separate class of nanomaterials with a wide range of morphologies due to the enormous number of studies and versatile applications.³ In Figure 1.2 we can see a schematic representation of this classification.

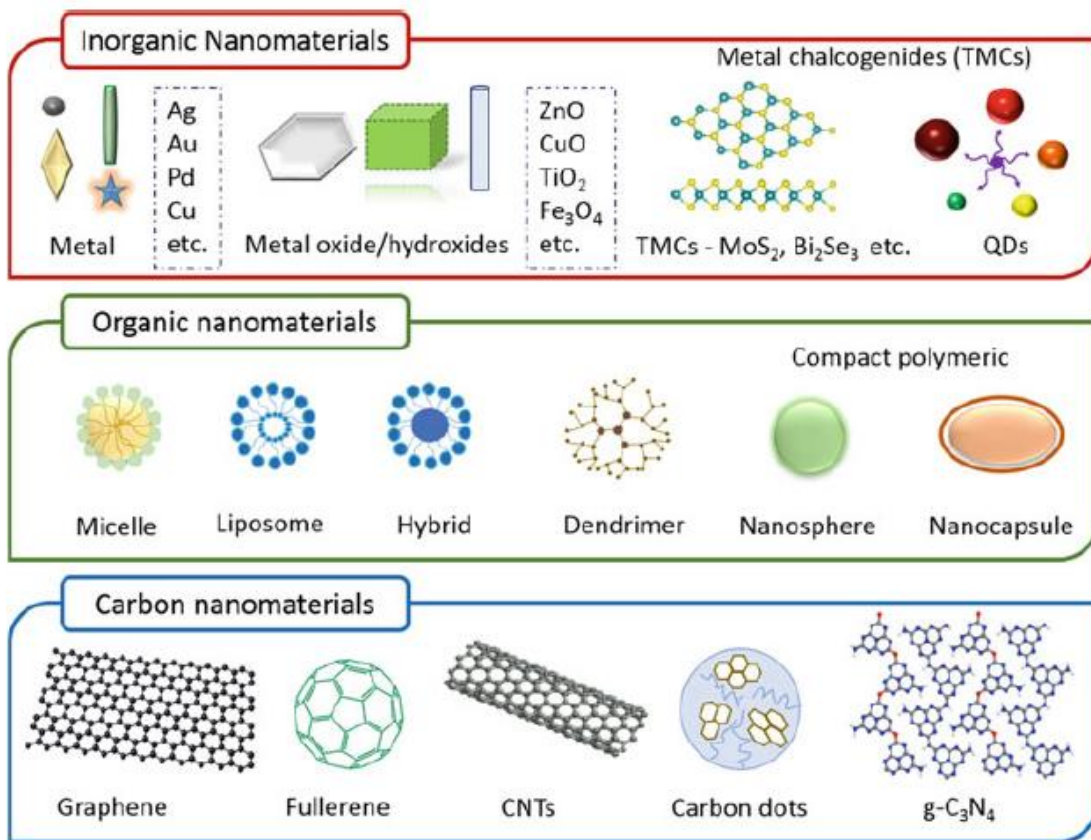


Figure 1.2 Basic nanomaterials classification: inorganic nanomaterials, organic nanomaterials, carbon-based materials.³

Metal oxides are considered one of the most stable naturally occurring compounds. They are formed by reaction between electronegative oxygen and electropositive metal.³ Metal oxides nanoparticles (MONPs) are among the widest used manufactured nanomaterials because of their unique properties such as nonlinear optical properties, higher ductility at elevated temperatures, cold welding properties, superparamagnetic behavior, unique catalytic, sensitivity, and selective activity. At the same time, MONPs exhibit unusual adsorptive properties and fast diffusivities; however, they are not stable in critical conditions.⁴

With growing demand and industrial interest, diverse types of versatile metal oxides have been synthesized for application in the water purification, cosmetics, bio-medical, energy, and environmental remediation fields. Some examples are Al₂O₃, TiO₂, Fe₃O₄, Fe₂O₃, SiO₂, ZnO, and CeO₂. These metal oxides can be easily modified by doping and surface modification,

resulting in hetero-structures and mixed oxides.³ The specific size of the resulting nanoparticle can alter magnetic, conducting, chemical, and electronic properties.⁴

1.3.3 Iron-oxide magnetic nanoparticles

Magnetic metal oxides nanoparticles have gained particular interest as their properties can be tuned based on their size and shape, besides they possess significant advantages including primary price (inexpensive to produce), stability, and compatibility, magnetic separation, sufficient physical and chemical stability, as well as biocompatibility and are environmentally safe.^{4,16}

Magnetite (Fe_3O_4), maghemite ($\gamma\text{-Fe}_2\text{O}_3$), and hematite ($\alpha\text{-Fe}_2\text{O}_3$) are the most prevailing types of iron oxide in nature, and they possess different physicochemical properties originated from the difference in their iron oxidation states.^{5,6} Hematite and maghemite shows weak, size-dependent magnetism while magnetite shows strong ferromagnetism and among all the iron oxides has been the most extensively studied because of the presence of the Fe^{2+} state with the potential of acting as an electron donor.^{6,17}

Iron has four different magnetic states that occur during its crystallization (Figure 1.3). In the paramagnetic state the crystal produces randomly aligned magnetic moments and the overall structure has zero net magnetization. When a paramagnetic state is subjected to an external magnetic field the moments align to produce a small net crystal magnetization. At the ferromagnetic and antiferromagnetic states, the individual moments are randomly aligned without an external magnetic field. In ferrimagnetism the magnetic fields associated with individual atoms spontaneously align themselves, some parallel, or in the same direction (as in ferromagnetism), and others generally antiparallel, or paired off in opposite directions (as in antiferromagnetism).^{6,18}

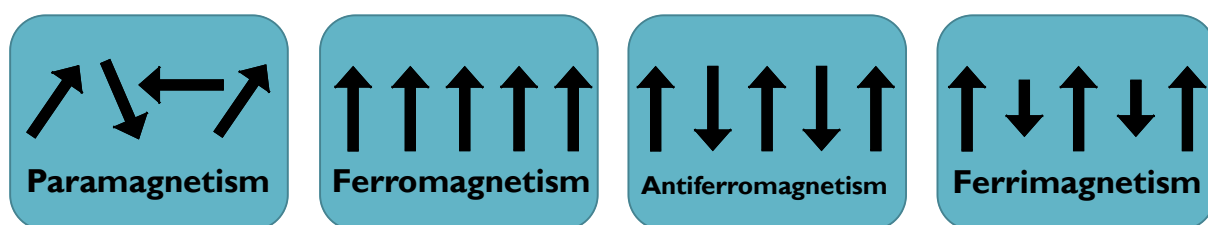


Figure 1.3 Alignment of the magnetic moment of individual atoms of iron.

A magnetic domain, also known as Weiss domain, in a ferromagnetic material, is a volume in which all magnetons are aligned in the same direction. This domain structure is the reason why the magnetic behavior of ferromagnetic material is size-dependent. Iron oxide nanoparticles can show superparamagnetic properties that are directly related to the nanoparticles' size and can be explained by analyzing the coercivity. Coercivity is defined as the minimum value of magnetizing intensity that is required to bring the material to its original state, when the nanoparticle diameter decreases the coercivity increases to a maximum and then falls toward zero. If the diameter of a single domain particle further decreases, the coercivity becomes zero and the particle goes from ferromagnetic to superparamagnetic.^{17,19} This behavior is schematized in Figure 1.4.

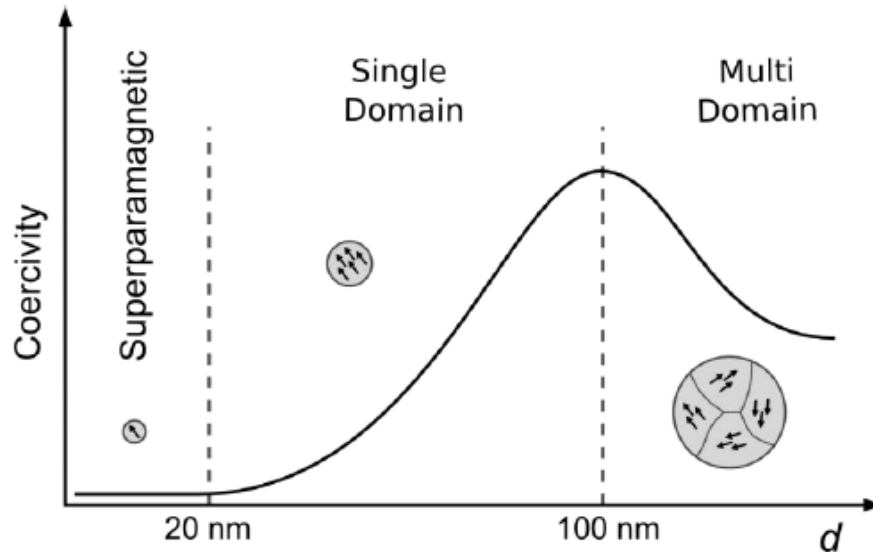


Figure 1.4 Coercivity variation with particle diameter.¹⁷

The magnetization curve of this kind of material is determined by its composition, solid structure, size and shape.¹⁹ To explain the response of magnetic and ferromagnetic materials in an applied field, it is necessary to make use of the hysteresis curve. In Figure 1.5, it can be observed that a superparamagnetic material reach a maximum of magnetization when an external magnetic field is applied and does not present remanent magnetization when this field is no longer applied, i.e. no hysteresis is produced such that they leave behind zero residual magnetization after an external magnetic field is removed.¹⁷ The same effect is observed for a paramagnetic material with the difference that it does not present the same level of

magnetization (it is lower) as a superparamagnetic material. Finally, a ferromagnetic material has remanent magnetization when an external magnetic field is no longer applied, this is the reason why it does not return to its original state.

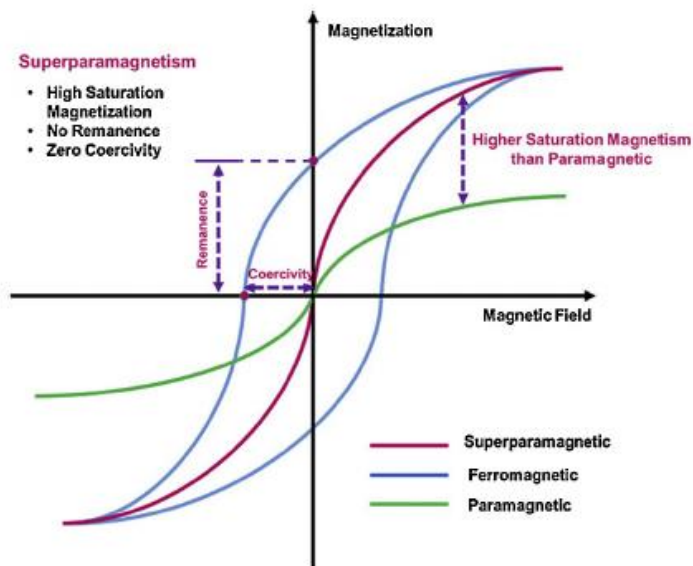


Figure 1.5 Magnetization characteristics of ferromagnetic materials.⁶

The domains of ferromagnetic nanoparticles and the magnetic moment of single domain superparamagnetic nanoparticles are well-illustrated in Figure 1.6, it shows how they align with the applied magnetic field. When the external magnet is removed ferromagnetic nanoparticles maintain their magnetization to a certain degree, while superparamagnetic nanoparticles will show zero net magnetization. Among naturally occurring minerals, magnetite is the one with the most attractive magnetic properties.¹⁷

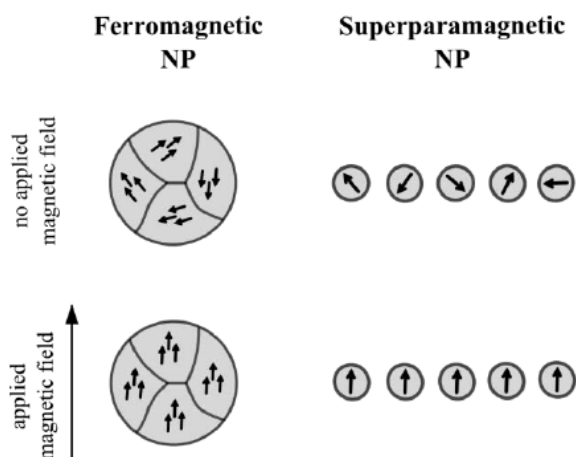


Figure 1.6 The domains of ferromagnetic and superparamagnetic nanoparticles.¹⁷

1.3.4 Synthesis of magnetic nanoparticles

In nanotechnology, a wide number of synthesis strategies and techniques are used, Figure 1.7 summarizes them.

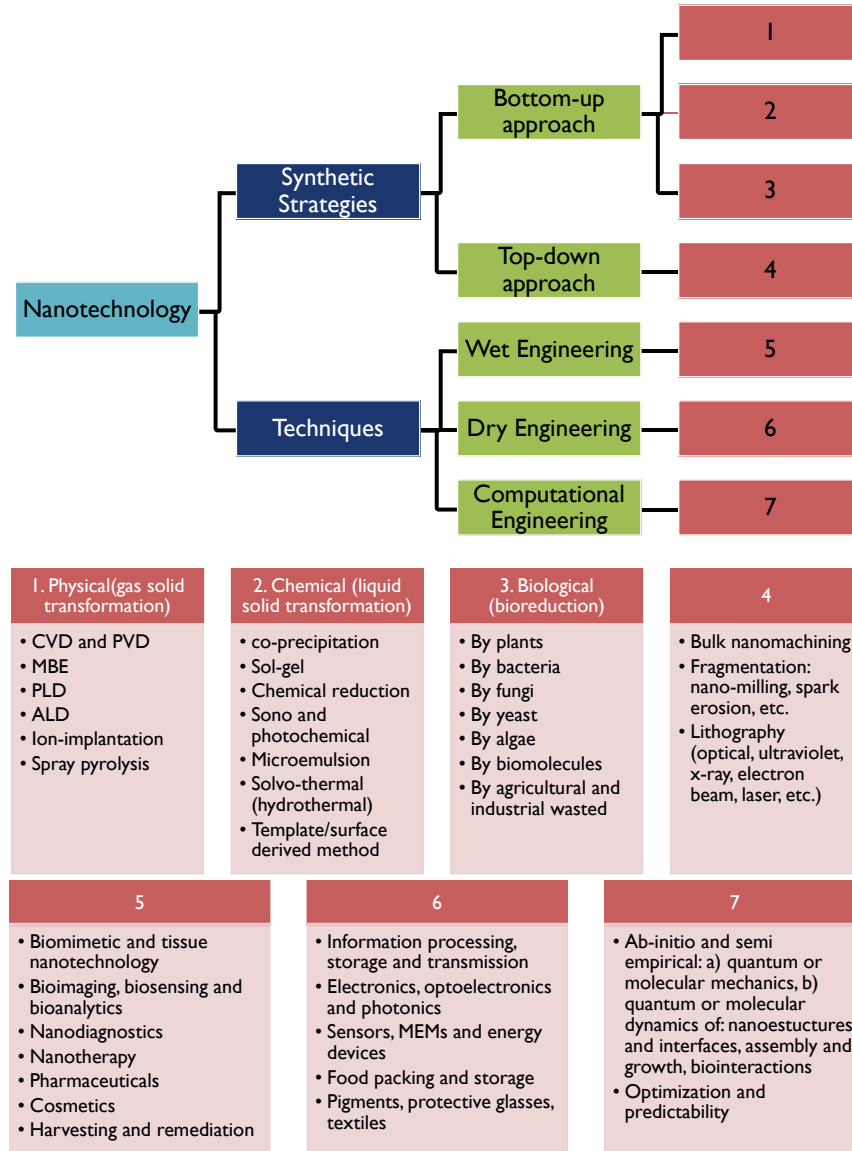


Figure 1.7 Synthetic strategies and techniques used in nanotechnology, enlisting the typical processes or applications that a certain strategy or technique includes.⁴

As synthetic strategies are concerned, there are in general two types of approaches to produce nanomaterials and the fabrication of nanostructures:

- i. Bottom-up approach that includes miniaturization of materials components up to atomic level with further self-assembly process leading to the formation of nanostructures thanks to the physical forces operating at the nanoscale which combine basic units into larger stable structures. This approach organizes atomic or molecular components in hierarchical nanocomplexes examples are quantum dots or nanoparticles formed from colloidal dispersion.
- ii. Top-down, that initiate with macroscopic structures controlling externally the process of formation of nanostructures, in other words, this approach adds or removes thin layers of bulk materials as do ball milling, mask etching, etc.⁴

Magnetic nanoparticles can be synthesized by three of the bottom-up methods: physical, chemical, and biological. Among these methodologies, chemical-based synthesis are mostly adopted (as seen in Figure 1.8) due to low production cost and high yield.⁸

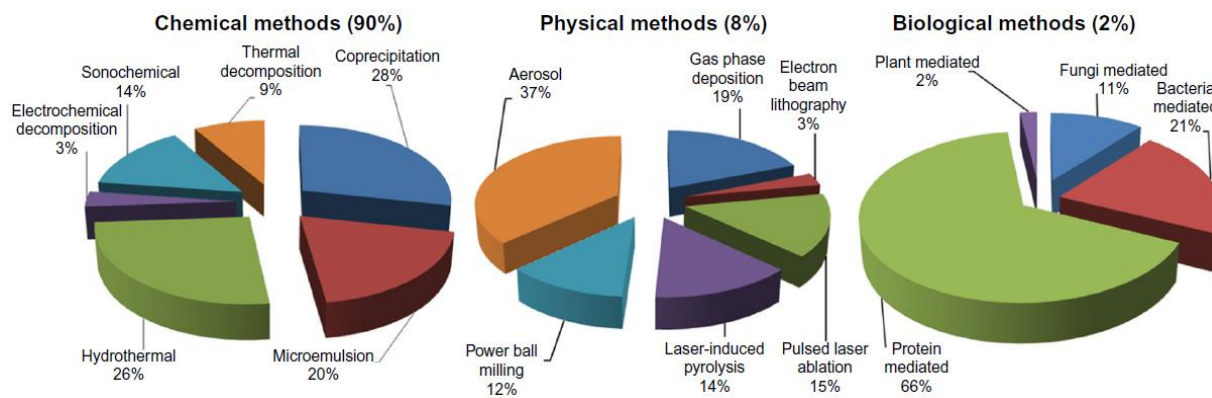


Figure 1.8 A comparison of the synthesis of superparamagnetic iron oxide nanoparticles by three different routes.⁸

In the last decades, researchers have been focusing especially on the chemical methods to synthesize magnetic nanoparticles since they are efficient routes to shape-controlled, highly stable, and monodisperse magnetic nanoparticles. The most popular and used chemical methods include co-precipitation, thermal decomposition and/or reduction, microemulsion, as well as hydrothermal synthesis. All of them can produce high-quality magnetic nanoparticles.^{7,8}

The principal advantages and disadvantages of the four above mentioned synthetic methods are summarized in Table 1.2. Briefly, the co-precipitation synthesis is the preferred route due to its simplicity. Thermal decomposition is the best method developed so far in terms

of size and morphology control of the nanoparticles. Microemulsions are a good alternative to synthesize monodispersed nanoparticles with various morphologies but require a large amount of solvent, and hydrothermal synthesis has been a relatively not much explored method although it allows the synthesis of high-quality nanoparticles. Until the moment of publication of this thesis, magnetic nanoparticles prepared from co-precipitation and thermal decomposition are the best studied, suitable and they can be prepared on a large scale.^{7,8}

Table 1.2 Comparison of the most common chemical synthetic methods.⁷

| Synthetic method | Synthesis | Reaction temp. (° C) | Reaction period | Solvent | Surface capping agents | Size distribution | Shape control | yield |
|------------------------|---------------------------------|----------------------|-----------------|------------------|--|-------------------|---------------|----------------|
| Co-precipitation | Very simple, ambient conditions | 20-90 | Minutes | Water | Needed, added during or after reaction | Relatively narrow | Not good | High/ scalable |
| Thermal decomposition | Complicated, inert atmosphere | 100-320 | Hours-days | Organic compound | Needed, added during reaction | Very narrow | Very good | High/ scalable |
| Microemulsion | Complicated, ambient conditions | 20-50 | Hours | Organic compound | Needed, added during reaction | Relatively narrow | Good | Low |
| Hydrothermal synthesis | Simple, high pressure | 220 | Hours ca. days | Water-ethanol | Needed, added during reaction | Very narrow | Very good | Medium |

The colloidal stability of magnetic nanoparticles synthesized by these four methods results either from steric or electrostatic repulsion, depending on the stabilizers, such as fatty acids or amines, and the polarity of the solvent used. Magnetite nanoparticles synthesized using co-precipitation were stabilized by repulsive electrostatic forces because the particles are positively charged, and nanoparticles synthesized by thermal decomposition are generally sterically stabilized in an organic solvent by fatty acids or surfactants.⁷

1.3.5 Surface modification and functionalization of magnetic nanoparticles

It is known that iron ions crystallize in more than 20 oxide and oxy-hydroxide forms. The divalent iron ions from tetrahedral sites in the surface of magnetite nanoparticles tending to oxidize quickly under ambient conditions and leading to be changed on its composition and properties, they also maintain their stability for a long period of time without agglomeration or precipitation (since stability is a crucial requirement for almost any application of magnetic nanoparticles). Thereupon, not only the synthesis conditions limit the applications of particles but also the environment where the particles are used.^{7,9}

Iron oxide nanoparticles must be stabilized against aggregation by reaching the equilibrium between attractive and repulsive forces in the magnetic colloidal suspension. There are four types of forces that theoretically contribute to the interparticle potential in the system:^{10,17}

1. Van der Waals forces, including strong short-range isotropic attractions.
2. Electrostatic repulsive forces that can be partially screened by adding salt to the suspension.
3. Magnetic dipolar forces between two particles, in the case of magnetic suspensions.
4. Steric repulsion forces, in the case of non-naked particles.

Stabilization of magnetic particles can be achieved by playing on one or both of the two repulsive forces mentioned above: electrostatic and steric repulsion (Figure 1.9). Controlling the strength of these forces is a key parameter to elaborate particles with good stability. The steric force can be difficult to predict and quantify but it is quite well-described theoretically for polymers and depends, among other parameters, upon the molecular weight and density of the polymer. The electrostatic repulsion can be followed through the knowledge of the diffusion potential that may be very close to the zeta potential (ζ), and the Debye-Huckel length that mainly depends of the ionic strength and pH of the solution.¹⁰

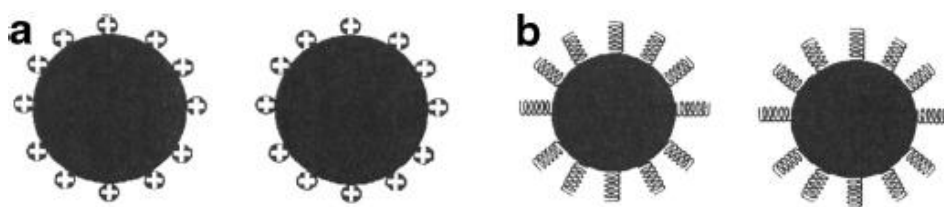


Figure 1.9 (a) Particles stabilized by the electrostatic layer. (b) Particles stabilized by steric repulsion.¹⁰

Therefore, it is necessary to develop efficient strategies to improve the chemical stability of magnetic nanoparticles. The most straightforward method seems to be protection by a layer so that oxygen can't reach the surface of the magnetic particles. Often, stabilization and protection of the particles are closely linked with each other. Regarding certain applications, the surface of particles can be adjusted with mild oxidation of the particle surface leading to thermodynamically more stable particles and different structure–property relationships.^{7,9}

Figure 1.10 shows a schematic representation of the modifications and functionalization of the magnetite. The majority of the protection strategies result in magnetic nanoparticles with a core-shell structure, this is the naked magnetic nanoparticle as a core coated by a shell, isolating the core against the environment. The coating strategies can be divided into two major groups:

- i. Coating with organic shells, including surfactant and polymers
- ii. Coating with inorganic components, including silica, carbon, precious metals (Ag, Au) or oxides, which can be created by gentle oxidation of the outer shell of the nanoparticles (a technique long known for the passivation), or additionally deposited (such as Y_2O_3).

As an alternative, magnetic nanoparticles can also be dispersed/embedded into a dense matrix, typically in polymer, silica, or carbon, to form composites, which also prevents or at least minimizes the agglomeration and oxidation.^{7,8,10}

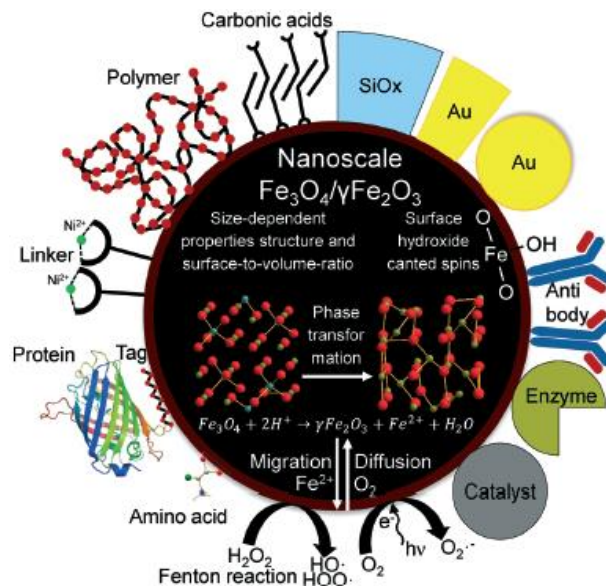


Figure 1.10 Schematic illustration of different applications, structural transformations, and surface interactions of nanoscale iron oxide nanoparticles.⁹

This protective layer will not only assure the magnetic nanoparticles against degradation but can also be used for further functionalization with specific components, like catalytically active species, drugs, specific binding sites, or other functional groups. Another method for the functionalization of magnetic nanoparticles is ligand exchange, by which the as-synthesized magnetic nanoparticles in an organic phase can be converted into water-soluble ones. The easy

separation and controlled placement of these functionalized magnetic nanoparticles through the use of an external magnetic field allows their application as catalyst supports, in immobilized enzyme processes, and the construction of magnetically controllable bio-electrocatalytic systems.⁷

1.3.5.1 Polymer Stabilizers

Several approaches have been developed to coat iron oxide nanoparticles using polymers, including in-situ coatings and post-synthesis coatings, and are often employed to passivate the surface of the nanoparticles during or after the synthesis to avoid agglomeration. In the in-situ approach, nanoparticles are coated during the synthesis. The post-synthesis coating method consists of grafting the polymer on the magnetic particles once synthesized.^{7,10}

Materials with polymeric coating can be classified as synthetic (polyethylene glycol, poly(vinyl alcohol), poly(lactic-co-glycolic acid), poly(vinyl-pyrrolidone), poly(ethylene-co-vinyl acetate), etc.) or natural (gelatin, dextran, chitosan, etc.).⁸ Table 1.3 shows the various summarized coating methods and materials of magnetic nanoparticles with polymers and their benefits.

Table 1.3 Different coating molecules/polymers for magnetic NPs to stabilize ferrofluids.⁸

| Molecules/Polymers | Benefits |
|--------------------|--|
| PEG | Improves biocompatibility by noncovalent immobilization of PEG on the surface, internalization efficiency of the NPs, and blood circulation time |
| Dextran | Stabilizes the colloidal solution and increases the blood circulation time |
| PVP | Stabilizes the colloidal solution and increases the blood circulation time |
| Fatty acids | Terminal functional carboxyl groups and colloidal stability |
| PVA | Gives rise to monodisperse particles and prevents coagulation of particles |
| Polyacrylic acid | Improves biocompatibility of the particles, also helps in bioadhesion, and increases the stability |
| Polypeptides | Worthy for cytology, such as targeting to cell |
| Phosphorylcholine | Coagulation activating and colloidal solution stabilizer |
| Poly(d, l-lactide) | Low toxicity and biocompatible |
| PolyNIPAAm | Cell separation and drug delivery |
| Chitosan | A widely used natural cationic linear polymer as nonviral gene delivery system, is biocompatible, used in medicine and food, applied in water treatment, polymers, textiles, biotechnology, hydrophilic, and used in agriculture |
| Gelatin | Biocompatible, natural polymer emulsifier hydrophilic, and used gelling agent |

Abbreviation: NPs, nanoparticles; PEG, polyethylene glycol; polyNIPAAm, poly(N-isopropylacrylamide); PVA, polyvinyl alcohol; PVP, polyvinyl pyrrolidone.

In general, polymers can be physically adsorbed or chemically anchored on magnetic nanoparticles to form a single or double layer. These kinds of interactions create repulsive forces to balance the magnetic one (mostly as steric repulsion) and the van der Waals attractive forces acting on the nanoparticles. Thus, by steric repulsion, the magnetic particles are stabilized in suspension. Polymers containing functional groups, such as carboxylic acids, phosphates, and sulfates, can bind to the surface of magnetite.^{7,10}

1.3.5.2 Carbon Coating

In recent years, carbon-protected magnetic nanoparticles are gaining more attention, because carbon-based materials have many advantages over polymer or silica, such as biocompatibility, and higher chemical and thermal stability. Especially, carbon-based new generation hybrid materials have been intensively investigated for analytical applications as adsorbent because of their high surface area, high mechanical stability for harsh medium, tailorability and functionality properties, this new generation of materials consist of carbon nanotubes, graphene, graphene oxide and nanodiamond.^{7,20}

It is possible to synthesize carbon-coated magnetic nanoparticles that are thermally stable and have high stability against oxidation and acid leaching. Moreover, carbon-coated nanoparticles are usually in the metallic state, and thus have a higher magnetic moment than the corresponding oxides. Although carbon-coated magnetic nanoparticles have many advantageous properties, these particles are often obtained as agglomerated clusters, owing to the lack of effective synthetic methods, and a low degree of understanding of the formation mechanism. Therefore, the synthesis of dispersible carbon-coated nanoparticles in isolated form is currently one of the challenges in this field.⁷

1.3.6 Hypothesis

- ❖ It will be possible to complete the synthesis of magnetic nanoparticles using the co-precipitation method.
- ❖ The magnetic nanoparticles will be successfully modified with the chosen organic modifiers (nanodiamond, chitosan and carbamoyl chitosan) producing

materials with still good magnetic properties and more stability in water than the raw materials.

1.4 Experimental and methods

1.4.1 Materials and reagents

All the reagents were obtained from Sigma Aldrich and used as purchased.

Nanodiamond (ND) powder was kindly provided by Qual Diamond Hi-tech Corporation, with high purity (95%) and a mean size of 30 nm, the material was used without any further modification.

- ❖ Low molecular weight chitosan (CH, assays, $\geq 75\%$)
- ❖ Iron (III) nitrate nonahydrate $\text{Fe}(\text{NO}_3)_3 \cdot 9\text{H}_2\text{O}$ (ACS reactive, $\geq 98\%$)
- ❖ Iron (II) sulfate heptahydrate $\text{FeSO}_4 \cdot 7\text{H}_2\text{O}$
- ❖ Ammonia hydroxide (30-32%)
- ❖ Deutero-hydrochloric acid (35% weight in D_2O , 99 %)
- ❖ Acetic acid (ACS reactive, $\geq 99.7\%$)
- ❖ Sodium hydroxide (ACS reactive, $\geq 97.0\%$)
- ❖ Hydrochloric acid (ACS reactive, 37%)
- ❖ 3,3',4,4'-Benzophenone Dianhydride

1.4.2 Equipment

- ❖ Analytical balance brand OHAUS model AV264

1.4.3 Methodology

1.4.3.1 Modification of Chitosan with a carbamoyl benzoic acid (CCH)

The chemical modification of chitosan with the carbamoyl benzoic acid (CCH) was obtained using the methodology reported by Martinez-Quiroz et al.²¹ as follow: 3,3',4,4'-Benzophenone dianhydride was dissolved in ethanol (0.3 equiv), subsequently, the CH was added (100 mL, 10 mg/mL, 7% acetic acid) and the mixture was let to react for 2 h under constant stirring. Afterward, naphthyl ethylamine (0.3 equiv) was added, and the reaction continued for 5 h. At the end of the reaction, the settle solution was filtered and allowed to dry. The solid obtained was pulverized and stored until its use.

1.4.3.2 Synthesis of Magnetic Nanoparticles (MNP)

Superparamagnetic iron-oxide nanoparticles were synthesized via chemical co-precipitation under alkaline conditions, maintaining a molar ratio of $\text{Fe}^{2+}:\text{Fe}^{3+}=1:2$ in an argon gas environment to avoid critical oxidation. This synthesis was inspired in the methodology reported by Liu et al²² with slight modifications: two iron salts ($\text{FeSO}_4 \cdot 7\text{H}_2\text{O}$ and $\text{Fe}(\text{NO}_3)_3 \cdot 9\text{H}_2\text{O}$) were weighed and dissolved in deionized water under vigorous magnetic stirring under an inert atmosphere, the solution was heated until 80 °C. Once this temperature was reached, 5 mL of NH_4OH (32%) was added and then stirred for 1 h. The product was washed with deionized water and separated by magnetic decantation. Finally, the product was dried in a desiccator for a couple days.

1.4.3.2 Surface modification and functionalization of Magnetic Nanoparticles

Magnetic nanodiamond, magnetic chitosan and magnetic carbamoyl chitosan (MND, MCH, and MCCH, respectively), were prepared by the co-precipitation method adding an extra step: the two salts of iron were mixed in water under an inert atmosphere until reach 50 °C, at that point 100 mg of nanodiamond, chitosan or carbamoyl chitosan (ND, CH, and CCH, respectively) was added to the mix and let the reaction pot under a vigorous magnetic stirring until reach 80 °C. At that temperature NH_4OH (32%) was added, and the mixture was let to react for 1 h. The final product was washed with deionized water and separated using magnetic decantation. The modified magnetite was dried for a couple days and stored until its use.

1.5 Results and discussions

The magnetic nanoparticles: MND, MCH, and MCCH, as well as raw magnetic iron-oxide nanoparticles (MNP), were synthesized and modified using the co-precipitation method in one step. These magnetic nanoscavengers are a proper combination of magnetite nanoparticles with other molecules (ND, CH and CCH) that can remove remaining substances in reclaimed water (RW) by adsorption or crystallization induction.

Figure 1.11 shows the raw MNP before (a) and after (b) the influence of a magnetic field (Niobium magnets) displaying its magnetic properties. It's well-observed that before applying the magnet the particles do not show any magnetization, but after the application of a magnetic force these particles react to the magnetic field showing a magnetization moment. This result will be further confirmed in the following chapter.

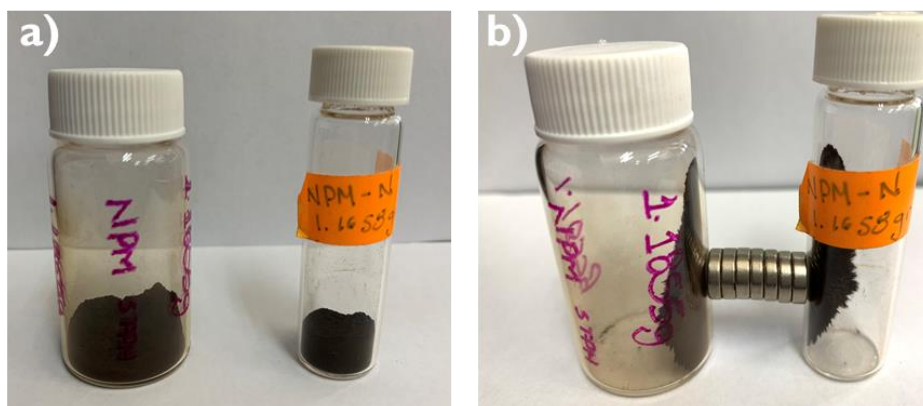


Figure 1.11 MNP before (a) and after (b) being under the influence of a Nb magnet.

All the modified magnetic nanoparticles have a black color and showed the same response to a magnetic field. Figure 1.12 illustrates the nanometric conception of magnetic nanoparticles with the three different types of molecules all of them will be tested based on its mechanical stability and chemical properties, and all their characterization will be shown and analyzed in the next chapter.

The modified magnetic nanoparticles will be further tested as nano-adsorbents to remove alkalinity and hardness from real water samples (RW samples), the working principle of the modified magnetic nanoparticles is represented in Figure 1.13, where the nanoparticles are dosed in water and recovered using magnetic decantation.

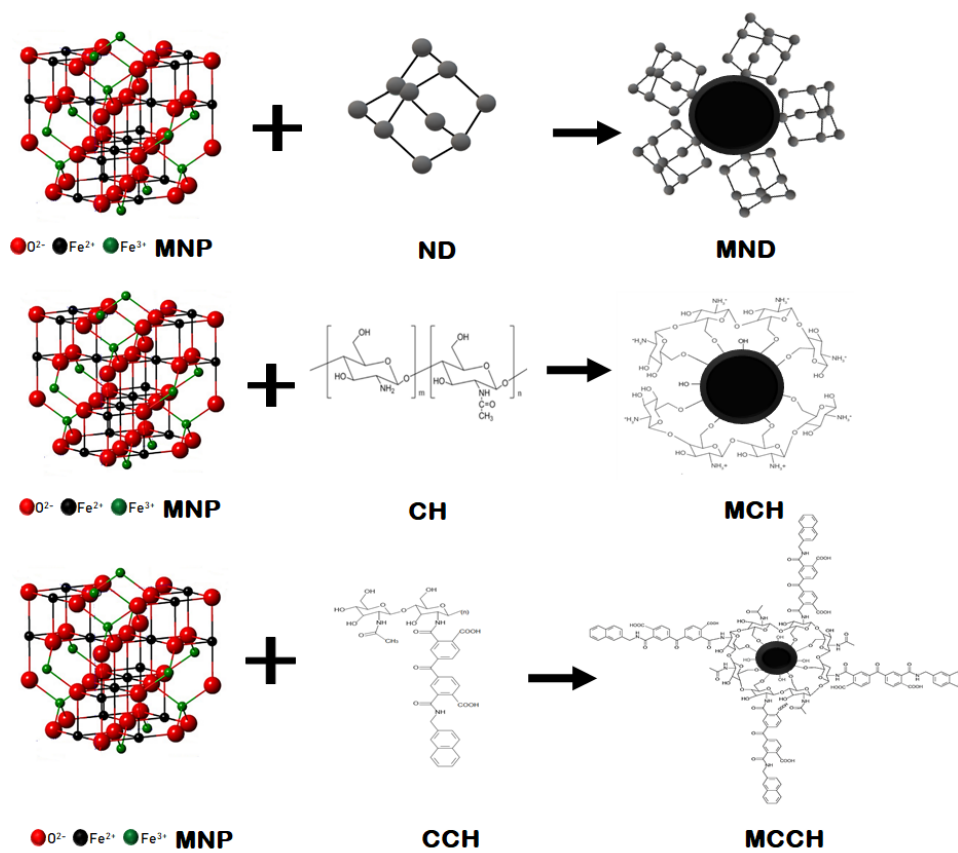


Figure 1.12 Schematic illustration of the formation of the nanoscavengers MND, MCH, and MCCH.

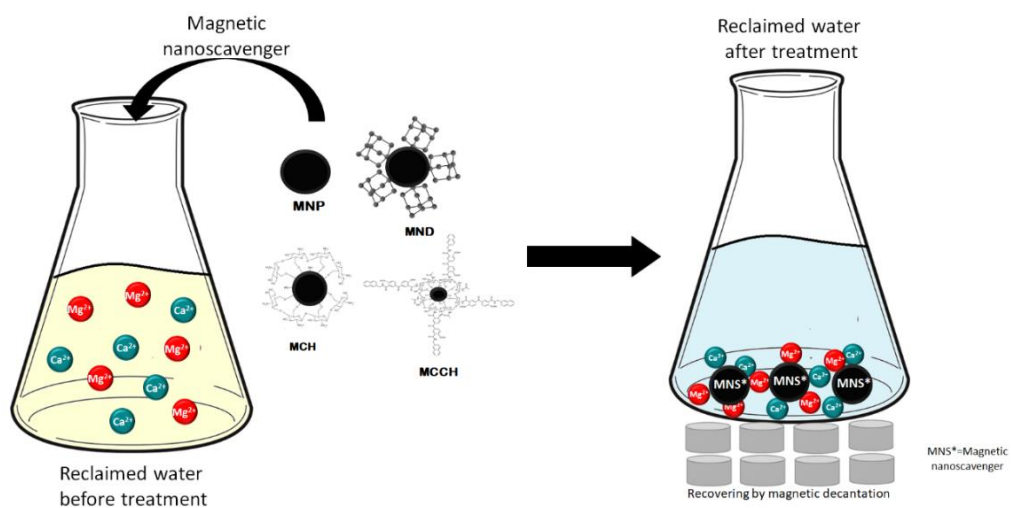


Figure 1.13 Working principle of the magnetic nanoscavengers.

1.6 Conclusions

Co-precipitation synthesis showed to be a very practical, simple, convenient, and fast methodology to synthesize magnetic nanoparticles. It does not present any problem with the reaction escalation.

It is important to point out that the co-precipitation synthesis is a good and greener technique not only to produce raw magnetic nanoparticles, but to modify and functionalize them adding just one more step to the synthesis route, where functionalized magnetite nanoparticles can be produced under mild conditions.

This technique allowed to obtain magnetic nanoparticles that show their response to a magnetic field and they do not present magnetic remanence after the magnet switch-off, pointing to a superparamagnetic property of the materials.

In the next chapter the physicochemical characterization of functionalized magnetites will be presented.

1.7 References

- (1) Vilarinho, P. *Scanning Probe Microscopy: Characterization, Nanofabrication and Device Application of Functional Materials*; Springer Science & Business Media, Algarve, Portugal, 2005; pp 3–33.
- (2) Xue, X.; Wang, F.; Liu, X. Emerging Functional Nanomaterials for Therapeutics. *J. Mater. Chem.* **2011**, *21*, 13107–13127.
- (3) Kumar, N.; Sinha Ray, S. *Synthesis and Functionalization of Nanomaterials: Introduction*. Springer Nature, Switzerland; 2018; pp 15–55.
- (4) Chavali, M. S.; Nikolova, M. P. Metal Oxide Nanoparticles and Their Applications in Nanotechnology. *SN Appl. Sci.* **2019**, *1*, 607.
- (5) Namdeo, M. Magnetite Nanoparticles as Effective Adsorbent for Water Purification-A Review. *Adv Recycl. Waste Manag.* **2017**, *2*, 135–147.
- (6) Mohammed, L.; Gomaa, H. G.; Ragab, D.; Zhu, J. Magnetic Nanoparticles for Environmental and Biomedical Applications: A Review. *Particuology* **2017**, *30*, 1–14.
- (7) Lu, A.; Salabas, E. L.; Schüth, F. Magnetic Nanoparticles: Synthesis, Protection, Functionalization, and Application. *Angew. Chemie Int. Ed.* **2007**, *46*, 1222–1244.
- (8) Ali, A.; Zafar, H.; Zia, M.; Ul Haq, I.; Phull, A. R.; Ali, J. S.; Hussain, A. Synthesis, Characterization, Applications, and Challenges of Iron Oxide Nanoparticles. *Nanotechnol. Sci. Appl.* **2016**, *9*, 49–67.
- (9) Schwaminger, S. P.; Bauer, D.; Fraga-García, P.; Wagner, F. E.; Berensmeier, S. Oxidation of Magnetite Nanoparticles: Impact on Surface and Crystal Properties. *Cryst. Eng. Comm.* **2017**, *19*, 246–255.
- (10) Laurent, S.; Forge, D.; Port, M.; Roch, A.; Robic, C.; Vander Elst, L.; Muller, R. Magnetic Iron Oxide Nanoparticles: Synthesis, Stabilization, Vectorization, Physicochemical Characterizations, and Biological Applications. *Chem. Rev.* **2008**, *110*, 2064–2110

-
- (11) Li, B.; Lavernia, E. *Pergamon Materials Series*; Elsevier Ltd, Kidlington, Oxford, 2001; Vol. 5, pp 253–304.
- (12) Kumar, A. Functional Nanomaterials: From Basic Science to Emerging Applications. *Solid State Phenom.* **2013**, *201*, 1–19.
- (13) Yin, Y.; Talapin, D. The Chemistry of Functional Nanomaterials. *Chem. Soc. Rev.* **2013**, *42*, 2484–2487.
- (14) Madamsetty, V. S.; Paul, M. K.; Mukherjee, A.; Mukherjee, S. Functionalization of Nanomaterials and Their Application in Melanoma Cancer Theranostics. *ACS Biomater. Sci. Eng.* **2020**, *6*, 167–181.
- (15) Hurts, M. N.; DeLong, R. K. Spectral Signature Analysis of Surface Functionalized Nanoparticles. *Molecular devices.* **2016**, 1–5.
- (16) Kudr, J.; Haddad, Y.; Richtera, L.; Heger, Z.; Cernak, M.; Adam, V.; Zitka, O. Magnetic Nanoparticles: From Design and Synthesis to Real World Applications. *Nanomaterials.* **2017**, *7*, 243
- (17) Marini, S. Magnetic Nanocomposites for Heavy Metals Removal from Stormwater, Ph.D. Thesis, Universidad de Padua, 2015, pp 21-26
- (18) The Editors of Encyclopaedia. Ferrimagnetism <https://www.britannica.com/science/ferrimagnetism> (accessed Apr 14, 2021).
- (19) Datta, P. *Woodhead Publishing Series in Biomaterials: Magnetic Gels*; Woodhead Publishing, United Kingdom, 2018; pp 441–465.
- (20) Yilmaz, E.; Ulusoy, H. İ.; Demir, Ö.; Soylak, M. A New Magnetic Nanodiamond/Graphene Oxide Hybrid (Fe₃O₄@ND@GO) Material for Pre-Concentration and Sensitive Determination of Sildenafil in Alleged Herbal Aphrodisiacs by HPLC-DAD System. *J. Chromatogr. B* **2018**, *1084*, 113–121.
- (21) Martínez-Quiroz, M.; López-Maldonado, E. A.; Ochoa-Terán, A.; Pina-Luis, G. E.; Oropeza-Guzman, M. T. Modification of Chitosan with Carbamoyl Benzoic Acids

for Testing Its Coagulant-Flocculant and Binding Capacities in Removal of Metallic Ions Typically Contained in Plating Wastewater. *Chem. Eng. J.* **2018**, *332*, 749–756.

(22) Liu, X.; Ma, Z.; Xing, J.; Liu, H. Preparation and Characterization of Amino–Silane Modified Superparamagnetic Silica Nanospheres. *J. Magn. Magn. Mater.* **2004**, *270*, 1–6.



Chapter II

Characterization of magnetic nanoparticles

2.1 Introduction

Characterization of materials is an important step in nanomaterials development, since it is used to determine the composition of the material, ensure the size, and verify the modification of the materials.¹ Each technique has its own requirements about types of samples able to be characterized, sample preparation, and limit of sensitivity in relation to the parameter that has to be determined.²

To characterize a functional material it is important to select the proper techniques, considering its potential uses and stability. Therefore, the correct characterization of magnetic nanomaterials (such as the previous one synthesized in this work) and the study of the influence of the chemical composition and the morphology on the magnetic properties are particularly important.

At this point it is imperative to remark that depending on the manner to characterize a nanomaterial is reaching a good nanoparticles dispersion. On the analytical method the sample must be conditioned. For example for TGA, VSM and FT-IR, magnetite nanoparticles (raw and functionalized) will be used in their powder presentation; and for TEM, DLS and ζ -potential the magnetic nanoparticles must be dispersed. In both cases the results must match with the expectations depending on the known properties (nanosized and magnetism) and the obtained results.

In this chapter we look closely at the most common characterization techniques for both magnetic nanoparticles and functionalized magnetic nanoparticles, and how all these techniques will provide us with the necessary information to inquire about the intrinsic and extrinsic properties of the synthesized materials. We also include the principle of each technique on the annexes (search by section number in annex).

2.2 Justification and objectives

2.2.1 Justification

In order to apply a functional material, it is necessary to know its intrinsic and extrinsic properties. Such properties are known through characterization techniques.

Since there is a wide variety of techniques, it is important to know the parameters that we want to study (such as size, shape, charge, magnetism, etc.) in order to have results that can confirm or deny the assumptions made about the material.

In the present work, it is essential to know the surface functionality of the synthesized materials, for which a variety of techniques have been chosen to help elucidate adsorption and recovery properties (by magnetic means) for further applications. Much attention is required to the sample preparation for each characterization technique, to ensure the quality of the results.

2.2.2 General objective

Characterize the previously synthesized magnetic nanoparticles and their modifications by techniques as:

- ❖ Transmission Electron Microscopy (TEM)
- ❖ Energy dispersive X-ray analysis (EDX)
- ❖ Fourier transform infrared (FT-IR)
- ❖ Thermogravimetric analysis (TGA)
- ❖ BET surface area analysis
- ❖ Vibrating sample magnetometry (VSM)
- ❖ Dynamic light scattering (DLS)
- ❖ Zeta potential (ζ -potential)

2.3 Background

2.3.1 Characterization of nanomaterials

In material science, the term “characterization” refers to the general and broad processes through which the properties and structure of the material are explored. This fundamental process is a must for scientific understanding of the material.¹

Characterization involves techniques required to explore material properties and microscopic structures, that is, any process that deals with material analysis such as mechanical testing, thermal analysis, and density calculation. Newer and advanced techniques are constantly emerging, joining characterization techniques that have been practiced for centuries. Characterization helps to determine the composition and structure of materials, and also allows us to assess whether the method was successful or not. Some techniques are qualitative, whereas some are quantitative.¹



Figure 2.1 Scheme of typical characterization techniques used with nanoparticles.^{1,2}

¡Error! No se encuentra el origen de la referencia. groups some of the main characterization techniques used with nanoparticles in connection to a range of possible features that needed to be studied. Special attention is needed, since the classification given may be misleading itself because most of the time a characterization method can provide more than one piece of information simultaneously.²

In particular, superparamagnetic nanomaterials are used in different areas such as ferrofluids, magnetically controlled drug carriers, magnetic resonance imaging and magnetic heterogeneous catalyst recovery. For this reason, the magnetic characterization of these new nanomaterials and the study of the influence of the chemical composition and the morphology on the magnetic properties are particularly important. Specifically, it is necessary the characterization of the dimensionality of these materials, the resulting magnetic properties, surface functionality, and other specific characterization techniques.^{3,4}

¡Error! No se encuentra el origen de la referencia. shows which parameter can be determined with a given technique. Each technique has its own requirements about types of samples able to be characterized, sample preparation procedures, and typical limit of sensitivity in relation to the parameter that has to be determined.

Table 2.1 Parameters and physicochemical characterization techniques.

| Entity characterized | Characterization techniques suitable |
|---|---|
| Size (structural properties) | TEM, XRD, DLS, NTA, SAXS, HRTEM, SEM, AFM, EXAFS, FMR, DCS, ICP-MS, UV-Vis, MALDI, NMR, TRPS, EPLS, magnetic susceptibility |
| Shape | TEM, HRTEM, AFM, EPLS, FMR, 3D-tomography |
| Elemental-chemical composition | XRD, XPS, ICP-MS, ICP-OES, SEM-EDX, NMR, MFM, LEIS |
| Crystal structure | XRD, EXAFS, HRTEM, electron diffraction, STEM |
| Size distribution | DCS, DLS, SAXS, NTA, ICP-MS, FMR, superparamagnetic relaxometry, DTA, TRPS, SEM |
| Chemical state-oxidation state | XAS, EELS, XPS, Mossbauer |
| Growth kinetics | SAXS, NMR, TEM, Cryo-TEM, Liquid-TEM |
| Ligands binding/composition/density/ arrangement/ mass, Surface composition | XPS, FTIR, NMR, SIMS, FMR, TGA, SANS |
| Surface area, specific surface area | BET, liquid NMR |
| Surface charge | Z-potential, EPM |
| Concentration | ICP-MS, UV-Vis, RMM-MEMS, PTA, DCS, TRPS |
| Agglomeration state | Z-potential, DLS, DCS, UV-Vis, SEM, Cryo-TEM, TEM |
| Density | DCS, RMM-MEMS |
| Single particle properties | Sp-ICP-MS, MFM, HRTEM, liquid TEM |
| 3D visualization | 3D-tomography, AFM, SEM |
| Dispersion of NP in matrices/supports | SEM, AFM, TEM |
| Structural defects | HRTEM, EBSD |
| Detection of NPs | TEM, SEM, STEM, EBSD, magnetic susceptibility |
| Optical properties | UV-Vis-NIR, PL, EELS-STEM |
| Magnetic properties | SQUID, VSM, Mossbauer, MFM, FMR, XMCD, magnetic susceptibility |

In the following sections we will approach some of the characterization techniques involved in this work.

2.3.2 Microscopy-based techniques

Optical microscopy helps to observe materials at a micron level with reasonable resolution. Imaging techniques like AFM, SEM, FE-SEM. STEM and TEM have been technologically advanced to detect materials with nanometer size. These techniques produce a highly magnified image, although the principles of the techniques change. In particular magnetic nanoparticles (MNP) can be observed through these imaging modalities.

2.3.2.1 Transmission Electron Microscopy (TEM)

TEM is a powerful analytical tool that can give direct information about the size and shape of a nanoparticle with inorganic cores. Making use of short wavelengths, achievable by highly accelerated electrons, this technique explores the structure of an MNP on the atomic level of detail, whereas by performing image analysis on the TEM micrograph obtained it is possible to provide quantitative results of the material's size distribution.^{5,6}

TEM helps researchers to take an in-depth look into the magnetite nanoparticles, being able to report a broad of different shapes that include dots/spheres, cubes, octahedrons, and nanorods,⁷⁻⁹ some examples can be seen in Figure 2.2. Additionally, TEM provides not only direct images of the sample but the most accurate estimation of the nanoparticle homogeneity.¹⁰

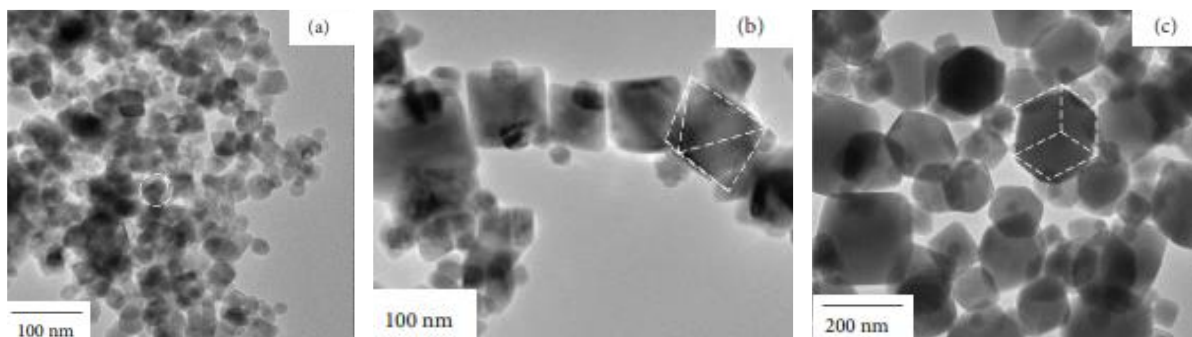


Figure 2.2. TEM micrographs of the magnetite nanoparticles.⁹

Contrary to SEM and STEM techniques a good image quality of surface-modified MNP can be obtained, allowing to elucidate the magnetite modification through a change in the particle size, either for an enlargement or shrink of its diameter (Figure 2.3).^{11,12}

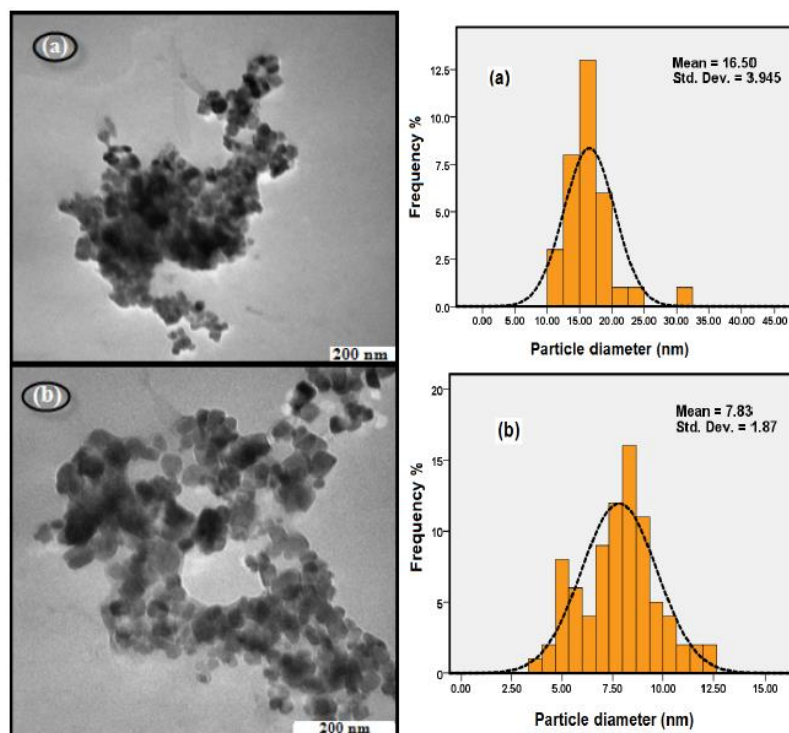


Figure 2.3. TEM images of (a) Fe₃O₄, and (b) Fe₃O₄/Oleic Acid.¹³

Since MNP tend to agglomerate due to strong magnetic dipole-dipole attractions between particles combined with van der Waals force and high surface energy,¹⁴ a good sample preparation is essential to get quality images, as will be discussed later in more detail. In the particular case of magnetite nanoparticles this means a better dispersion by sonication. Mérida *et al.* used TEM to report that their synthesized MNP were roughly spherical with diameters going from 12 to 20 nm with a few agglomerates, the authors did special emphasis that a strong sonication translated into an evident reduction in aggregates' sizes.⁵

2.3.2.2 Energy dispersive X-ray analysis (EDX)

EDX is often used together with SEM, FE-SEM, STEM and TEM. EDX can provide more information about the sample with the elemental composition analysis, allowing to corroborate that MNP has been synthesized with no impurities.¹⁵

Mohamed *et al.* obtained iron-oxide magnetic nanoparticles for protein/enzyme immobilization purposes; the authors show the EDX spectra (**¡Error! No se encuentra el origen de la referencia.**) for the MNP with no impurities. Additionally, the authors observed the changes in the elemental composition on the MNP before and after the immobilization of the enzyme and use these results to estimate the amount of enzyme immobilized on the particles.¹⁶

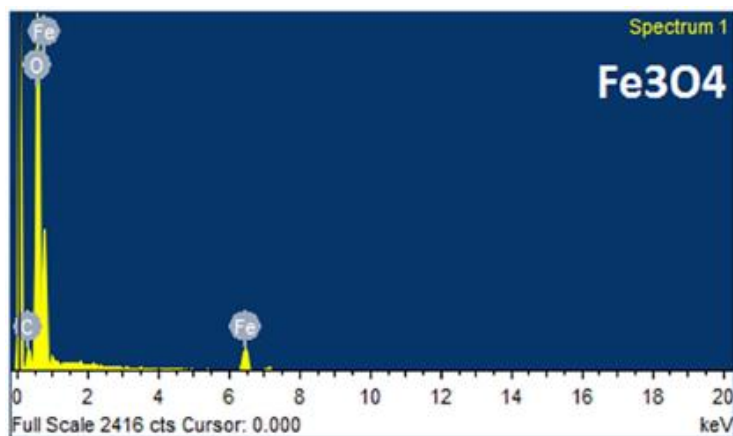


Figure 2.4 SEM–EDX spectra of Fe₃O₄ magnetic nanoparticle.¹⁶

In other study, Chen *et al.* doped magnetic nanodiamonds with Fe using ion implantation technique, where EDX was used to look at the content of various elements in the ND and search

for the new Fe signals that confirmed the implantation of this element in the formation of magnetic nanodiamond (**¡Error! No se encuentra el origen de la referencia.**)¹⁷

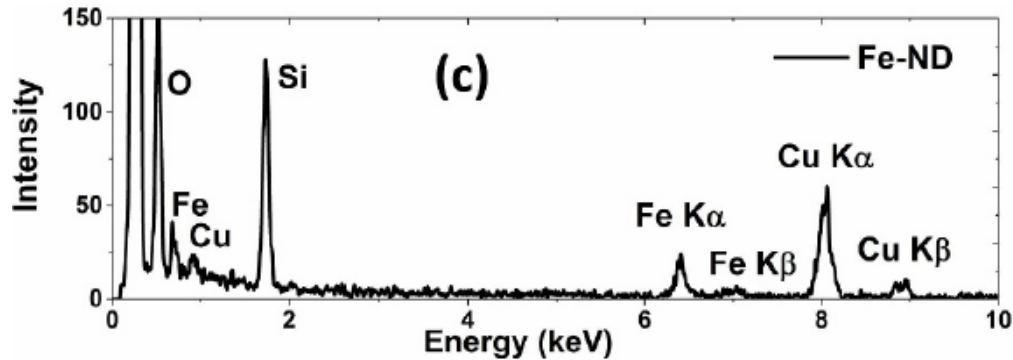


Figure 2.5 EDX spectrum of the Fe-implanted ND.¹⁷

2.3.4 Sample preparation for microscopy-based techniques (TEM and EDX)

A very important thing to have in consideration is the sample preparation. Microscopy-based techniques (SEM, STEM, EDX and TEM) analysis will only work if the samples are prepared properly. The primary concern with the samples is conductivity; for artifact-free images to be collected, the sample must be adequately conductive and grounded to the sample stub to avoid surface charging caused by the bombardment of electrons from the beam building upon the surface of the sample until discharge, making the image seem to pulse. Since metals already conduct electricity when bombarded with electrons, they do not require any preparation. However, the nonmetals need to be prepped with a sputter coater. Only a few angstroms of conductive material are required, and a carefully coated sample can still maintain its surface morphology, but care should be taken to be selective in the choice of conductive coating if elemental analysis is required.^{1,15}

Removal of water is also important in traditional, as the water molecules will vaporize in a vacuum, creating an obstacle for the electron beams and obscuring the clarity of the image. Newer SEMS no longer require a full vacuum to operate. These devices produce lower resolution images, but they open up the possibility of examining a whole range of previously unexaminable samples that are vital for industries and other disciplines.¹

2.3.3 Spectroscopy-based characterization techniques

Spectroscopy-based techniques help toward the determination of the structure, the composition, the size and other basic features of the NPs.

2.3.3.1 Fourier transform infrared spectroscopy (FT-IR)

FT-IR analysis is used for the identification of a broad range of organic, inorganic, and polymeric materials utilizing infrared light for scanning the samples.^{1,10} FT-IR is a fast, simple and reliable technique. FT-IR is very useful to characterize magnetite since a typical band below 700 cm^{-1} is easily recognizable due to the stretching vibration of the Fe-O bonds, characteristic of magnetite.¹²

Additionally to raw magnetite characterization, FT-IR is useful to a fast detection of the surface modification of the MNP (functionalization) with the appearance of new bands and change in the intensity of the same, these changes can suggest the cross-linking of the magnetite with other species.

Shalaby *et al.* synthesized iron-oxide nanoparticles for hyperthermia applications by co-precipitation method, they obtained the FT-IR spectrum for this material (**¡Error! No se encuentra el origen de la referencia.**), where the typical bands for MNP are observed, special attention was placed for the band at low wavenumbers ($\leq 700\text{ cm}^{-1}$) due to the vibrations of the Fe-O bond.¹⁸ A similar spectrum is reported by Amritphale *et al.*¹⁹

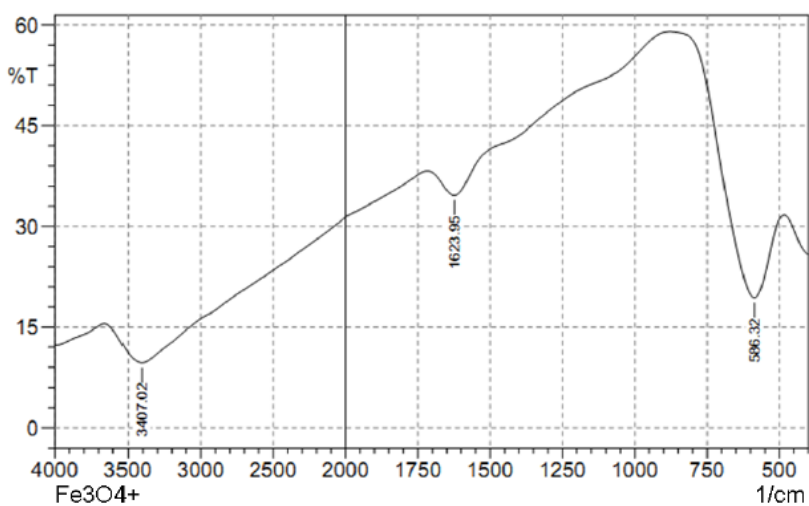


Figure 2.6 Spectra FT-IR of iron oxide magnetic nanoparticles.¹⁸

Other authors functionalize MNP with different organic molecules and they used FT-IR, among other techniques, to infer the correct functionalization for the nanoparticles. For example, Jun et al. synthesized silica-coated MNP and Amaro-Reyes et al. synthesized MNP coated with chitosan, and they confirmed the modification of the magnetite nanoparticles with the apparition of new bands (from the modifying molecules) on the FT-IR spectrums.^{12,20}

2.3.4 Other characterization techniques

2.3.4.1 Thermogravimetric analysis (TGA)

Thermogravimetric analysis (TGA) measures changes in physical properties and chemical properties by increasing temperature as a function of time. TGA can also determine either mass loss or gain due to decomposition or oxidation and it is possible to evaluate the thermal stability of a material.^{21,22}

The TGA is a simple and direct technique, and no special treatment is need for sample preparation, apart from having the sample in dry state and only a few milligrams of the nanomaterial sample are required. When having a modified nanoparticle, FT-IR offers information about the interaction and conformation between a NP and the stabilizer type but does not give insights on the extent of surface coverage or the mass-to-mass ratio of NP to stabilizer.¹⁰

A typical thermogram of raw MNP does not show any endothermic and exothermic peaks, and it has a very stable behavior since low weight loss is obtained.²³ Authors report weight loss going from 10 to 5% or less for uncoated Fe₃O₄.^{24,25} When the first weight loss is due to residual water and other contaminants, as well as for physically adsorbed molecules.²⁵ Then, the second weight loss is due to the elimination of organic matter, which can come from both the solvents used and the secondary reaction products.²⁴

When magnetite is coated a variation on the % of weight loss and the regions where these losses occur are going to be different from the raw materials used to synthesize the new materials. MNP coated organic molecules will show a slight difference in the weight loss but are easily attributed to the surface modification on the magnetic material.²³ Danafar *et al.* and Lesiak *et al.* functionalized magnetite with natural and biocompatible molecules, and they found

out that those new materials presented different weight losses, attributed them to the surface modification of the magnetite (**Error! No se encuentra el origen de la referencia.**a and b).^{23,25}

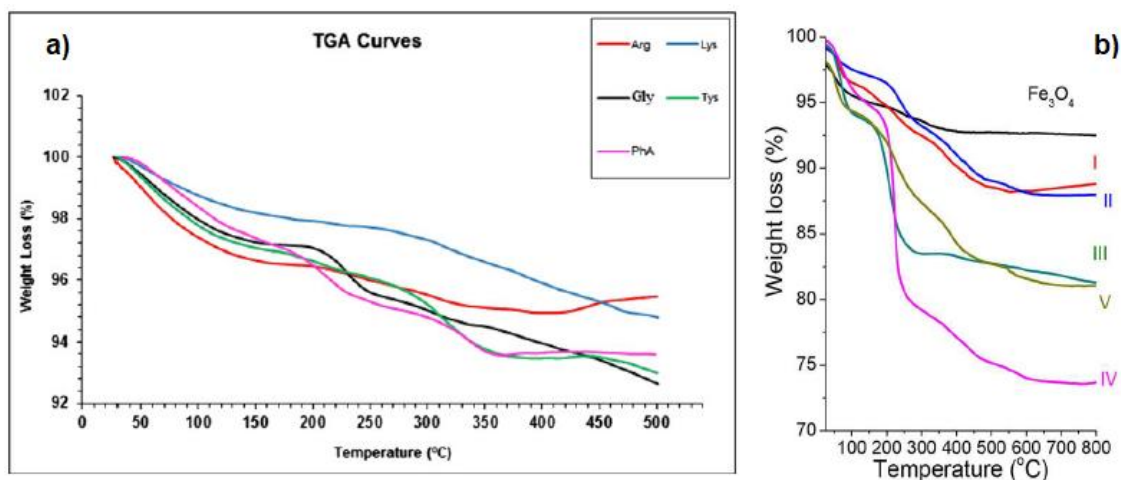


Figure 2.7 a) TGA curves of MNP coated with L-tyrosine (Tys), L-phenylalanine (PhA), L-arginine (Arg), glycine (Gly) and L-lysine (Lys).²³ b) TGA of MNP and MNP functionalized with oxalic, succinic, glutamic acids, and L-arginine.²⁵

2.3.4.2 Dynamic light scattering (DLS)

DLS is a widely employed technique to find the size of NPs in colloidal suspensions in the nano- and sub-micrometer ranges. DLS is noninvasive, and thus the sample can be reused for other purposes after the analysis. In addition, no specific modification is needed (except dilution), and a small sample volume (1–1.5 mL) is sufficient for the analysis.²⁶

When performing DLS it is important to take in consideration the concentration of the solution. Lim *et al* performed a complete study of magnetic nanoparticles and their behavior in DLS varying the concentration of the analyzed solution. The authors found out that MNPs show strong concentration dependency as their hydrodynamic diameter increases with the concentration increment (**Error! No se encuentra el origen de la referencia.**).⁶

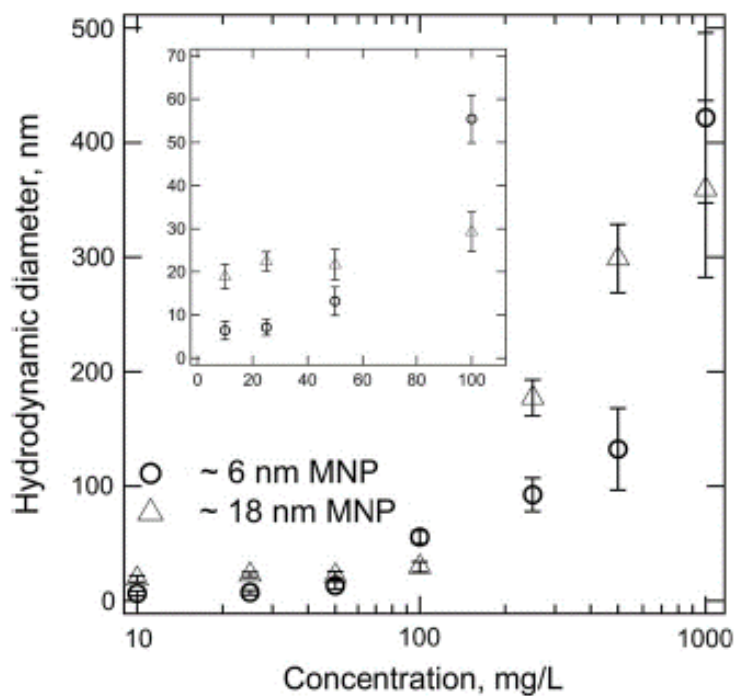


Figure 2.8 Particle concentration effects on the measurement of hydrodynamic diameter by DLS.⁶

As mentioned in the last chapter, MNP are generally coated to reduce aggregation effects, but usually this coating results in an increase of the particle size in suspension.²⁷ Zavisova et al. studied the variation on the DLS sizes of iron oxide nanoparticles with different modifications finding that raw magnetite have the smaller size in suspension, while for most of the modification showed bigger sizes when coated with organic molecules.²⁷

In other work, Gu *et al* also studied different functionalized MNP by DLS where they found particles with kind of irregular agglomerates and had three size distributions (**¡Error! No se encuentra el origen de la referencia.**). They attributed the larger hydrodynamic size of magnetic nanoparticles to the coating layer, hydration layer and the aggregations in water.²⁸

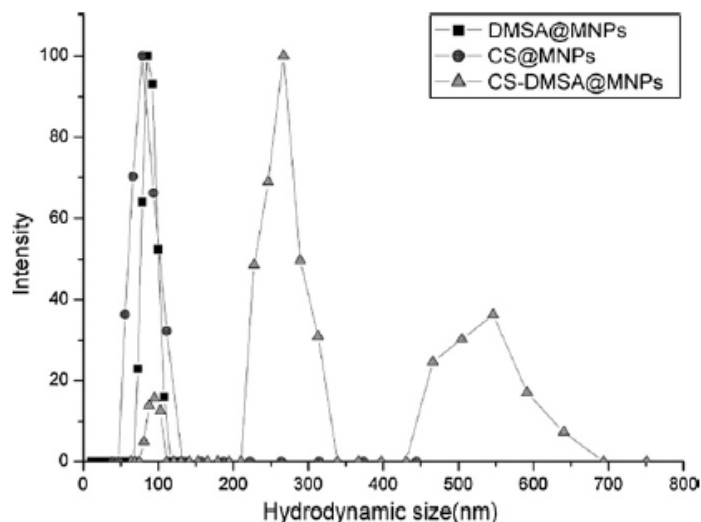


Figure 2.9 Hydrodynamic size distributions of DMSA@MNPs, CS@MNPs, CSDMSA@MNP by DLS.²⁸

2.3.4.3 Zeta Potential (ζ -potential)

Nanoparticles or colloidal particles will have a surface charge in suspension.¹ Highly positively or negatively charged particles tend to repel each other resulting in more stability and with a minor trend to agglomerate. Such highly charged particles are related to pH values which are far from the so-called ‘isoelectric point’ (IEP) of a solution, which refers to the pH value at which the zeta potential is zero. Contrarily, at low ζ -potential values in a colloidal nanoparticles dispersion causes the flocculation of the colloids and it corresponds to values closer to the IEP of the system.^{10,15}

The electrostatic interaction of the magnetite nanoparticles can be controlled by variation in their surface charges.²⁸ Magnetite, being an amphoteric solid, presents charges on the protonation or deprotonation reactions on the Fe-OH sites over the surface of the nanoparticles.²⁹ Therefore, the ζ -potentials of the iron oxides vary in range from positive to negative charges. The zeta potential of MNP shows a decreasing trend when the pH increases from 2 to 6-7, while IEP is often observed close to pH 6-7. After the IEP the charge of the MNP continues decreasing, resulting in more negative values.^{30,31} The above mentioned can be observed in ¡Error! No se encuentra el origen de la referencia..

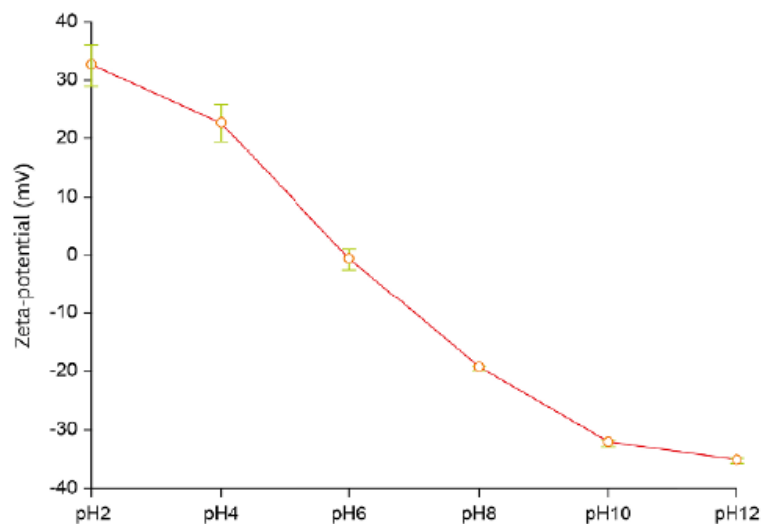


Figure 2.10 ζ -potential of iron oxide particles at different pH levels.³⁰

When magnetite is modified with a molecule, a change in the superficial charge will be observed, as well as a change in the IEP. The superficial charge of a functionalized magnetite will vary depending on the functional groups of the molecule used for the functionalization.²⁸

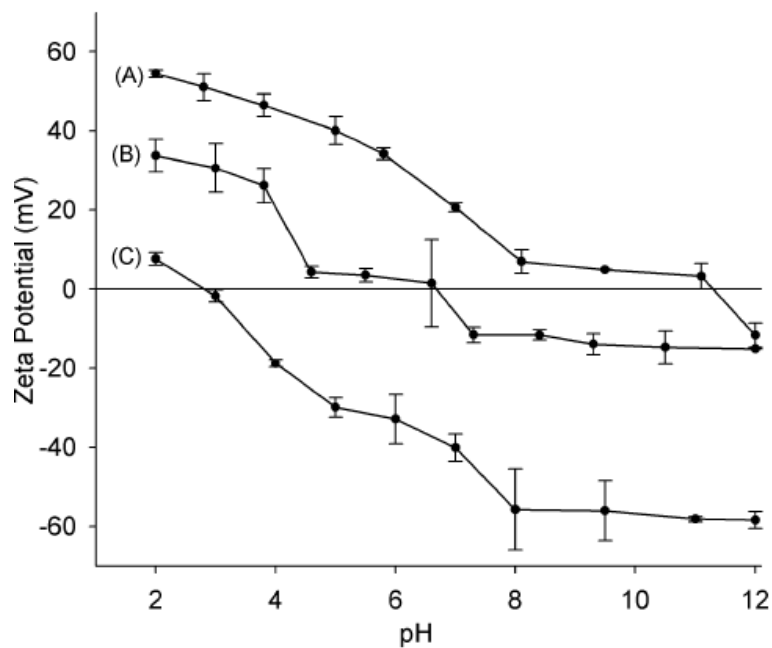


Figure 2.11 ζ -potential measurements of (A) Fe_3O_4 -CS, (B) Fe_3O_4 -CSO, and (C) Fe_3O_4 -silaneCOOH nanoparticles.³²

Rinaldi et al functionalized magnetite using chitosan (CS), oligosaccharide chitosan (OCS), and silane-carboxylic groups (silane-COOH), to study their stability in aqueous media

and biological buffers for potential biomedical applications. The authors performed ζ -potential measurements to evaluate the behavior of the nanoparticles and their dependence on the pHs (**¡Error! No se encuentra el origen de la referencia.**). Each magnetic material showed a different charge at every pH; hence each material had a different IEP. With this, the authors were able to propose a colloidal stability mechanism for each magnetic nanoparticle (electrostatic or steric repulsions).³²

2.3.4.4 Brunauer-Emmett-Teller (BET) surface area analysis of nanoparticles

Besides optical and spectroscopic techniques, structural and textural properties are important parameters to study, especially when iron oxides are used as catalysts. The specific surface area, pore size, and shape are classified as textural properties and are highly dependent on its particle characteristics. Brunauer-Emmett-Teller (BET) method is commonly used to obtain the specific surface area of a solid.³³

According to literature, the values of surface area and porosity are dependent on synthesis methods. Using co-precipitation, microwave and microlesion synthesis method, magnetite nanoparticles usually present areas from 85 to 120 m²/g.³⁴⁻³⁶

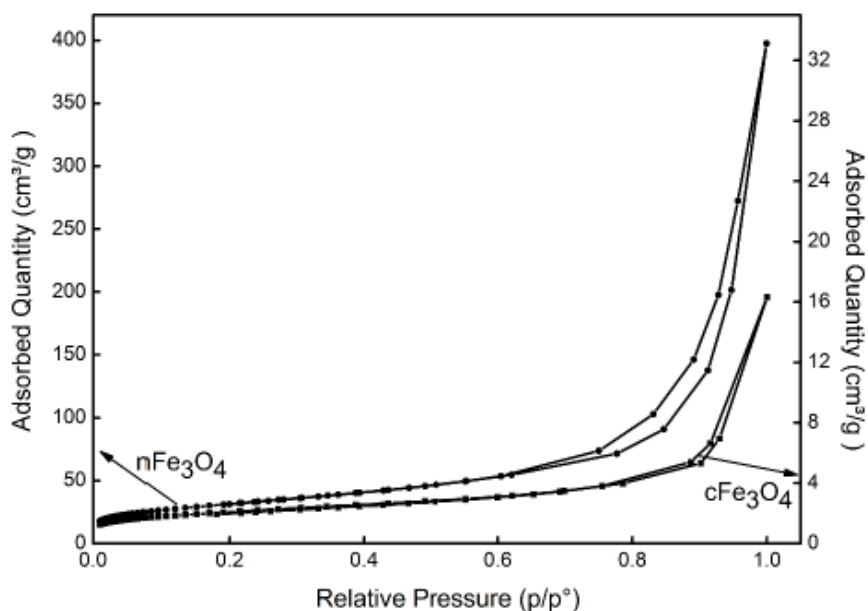


Figure 2.12 Nitrogen sorption/desorption isotherm of cFe₃O₄ (commercial) and nFe₃O₄ (synthesized) magnetite samples.³⁷

Motelica-Heino *et al* compared commercial magnetite versus synthesized magnetite (by co-precipitation) and studied their intrinsic properties for possible environmental applications as adsorbents. The authors compared both magnetites resulting that synthesized magnetite displayed a wide specific surface area of 100 m²/g and with sizes close to 10 nm, smaller than the commercial ones with sizes near to 80 nm showing a BET surface area of 100 m²/g. Both isotherms are displayed on **¡Error! No se encuentra el origen de la referencia.** where it can be seen a type IV isotherm behavior for both MNP, agreeing with the work of Sharma *et al* where a similar isotherm is obtained for co-precipitated magnetite. Finally, Motelica-Heino *et al.* and Sharma *et al.* conclude that MNP are good materials to remove the pollution of drinking water, and they can be successfully used as an adsorption technique for removing the pollutant species from wastewater.^{34,37}

2.3.4.5 Vibrating sample magnetometry (VSM)

VSM is used to measure the magnetic properties of materials as a function of magnetic field, temperature, and time. Since magnetite (Fe₃O₄) is the most magnetic naturally occurring mineral and is a ferrimagnetic material that can exhibit superparamagnetism at the nanoscale (with a reported upper limit for single domain), it becomes essential use VSM to characterize the material.³⁸

Magnetic behavior of ferromagnetic material is size-dependent (as mentioned in previous chapter), subsequently the superparamagnetism on the MNP is also attached to its size. In the literature we can find that the reported magnetization curves for unfunctionalized MNP, synthesized by co-precipitation, varies from 47 to 75 emu/g, where higher values correspond to smaller nanoparticle sizes.^{34,39,40}

Additionally, MNP functionalized with polymers and organic molecules tend to show smaller saturation magnetization values than unmodified ones. Despite this, it's possible to synthesize functionalized magnetite with good to great magnetic properties, as shown in the work of Fechine *et al.*, where the surface modification of MNP with biopolymers and organic molecules did not reduce the magnetization drastically (**¡Error! No se encuentra el origen de la referencia.**)⁴¹

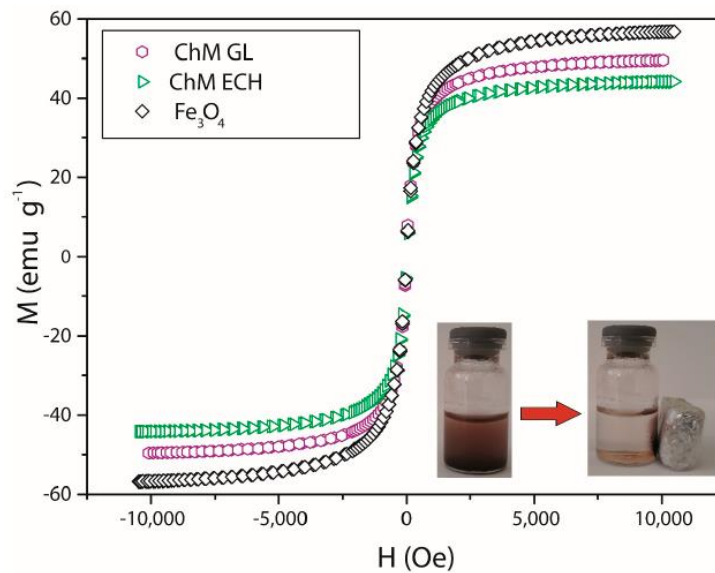


Figure 2.13 Magnetization curves normalized per gram of sample (emu/g).⁴¹

2.3.5 Hypothesis

- ❖ It will be possible to corroborate the modification of MNP with ND, CH, and CCH using techniques such: FT-IT, TGA, TEM, DLS, VSM and ζ -potential
- ❖ MNP will present strong magnetism due to their size (superparamagnetism). MND, MCH, and MCCH, will lower their magnetism measure but they will be superparamagnetic still.
- ❖ BET analysis, DLS and ζ -potential will provide hints about the possible application for the magnetite-base materials to trap cationic species and how is the behavior of these materials in water, for water treatment applications

2.4 Experimental and methods

2.4.1 Equipment

- ❖ Analytical balance brand OHAUS model AV264
- ❖ Shimadzu FT-IR, IRSpirit with ATR mode
- ❖ Perkin Elmer TGA 4000
- ❖ Quantachrome Instruments, model autosorb iQ operated with the software Quantachrome AsiQwin
- ❖ Scanning/transmission electron microscope, Termofisher, Talos F200X
- ❖ Dual-beam focused ion beam/field emission scanning transmission electron microscope, Tescan Lyra 3GM
- ❖ Anton Paar Litesizer 500

2.4.2 Methodology

2.4.2.1 FT-IR analysis

The MNP, MND, MCH, and MCCH were characterized in powder by Fourier transform infrared spectroscopy (FT-IR) using a Shimadzu FT-IR (IRSpirit) ATR mode, to compare the functional groups on each material and validate the correct modification of the magnetite. These same powder samples were characterized with this technique after using them to treat RW, to determine if there was a change in the spectrums.

2.4.2.2 TGA analysis

Thermogravimetric analysis (TGA) was performed for all the magnetic nanoscavengers using a Perkin Elmer equipment (TGA 4000) to examine the thermal decomposition in an inert atmosphere of argon ($10\text{ }^{\circ}\text{C min}^{-1}$). The samples were heated from a temperature of $30\text{ }^{\circ}\text{C}$ to $800\text{ }^{\circ}\text{C}$. The results were compared to evaluate the modification of the magnetic materials.

2.4.2.3 TEM images and size distribution

TEM images for MND, MCH, and MCCH were performed using a scanning/transmission electron microscope (Termofisher, Talos F200X). The micrographs were acquired with an

operating voltage of 200 kV. The size distribution was calculated using imagej to measure the particles and then the data was processed using origin 9 pro.

2.4.2.4 EDX

EDX were performed in an accelerating voltage of 13.0kV performed using a dual-beam focused ion beam/field emission scanning transmission electron microscope (Tescan Lyra 3GM).

2.4.2.5 VSM measurements

The VSM data was collected using the VSM option of the Versalab platform (Quantum Design, Inc). All measurements were performed at 300 K. The field was swept from +30 kOe to -30 kOe back to +30 kOe at a sweep rate of 35 Oe/s.

2.4.2.6 BET surface area analysis

Magnetic nanoscavengers surface areas were estimated by Brunauer-Emmett-Teller method (BET) in a Quantachrome Instruments, model autosorb iQ operated with the software Quantachrome AsiQwin.

2.4.2.7 DLS measurements

DLS was performed in an Anton Paar (Litesizer 500) to analyze the size of the nanoparticles and its dependence on the pH, on a scale from 2 to 12. The pH was adjusted with 0.1 M HCl to pH = 2 and 0.1 M NaOH to pH 12.

2.4.2.8 Zeta Potential measurements

The physicochemical performance of all nanoparticles (MNP, MND, MCH, and MCCH), was determined by Zeta Potential and pH measurements in an Anton Paar (Litesizer 500). The pH was adjusted with 0.1 M HCl and 0.1 M NaOH from pH 2 to pH 12.

2.5 Results and discussions

2.5.1 FT-IR analysis

All the nanoparticles synthesized were first characterized by FT-IR spectroscopy. The spectra obtained are shown in **¡Error! No se encuentra el origen de la referencia.** For the raw material (MNP, black line) we can observe the following characteristic signals: at 3280 cm^{-1} the stretching signal of the O-H bonds, at 1637 cm^{-1} a small signal assigned to the bending vibration of the H-O-H bonds, and the large and characteristic signal around 578 cm^{-1} is related to the stretching of Fe-O bonds in Fe_3O_4 , which indicates the correct synthesis of magnetite. As it can be seen, all the other materials have the same dominant magnetic iron-oxide base. The spectrum obtained is similar to those reported in the literature.⁴²⁻

44

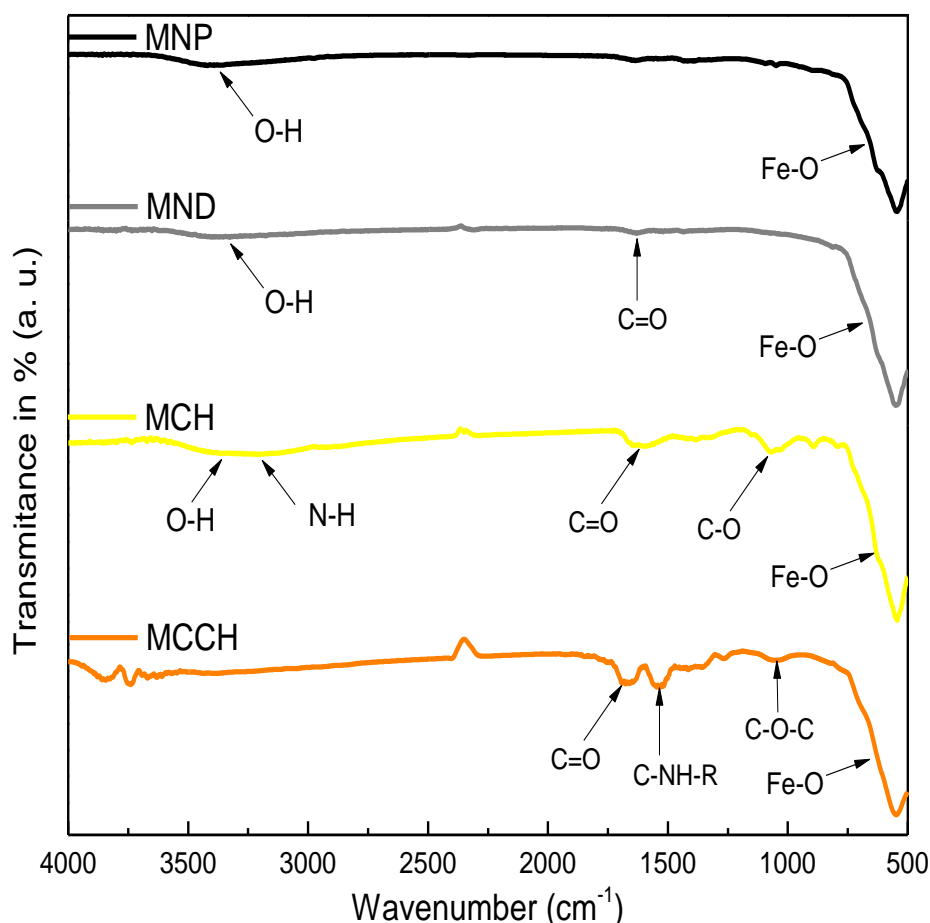


Figure 2.14. FT-IR of MNP (black line), MND (grey line), MCH (yellow line), MCCH (orange line), and their principal functional groups.

The spectrum obtained for MND (grey line) shows a signal at 3331 cm^{-1} due to the presence of hydroxyl groups (O-H) which overlap the signals of symmetric and asymmetric stretching of CH_2 and CH_3 . The absorption band at 1630 cm^{-1} corresponds to the bending vibration of the hydroxyl group (OH) related to the deformation oscillations of adsorbed water molecules, which tend to overlap with the oscillations of the carbonyl group (C=O) from the nanodiamond. At the end of the spectra, we find the characteristic peak of magnetite, the stretching signal of the Fe-O bonds for Fe_3O_4 at 539 cm^{-1} .⁴⁵⁻⁴⁸

On the MCH spectrum (yellow line), we can find the contribution of CH, showing at 3168 cm^{-1} the stretching vibration of OH that is overlapped with the stretching vibration signal of NH, at 2869 cm^{-1} it is located the stretch signal of the C-H aliphatic, close to 1650 cm^{-1} we find the stretching vibration of the carbonyl of primary amide and at 1055 cm^{-1} the stretching signal of C-O.^{42,49,50}

The spectrum for MCCH (orange line) has a band around 3416 cm^{-1} indicating the O-H stretching vibration overlapping with that of the amine (N-H) stretching vibration. At 1681 cm^{-1} the C=O signal from the benzoic acid, at 1546 cm^{-1} the secondary amide bending signal (C-NH-R). In the region close to 1255 cm^{-1} the carbonyl torsion signal is located. Then, at 1058 cm^{-1} the bending vibration C-O-C is observed. Finally, at 545 cm^{-1} , the characteristic signal of the Fe-O stretching from the magnetite is observed.⁵¹ Comparisons between raw MNP and each of the modifier FT-IRs are shown in annexes 2.8.1

2.5.2 TGA analysis

Consecutively, TGA was performed to analyze the effectiveness of surface modification and confirm the surface functionalization of the MNP with ND, CH, and CCH. The content of the surface-modified molecule was evaluated based on the weight loss ratio. As shown in **¡Error! No se encuentra el origen de la referencia.**, the mass losses until $100\text{ }^\circ\text{C}$ of MNP, MND, MCH, and MCCH were 0.36%, 1.4%, 3.4%, and 1.3%, respectively, which can be attributed to the water content in all the samples (as humidity).^{19,52} For the MNP (black line),

another loss of mass is observed (approximately 1.6% by weight) in the range of 200-350 °C, which corresponds to the elimination of organic matter probably coming from both the solvents used and the secondary reaction products.²⁴ The slight degradation of the material due to the effect of temperature indicates that it has good stability. The MND thermogram (grey line) shows a second mass loss due to the elimination of organic matter related to the remaining sp² carbon content from the ND.^{53,54} It is also notable that the MND nanoscavenger has a degradation of 13.56%, which indicates the modification of the magnetite with ND.

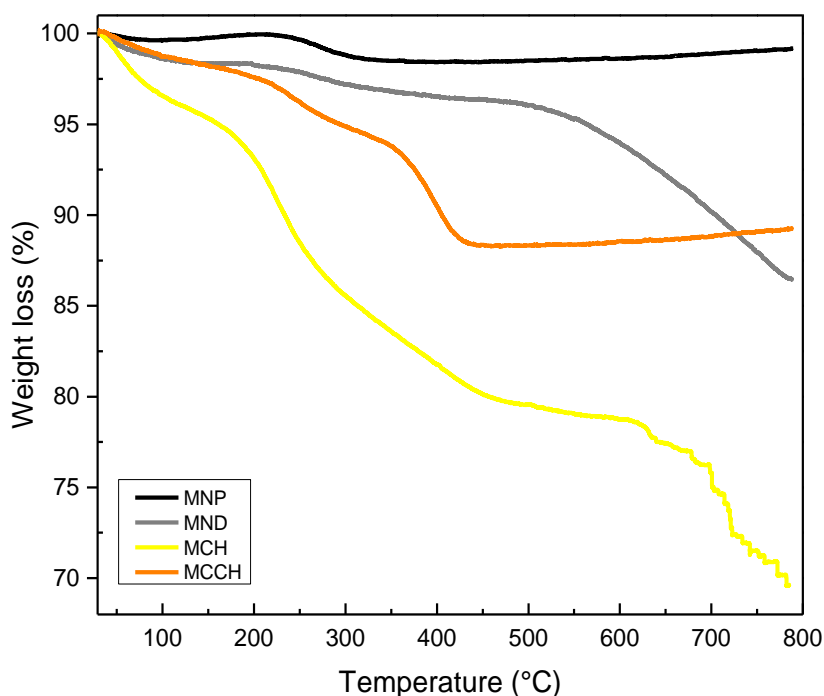


Figure 2.15. TGA of MNP (black line), MND (grey line), MCH (yellow line), MCCH (orange line).

On the MCH thermogram (yellow line), we found that in the second part of the degradation process there is a considerable weight loss of the material from 250 °C, which is caused by the elimination of H₂O, NH₃, CO, CO², and CH₃COOH, due to the pyrolytic degradation of chitosan.⁵⁵ This culminates in a total material weight loss of 30.37%, indicating an effective chemical modification of the MNP.

Finally, for MCCH (orange line) there is a second degradation stage between 200 and 350 °C due to the degradation of benzoic acid, and a third subsequent stage at 350 °C due to pyrolytic degradation due to the CH content. At the end of the degradation process, the MCCH

nanoscavenger presents a weight loss of 11.78% and greater thermal stability than MCH. It is important to mention that CCH is a grafted chitosan that has an acidic substitution that changes the surface chemical bonding capability. In other words, the surface composition of the magnetic nanoscavenger differs when CH has been previously modified with a bulky carbamoyl acid. Comparisons between raw MNP and each of the modifier TGAs are shown in annexes 2.8.2

2.5.3 TEM characterization

The obtained iron-oxide magnetic nanoparticles (MNP) and its modifications, magnetic chitosan (MCH) and magnetic carbamoyl-chitosan (MCCH), were characterized by TEM to prove the nanometric scale and morphology type of the materials. In Figure 2.16a, b, c and d are presented the TEM micrographs for MNP, MCH and MCCH, respectively, along with their sizes distributions (Figure 2.16e, f, g, and h). These images evidence the nanometric dimension of the magnetite particles where the MNP exhibit larger sizes with 15.7 nm followed by MND and MCCH with 13 and 12.4 nm, respectively. MCH are the smaller particles with 10.4 nm. These results prove that the surface modification of the raw material improves their dispersibility resulting in a lower agglomeration and size of the materials. The sizes of the materials and the surface modification of the materials are correlated to their intrinsic magnetism as will be detailed later.

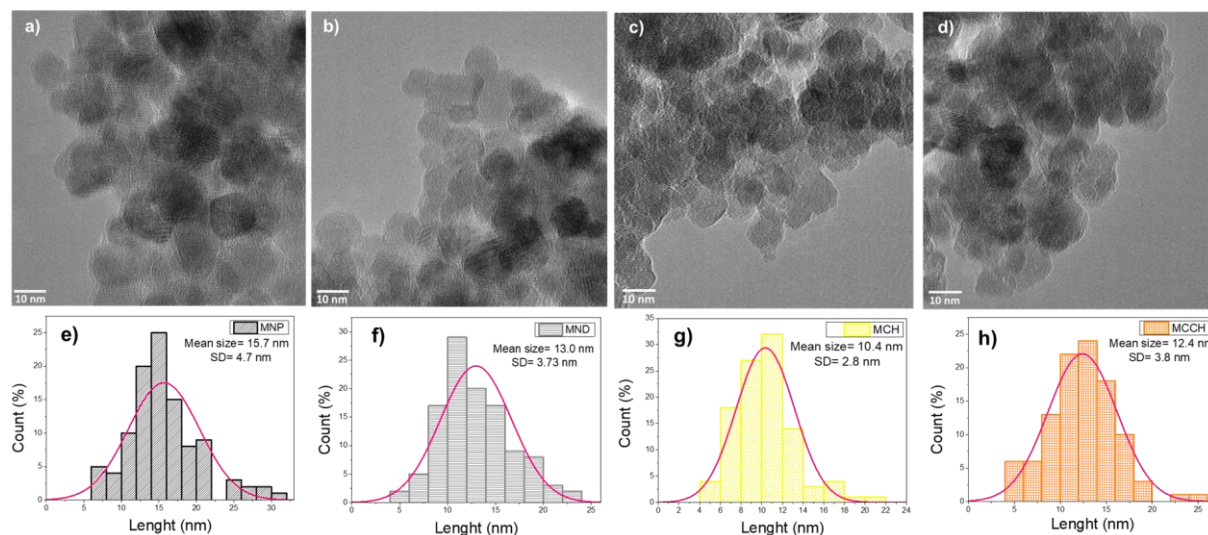


Figure 2.16. TEM micrographs of a) MNP, b) MND, c)MCH, and d) MCCH. Size distribution of e) MNP, f) MND, g) MCH, and h) MCCH.

2.5.4 EDX characterization

A mapping of each material was carried out using EDX obtained from SEM/TEM images (see annex 2.8.3A), it was found that all materials are mainly composed of Iron and Oxygen, the main ingredients of magnetite. In **¡Error! No se encuentra el origen de la referencia.** we can see the EDX bands for each synthesized material. The C signal appearing on the MNP spectra is a contribution due to the cell where the sample was mounted (carbon cell). With these results we can ensure the quality of the synthesis of the magnetic material, since they are not contaminated with any other element. The tables of each material with their elements and % in weight and % in atomic weight can be found in the annex 2.8.3B

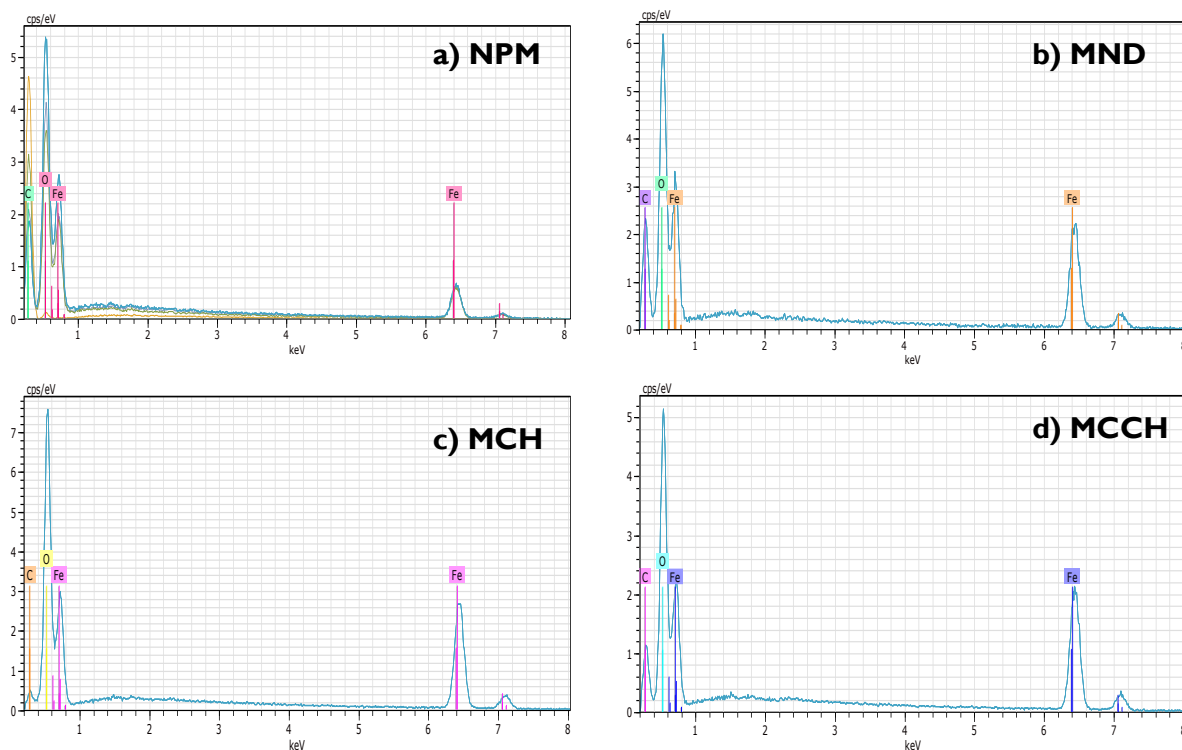


Figure 2.17. EDX spectra for MNP, MND, MCH, and MCCH.

2.5.5 VSM measurements

The magnetic response of the synthesized materials was evaluated using VSM measurements. As can be seen in **¡Error! No se encuentra el origen de la referencia.** the coercivity of all the nanoparticles synthesized is equal to zero, they do not exhibit a hysteresis

loop, meaning that they are superparamagnetic, as expected. Therefore nanoparticles are stable, they do not aggregate, and they maintain their properties over time.

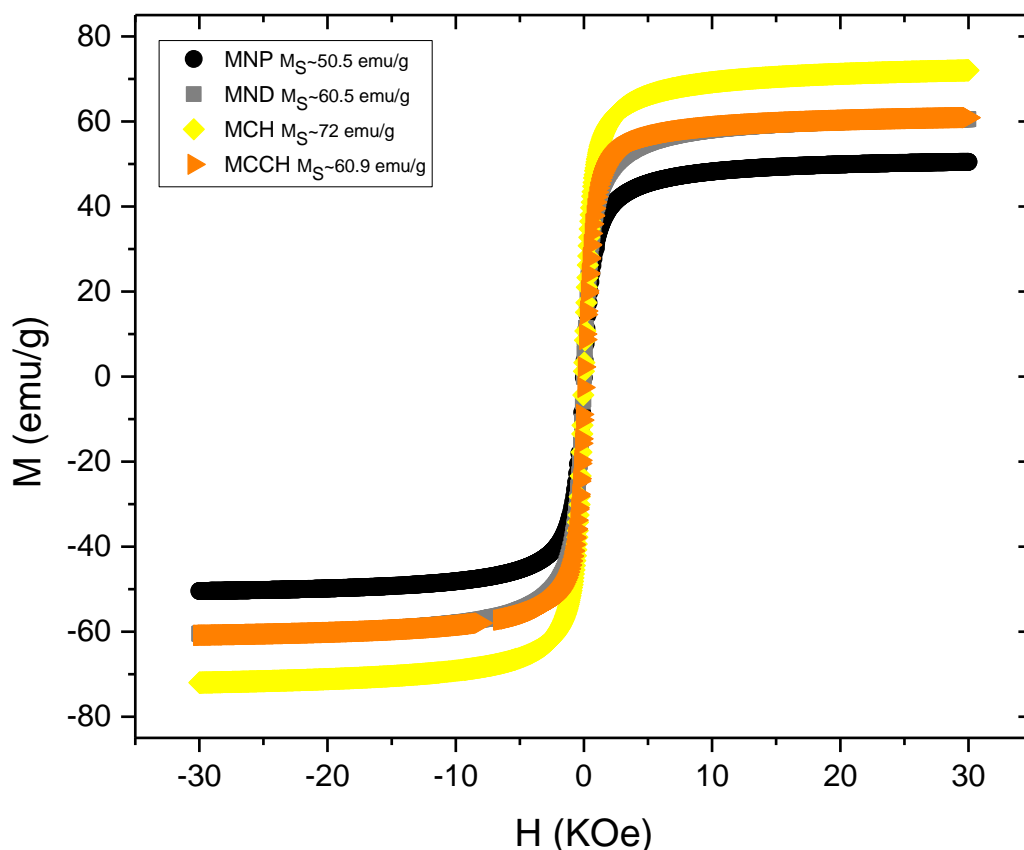


Figure 2.18. Magnetization curves of MNP (black), MND (gray), MCH (yellow), and MCCH (orange).

According to literature, the saturation magnetization (M_S) of bulk magnetite and maghemite are higher than those of the nanoparticles, which means that the nanoparticles are less magnetic than the bulk material, but unlike them the nanoparticles have superparamagnetism and zero magnetization remanence.⁵⁶

MNP present the lower M_S of 50.5 emu/g due to a possible surface oxidation since the material was stored at normal atmosphere. It has been found out that exist a decrease of the M_S and attributed to an increase of the oxide layer on the surfaces leading to a diminishing of the magnetic core. This is oxidation over time is avoided when magnetite is functionalized, since surface modification of magnetite not only avoids aggregation but also the oxidation of magnetite nanoparticles, therefore both modified magnetites (MND, MCH and MCCH) possess

a higher M_s ⁵⁷. MCH have a greater magnetization (72 emu/g) than MND and MCCH (60.9 emu/g) since the magnetic behavior of ferromagnetic materials is size-dependent⁵⁸, and as seen on the TEM micrographs, MCCH has a bigger size than MCH.

Bulk magnetite has a M_s of 100 emu/g and bulk maghemite 80 emu/g or synthesized raw MNP have almost 51% and 63% of magnetism than magnetite and maghemite in bulk, respectively. But the surface modification of the MNP improved their stabilization and magnetism by ~11% ND and CCH, and by 22% using CH, compared only with bulk magnetite.

The above mentioned is evidence of the physicochemical effect of MNP modification where the addition of different molecules to the magnetite structure can provide some stabilizing effects with a better space distribution, leading to an increase of magnetization. In the particular case of MCH and MCCH, both coatings improve the magnetism on the magnetite but a smaller increase on its observed for MCCH due to the size of the coating molecule (CH modified with a carbamoyl benzoic acid).

Additionally, it is known that as the particle size decreases a large percentage of all the atoms in a nanoparticle become surface atoms, which implies that surface and interface effects are more important. Owing to this large surface atoms/bulk atoms ratio, the surface spins make an important contribution to magnetization.⁵⁹

2.5.6 BET surface area measurements

The isotherm of adsorption and desorption of nitrogen for each material is shown in **¡Error! No se encuentra el origen de la referencia..** All the isotherms of these materials are classified as type IV where the initial behavior consists of the formation of a monolayer, followed by a multilayer formation behavior until reaching a maximum “multilayer thickness” at a maximum pressure P_o , with their distinctive hysteresis loops. The hysteresis loop is characteristic of mesoporous solids which is due to the filling process of the mesopores and is governed by the phenomenon of capillary condensation and by the percolative properties of the solid.⁶⁰ Additionally, it is observed that the hysteresis between adsorption and desorption are in a range of 0.7, 0.6, 0.5, and 0.6, to 1 P/P_o , for MNP, MND, MCH and MCCH, respectively which is indicative of the presence of mesopores in magnetite-base nanoparticles.⁶¹

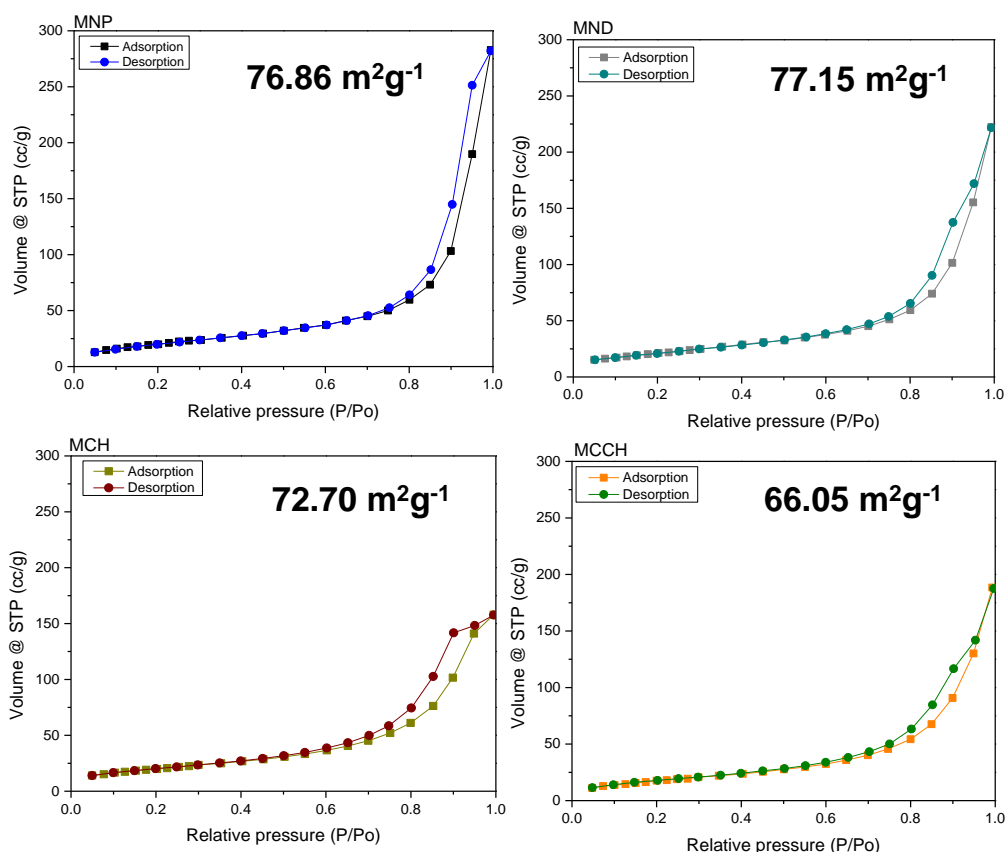


Figure 2.19. Physisorption measurements and BET area of MNP, MDN, MCH and MCCH.

A BET analysis was performed to estimate the surface area of magnetic nanoscavengers indicating that MND has the larger one ($77.15 \text{ m}^2\text{g}^{-1}$), followed by MNP ($76.86 \text{ m}^2\text{g}^{-1}$), MCH ($72.70 \text{ m}^2\text{g}^{-1}$) and MCCH ($66.05 \text{ m}^2\text{g}^{-1}$). It is meaningful to point that the smallest areas were presented for the materials with the wider hysteresis loops and the biggest areas were shown for the materials with the narrow hysteresis loops. In all cases the estimation of surface area allows classifying the magnetic nanoscavengers as materials with moderated surface area compared with common active carbon that has around $500 \text{ m}^2\text{g}^{-1}$.

Despite of the aforementioned, other authors have carried out studies on natural and synthetic magnetite samples finding that for natural samples the surface areas are ranging from 1.4 to $7.6 \text{ m}^2/\text{g}$ and for synthetic samples the surface area is $7.3 \text{ m}^2/\text{g}$ when they are slightly less than $5 \mu\text{m}$ and $39.3 \text{ m}^2/\text{g}$ when they are below 50 nm , indicating that the smaller the size of the material the greater the surface area. Furthermore, a comparison between different synthetic

magnetites showed that those with sizes from 8 to 22 nm with surface areas between 95.5 and 39.3 m²/g, respectively, showed higher adsorption capacities of 2⁺ metals such as Pb (II) and Zinc (II) ranging from 160 to 180 μmol/g.⁶² The foregoing confirms that the magnetic nanomaterials that we previously synthesized, with sizes smaller than 50 nm (as observed by TEM) will present adsorption capacities for 2⁺ metal ions such as Ca²⁺ and Mg²⁺.

2.5.7 DLS measurements

Aqueous dispersions of the different magnetic nanoparticles systems were prepared at different pH to determine its influence over the future applications of the materials on the uptake/remotion of ionic from water. **¡Error! No se encuentra el origen de la referencia.** shows the comparison of the hydrodynamic diameter and its dependence on the pH for studied magnetic nanomaterials.

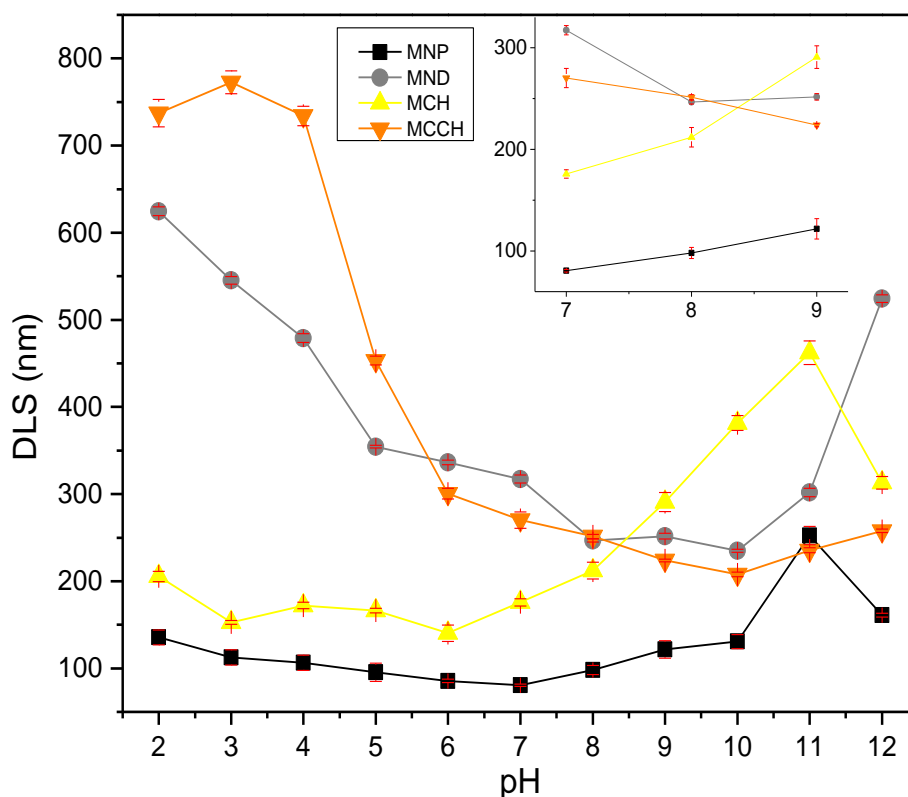


Figure 2.20. a) DLS of MNP (black line), MND (grey line), MCH (yellow line), MCCH (orange line). b) Zeta potential of MNP (black line), MND (grey line), MCH (yellow line), MCCH (orange line).

We can observe a particle size difference between DLS and STEM measurements, attributed to wet and dried particles used in each case. The hydrodynamic diameter of magnetic nanoparticles, in colloidal suspension, is commonly greater than STEM due to adsorbed water molecules on the magnetite surface.⁶³ The use of DLS to characterize magnetic nanomaterials relies on the effectiveness of the technique to monitor the colloidal stability of the particles,⁶⁴ showing the hydrodynamic size, that is, of a particle in motion, interacting with the medium.

MNP (black line) shows the lower and most stable hydrodynamic diameter, this is not affected by the pH in an interval of pH from 2 to 10, the increase in suspended particle size at pH greater than 10 is due to the aggregation of the material and suggests iron hydroxides nucleation, as previously reported.⁶⁵ Demangeat et al. argue that the particle size distribution is pH dependent since MNP are smaller than 40 nm at $3 < \text{pH} < 5$ and this value decreases after the isoelectric point (IEP).

The increase of hydrodynamic diameter in the other synthesized magnetite-based nanomaterials is another evidence of the physicochemical effect of MNP modification, as has been previously discussed.¹² MCH has a very similar particle size behavior to MNP, having a more evident size increment due to agglomeration as pH increases. On the opposite, MND and MCCH show larger sizes at lower pH values. These larger hydrodynamic diameters, especially for MCCH, are due to the rapid aggregation and subsequent chain-like gelation favored by the presence of the modified polymer (CCH).⁶⁴

2.5.8 ζ -potential measurements

Since the application of magnetic nanoscavengers will be in water conditioning, zeta potential and particle size vs. pH profiles were obtained to determine the surface charge of each material and it can be seen in **¡Error! No se encuentra el origen de la referencia..**

The discussion mentioned in the above section of hydrodynamic diameter is consistent with the zeta potential measurements since aggregation is commonly favored at pH close to the IEP. Since the IEPs for the MNP, MCH, MND, and MCCH are 5.8, 9, 3.2, and 3.5 mV, respectively, these particles exhibit their greater sizes close to those pH values due to favorable

electrostatic interactions likely formed coarse aggregates.¹² Moreover, the IEPs of four nanomaterials show an interesting pH scale of adsorbent materials.

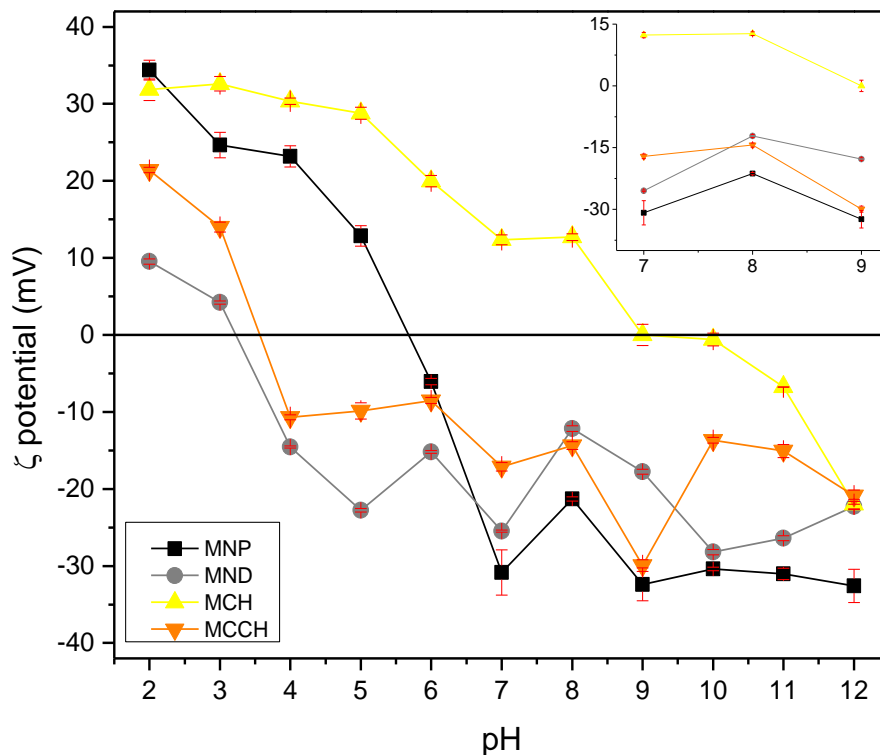


Figure 2.21. ζ -potential of MNP (black line), MND (grey line), MCH (yellow line), MCCH (orange line).

Thus, the addition of different molecules to the magnetite structure brings different stabilizing effects (electrostatic and binding forces) in which the magnetic nanoscavengers reach a colloidal stable state. When the MNP is in the presence of small molecules (as ND), the IEP shifts close to 3 mV, having consequently narrow pH-range stability. Magnetic nanoparticles modified with carboxylic acids also shifts the IEP to a more acidic value, which explains that adding a carbamoyl benzoic acid to chitosan has a significant effect of steric hindrance on dispersion stability and its IEP.⁶⁶ These results emphasize that the pH-dependent stability of magnetic nanoscavengers, and hence their hydrodynamic size, shifts in parallel with IEP in each case. At this point colloidal stability can be related to a schematic space distribution represented in Figure 1.12 from chapter I.

2.6 Conclusions

We proved that magnetite was satisfactorily modified with ND, CH and MCCH. Using FT-IR we could observe the characteristic band of the bond Fe-O of the magnetite on the raw material and all their modification and the characteristic groups from the modifiers as well. With TGA was possible to relate those groups coming from the raw material with the attributed weight loss in each modified magnetite, we also found out that raw magnetite with no modification is a pretty stable material with no great degradation due to high temperatures.

TEM images gave us a panorama of the morphology of the particles, and along with their size distribution analysis, we could infer their sizes. TEM analysis for MNP suggests sizes close to 16 nm. Additionally, TEM images allowed us to observe the deagglomeration effect caused by the modifier, finding sizes of 13, 10.4 and 12.4 nm for MND, MCH, and MCCH, respectively. It's important to point to the fact that CCH provides better stabilization and less agglomeration effect than only CH as a coating on the magnetite. BET analysis indicates that all the materials have a type IV isotherm with surface areas from 66 to ~ 77 m²/g, along with the literature we can say that our materials fit with magnetites smaller than 50 nm (as observed by TEM) and can present adsorption capacities for 2⁺ metal ions such as Ca²⁺ and Mg²⁺.

We found out that all the synthesized materials have a superparamagnetic behavior since they don't present remanence or hysteresis loop at the VSM measurements. Where the modification of the magnetite surface led to an increase of their magnetic properties due to its reduction in size. The magnetization moments observed were 50.5, 60.5, 72, and 60.9 emu/g for MNP, MND, MCH and MCCH, respectively.

DLS and ζ -potential measurements show that the materials present aggregation at pH close to the IEP, where MNP have the lower and most stable hydrodynamic diameter and the increase of hydrodynamic diameter in the other synthesized magnetite-based nanomaterials is another evidence of the physicochemical effect of MNP modification. Additionally, the IEPs of the four nanomaterials show a varied pH scale of adsorbent materials that can be convenient and suitable for water treatment applications.

2.7 References

- (1) Titus, D.; James Jebaseelan Samuel, E.; Roopan, S. M. Chapter 12 - Nanoparticle Characterization Techniques. In *Micro and Nano Technologies*; Eds.; Elsevier: Vellore, India, 2019; pp 303–319.
- (2) Imbraguglio, D.; Giovannozzi, A.; Rossi, A. Nanometrology. **2013**, *185*, 193–220.
- (3) Galletti, A.; Bertolucci, E.; Marracci, M.; Tellini, B.; Visone, C. Characterization of Magnetite Nanoparticles. In *Conference Record - IEEE Instrumentation and Measurement Technology Conference*; 2014; pp 464–467.
- (4) Sandler, S. E.; Fellows, B.; Mefford, O. T. Best Practices for Characterization of Magnetic Nanoparticles for Biomedical Applications. *Anal. Chem.* **2019**, *91*, 14159–14169
- (5) Mérida, F.; Chiu, A.; Bohórquez, A.; Maldonado-Camargo, L.; Pérez, M.-E.; Pericchi, L.; Torres-Lugo, M.; Rinaldi, C. Optimization of Synthesis and Peptization Steps to Obtain Iron Oxide Nanoparticles with High Energy Dissipation Rates. *J. Magn. Magn. Mater.* **2015**, *394*, 361–371.
- (6) Lim, J.; Yeap, S. P.; Che, H. X.; Low, S. C. Characterization of Magnetic Nanoparticle by Dynamic Light Scattering. *Nanoscale Res. Lett.* **2013**, *8*, 381.
- (7) Jana, N. R.; Chen, Y.; Peng, X. Size- and Shape-Controlled Magnetic (Cr, Mn, Fe, Co, Ni) Oxide Nanocrystals via a Simple and General Approach. *Chem. Mater.* **2004**, *16*, 3931–3935.
- (8) Lenart, V. M.; Gómez, S.; Calatayud, M. P.; Goya, G. Size and Shape Control of Magnetite Nanoparticles with a Nonselective Binding Surfactants. **2014**, *1408*, 1-2
- (9) Torres-Gómez, N.; Nava, O.; Argueta-Figueroa, L.; García-Contreras, R.; Baeza-Barrera, A.; Vilchis-Nestor, A. R. Shape Tuning of Magnetite Nanoparticles Obtained by Hydrothermal Synthesis: Effect of Temperature. *J. Nanomater.* **2019**, *2019*, 7921273.
- (10) Mourdikoudis, S.; Pallares, R.; Thanh, N. Characterization Techniques for Nanoparticles:

Comparison and Complementarity upon Studying Nanoparticle Properties. *Nanoscale* **2018**, *10*, 12871–12934.

- (11) Ardelean, I. L.; Stoencea, L. B. N.; Fikai, D.; Fikai, A.; Trusca, R.; Vasile, B. S.; Nechifor, G.; Andronescu, E. Development of Stabilized Magnetite Nanoparticles for Medical Applications. *J. Nanomater.* **2017**, *2017*, 1–9.
- (12) Díaz-Hernández, A.; Gracida, J.; García-Almendárez, B. E.; Regalado, C.; Núñez, R.; Amaro-Reyes, A. Characterization of Magnetic Nanoparticles Coated with Chitosan: A Potential Approach for Enzyme Immobilization. *J. Nanomater.* **2018**, *2018*, 1–11.
- (13) Mahdavi, M.; Ahmad, M.; Haron, M. J.; Namvar, F.; Nadi, B.; Rahman, M.; Amin, J. Synthesis, Surface Modification and Characterisation of Biocompatible Magnetic Iron Oxide Nanoparticles for Biomedical Applications. *Molecules* **2013**, *18*, 7533–7548.
- (14) Singh, D.; McMillan, J. M.; Liu, X.-M.; Vishwasrao, H. M.; Kabanov, A. V.; Sokolsky-Papkov, M.; Gendelman, H. E. Formulation Design Facilitates Magnetic Nanoparticle Delivery to Diseased Cells and Tissues. *Nanomedicine (Lond)*. **2014**, *9* (3), 469–485.
- (15) Campbell, J.; Burkitt, S.; Dong, N.; Zavaleta, C. Chapter 9 - Nanoparticle Characterization Techniques. In *Micro and Nano Technologies*; Eds.; Elsevier, 2020; pp 129–144.
- (16) Mohammed, L.; Gomaa, H. G.; Ragab, D.; Zhu, J. Magnetic Nanoparticles for Environmental and Biomedical Applications: A Review. *Particuology* **2017**, *30*, 1–14.
- (17) Chen, C.; Cho, I. C.; Jian, H.-S.; Niu, & H. Fe Doped Magnetic Nanodiamonds Made by Ion Implantation. *Nat. Publ. Gr.* **2017**.
- (18) Shalaby, T.; Yousef, Y. S.; Ahmed, M.; Badawy, H. A.; Gebreel, D. T. Magnetic Iron Oxide Nanoparticles: Preparation and Hyperthermia Applications. *Int. J. Nanoparticles* **2015**, *8*, 115–131.
- (19) Mishra, D.; Arora Soni, R.; Lahiri, S.; Amritphale, S.; Chandra, N. Synthesis and Characterization of Iron Oxide Nanoparticles by Solvothermal Method. *Prot. Met. Phys.*

Chem. Surfaces **2014**, *50*, 628–631.

- (20) Pham, X.-H.; Hahm, E.; Kim, H.-M.; Son, B. S.; Jo, A.; An, J.; An, T.; Thi, T.; Nguyen, D. Q.; Jun, B.-H. Silica-Coated Magnetic Iron Oxide Nanoparticles Grafted onto Graphene Oxide for Protein Isolation. *Nanomaterials* **2020**, *10*, 117–131.
- (21) Jalvandi, J. Novel Chemical and Physical Approaches for Sustainable Drug Release from Biodegradable Electrospun Nanofibres, 2016, pp 58–71.
- (22) Hashemifard, S. A.; Khosravi, A.; Abdollahi, F.; Alihemati, Z.; Rezaee, M. Chapter 11 - Synthetic Polymeric Membranes for Gas and Vapor Separations; Eds.; Elsevier: Bushehr, Iran, 2020; pp 217–272.
- (23) Nosrati, H.; Salehiabar, M.; Attari, E.; Davaran, S.; Danafar, H.; Manjili, H. K. Green and One-Pot Surface Coating of Iron Oxide Magnetic Nanoparticles with Natural Amino Acids and Biocompatibility Investigation. *Appl. Organomet. Chem.* **2018**, *32*, e4069–e4079.
- (24) Caamaño Chico, K. Síntesis, Caracterización y Funcionalización de Nanopartículas Magnéticas Para Detección de Patógenos. Estudio de La Funcionalización Con SiO₂ Mesoporoso., Universidade da Coruña, 2016, pp 50–68.
- (25) Lesiak, B.; Rangam, N.; Jiricek, P.; Gordeev, I.; Tóth, J.; Kövér, L.; Mohai, M.; Borowicz, P. Surface Study of Fe₃O₄ Nanoparticles Functionalized With Biocompatible Adsorbed Molecules. *Front. Chem.* **2019**, *7*, 1–16.
- (26) Leong, S. S.; Ng, W. M.; Lim, J.; Yeap, S. P. Dynamic Light Scattering: Effective Sizing Technique for Characterization of Magnetic Nanoparticles BT - Handbook of Materials Characterization; Sharma, S. K., Ed.; Springer International Publishing: Cham, 2018; pp 77–111.
- (27) Zavisova, V.; Koneracka, M.; Kovac, J.; Kubovcikova, M.; Antal, I.; Kopcansky, P.; Bednarikova, M.; Muckova, M. The Cytotoxicity of Iron Oxide Nanoparticles with Different Modifications Evaluated in Vitro. *J. Magn. Magn. Mater.* **2015**, *380*, 85–89.

-
- (28) Ge, Y.; Zhang, Y.; Xia, J.; Ma, M.; He, S.; Nie, F.; Gu, N. Effect of Surface Charge and Agglomerate Degree of Magnetic Iron Oxide Nanoparticles on KB Cellular Uptake in Vitro. *Colloids Surfaces B Biointerfaces* **2009**, *73*, 294–301.
- (29) De La Rosa, L. M. Síntesis y Funcionalización de Nanopartículas Magnéticas Para El Reconocimiento y Remoción de Especies Ambientales, Instituto tecnologico de Tijuana, 2011, pp 11–17
- (30) Meng, X.; Ryu, J.; Kim, B.; Ko, S. Application of Iron Oxide as a PH-Dependent Indicator for Improving the Nutritional Quality. *Clin Nutr Res* **2016**, *5*, 172–179.
- (31) Chang, Y.-C.; Chen, D.-H. Preparation and Adsorption Properties of Monodisperse Chitosan-Bound Fe₃O₄ Magnetic Nanoparticles for Removal of Cu(II) Ions. *J. Colloid Interface Sci.* **2005**, *283*, 446–451.
- (32) López-Cruz, A.; Barrera, C.; Calero-DdelC, V. L.; Rinaldi, C. Water Dispersible Iron Oxide Nanoparticles Coated with Covalently Linked Chitosan. *J. Mater. Chem.* **2009**, *19*, 6870–6876.
- (33) Campos, E. A.; Pinto, D. V. B. S.; Oliveira, J. I. S. de; Mattos, E. da C.; Dutra, R. de C. L. Synthesis, Characterization and Applications of Iron Oxide Nanoparticles - a Short Review . *J. Aerosp. Technol. Manag.* 2015, pp 267–276.
- (34) Srivastava, V.; Singh, P.; Weng, C.-H.; Singh, V.; Sharma, Y. C. Economically Viable Synthesis of Fe₃O₄ Nanoparticles and Their Characterization. *Polish J. Chem. Technol.* **2011**, *13*, 1–5
- (35) Ang, B. C.; Yaacob, I. I. Synthesis and Characterization of Iron Oxides Nanoparticles. *Key Eng. Mater.* **2006**, *306–308*, 1115–1120.
- (36) Acarbas, O.; Ozenbas, M. Preparation of Iron Oxide Nanoparticles by Microwave Synthesis and Their Characterization. *J. Nanosci. Nanotechnol.* **2008**, *8*, 655–659.
- (37) Iconaru, S. L.; Guégan, R.; Popa, C. L.; Motelica-Heino, M.; Ciobanu, C. S.; Predoi, D. Magnetite (Fe₃O₄) Nanoparticles as Adsorbents for As and Cu Removal. *Appl. Clay Sci.*

2016, 134, 128–135.

- (38) Savliwala, S.; Chiu-Lam, A.; Unni, M.; Rivera-Rodriguez, A.; Fuller, E.; Sen, K.; Threadcraft, M.; Rinaldi, C. Chapter 13 - Magnetic Nanoparticles. In *Micro and Nano Technologies*; Eds.; Elsevier, 2020; pp 195–221.
- (39) Mohseni-Bandpi, A.; Kakavandi, B.; Kalantary, R. R.; Azari, A.; Keramati, A. Development of a Novel Magnetite–Chitosan Composite for the Removal of Fluoride from Drinking Water: Adsorption Modeling and Optimization. *RSC Adv.* **2015**, *5*, 73279–73289.
- (40) Sundar, L. S.; Irurueta, G. O.; Venkata Ramana, E.; Singh, M. K.; Sousa, A. C. M. Thermal Conductivity and Viscosity of Hybrid Nanofluids Prepared with Magnetic Nanodiamond-Cobalt Oxide (ND-Co₃O₄) Nanocomposite. *Case Stud. Therm. Eng.* **2016**, *7*, 66–77.
- (41) Freire, T. M.; Fechine, L. M. U. D.; Queiroz, D. C.; Freire, R. M.; Denardin, J. C.; Ricardo, N. M. P. S.; Rodrigues, T. N. B.; Gondim, D. R.; Junior, I. J. S.; Fechine, P. B. A. Magnetic Porous Controlled Fe(3)O(4)-Chitosan Nanostructure: An Ecofriendly Adsorbent for Efficient Removal of Azo Dyes. *Nanomater.* **2020**, *10*, 1194–1219.
- (42) Abdelhamid, H. N.; Lin, Y. C.; Wu, H.-F. Magnetic Nanoparticle Modified Chitosan for Surface Enhanced Laser Desorption/Ionization Mass Spectrometry of Surfactants. *RSC Adv.* **2017**, *7*, 41585–41592.
- (43) Hussein-Al-Ali, S. H.; El Zowalaty, M. E.; Hussein, M. Z.; Geilich, B. M.; Webster, T. J. Synthesis, Characterization, and Antimicrobial Activity of an Ampicillin-Conjugated Magnetic Nanoantibiotic for Medical Applications. *Int. J. Nanomedicine* **2014**, *9*, 3801–3814.
- (44) Garcia Casillas, P. E.; Rodriguez, C.; Martinez Perez, C. Infrared Spectroscopy of Functionalized Magnetic Nanoparticles. In *Infrared spectroscopy-Materials Science*; Ed. BoD–Books on Demand 2012; pp 405–420.
- (45) Islam, N.; Dihingia, A.; Manna, P.; Das, T.; Kalita, J.; Dekaboruah, H. P.; Saikia, B. K.

Environmental and Toxicological Assessment of Nanodiamond-like Materials Derived from Carbonaceous Aerosols. *Sci. Total Environ.* **2019**, *679*, 209–220.

- (46) Gaur, P.; Banerjee, S. C-N Cross Coupling: Novel Approach towards Effective Aryl Secondary Amines Modification on Nanodiamond Surface. *Diam. Relat. Mater.* **2019**, *98*, 107468–107478
- (47) Gutiérrez B., J. M.; Conceição, K.; de Andrade, V. M.; Trava-Airoldi, V. J.; Capote, G. High Antibacterial Properties of DLC Film Doped with Nanodiamond. *Surf. Coatings Technol.* **2019**, *375*, 395–401.
- (48) Dolmatov, V. Y.; Kulakova, I. I.; Myllymäki, V.; Vehanen, A.; Panova, A. N.; Voznyakovskii, A. A. IR Spectra of Detonation Nanodiamonds Modified during the Synthesis. *J. Superhard Mater.* **2014**, *36*, 344–357.
- (49) Liu, X.; Hu, Q.; Fang, Z.; Zhang, X.; Zhang, B. Magnetic Chitosan Nanocomposites: A Useful Recyclable Tool for Heavy Metal Ion Removal. *Langmuir* **2008**, *25*, 3–8.
- (50) UNSOY, G.; Yalcin, S.; Khodadust, R.; Gündüz, G.; Gunduz, U. Synthesis Optimization and Characterization of Chitosan-Coated Iron Oxide Nanoparticles Produced for Biomedical Applications. *J. Nanoparticle Res.* **2012**, *14*, 1–13.
- (51) Gable, K. Carboxylic Acid Derivatives: IR Spectra <https://sites.science.oregonstate.edu/~gablek/CH336/Chapter20/Derivspeg.htm> (accessed Sep 9, 2021).
- (52) Karimzadeh, I.; Aghazadeh, M.; Doroudi, T.; Ganjali, M.; Kolivand, P. Superparamagnetic Iron Oxide (Fe₃O₄) Nanoparticles Coated with PEG/PEI for Biomedical Applications: A Facile and Scalable Preparation Route Based on the Cathodic Electrochemical Deposition (CED) Method. *Adv. Phys. Chem.* **2017**, *2017*, 1–8.
- (53) Tiainen, T.; Myllymäki, T. T. T.; Hatanpää, T.; Tenhu, H.; Hietala, S. Polyelectrolyte Stabilized Nanodiamond Dispersions. *Diam. Relat. Mater.* **2019**, *95*, 185–194.
- (54) Yang, G.; Huang, H.; Chen, J.; Gan, D.; Deng, F.; Huang, Q.; Wen, Y.; Liu, M.; Zhang,

-
- X.; Wei, Y. Preparation of Ionic Liquids Functionalized Nanodiamonds-Based Composites through the Michael Addition Reaction for Efficient Removal of Environmental Pollutants. *J. Mol. Liq.* **2019**, *296*, 111874–111882.
- (55) Corazzari, I.; Nisticò, R.; Turci, F.; Faga, M. G.; Franzoso, F.; Tabasso, S.; Magnacca, G. Advanced Physico-Chemical Characterization of Chitosan by Means of TGA Coupled on-Line with FTIR and GCMS: Thermal Degradation and Water Adsorption Capacity. *Polym. Degrad. Stab.* **2015**, *112*, 1–9.
- (56) Marini, S. Magnetic Nanocomposites for Heavy Metals Removal from Stormwater, Universidad de Padua. Italia, 2015, pp 7–26.
- (57) Dung, T. T.; Danh, T. M.; Hoa, L. T. M.; Chien, D. M.; Duc, N. H. Structural and Magnetic Properties of Starch-Coated Magnetite Nanoparticles. *J. Exp. Nanosci.* **2009**, *4*, 259–267.
- (58) Akbarzadeh, A.; Samiei, M.; Davaran, S. Magnetic Nanoparticles: Preparation, Physical Properties, and Applications in Biomedicine. *Nanoscale Res. Lett.* **2012**, *7*, 144.
- (59) Lu, A.; Salabas, E. L.; Schüth, F. Magnetic Nanoparticles: Synthesis, Protection, Functionalization, and Application. *Angew. Chemie Int. Ed.* **2007**, *46*, 1222–1244.
- (60) Rosas-García, V. M. Adsorción: isothermas de adsorción <http://lqi.tripod.com/FQAv/isoterms.htm> (accessed Dec 6, 2020).
- (61) Ma, J.; Wang, L.; Wu, Y.; Dong, X.; Ma, Q.; Qiao, C.; Zhang, Q.; Zhang, J. Facile Synthesis of Fe₃O₄ Nanoparticles with a High Specific Surface Area. *Mater. Trans.* **2014**, *55*, 1900–1902.
- (62) Salazar Camacho, C. A.; Villalobos Peñalosa, M. CHARACTERIZATION AND SURFACE REACTIVITY OF NATURAL AND SYNTHETIC MAGNETITES: II. ADSORPTION OF Pb(II) AND Zn(II). *Rev. Int. Contam. Ambient.* **2017**, *33*, 165–176.
- (63) Sagar, V.; Atluri, V. S. R.; Tomitaka, A.; Shah, P.; Nagasetti, A.; Pilakka-Kanthikeel, S.; El-Hage, N.; McGoron, A.; Takemura, Y.; Nair, M. Coupling of Transient near Infrared

Photonic with Magnetic Nanoparticle for Potential Dissipation-Free Biomedical Application in Brain. *Sci. Rep.* **2016**, *6*, 29792–29803.

- (64) Lim, J.; Yeap, S. P.; Che, H. X.; Low, S. C. Characterization of Magnetic Nanoparticles by Dynamic Light Scattering. *Nanoscale Res. Lett.* **2013**, *8*, 381–395.
- (65) Demangeat, E.; Pédrot, M.; Dia, A.; Bouhnik-le-Coz, M.; Grasset, F.; Hanna, K.; Kamagate, M.; Cabello-Hurtado, F. Colloidal and Chemical Stabilities of Iron Oxide Nanoparticles in Aqueous Solutions: The Interplay of Structural, Chemical and Environmental Drivers. *Environ. Sci. Nano* **2018**, *5*, 992–1001.
- (66) Tombácz, E.; Tóth, I. Y.; Nesztor, D.; Illés, E.; Hajdú, A.; Szekeres, M.; L.Vékás. Adsorption of Organic Acids on Magnetite Nanoparticles, PH-Dependent Colloidal Stability and Salt Tolerance. *Colloids Surfaces A Physicochem. Eng. Asp.* **2013**, *435*, 91–96.



Chapter III

Reclaimed water and its characteristics

3.1 Introduction

As the demand for water increases and the development of new sources of supply becomes more expensive, there is an increasing need to use water more than once during the hydrological cycle. Wastewater from point sources, such as sewage treatment plants, industries, and thermal power plants, can provide an excellent source of reusable water because this water is generally reliable, available, can be accessed at a single point, and has a known quality.

These sources can be reused within the same industry or for completely different purposes, helping to maintain the environmental quality upstream by reducing demand for new water sources and offering to the communities an opportunity for pollution mitigation by reducing effluent discharge to clean water sources.¹

A great challenge of our century will consist of managing the planet's water resources in a more pertinent way. Using reclaimed water will undoubtedly become common practice as freshwater sources become increasingly scarce around the world. The reuse of water through different levels of treatment will then be convenient to promote greater use of this vital resource.

Hence, treatment and reuse already play a fundamental role in the administration and management of water in all countries, especially in those with problems of scarcity or contamination such as México and USA.

The types of reclaimed water can be classified into different categories depending on their final destination, which will demand different characteristics in terms of their content and quality. Therefore, it is necessary to study each case of reclaimed water application before its use, to meet the water quality criteria and optimize their treatment and operation cost.

3.2 Justification and objectives

3.2.1 Justification

Guarantee water sustainability and use for this and future generation can be achieved by water recycling. The reclaimed water uses can be widely exploited since their applications are vast, and the treatment needed for this water will depend on its final destination.

Therefore, for the purpose of this thesis, it becomes essential to know the chemistry and quality of the water previous to a specific treatment.

3.2.2 General objective

Characterize RW through, DLS, ζ -potential, Alkalinity, and Hardness, to establish the reference measurements for further comparisons.

3.3 Background

3.3.1 Water reuse and reclaimed water

Water is the core of sustainable development, but it is a limited resource. In México, the National Council of Water Resources (CONAGUA) identifies at least 106 municipalities with high vulnerability to drought. Specifically, the state of Baja California is in water scarcity, being one of the main problems the depletion and deterioration suffered by its basins and aquifers, as well as their overexploitation, which ends up restricting the water supply.^{2,3}

The ultimate goal, when managing resources in water scarce areas, is to reach a balance among demand and offer (availability) of those resources. Therefore, environmentally sustainable development and management of water resources is a critical and complex issue for rich and poor countries.^{4,5}

In response to this problem, hydric resources should be managed more efficiently. As the demand for water increases and new sources of supply become more expensive to develop, there is an increasing need to use water more than once during the hydrological cycle. A feasible alternative is to apply environmentally sustainable treatments to wastewater to reclaim it for future purposes.¹

While options for developing water supplies via traditional approaches are limited, municipal wastewater is readily available, as it is produced at the proximity of the demands, is reliable, and may be treated to meet required standards at a reasonable cost. The technological improvement and economic affordability of wastewater treatment have made wastewater recycling a reality and broadened the most sustainable use of recycled water.^{6,7}

Reclaimed (recycled) water is the treated wastewater after removing solids and certain impurities, and its characteristics will depend on its source, treatment level and geographic location. Reclaimed water (RW) possesses many financial, technical, and institutional challenges than traditional sources, although a range of treatment options are available such that any level of water quality can be achieved depending upon the use of the reclaimed water.^{7,8}

To achieve economic efficiency and environmental sustainability a combination of water treatment technologies with a disinfection process can offer an increase in water quality, where the right level of treatment can be dictated by the end application of the RW (Figure 3.1)⁸



Figure 3.1 Treatment technologies to achieve any desired level of water quality.⁸

3.3.2 Reclaimed water (RW) application opportunities

The potential uses for RW are indeed numerous and widely varied since can be treated to meet the most stringent quality requirements and could be used for any purposes desired. However, reclaimed water has been used most commonly for non-direct consumption and non-body contact purposes. These possible applications can be observed in Figure 3.2.

There are many ways to classify the uses of RW but they can be large-grouped as follow:⁹

- I. Urban reuse
- II. Agricultural reuse
- III. Industrial reuse, cooling water
- IV. Industrial reuse, water for boilers
- V. Reuse in public services
- VI. Reuse for aquaculture activities
- VII. Reuse for recreational activities
- VIII. Reuse for aquifer recharge

The current drawbacks of reuse are mainly related to the difficulty of assessing health problems related to the capacity of a reclamation system to consistently obtain good quality water, in

Table 3.1 we can see some examples of the problems related to the RW.

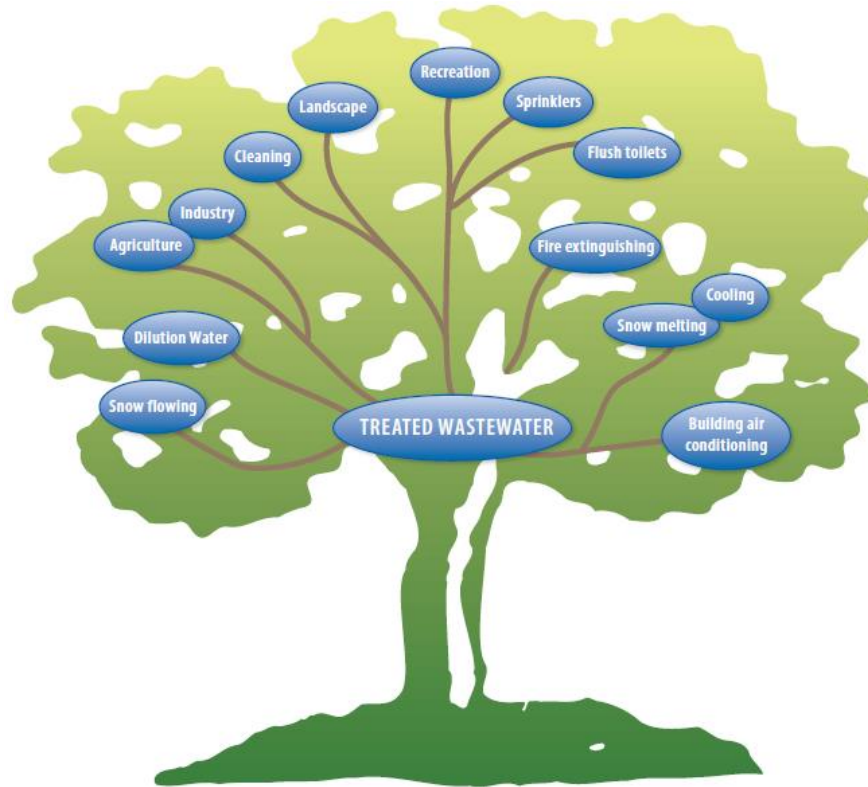


Figure 3.2 Reclaimed water opportunities.⁶

Table 3.1 Main reclaimed wastewater uses and main related problems.⁵

| Type | Problem | In relation with | End uses/ comments |
|-------------------------------|---|--|--|
| Agriculture | Salinity Plant illnesses Toxicity | Soils, plants Plant pathogens Accumulation of toxics in matrices | Expensive to be reduced Scarce standards can affect crops Transmission to the consumers |
| Urban uses (not for drinking) | Environment pollution (urban) | Aerosols, runoff, animal health | Mainly irrigation, but also cleaning and industrial uses |
| Industry | Salinity Human health | Scaling Aerosols, pathogens | For cooling, cleaning, processes, ... |
| Leisure | Human health | Aerosols, ingestion | Irrigation (golf courses, theme parks...), swimming pools |
| Recovery of water bodies | Environment pollution | Pathogens, toxics, nutrients | Increase the amount of water in the neighboring bodies |
| Groundwater recharge | Pollution | Chemicals, physical pollution, microorganisms | Water for several uses |
| Potable | Pollution of ground water | Drinking water safety | Direct reuse, drinking water |

3.3.3 RW quality

There is no specific regulation for reuse water in general since the quality criteria will depend on the purpose or the use that will be given to this water.

Table 3.2 Microbiological criteria for different applications of wastewater reclamation.¹

| Application | Fecal coliforms (geometric mean; no. per 100 ml) |
|---------------------------|---|
| Irrigation (restricted) | No standards recommended |
| Irrigation (unrestricted) | ≤ 1000* |
| Aquaculture | ≤ 1000* (measured in the fishponds) |
| Landscape irrigation | ≤ 200* |
| Groundwater recharge | 23** |
| Non-potable urban use | 3-1000** |
| Recreation | 2.2-1000** |
| Drinking water | Must not be detectable* |

* WHO standards

** USA-EPA standards

The WHO (world health organization) guidelines emphasize microbiological safety because more than half of the world population is still exposed to waters that contain pathogenic organisms to some degree. Table 3.2 summarizes some microbiological criteria for different wastewater reuse applications according to the WHO guidelines.¹

| Physical parameters | Chemical parameters | Biological parameters |
|---|--|--|
| <ul style="list-style-type: none"> • Turbidity • Total solids • Settling solids • Total dissolved solids • Colour • Odor • Temperature | <ul style="list-style-type: none"> • pH • Alkalinity • Acidity • Dissolved oxygen • Chemical oxygen demand • Total nitrogen • Ammonia nitrogen • Nitrite Nitrogen • Nitrogen from nitrates • Phosphor • Chloride • Fats and oils | <ul style="list-style-type: none"> • Total coliforms • Fecal coliforms • Helminth eggs • Protozoa • Virus |

Figure 3.3 Important parameters to characterize reclaimed water.¹⁰

There are other specific parameters to characterize wastewater for reuse (shown in Figure 3.3) but these parameters can vary depending on the application.¹⁰ We will address some of them below.

3.3.3.1 Urban reuse

Urban reuse is one of the highest volumes use in Mexico and USA.^{8,9} The application under this classification can be many such as recreational field, golf course irrigation, landscape irrigation, fire protection and toilet flushing; and all of them are important components of the RW portfolio of many urban reuse programs.

Urban reuse is often divided into applications that are either accessible to the public or have restricted access (restricted by physical or institutional barriers). When RW is used to irrigate residential areas, golf courses, public school yards, and parks, receives treatment and high-level disinfection and is not considered a threat to public health, but it differs from drinking quality water. Of particular importance are the salts and nutrients in reclaimed water, and special management practices for both end uses may be required depending on the concentrations in the RW.⁸ Table 3.3 shows the parameters for a RW used specifically for golf courses and recreational field irrigation according to the EPA (environmental protection agency, USA).

Table 3.3 Interpretation of RW quality.⁸

| Parameter | Units | Degree of restriction on use | | |
|--|--------------------|------------------------------|--------------------|---------|
| | | None | Slight to moderate | severe |
| Salinity | | | | |
| Electrical conductivity (E _{cw}) | dS m ⁻¹ | < 0.7 | 0.7 – 3.0 | > 3.0 |
| Total dissolved solids (TDS) | mg/L | < 450 | 450 – 2,000 | > 2,000 |
| Iron toxicity | SAR | < 3 | 3 – 9 | > 9 |
| Sodium (Na) | meq/L | < 3 | > 3 | |
| Root absorption | mg/L | < 70 | > 70 | |
| Foliar absorption | meq/L | < 2 | 2 – 10 | > 10 |
| Chloride (Cl) | mg/L | < 70 | 70 – 355 | > 355 |
| Root absorption | meq/L | < 3 | > 3 | |
| Foliar absorption | mg/L | < 100 | > 100 | |
| Boron | mg/L | < 1.0 | 1.0 – 2.0 | > 2.0 |
| pH | | | 6.5 – 8.4 | |

In urban reuse, RW is distributed to customers by a parallel network of pipes, separate of the drinking water distribution system. The requirements regarding water quality in México and USA (including specific states) for this type of reuse are presented in Table 3.4 and Table 3.5, extensive parameters are shown in the annex 3.8.1.

Table 3.4 Water quality for urban reuse (not restricted).⁹

| Parameter | EPA | Arizona | California | New México | NOM-003-SEMARNAT-1997 |
|------------------------------------|---------------|-------------------------------|--------------------------------|------------|-----------------------|
| pH | 6 – 9 | 4.5 – 9.0 | ----- | ----- | ----- |
| DBO ₅ (mg/L) | ≤ 10 | ----- | ----- | ----- | ----- |
| Turbidity (NTU) | ≤ 2 | 5 | 2 | ----- | ----- |
| Fecal coliforms (organisms/100 mL) | No detectable | 25 (median) 75 (simple m.) | 2.2 (median) 23 (simple m.) | 100 | 240 |
| Residual chlorine (mg/L) | 1 | ----- | ----- | ----- | ----- |
| Helminth eggs (organisms/ L) | ----- | ----- | ----- | ----- | ----- |

Table 3.5 Water quality for urban reuse (restricted).⁹

| Parameter | EPA | Arizona | California | New México | NOM-003-SEMARNAT-1997 |
|------------------------------------|-------|----------------------------------|--------------------------------|------------|-----------------------|
| pH | 6 – 9 | 4.5 – 9.0 | ----- | ----- | ----- |
| DBO ₅ (mg/L) | ≤ 30 | ----- | ----- | ----- | ----- |
| Settleable solids (mg/L) | ≤ 30 | ----- | ----- | ----- | ----- |
| Fecal coliforms (organisms/100 mL) | ≤ 200 | 25 (median) 1,000 (simple m.) | ----- | 1,000 | < 1,000 |
| Residual chlorine (mg/L) | 1 | ----- | 23 (median) 240 (simple m.) | ----- | ----- |
| Total coliforms | | | | | |
| Helminth eggs (organisms/ L) | ----- | ----- | ----- | ----- | ----- |

3.3.3.2 Agricultural reuse

The use of water in agriculture represents a significant fraction of the total demand for water since almost 60% of all the world's freshwater withdrawals go towards irrigation uses. And it's important to considerate that farming could not provide food for the world's current populations without adequate irrigation.^{8,9}

Agricultural use of RW has a long history and in USA already represents a significant percentage of the use of this water. RW from municipal and agricultural sources provides many advantages, such as:⁸

- ❖ The RW supply is highly reliable and typically increases with population growth.
- ❖ The cost of treating wastewater to secondary (and sometimes even higher) standards is generally lower than the cost of potable water from unconventional water sources (e.g., desalination).
- ❖ The option of allocating RW to irrigation is often the preferred and least expensive management alternative for municipalities.
- ❖ RW is an alternative to supplement and extend freshwater sources for irrigation.
- ❖ In many cities, RW might be the highest quality water available to farmers and could represent an inexpensive source of fertilizer. However, this advantage is conditional on proper quantities and timing of water and nutrients. Depending on the stage of growth, excess nutrients can negatively affect yields.

Irrigation of crops (food and non-food) with untreated wastewater is widely practiced in many parts of the developing world with accompanying adverse public health outcomes. Various international aid organizations have mobilized to improve upon these irrigation practices and provide barriers against transmission of disease-carrying agents (WHO and food and agricultural organization, FAO). Complementary to the above discussed, it is important to identify the key constituents of concern for agricultural irrigation, like plant sensitivity (the plant's tolerance to constituents encountered in the root zone or deposited on the foliage) since there are higher concentrations of some constituents in RW than the groundwater or surface water sources from which the water supply is drawn.⁸

The types and concentrations of constituents in RW will depend on the municipal water supply, the influent waste streams, the amount, and composition of infiltration in the wastewater collection system, the treatment processes, and the type of storage facilities. A summary of these recommendations is provided in Table 3.6.⁸

Table 3.6 Guidelines for interpretation of water quality for irrigation.⁸

| Potential irrigation problem | Units | Degree of restriction on irrigation | | |
|---|---------|-------------------------------------|--------------------|--------|
| | | None | Slight to moderate | Severe |
| Salinity (affects crop water availability) ² | | | | |
| EC _w | dS/m | < 0.7 | 0.7 – 3.0 | > 3.0 |
| TDS | mg/L | < 450 | 450 – 2000 | > 2000 |
| Infiltration (affects infiltration rate of water into the soil; evaluate using EC _w and SAR together) ³ | | | | |
| SAR | 0 – 3 | and EC _w = | > 0.7 | < 0.2 |
| | 3 – 6 | | > 1.2 | < 0.3 |
| | 6 – 12 | | > 1.9 | < 0.5 |
| | 12 – 20 | | > 2.9 | < 1.3 |
| | 20 – 40 | | > 5.0 | < 2.9 |
| Specific ion toxicity (affects sensitive crops) | | | | |
| Sodium (Na) ⁴ | | | | |
| Surface irrigation | SAR | < 3 | 3 – 9 | > 9 |
| Sprinkler irrigation | meq/L | < 3 | > 3 | |
| Chlorine (Cl) ⁴ | | | | |
| Surface irrigation | meq/L | < 4 | 4 – 10 | > 10 |
| Sprinkler irrigation | meq/L | < 3 | > 3 | |
| Boron (B) | meq/L | < 0.7 | 0.7 – 3.0 | > 3.0 |
| Miscellaneous effects (affects susceptible crops) | | | | |
| Nitrate (NO ₃ -N) | mg/L | < 5 | 5 – 30 | > 30 |
| Bicarbonate (HCO ₃) | meq/L | < 1.5 | 1.5 – 8.5 | > 8.5 |
| pH | | Normal range 6.5 – 8.4 | | |

2 EC_w means electrical conductivity, a measure of the water salinity, reported in deciSiemens per meter at 25°C (dS/m) or in millimhos per centimeter (mmho/cm); both are equivalent.

3 SAR is the sodium adsorption ratio; at a given SAR, infiltration rate increases as water salinity increases.

4 For surface irrigation, most tree crops and woody plants are sensitive to sodium and chloride; most annual crops are not sensitive. With overhead sprinkler irrigation and low humidity (< 30 percent), sodium and chloride may be absorbed through the leaves of sensitive crops.

The parameters of the RW that are of concern if it replaces the first-use water are: salinity, sodium, excessive residual chlorine and nutrients, and trace elements. The sensitivity is generally a function of the tolerance of the plants to these constituents from the root or deposited on the foliage.⁹ In **¡Error! La autreferencia al marcador no es válida.** to 3.10 are shown the quality parameters of the water for this reuse, extensive parameters are shown in the annex 3.8.2.

Table 3.7 Water quality required for reuse in agriculture (non-commercially processed food crops).⁹

| Parameter | EPA | Arizona | California | New México |
|------------------------------|-------|-------------------------------------|--------------|------------|
| pH | 6 – 9 | 4.5 – 9.0 | ----- | ----- |
| DBO ₅ (mg/L) | ≤ 30 | ----- | ----- | ----- |
| SS (mg/L) | ≤ 30 | ----- | ----- | ----- |
| Fecal coliforms (org/100 mL) | ≤ 200 | 1,000 (median) 2,500 (simple m.) | ----- | 1,000 |
| Residual chlorine (mg/L) | 1 | ----- | ----- | ----- |
| Total coliforms (org/100 mL) | ----- | ----- | 2.2 (median) | ----- |

Table 3.8 Water quality required for reuse in agriculture (commercially processed food crops, surface irrigation of orchards and vineyards).⁹

| Parameter | EPA | Arizona | California | New México |
|------------------------------|-------|-------------------------------------|--------------|------------|
| pH | 6 – 9 | 4.5 – 9.0 | ----- | ----- |
| DBO ₅ (mg/L) | ≤ 30 | ----- | ----- | ----- |
| SS (mg/L) | ≤ 30 | ----- | ----- | ----- |
| Fecal coliforms (org/100 mL) | ≤ 200 | 1,000 (median) 2,500 (simple m.) | ----- | 1,000 |
| Residual chlorine (mg/L) | I | ----- | ----- | ----- |
| Total coliforms (org/100 mL) | ----- | ----- | 2.2 (median) | ----- |

Table 3.9 Water quality required for reuse in agriculture (for non-food crops, dairy pasture, feed, fiber, and seed crops)⁹

| Parameter | EPA | Arizona | California | New México |
|------------------------------|-------|-----------------------------------|------------|------------|
| pH | 6 – 9 | 4.5 – 9.0 | ----- | ----- |
| DBO ₅ (mg/L) | ≤ 30 | ----- | ----- | ----- |
| SS (mg/L) | ≤ 30 | ----- | ----- | ----- |
| Fecal coliforms (org/100 mL) | ≤ 200 | 100 (median) 4,000 (simple m.) | ----- | ≤1,000 |
| Residual chlorine (mg/L) | I | ----- | ----- | ----- |
| Total coliforms (org/100 mL) | ----- | ----- | ----- | ----- |

Table 3.10 Recommended limits of trace elements and dissolved solids for irrigation with treated water.⁹

| Parameter | Long term use (mg/L) | Short term use (mg/L) |
|-------------------------------|----------------------|-----------------------|
| Aluminum | 5.0 | 20.0 |
| Arsenic | 0.10 | 2.0 |
| Beryllium | 0.10 | 0.5 |
| Boron | 0.75 | 2.0 |
| Cadmium | 0.01 | 0.05 |
| Chlorine | 0.1 | 1.0 |
| Cobalt | 0.05 | 5.0 |
| Copper | 0.2 | 5.0 |
| Fluorine | 1.0 | 15.0 |
| Iron | 5.0 | 20.0 |
| Lead | 5.0 | 10.0 |
| Lithium | 2.5 | 2.5 |
| Manganese | 0.2 | 10.0 |
| Molybdenum | 0.01 | 0.05 |
| Nickel | 0.2 | 2.0 |
| Selenium | 0.02 | 0.02 |
| Vanadium | 0.1 | 1.0 |
| Zinc | 2.0 | 10.0 |
| Other parameters | | |
| parameter | Recommended limit | |
| Total dissolved solids (mg/L) | 500 – 2,000 | |

3.3.3.3 Industrial reuse

Traditionally, pulp and paper, textile, and other facilities using RW for cooling tower purposes have been the primary industrial users. Over the past decade, the industrial use of RW has grown in a variety of industries ranging from electronics to food processing, as well as a broader adoption by the power-generation industry, for purposes ranging from process water, boiler feed water, and cooling tower use to flushing toilets and site irrigation.⁸

Table 3.11 Water quality required in cooling water (recirculation systems).⁹

| Parameter* | WPCF | EPA | DGCOH |
|-------------------------------------|-----------|-----------|---------|
| Chloride | 500 | ----- | ----- |
| Total dissolved solids | 500 | ----- | 1,200 |
| Hardness | 650 | ----- | 325 |
| Alkalinity | 350 | ----- | 300 |
| pH | 6.9 – 9.0 | 6.9 – 9.0 | 5 – 8.3 |
| Chemical oxygen demand | 75 | ----- | 75 |
| Total suspended solids | 100 | ≤ 30 | 500 |
| Turbidity | 50 | ----- | 10 |
| Biochemical oxygen demand | 25 | ≤ 30 | 20 |
| Active substances to methylene blue | 1.0 | ----- | 0.5 |
| Ammonia nitrogen | 1.0 | ----- | 0.5 |
| Phosphates | 4 | ----- | 1.0 |
| Silicon oxides | 50 | ----- | ----- |
| Aluminum | 0.1 | ----- | 1.0 |
| Iron | 0.5 | ----- | 0.5 |
| Manganese | 0.5 | ----- | 0.5 |
| Calcium | 50 | ----- | ----- |
| Magnesium | 0.5 | ----- | ----- |
| Bicarbonate | 24 | ----- | ----- |
| Sulfates | 200 | ----- | 700 |
| DBO ₅ | ----- | ≤ 30 | ----- |
| Standard account (Col/L) | ----- | ----- | 2,000 |
| Total coliform (org/ 100 mL) | ----- | ----- | 10,000 |
| Fecal coliform (org/ 100 mL) | ----- | ≤ 200 | ----- |
| Residual chlorine | ----- | 1 | 0.2 |

DGCOH= Dirección General de Construcción y Operación Hidráulicas (DGCOH)

WPCF = Water Pollution Control Federation

*All values in mg/L with the exception of pH and the indicated.

Cooling towers are recirculating evaporative cooling systems that use the RW to absorb process heat and then transfer the heat by evaporation. As the cooling water is recirculated, makeup water (RW) is required to replace water lost through evaporation. Some industries require large volumes of water for cooling being the most frequent water quality problems scale formation (hardness), corrosion, biological growth and foam production.^{8,9}

This problem occurs both from contaminants in drinking water and in RW, but the concentrations of some contaminants in RW can be very high. Table 3.11 presents the water quality criteria for cooling process.

Table 3.12 Recommended boiler water limits.⁸

| Drum operating pressure (psig) | 0 – 300 | 301 – 450 | 451 – 600 | 601 – 750 | 751 – 900 | 901 – 1000 | 1001 – 1500 | 1501 – 2000 | OTSG |
|--|-------------|------------|------------|------------|------------|------------|-------------|-------------|------------|
| Steam | | | | | | | | | |
| TDS max (ppm) | 0.2 – 1.0 | 0.2 – 1.0 | 0.2 – 1.0 | 0.1 – 0.5 | 0.1 – 0.5 | 0.1 – 0.5 | 0.1 | 0.1 | 0.05 |
| Boiler water | | | | | | | | | |
| TDS max (ppm) | 700 – 3500 | 600 – 3000 | 500 – 2500 | 200 – 1000 | 150 – 750 | 125 – 625 | 100 | 50 | 0.05 |
| Alkalinity max (ppm) | 350 | 300 | 250 | 200 | 150 | 100 | n/a | n/a | n/a |
| TSS max (ppm)15 | 10 | 8 | 3 | 2 | 1 | 1 | 1 | n/a | n/a |
| Conductivity max (µmho/cm) | 1100 – 5400 | 900 – 4600 | 800 – 3800 | 300 – 1500 | 200 – 1200 | 200 – 1000 | 150 | 80 | 0.15 -0.25 |
| Silica max (ppm SiO ₂) | 150 | 90 | 40 | 30 | 20 | 8 | 2 | 1 | 0.02 |
| Feed water (Condensate and Makeup, after Deaerator) | | | | | | | | | |
| Dissolved oxygen (ppm O ₂) | 0.007 | 0.007 | 0.007 | 0.007 | 0.007 | 0.007 | 0.007 | 0.007 | n/a |
| Total iron (ppm Fe) | 0.1 | 0.05 | 0.03 | 0.025 | 0.02 | 0.02 | 0.01 | 0.01 | 0.01 |
| Total copper (ppm Cu) | 0.05 | 0.025 | 0.02 | 0.02 | 0.015 | 0.015 | 0.01 | 0.01 | 0.002 |
| Total hardness (ppm CaCO ₃) | 0.3 | 0.3 | 0.2 | 0.2 | 0.1 | 0.05 | ND | ND | ND |
| pH @ 25 °C | 8.3- 10.0 | 8.3- 10.0 | 8.3- 10.0 | 8.3- 10.0 | 8.3- 10.0 | 8.8 – 9.6 | 8.8 – 9.6 | 8.8 – 9.6 | n/a |
| Nonvolatile TOC (ppm C) | 1 | 1 | 0.5 | 0.5 | 0.5 | 0.2 | 0.2 | 0.2 | ND |
| Oily matter (ppm) | 1 | 1 | 0.5 | 0.5 | 0.5 | 0.2 | 0.2 | 0.2 | ND |

The use of RW for boiler make-up water differs little from the use of conventional potable water but both require extensive pretreatment. Water quality requirements for boiler make-up water depend on the pressure at which the boiler is operated; in general, higher pressures require higher-quality water. The primary concern is scale buildup and corrosion of equipment and for instance control or removal of hardness from any source of water is required; additionally, control of insoluble scales of calcium and magnesium, and control of silica and alumina, are also required.^{8,11}

Alkalinity of the RW, determined by its bicarbonate, carbonate, and hydroxyl content, is also a concern because excessive alkalinity concentrations contribute to foaming and other forms of carryover, resulting in deposits. Bicarbonate alkalinity in feed water breaks down under the influence of boiler heat to release carbon dioxide, a major source of localized corrosion in steam-using equipment and condensate-return systems.^{8,11,12} The water quality required for this purpose is shown in Table 3.12.

3.3.3.4 *Aquifer recharge reuse*

Water recharge to aquifers not used for potable water has been practiced for many years and often viewed as a disposal method for treated wastewater effluent, but additionally RW can provide a several other benefits including:^{8,9}

- ❖ Recovery of RW for subsequent reuse or discharge
- ❖ Recharge of adjacent surface streams
- ❖ Seasonal storage of RW beneath the site for agriculture
- ❖ Establish a barrier to the invasion of salty waters in coastal aquifers
- ❖ Increase the volume of aquifers with water of adequate quality
- ❖ To control or prevent subsidence of the land

Recharge methods can be either by surface spread or direct injection. For surface spread, the RW is moved from the ground surface to the aquifer by infiltration and percolation through the soil matrix, and the techniques include flooding, ridge and furrow systems, channel division, and infiltration basins. On the other hand, direct injection involves pumping RW directly into the aquifer zone, which is generally a well-confined aquifer, in depth or where hydrogeological conditions are not appropriate for surface dissemination. Direct injection requires a better-quality water than the one recommended for surface dissemination, because in direct injection soil treatment is absent.⁹

The system to be used depends on many similar factors such as soil type and porosity, aquifer depth, topography, and quantity of the RW. The quality of the water required for this type of recharge depends on the specific site and the use, therefore, it is necessary to study each case. Table 3.13 shows the water quality criteria water required for use in aquifer recharge.

Table 3.13 Water quality required for its reuse in the recharge of aquifers⁹

| Parameter | EPA | DGCOH |
|---|---------------|-------|
| General | | |
| Total dissolved solids (mg/L) | 500 | 500 |
| pH | 6.5 – 8.5 | 7 – 9 |
| Turbidity (NTU) | 1.0 | 5 |
| Color | 15.0 | 5 |
| Asbestos, million fibers/L | 7.0 | ----- |
| Residual chlorine (mg/L) | 1.0 | 0.2 |
| Active substances to methylene blue | 0.5 | 0.5 |
| Temperature °C | ----- | ----- |
| Oils and fats | ----- | 0 |
| Floating matter | ----- | ----- |
| Settleable solids (mL/L) | ----- | ----- |
| Total suspended solids (mg/L) | ----- | 2 |
| DBO ₅ (mg/L) | ----- | 2.5 |
| Total hardness (as CaCO ₃) | ----- | 500 |
| Microbiological | | |
| Total coliforms (org/100 mL) | 1 | 1,000 |
| Fecal coliforms (org/100 mL) | No detectable | ----- |
| Helminth eggs (organisms/ L) | ----- | 0 |
| Standard account (Col/ mL) | ----- | 200 |
| Inorganics (mg/L) | | |
| Arsenic | 0.05 | 0.5 |
| Cadmium | 0.01 | 0.01 |
| Chloride | 250 | 250 |
| Chromium | 0.05 | 0.05 |
| Copper | 1.0 | 1.0 |
| Cyanide | 0.2 | 0.2 |
| Total iron | 0.3 | 0.3 |
| Fluorides | 2.0 | 1.5 |
| Total phosphorus | ----- | 1.0 |
| Total manganese | 0.05 | ----- |
| Mercury | 0.002 | 0.002 |
| Nitrogen – nitrate | 10 | 10 |
| Nitrogen – nitrite | 1.0 | 0.1 |
| Ammonia nitrogen | ----- | 0.5 |
| Nickel | 0.1 | 0.05 |
| Selenium | 0.01 | 0.01 |
| Sulfates | 250 | 250 |
| Lead | 0.05 | 0.05 |
| Zinc | 5 | 5 |
| Barium | 1.0 | 1.0 |
| Silver | 0.05 | 0.05 |
| Thallium | 0.0002 | ----- |
| Sodium adsorption reaction (RAS) (dimensionless) | ----- | 6 |

DGCOH= Dirección General de Construcción y Operación Hidráulicas (DGCOH)

* By injection into potable aquifers.

3.3.4 RW composition in Tijuana, Baja California, México

In the specific case for the Tijuana region, in the state of Baja California in Mexico, wastewater is treated for its reuse, which is not suitable for human consumption. This water has been previously characterized in its physicochemical parameters at a pH ~ 8 (pH at which it is obtained at the end of the treatment in the wastewater treatment plant, WWTP). Also, this RW was characterized based on its cationic and anionic content at the mentioned pH (Table 3.14).

Table 3.14 Composition of reclaimed water, obtained from the wastewater plant treatment "La Morita" in Tijuana, Baja California, México.

| Parameter | Reclaimed Water | Cations in Reclaimed water | Units (ppm) | Anions in Reclaimed water | Units (ppm) |
|-------------------------------------|-----------------|----------------------------|-------------|-------------------------------|-------------|
| Turbidity (NTU) | 23 | Li ⁺ | 0 | F ⁻ | 0 |
| pH | 7.9 | Na ⁺ | 287.59 | Cl ⁻ | 378.55 |
| Color (HU) | 253 | K ⁺ | 33.95 | NO ₂ ⁻ | 4.30 |
| Total suspended solids (mg/L) | 15.3 | Ca ²⁺ | 57.37 | Br ⁻ | 0 |
| Particle size (nm) | 566.9 | Mg ²⁺ | 126.64 | NO ₃ ⁻ | 117.41 |
| Zeta potential (mV) | -0.9 | | | SO ₄ ²⁻ | 383.55 |
| chemical oxygen demand (COD) (mg/L) | 74.0 | | | | |
| Total organic carbon (TOC) (mg/L) | 19.4 | | | | |
| Electrical conductance (mS/cm) | 2.8 | | | | |

Although a large majority of the parameters have been studied for the RW of Tijuana, more studies must be carried out to understand its future interaction with other components (nanotechnologies / materials) to adapt this water to any type of final destination.

3.3.5 Hard water

Using RW from a wide range of sources is an attractive way to meet the growing water demand. However, most of these water sources have a hardness level that does not make them attractive for industrial and domestic usages since requiring salts to be removed.¹³

Technically, hard water is water that contains dissolved positive ions with multiple plus charges due to cations such as calcium and magnesium (divalent cations, 2⁺) and to a lesser extent to aluminium, iron, and other divalent and trivalent cations.^{14,15}

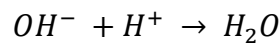
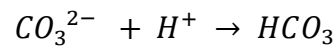
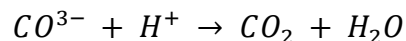
Generally, calcium ions are predominant, like 75% or more of the hardness. Calcium carbonate is the precipitated form of the Ca ion contribution to hardness which is also known as lime scale or hard water scale. This scale adheres to surfaces and is difficult to remove.¹⁶

The removal of excessive amounts of Ca and Mg from water used for consumption would make healthy feeding and organism functioning possible. At the same time, water softening could make possible industry and household usage ensuring long-lasting operation of equipment and pipes.¹⁷

3.3.5.1 Alkalinity

The EPA defines alkalinity as "a measure of the buffering capacity of water".¹² In other words, alkalinity is a measure of the water's ability to neutralize acidity. This buffering capacity is important for water quality, since pH has a direct effect on organisms, and indirect effect on the toxicity of some other contaminants in the water.

The alkalinity of water is mainly due to the presence of bicarbonate, carbonate and hydroxide ions, where these 3 ions react with H⁺ ions to reduce acidity, increasing alkalinity and pH:¹⁸



The primary source of alkalinity is the carbonate system, although phosphates, silicates, borates, carboxylates, and other weak acid systems can also contribute, but sometimes some of these contributions are not significant to be taken into account.¹⁹

Figure 3.4 is displayed to have a better understanding about the dependence of pH and alkalinity. At a pH close to 4.3 or lower there is no alkalinity present, there is only free mineral

acidity and dissolved carbon dioxide (dissolved CO_2 is sometimes expressed as carbonic acid, H_2CO_3).

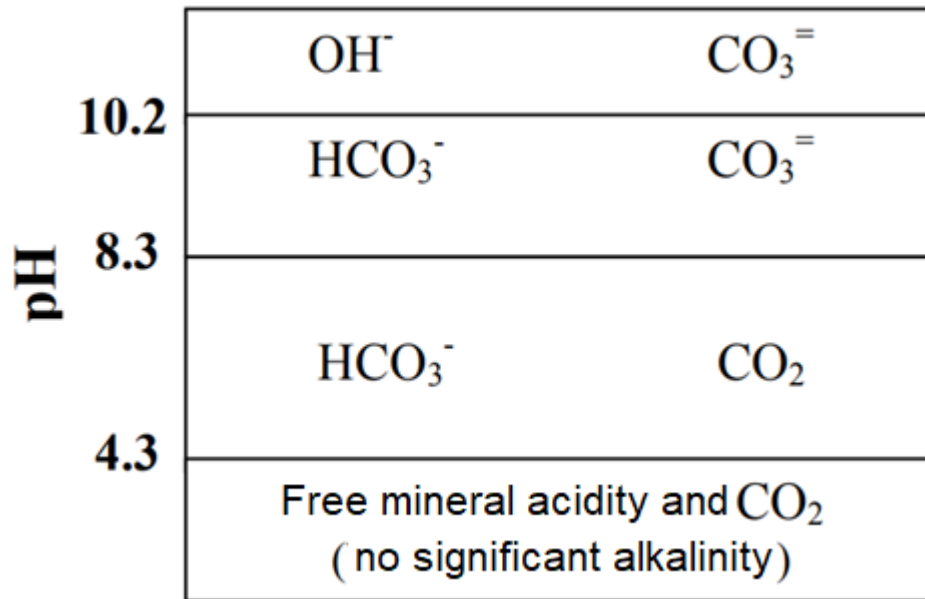


Figure 3.4 Alkalinity and pH diagram.²⁰

As the pH increases, between 4.3 and 8.3, the dissolved carbon dioxide begins to convert into bicarbonate ion, and this conversion is completed at a pH close to 8.3. When the pH is increased above 8.3 the bicarbonate ion now turns into a carbonate ion and this conversion is completed at a pH of around 10.2. If the pH continues increasing (above 10.2) measurable levels of hydroxide along with carbonate ions can be seen.²⁰

Therefore, alkalinity is a significant parameter in the drinking water and wastewater treatment processes since it acts as a pH buffer in the coagulation and softening of water with lime and soda. In wastewater treatment, alkalinity is also important to determine the suitability of the waste for the treatment and control processes such as anaerobic digestion, where any fraction of bicarbonate alkalinity and total alkalinity contributed by volatile acid salts needs to be considered.²¹

3.3.5.2 Hardness

Hardness is a chemical parameter that is due to polyvalent metal ions dissolved in water; in freshwater these are mainly calcium and magnesium, although other metals such as iron, strontium and manganese may have contributions.¹² Generally, hardness refers to the total

concentration of calcium and magnesium ions, where calcium typically represents 2/3 of total hardness and mg about 1/3, given in milliequivalents per liter:^{18,19}

$$\text{Hardness, eq/L} = 2[\text{Ca}^{2+}] + 2[\text{Mg}^{2+}]$$

It is called hardness because if calcium and magnesium are present in the water, lathering for washing is “Hard” (difficult) to do. Therefore, cleaning with hard water is "hard". Hardness is often confused with alkalinity, this confusion is due to the term used to inform both measurements, mg/L of CaCO₃. Additionally, the fact that if limestone is the primary source of hardness and alkalinity, both concentrations will be similar (if not identical) contributing to this confusion. And, as expected, hard water is likely to have a high pH as well due to the high content of carbonates that buffer the pH towards the alkaline side.^{12,18}

Two general types of hardness are of interest:^{16,19}

- ❖ Temporary hardness or carbonate hardness. It is associated with HCO₃⁻ and CO₂⁻³ and they can cause scale-formation.
- ❖ Permanent hardness or non-carbonate hardness. It is associated with other anions, particularly Cl⁻ and SO₂⁻⁴. This group, contains hard water ions (such as calcium and/or magnesium) as in temporary hardness, but it does not contain the bicarbonate ion. Therefore, this hardness does not form scale upon heating.

Maintenance is always a concern with equipment when hard water containing temporary hardness is present due to its scale forming potential, especially when water is heated to produce steam. Therefore, conserve the balance between carbonate and noncarbonate hardness is important in water softening (hardness removal) and in scale formation (because HCO₃⁻ dissociates at high temperatures).¹⁶

3.3.6 Hypothesis

- ❖ RW obtained from the WWTP “La Morita” will have a large size of suspended particles bigger than a half of micron.
- ❖ RW water will present size dependency with pH, and surface potential charge with pH.

-
- ❖ RW studied will have a higher amount of alkalinity and hardness than potable water, reason why will need further treatment to meet the regulations for some applications.

3.4 Experimental and methods

3.4.1 Materials and reagents

- ❖ Sodium hydroxide (ACS reactive, $\geq 97.0\%$)
- ❖ Hydrochloric acid (ACS reactive, 37%)
- ❖ Alkalinity test kit, Hach
- ❖ Total hardness test kit, Hach

3.4.2 Equipment

- ❖ Analytical balance brand OHAUS model AV264
- ❖ Anton Paar Litesizer 500
- ❖ Horiba Laqua PC1100 Dual Channel pH/Ion Meter

3.4.3 Methodology

The water samples for this study were obtained from the WWTP “La Morita” located in the city of Tijuana in the state of Baja California, México. Since this water is transported in purple pipes is denominated “Purple water”. The quality of this water does not meet the regulation to be classified as potable for domestic consumption, but it is close to fit the quality for irrigation/agricultural use, reason why it is the object of this study.

The RW was characterized in previous work, by the parameters shown in Table 3.14; additionally, DLS, ζ -potential, and alkalinity and hardness test at different pH values were performed. For Alkalinity and hardness determinations we select to work at pH 7, 8, and 9 since the natural pH of RW is 8 and to evaluate the behavior in the surrounding pHs. The pH was adjusted using 0.001 M HCl and 0.001 M NaOH solutions.

3.4.3.1 DLS characterization of RW

DLS was performed in an Anton Paar (Litesizer 500) to analyze the size of suspended particles present in the water samples and its dependence on the pH, on a scale from 2 to 12. The pH was adjusted with 0.1 M HCl to pH = 2 and 0.1 M NaOH .

3.4.3.2 ζ -potential characterization of RW

The physicochemical performance of RW was determined by Zeta Potential and pH measurements in an Anton Paar (Litesizer 500). The pH was adjusted with 0.1 M HCl and 0.1 M NaOH from pH 2 to pH 12.

3.4.3.3 Alkalinity test procedure for RW

Hach commercial kit was used to determine the alkalinity of the samples at three different pH values: 7, 8, and 9, following the standard titration procedure as described:

For the test, with a 50 mL sample of RW, we used H₂SO₄ 0.020 N as titrant. A 25 mL burette was filled to the zero mark with the titrant. The sample was poured into a 250 mL Erlenmeyer flask and the content of one phenolphthalein indicator powder pillow was added to the sample and swirled to mix. Since no change of color was observed, the content of one bromocresol green-methyl green indicator powder pillow was also added and swirled to mix. The flask was placed under the burette adding titrant swirling the flask until a change of color was observed from green to a light pink color. Finally, we multiplied the mL of titrant used by 20 to calculate the concentration in mg/L as CaCO₃ total alkalinity.

The commercial Hach kit for alkalinity is comparable to the Mexican standard “NMX-AA-036-SCFI-2001” for the determination of acidity and alkalinity. The described procedure can be used for Standard Methods for the Examination of Water and Wastewater 2320 B (alkalinity) accepted for EPA and NPDES (National Pollutant Discharge Elimination System).

3.4.3.4 Total hardness test procedure for RW

Hach commercial kit was also used to determine the total hardness of the samples at the pH values: 7, 8, and 9, following the standard titration procedure as follow:

The test was carried with a 50 mL sample of RW using EDTA 0.020 N as the titrant. A 25 mL burette was filled to the zero mark with the titrant. The sample was poured into a 250 mL Erlenmeyer flask adding 1 mL of KOH 1 N (standard solution) and swirled to mix. The content of one CalVer 2 calcium indicator powder pillow was added to the sample and swirled to mix. The flask was placed under the burette adding titrant swirling the flask until a change of

color was observed from red to a pure blue color. Finally, we multiplied the mL of titrant used by 20 to calculate the concentration in mg/L of Ca as CaCO₃.

The commercial Hach kit for hardness is comparable to the Mexican standard “NMX-AA-072-SCFI-2001” determination of total hardness. The described procedure was adapted from Standard Methods for the Examination of Water and Wastewater 2340 (hardness) accepted for EPA and NPDES (when 0.020 N titrant is used).

3.5 Results and discussions

Model RW was obtained from a wastewater treatment plant in Tijuana, B. C. presumably containing Ca^{2+} and Mg^{2+} as well as carbonates and other salts (Table 3.14). This water accomplishes the Mexican regulation NOM-003-SEMARNAT-1997 that is equivalent to regulations of RW mentioned in EPA/600/R-12/618. RW was characterized by the same dispersion properties (DLS and ζ -Potential) as the magnetite-base materials (mentioned in previous chapters in order to analyze its behavior vs pH and compare it with the MNP, MND, MCH and MCCH).

3.5.1 DLS and ζ -potential characterization of RW

Figure 3.5 reveals the average particle size (black line) and the ζ -potential (blue line) estimated for the RW at different pHs (2 to 12).

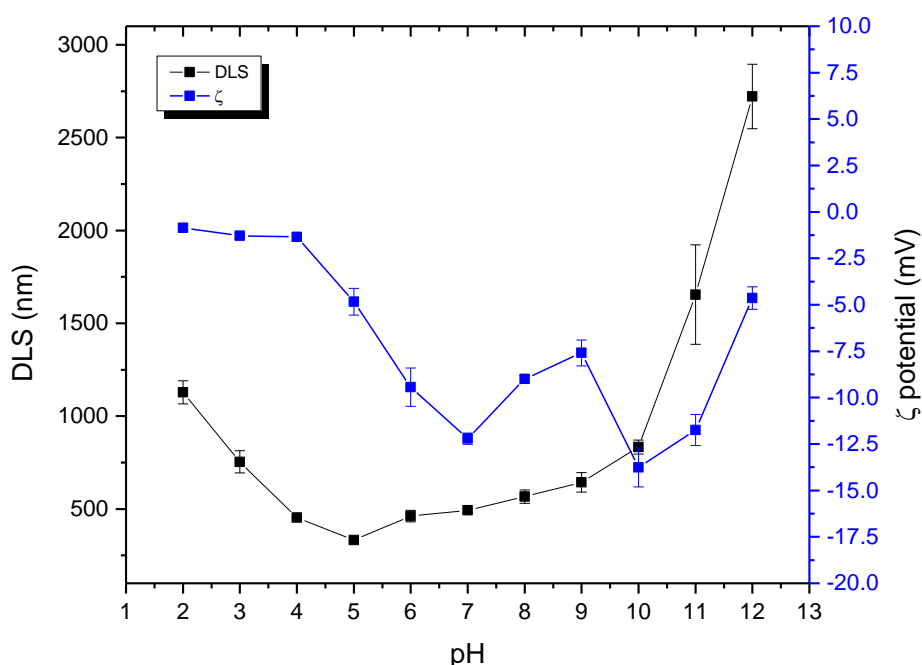


Figure 3.5 DLS (black line) and ζ -potential (blue line) of the RW from the WWTP “la Morita”. The pH was adjusted using solutions of 0.001 M HCl and 0.001 M of NaOH.

From DLS study, we can observe the dependence of the size of the suspended solids present in RW with the pH and how it's also affected by the electrostatic interactions. As we can notice, the particles have a size close to a micron at pH 2 and this decreases to a minimum size close to 300 nm at a pH of 5, After this value, the size begins to gradually increase again

up to a pH of 10, and it is at a pH of 11 and 12 that this value increases to sizes greater than one micron.

Placing the attention now on the ζ -potential of the RW we can see that an isoelectric point is not reached, and all the potential readings are negative, however, at more acidic pH values (2 to 4) the electric potential is closer to its IEP, which explains the agglomeration of the suspended solids in the water. By increasing the pH, the potential value is also affected, increasing in more negative values, due to the desorption of protons, which increases the charge density on the surface, this modifies the electrostatic interactions and increases the repulsion forces between the molecules, which is why the size of the suspended particles decreases. Finally, at a more basic pH, the value of the potential decreases again, having as an effect a greater agglomeration of the suspended solids due to the variation of the charge density.

3.5.2 Alkalinity and hardness characterization of RW

Figure 3.6 shows the results of the alkalinity and hardness tests made for the RW, we can see that increasing the pH increases the alkalinity, but the hardness levels are maintained.

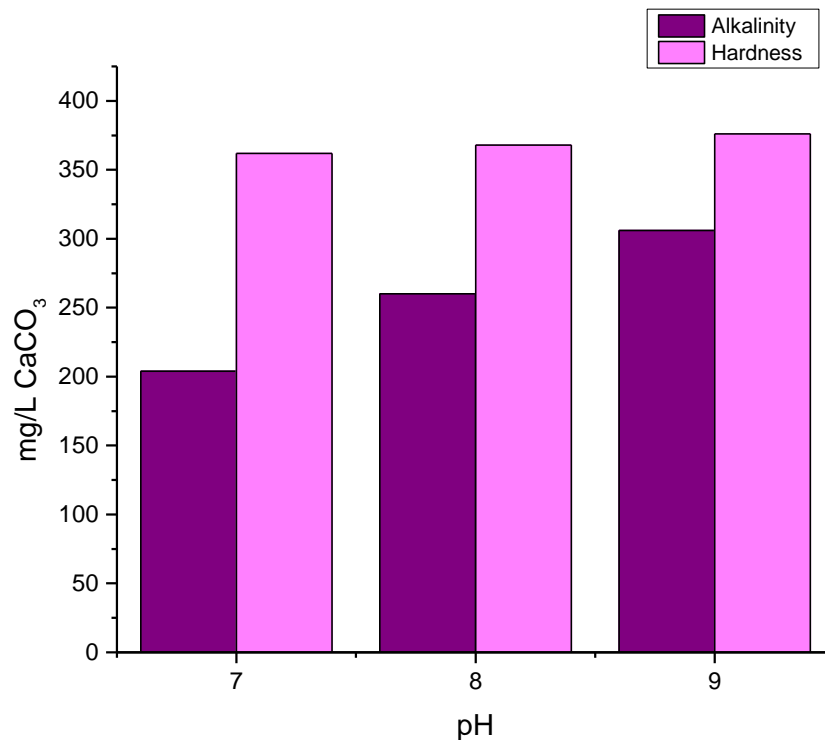


Figure 3.6 Alkalinity(purple) and hardness (pink) measurements for RW from the WWTP “La Morita” at pH 7, 8, and 9 expressed as mg L-1 of CO₃.

The alkalinity values are 200, 250, and 300 mg/L at pH 7, 8, and 9 respectively, the EPA indicates that the typical ranges for a RW should be between 50-150 mg/L. Regarding the hardness values found for these samples, they remain around 350 mg/L in each pH, for this parameter the EPA does not establish minimum or maximum values for reuse water, but it does establish values of 113 ± 19.3 mg/L for water raw residual, and 105.6 ± 24.2 mg/L for reuse water that goes to a power plant. These results indicate that the RW from the WWTP “La Morita” needs further treatment to reduce the alkalinity and hardness values present in the water

3.5.3 DLS comparison of RW and magnetic nanomaterials (MNP, MND, MCH, and MCCH)

Figure 3.7 shows the comparison between DLS for RW and magnetic nanomaterial dispersed in deionized water (MNP, MND, MCH, and MCCH). Among all, raw magnetite has the most stable size (close to 100 nm) in deionized water dispersion (as mentioned in the last chapter), and RW presents much higher diameters of suspended particles than any other magnetite-based material with sizes from 500 to 700 nm.

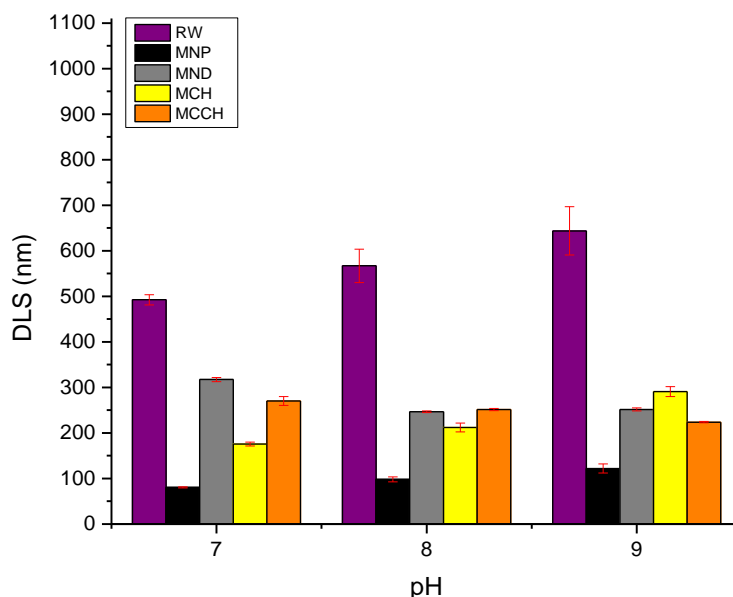


Figure 3.7 Comparison of the DLS measurements of RW (purple), MNP (black), MND (gray), MCH (yellow), and MCCH (orange) at pH of 7, 8, and 9.

It is important to point that RW has “natural” a yellowish color, from the water treatment train applied, and those suspended particles are not visible at naked-eye, but they tend to agglomerate and precipitate to the bottom after a few days (Figure 3. 8).

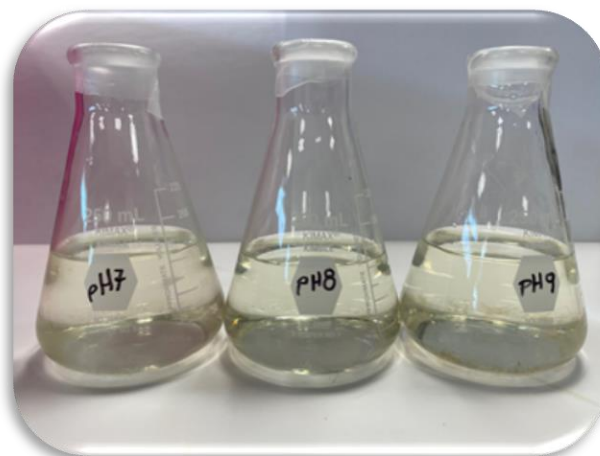


Figure 3. 8. RW at pH 7, 8 and 9.

3.5.4 ζ -potential comparison of RW and magnetic nanomaterials (MNP, MND, MCH, and MCCH)

ζ -potential comparison of RW and magnetic nanomaterial dispersed in deionized water (MNP, MND, MCH, and MCCH) are shown in Figure 3.9.

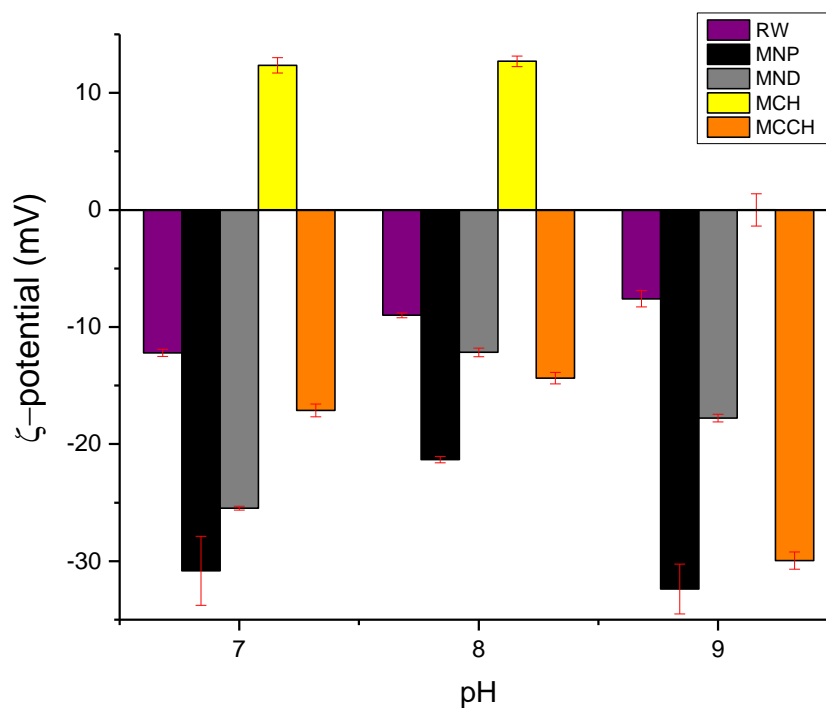


Figure 3.9 Comparison of the Zeta Potential measurements of RW (purple), MNP (black), MND (gray), MCH (yellow), and MCCH (orange) at pH of 7, 8, and 9.

We can note that only MCH at pH 9 reaches the IEP, with no other particle or the RW close to the IEP at those pHs. The most stable ζ -potential values are reached for MNP at pH 7 and 9, and while all the systems show negative potentials MCH have positive values. This can be an indication that MCH possess a potential to interact better with ions present in RW, since this water has negative measurements.

3.6 Conclusions

The characterization of the RW from the WWTP “La Morita” was carried out by DLS and ζ -potential where we could evaluate the size dependence with the pH and how it’s also affected by the electrostatic interactions. The IEP was not reached for this water in all the study (pH 2 to 12) which clearly affected the potential values modifying the electrostatic interactions. We found out that when the repulsion forces increased between the molecules the size of the suspended particles decreases, and when the value of the potential decreases, an agglomeration effect of the suspended solids occurs, due to the variation of the charge density resulting in sizes larger than a micron.

Since the natural pH of RW is 8, a pH range between 7 and 9 was analyzed so we can evaluate the electrostatic interaction between magnetic nanoscavengers for RW alkalinity and hardness removal in the next chapter. We found out that the alkalinity and hardness of RW is around 200-300 mg/L and 350 mg/L, respectively, having good parameters for irrigation for urban and crops reuses but not as good for some industrial applications and water recharge or potable uses, even those parameters are not “bad” and barely accomplish the Mexican regulation and RW needs further treatment for other reuses and to avoid scale and corrosion on pipelines and other machinery.

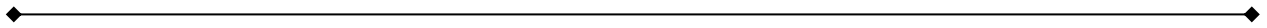
Additionally, we compared DLS and ζ -potential of RW with the measurements of the magnetite-base materials previously synthesized, we correlated their behavior previous to their mutual interaction (RW and magnetic material) where we expect that the presence of ionic species in RW can be absorbed using of magnetite-base materials.

With all these measurements and comparisons we presume to evaluate the electrostatic interaction between magnetic materials for RW alkalinity and hardness removal.

3.7 References

- (1) The world bank. *Water Resources and Environment Technical Note F.3*; DAVIS, R., HIRJI, R., Eds.; The International Bank for Reconstruction and Development/The world bank, 2003, pp 8-19
- (2) Comisión Nacional del agua. *Estadísticas Del Agua En México, Edición 2018*; Secretaría de Medio Ambiente y Recursos Naturales: Ciudad de México, México, 2018.
- (3) Secretaria de medio ambiente y recurzos naturales (SEMARNAT). Disponibilidad del agua https://apps1.semarnat.gob.mx:8443/dgeia/informe_12/pdf/Cap6_agua.pdf. (Accessed May 23 2021)
- (4) Garrido-Cárdenas, J.; Esteban-García, B.; Agüera, A.; Sánchez Pérez, J. A.; Manzano-Agugliaro, F. Wastewater Treatment by Advanced Oxidation Process and Their Worldwide Research Trends. *Int. J. Environ. Res. Public Health* **2019**, *17*, 170.
- (5) Salgot, M.; Folch, M. Wastewater Treatment and Water Reuse. *Curr. Opin. Environ. Sci. Heal.* **2018**, *2*, 64–74.
- (6) Wu, L.; Chen, W.; French, C.; Chang, A. C. *Safe Application of Reclaimed Water Reuse in the Southwestern United States*; UCANR Publications, USA 2009; pp 1-9
- (7) Maheshwari, B.; Singh, V.; Thoradeniya, B. *Balanced Urban Development: Options and Strategies for Liveable Cities*; Springer Open; College Station, TX , USA, 2016, pp 261-339.
- (8) U.S. Environmental Protection Agency. *2012 Guidelines for Water Reuse*; Washington, D.C., 2012, pp 37-251
- (9) Escalante Estrada, V. E. *Reúso Del Agua Residual En México*, Curso inte.; Instituto Mexicano de Tecnología del Agua: Morelos: Morelos, México, 2004, pp 249-282.
- (10) Dirección de Recursos Hídricos de Tucumán. Calidad del Agua <http://www.recursohidricos.gov.ar/webback/index.php/nuestra-funcion/2017-03-23-14-12-06/calidad-de-agua> (accessed May 3, 2021).

-
- (11) United States Environmental Protection Agency, E. Total Alkalinity
<https://archive.epa.gov/water/archive/web/html/vms510.html>. (accessed May 3, 2021).
- (12) U.S. Environmental Protection Agency. *Quality Criteria for Water*, 1st edition.; U.S. Environmental protection agency: Washington, D.C., 1976, pp 1-136.
- (13) Anim-Mensah, A. R.; Krantz, W. B.; Govind, R. Studies on Polymeric Nanofiltration-Based Water Softening and the Effect of Anion Properties on the Softening Process. *Eur. Polym. J.* **2008**, *44*, 2244–2252.
- (14) Entezari, M. H.; Tahmasbi, M. Water Softening by Combination of Ultrasound and Ion Exchange. *Ultrason. Sonochem.* **2009**, *16*, 356–360.
- (15) Yildiz, E.; Nuhoglu, A.; Keskinler, B.; Akay, G.; Farizoglu, B. Water Softening in a Crossflow Membrane Reactor. *Desalination* **2003**, *15*, 139–152.
- (16) Felber, S. Water Hardness. In *Water fundamentals handbook*; DRI-STEEM Corporation: Minesota, USA, 2017, pp 7-14.
- (17) Bodzek, M.; Koter, S.; Wesółowska, K. Application of Membrane Techniques in a Water Softening Process. *Desalination* **2002**, *145*, 321–327.
- (18) Mealy, R.; Bowman, G. *Importance of General Chemistry Relationships in Water Treatment*; Wisconsin, USA, 2014, pp 10-24
- (19) Crittenden, J. C.; Trussell, R. R.; Hand, D. W.; Howe, K. J.; Tchobanoglous, G. *MWH's Water Treatment: Principles and Design*; John Wiley & Sons, Hoboken, New Jersey, 2012, pp 1117-1481.
- (20) McDonald, J. Alkalinity & pH relationships
<http://www.veoliawatertech.com/crownsolutions/ressources/documents/2/21951,Water-pp393-394.pdf> (accessed Sep 17, 2020).
- (21) Haach. *Alkalinity for Water, Wastewater and Seawater*; New Zeland, 2020.



Chapter IV

Reclaimed water treatment with functionalized magnetic nanoparticles

4.1 Introduction

While the worldwide concern for the development of new wastewater treatment technologies that allow their recovery and use for other purposes, nanotechnology provides new alternatives to be implemented alone or in conjunction with the traditional water treatment techniques.

Among all nanotechnologies available, the utilization of iron-oxide nanomaterials has received much attention due to their unique properties and advantages that could help in water treatment and making the separation process more efficient.

The principal process to remove contaminants from water using magnetite nanoparticles is mainly by adsorption (as nano-adsorbent), where various types of interactions can take place between the nanoparticles and the contaminants in the water.

New advances in magnetic nanoparticles are needed to keep developing the next generation of nano-adsorption systems that could potentially be applied to many different water types depending on the needs of their future application.

In this chapter, we will address the nano-adsorption capabilities of magnetite nanoparticles and their functionalization with organic molecules to treat reclaimed water. We will focus on the change of the physicochemical properties of this water along with the improvement of its quality parameters (alkalinity and hardness). Finally, we will study the recovered nano-adsorbents to evaluate the changes in their mass and surfaces and determine if these materials can remove the targeted contaminants from water.

4.2 Justification and objectives

4.2.1 Justification

Nanomaterials have been suggested as an efficient, cost-effective, and environmentally friendly alternative to existing treatment materials, where magnetite nanoparticles excel for their enhanced removal efficiency, adaptability to different types of pollutants, and practicality.

Nevertheless, more studies are needed about unconventional contaminants and water conditioning for different reuse purposes using new functionalized magnetic nanoparticles.

4.2.2 General Objective

Study the adsorption capacity of magnetites as Ca^{2+} and Mg^{2+} captors in the softening of RW.

4.2.2.1 Specific objectives

- Study the physicochemical interaction between a magnetite-base nanoparticle (MNP, MND, MCH, and MCCH) and RW, using DLS and ζ -potential.
- Study the physicochemical properties of the RW after being treated with magnetic nanoparticles (MNP, MND, MCH, and MCCH) and their alkalinity and hardness removal.

4.3 Background

4.3.1 Wastewater treatment process

According to the Official Mexican Standard (NOM) NOM-001-SEMARNAT-1996, wastewater is defined as water of varied composition from discharges of municipal, industrial, commercial, service, agricultural, livestock, and domestic residues, and in general of any other use, as well as the mixture of them.¹

Wastewater discharges are classified as (i) municipal, those generated in population centers and collected in urban sewerage systems; and (ii) non-municipal, generated by other uses (such as self-supplied industry) and which are discharged directly into national water bodies.²

There are two main objectives when treating wastewater:³

- 1) Clean up as many settlements as possible by safely disposing of the collected wastewater into the environment after treatment, thus meeting the disposal regulations of each region (this objective is the most common).
- 2) Reuse these treated waters for different activities.

Wastewater treatment systems tend to copy natural, biological, physical, and chemical processes. Conventional water treatment includes coagulation and flocculation, sedimentation, filtration, adsorption, and disinfection. These are physical-chemical processes that eliminate turbidity, organic matter, and pathogens.⁴ There are four stages in the water treatment process:⁵

I. Pre-treatment: it is a physical treatment where solids contained in the wastewater are removed through bars and detanglers.

II. Primary treatment: can be both physical and physicochemical; it is carried out in sedimentation tanks to remove part of the contaminants as sludge at the bottom of the tanks. The sludge can be further processed for other use.

III. Secondary treatment: it is a biological treatment where bacteria are used to consume another part of the contaminants that were not removed with the primary treatment. Aeration (incorporation of oxygen/air into the water) is used to aid bacterial growth.

IV. Advanced treatment: it is used after the previous treatments to eliminate nutrients that help the growth of aquatic flora (algae and lilies) such as phosphorus and ammonia, using techniques such as filtration (through granular materials of various types and sizes) and disinfection (using chlorine or ultraviolet rays).

Examples of common treatment train processes are presented in Figure 4.1

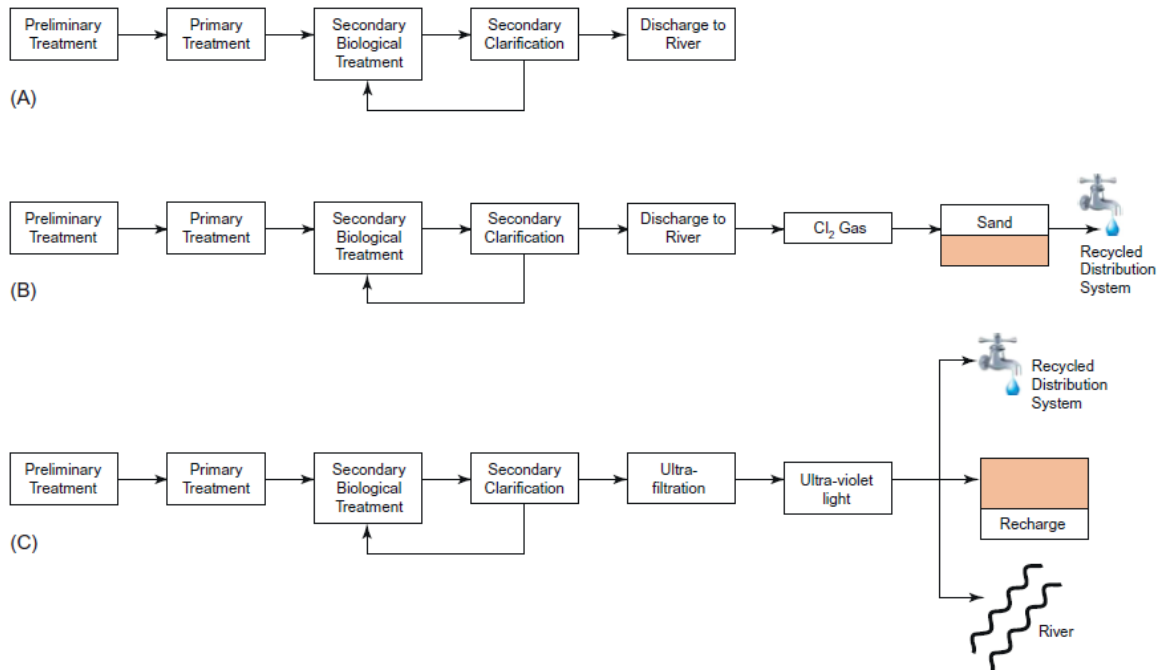


Figure 4.1 Wastewater treatment trains. (A) Preliminary treatment: screening of debris. Primary treatment: physical treatment. Secondary treatment: biological treatment via aerobic microbial degradation of organic matter. Secondary clarification: biological floc settles out as secondary sludge. Discharge: secondary effluent is discharged to the river. (B) Similar to treatment train (A) but with the addition of disinfection via chlorine gas and sand filtration to remove particulates before distribution for irrigation. (C) Advanced treatment: utilizes ultrafiltration to remove particulates and ultraviolet light for water disinfection before discharge for irrigation, groundwater recharge, or surface water.

It is necessary to consider that the purpose of nutrient elimination is to finally dispose of legally treated wastewater and comply with the regulations, and reclamation purpose is to guarantee that reclaimed water has enough quality to be safely and legally reused.³

By taking factors such as regulations, water quality of the wastewater effluent, water quality goals, end uses of the treated water, and public influence, the designed treatment process can be matched with the intended use without expending unnecessary funds or energy meanwhile minimizing other environmental and social costs. Therefore, the concept of “Fit for

Purpose” emphasizes the efficiencies realized by designing reuse for specific end applications, as can be seen in Figure 4.2.⁶

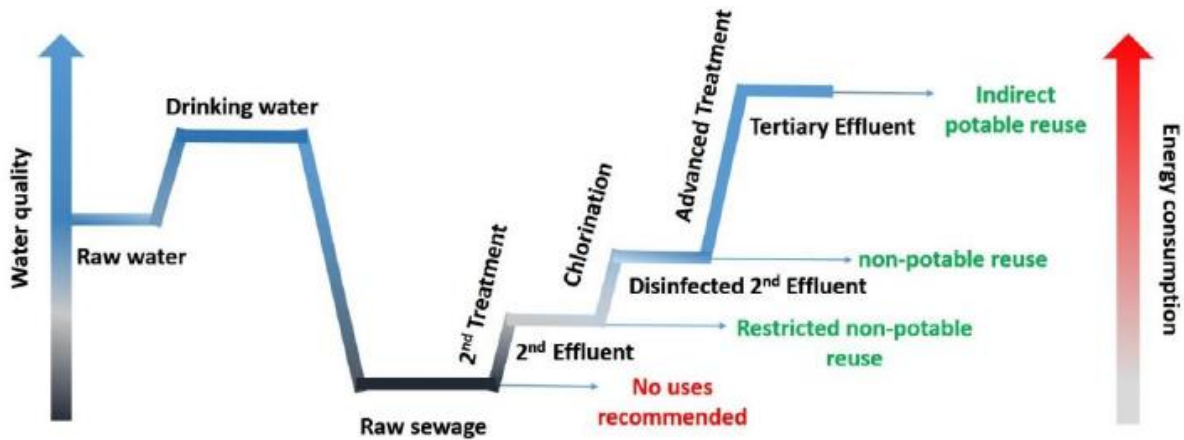


Figure 4.2 Fit for Purpose - Treat the wastewater for potential uses (adapted from 2012 US EPA Guidelines for Water Reuse).⁶

4.3.2 RW treatment strategies

There are three main types of reclamation treatment considered:³

- a) Secondary treatments capable of obtaining water suitable for reuse
- b) Tertiary treatments without disinfection, with an end-product allowing reuse
- c) Full tertiary treatments, including pre-treatment for disinfection and disinfection

It is important to realize that higher forms of treatment always include the lower; therefore, tertiary treatment is always preceded by primary and secondary treatment, as advanced treatment is always preceded by primary, secondary, and tertiary treatment. Usual reclamation technologies for advanced treatment of secondary wastewater (not exhaustive) before disinfection are described in Table 4.1.

When reusing RW, disinfection is basic since one of the main legal, compulsory limitations of this practice is the microbiological quality. The technologies previously employed are mainly used for preparing the water to be easily disinfected. The main disinfection technologies used for the reclamation/reuse systems are shown in Table 4.2.

The selection of the technology to be used in a wastewater treatment facility relies on many circumstances, but in general, high-tech facilities are more suitable for large cities, and systems that rely on natural technologies are more suitable for small towns and villages.³ The

latest in water reuse/recycling technology is not so much the technology itself but how that technology is being applied.

Table 4.1 RW technologies for secondary treatment of wastewater.³

| Type | Technology | Comments |
|--------------------------------|---|---|
| Physical | Additional settling | Maturation lagoons, settlers... |
| | Coagulation–flocculation | Reactive should be added. Stirring is necessary for a good mixing. Needs a settling step |
| | Filtration | Membrane technologies (nano and ultrafiltration, reverse osmosis), extensive systems with filtering materials (sand, organic matter, coal, multilayer filters...) |
| Chemical (not disinfection) | Desalination | Usually membrane technologies (reverse osmosis, electrodialysis reversal) |
| | Coagulation–flocculation | Reactive should be added. Stirring is necessary. Needs a settling step |
| | Fixed biofilms technologies (e.g. wetlands, infiltration-percolation) | Transformation of nutrients (mainly N forms), chemicals and organic matter (depending on the redox conditions) |
| Microbiological | Maturation lagoons | Settling, algae can grow at big pace |
| | Extensive systems (apart from lagooning) | Surface and in-depth filtration in systems with sand, soil, substrate... Active role of fixed biofilms. Transformation of N forms depending on the aerobic, anoxic, or anaerobic conditions |
| Combined system | MBR (Membrane Biological Reactors) | Combines a classical activated sludge (biological reactor) and in the same tank a membrane to separate activated sludge flocs) |

Table 4.2 Disinfection technologies used for the RW systems.³

| Technology | Variations | Observations |
|------------------------------|---|--|
| Physical | Ultraviolet radiation (UV) | Multiple lamp systems are recommended for wastewater disinfection. The lamps should be changed after the end of their theoretical lifespan. Not useful with high turbidity |
| | Gamma radiation | Rarely employed in Europe. Not used for wastewater treatment and reclamation at small scale |
| | Membrane-based technologies | Several types, the pore diameter defines the disinfection capacity. Ultrafiltration and nanofiltration as well as reverse osmosis are the main technologies quoted. Could not be useful after some natural systems because of the high contents of algae or suspended solids |
| Chemical | Chlorination (several types) | The most used technology. Residual action is its most important feature. Also used in combination with other technologies, mainly UV. By-products generation while reacting with organic matter and other pollutants |
| | Peracetic acid (PAA) | Used to be expensive, the price was reduced and is gaining market. No by-products |
| | Ozone | Not used after extensive treatments and for small facilities. Expensive technology difficult to manage |
| Other | Additional lagooning (maturation) systems | The natural UV radiation disinfects. Other processes are natural die-off, predation... It is necessary to eliminate algae after this treatment |
| | Constructed wetlands, infiltration-percolation... | Use of soil/biofilms disinfection capacity as well as filtration capacity (organisms associated with the solids) |
| Combinations of technologies | UV-chlorination is the classical example. Also membranes + chlorination ... | UV acts eliminating pathogens and chlorine is used for final elimination and for maintaining a residual disinfection capacity |

Taking into consideration the key unit processes and operations used in water reclamation, an almost endless number of treatment process flow diagrams can be developed to meet the water quality requirements of a certain reuse application (Figure 4.3).⁷

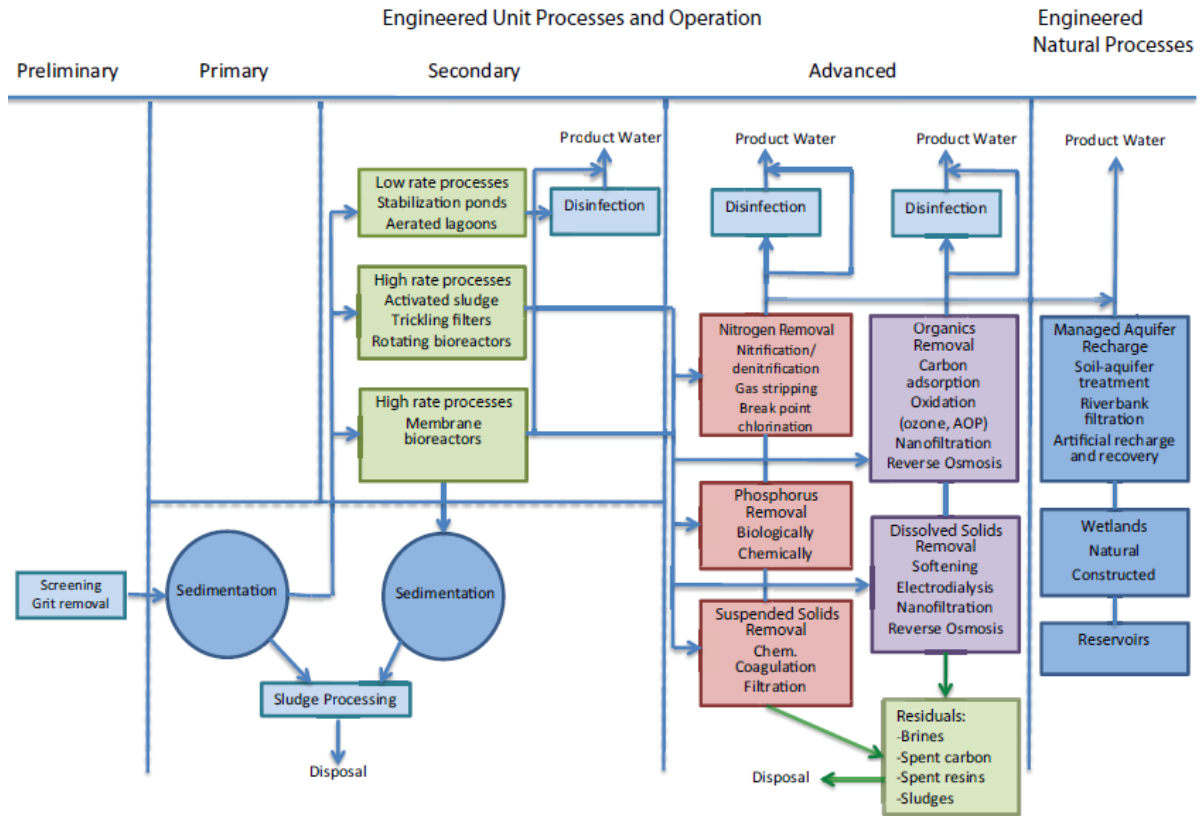


Figure 4.3 Treatment processes commonly used in water reclamation.⁷

4.3.3 Advanced engineered treatment

Advanced treatment plays a critical role in the effective treatment of municipal and industrial wastewater to meet water quality objectives for water reuse and to protect public health. Modern engineered unit processes and operations are arranged into engineering systems targeting the removal of nutrients, organic constituents, reduction of total dissolved solids (TDS) or salinity, and additional treatment barriers to pathogens. Nutrients can be reduced through biological nitrification or denitrification processes, gas stripping, chemical precipitation, and breakpoint chlorination. Organic constituents can be further eliminated using a broad of advanced processes that include activated carbon, nanofiltration (NF), reverse osmosis (RO),

and chemical oxidation (ozone, advanced oxidation processes [AOPs]). Dissolved solids are maintained during softening, electro dialysis, NF, and RO.⁷

As mentioned before, after conventional biological treatment processes, tertiary or advanced treatment can be applied, some conventional treatments are discussed below.

4.3.3.1 Adsorption

Adsorption is a mass transfer process in which substances present in a liquid phase are adsorbed or accumulated on a solid phase and thus removed from the liquid and is mainly used for the removal of taste- and odor-causing compounds, synthetic organic chemicals, color-forming organics, and disinfection of by-product precursors. Other Inorganic constituents that could represent a health hazard (such as perchlorate, arsenic, and some heavy metals) are also removed by adsorption.⁸

Adsorption involves the movement of contaminants from solution to the soil particles where the constituent that undergoes adsorption onto a surface is called adsorbate, and the solid onto which the constituent is adsorbed is referred to as the adsorbent. During the adsorption process, dissolved species are transported into the porous solid adsorbent granule by diffusion and are then adsorbed onto the extensive inner surface of the adsorbent.^{8,9}

Dissolved species are concentrated on the solid surface either for a chemical reaction (chemisorption) or physical attraction (physical adsorption) to the surface. Physical adsorption is the most common mechanism by which adsorbates are removed in water treatment. It is a rapid process caused by nonspecific binding mechanisms such as van der Waals forces and it is reversible, which means that the adsorbate desorbs in response to a decrease in solution concentration. On the other hand, chemisorption is usually not reversible (because the adsorbate is chemically bonded to the surface), and desorption, if it occurs, is accompanied by a chemical change in the adsorbate.^{8,9} Physical adsorption and chemisorption mechanisms are listed in Table 4.3.

Three interactions compete when considering physical adsorption in aqueous solutions: (1) adsorbate–water interactions, (2) adsorbate–surface interactions, and (3) water–surface interactions. The extent of adsorption is determined by the strength of adsorbate–surface

interactions as compared to the adsorbate–water and water–surface interactions. Adsorbate–surface interactions are determined by surface chemistry, and adsorbate–water is related to the solubility of the adsorbate. Water–surface interactions are determined by the surface chemistry, for example, a graphitic surface is hydrophobic, and oxygen-containing functional groups are hydrophilic. For Water–surface interactions are determined by the surface chemistry.⁸ Some of the forces that occur between the adsorbent surface and adsorbates are illustrated in Figure 4.4.

Table 4.3 Comparison of adsorption mechanisms between physical adsorption and chemisorption.⁸

| Parameter | Physical Adsorption | Chemisorption |
|-------------------------|---|--|
| Use for water treatment | Most common type of adsorption mechanism | Rare in water treatment |
| Process speed | Limited by mass transfer | Variable |
| Type of bonding | Nonspecific binding mechanisms such as van der Waals forces, vapor condensation | Specific exchange of electrons, chemical bond at surface |
| Type of reaction | Reversible, exothermic | Typically nonreversible, exothermic |
| Heat of adsorption | 4–40 kJ/mol | >200 kJ/mol |

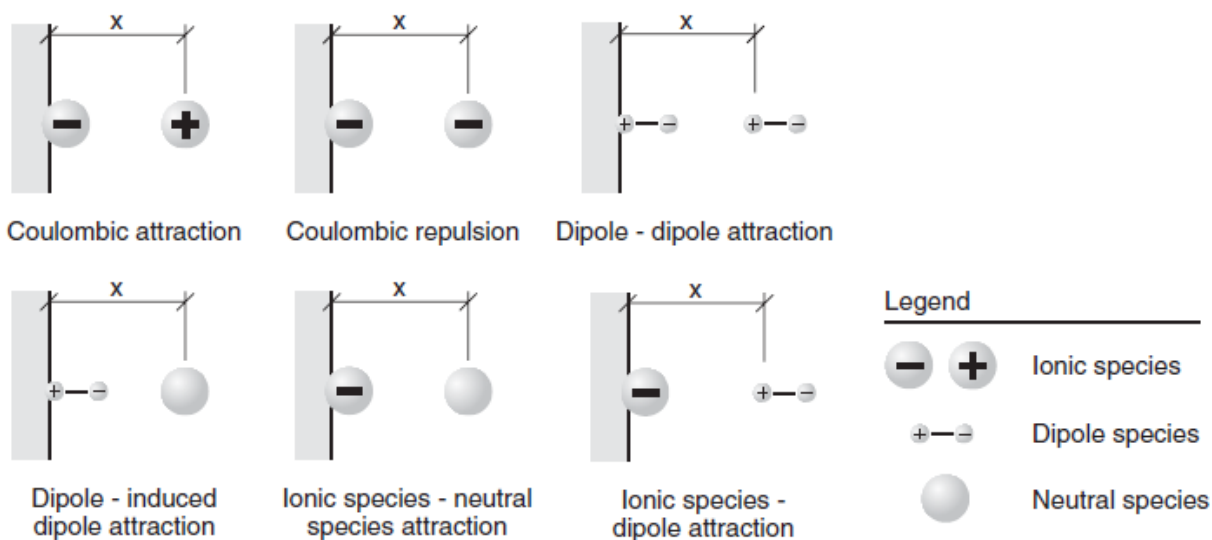


Figure 4.4 Surface functional groups and forces of attraction.

The interactions and forces mentioned above are not easily measurable, but in general, they can be related to some properties of the adsorbate and solvent. Solubility is a direct indication of adsorption strength or magnitude of the adsorption force, where the lower the

solubility of adsorbate in the solvent, the higher the adsorption strength. Therefore, adsorption strength is inversely proportional to solubility. Unfortunately, there are other factors for different classes of organics where solubility alone is not the only indicator of adsorbability. Polar, neutral, and charged compounds must be considered separately.⁸

The primary adsorbent materials used in the adsorption process are powdered activated carbon (PAC) and granular activated carbon (GAC). Activated carbon adsorption is effective in removing hydrophobic organic compounds from surface and groundwater sources. Compounds with low water solubilities, such as organic solvents and chlorinated organic solvents, are adsorbable because of their low water solubility. Water-soluble compounds and larger compounds are better removed by oxidation or ultrafiltration.^{8,10}

4.3.3.2 Reverse osmosis (RO)

Osmosis is the process by which a solvent passes through a semi-permeable membrane, from a dilute solution to a concentrated solution, until the difference in concentrations on both sides of the membrane is equalized (ionic balance). The pressure required for this phenomenon to occur is known as osmotic pressure.¹¹

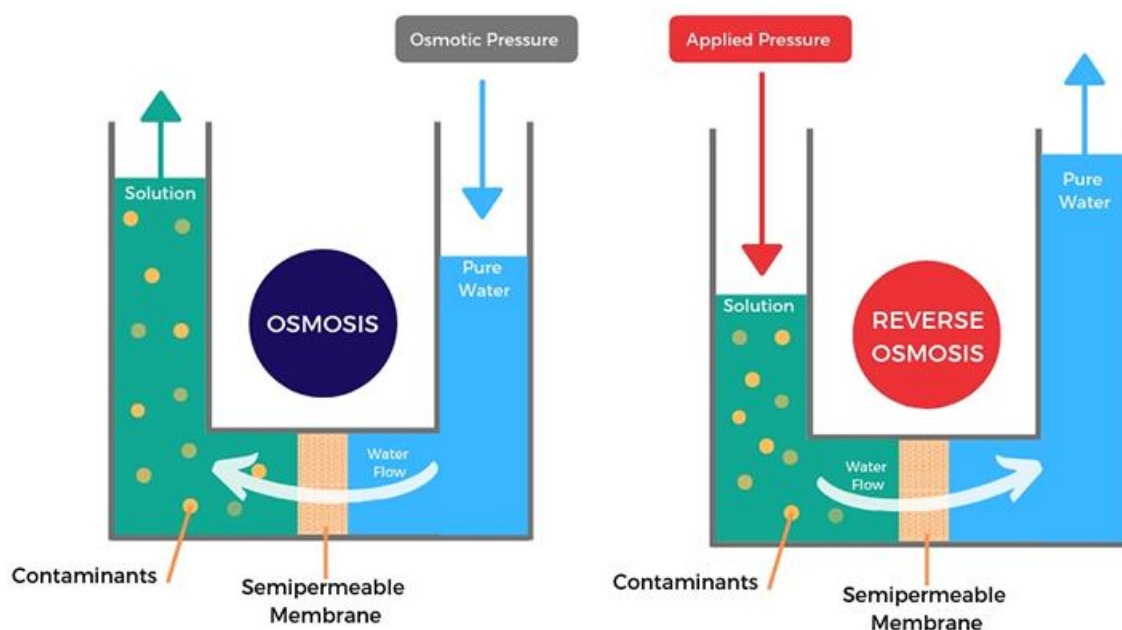


Figure 4.5 Osmosis and reverse osmosis process diagram.¹²

RO is the opposite process of osmosis, where a solvent is transferred through a semi-permeable membrane from a concentrated solution to a dilute solution. In this case, it is necessary to overcome the osmotic pressure to make the solution flow through the membrane with a pushing force greater than the osmotic pressure in the opposite direction to the osmosis process (Figure 4.5), consequently, a pump is needed.^{8,11,13}

Thus, RO is a membrane water treatment process that is used to separate dissolved solutes. An ordinary RO membrane is made of semi-permeable synthetic material, permeable to some components in the feed stream and impermeable to other components and with a thickness less than 1 mm. Water is pumped under high pressure through the membrane surface, which causes a part of the water to pass through the membrane. As shown in Figure 4.6, the water that passes through the membrane (permeate) is relatively free of specific dissolved solutes, while the remaining water (concentrate) goes out at the other end of the pressured vessel.^{8,13}

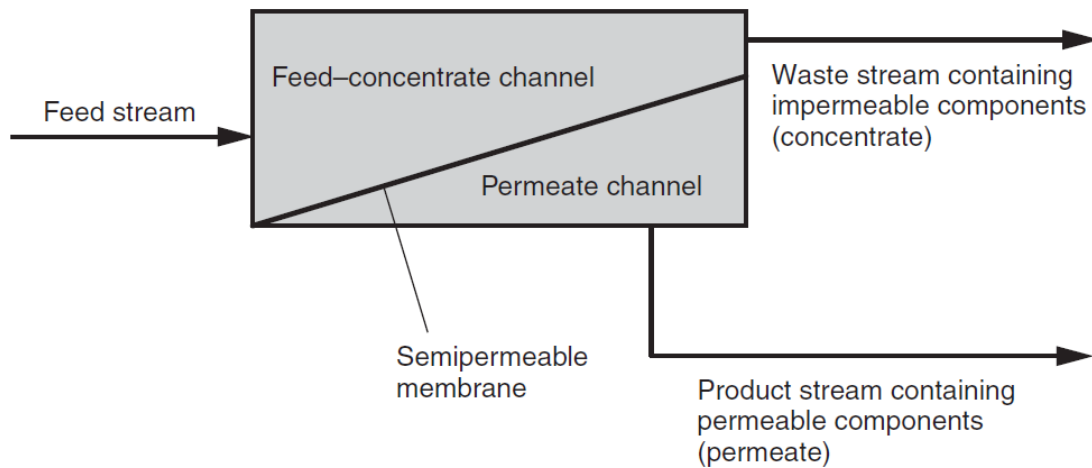


Figure 4.6 Separation process through reverse osmosis membrane.⁸

RO's ability to remove contaminants from water, including many synthetic organic chemicals, has increased interest in incorporating RO into wastewater treatment process trains as an advanced treatment process. The uses of reverse osmosis in water treatment and alternative processes are listed in Table 4.4, ranging from seawater desalination, advanced treatment for water reuse, softening, removal of natural organic matter (*NOM*) to control the formation of disinfection by-products (*DBP*), up to the elimination of specific contaminants.

Table 4.4 Reverse osmosis objectives and alternative processes.⁸

| Process Objective | Membrane Process Name | Alternative Processes |
|---|-------------------------------|---|
| Ocean or seawater desalination | High-pressure RO, seawater RO | Multistage flash (MSF) distillation, multi-effect distillation (MED), vapor compression distillation (VCD) |
| Brackish water desalination | RO, low-pressure RO, NF | Multistage flash distillation, ^a multi-effect distillation, ^a vapor compression, ^a electrodialysis, electrodialysis reversal |
| Softening | Membrane softening, NF | Lime softening, ion exchange |
| NOM removal for DBP control | NF | Enhanced coagulation/softening, GAC |
| Specific contaminant removal ^b | RO | Ion exchange, activated alumina, coagulation, lime softening, electrodialysis, electrodialysis reversal |
| Water reuse | RO | Advanced oxidation |
| High-purity process water | RO | Ion exchange, distillation |

4.3.3.3 Ion Exchange

Ion exchange is a chemical process used to remove unwanted dissolved ionic components, which are exchanged for other ions of similar charge. In water treatment applications, ion exchange is mainly used to soften and demineralize water, for example, to remove Ca^{2+} , Mg^{2+} , Na^+ , Cl^- , SO_4^{2-} , NO_3^- ,⁸ and to a lesser extent for barium, radium, arsenic, perchlorate, chromate, and other heavy metals.¹⁴

The processes that use ion exchange are the following:¹⁵

- ❖ Water softening (removal of hardness)
- ❖ Dealkalization (remove carbonates)
- ❖ Decationization (removal of all cations)
- ❖ Demineralization (removal of all ions)
- ❖ Mixed bed (Nitrates and demineralization)
- ❖ Metal removal

Ion exchange involves the exchange of an ion in the solid phase and an ion in the aqueous phase. The solid phase (exchangers) is insoluble and can be either of natural origin (kaolinite and montmorillonite minerals) or of synthetic origin (polymeric resin).^{8,15}

These exchangers have fixed charged functional groups (either positively or negatively) located on their external and/or internal surfaces (Figure 4.7). In addition, there is the presence of other ions of opposite charge called "counterions" that are associated with each functional group by electrostatic attraction. Depending on the charge of the functional group in the exchanger the counterion can be a cation (if the functional group is negative) or an anion (if the functional group is positive), thus fulfilling the electroneutrality criteria within the exchange material as in the aqueous solution, granting it the ability to be exchanged with another counterion in the aqueous phase.⁸

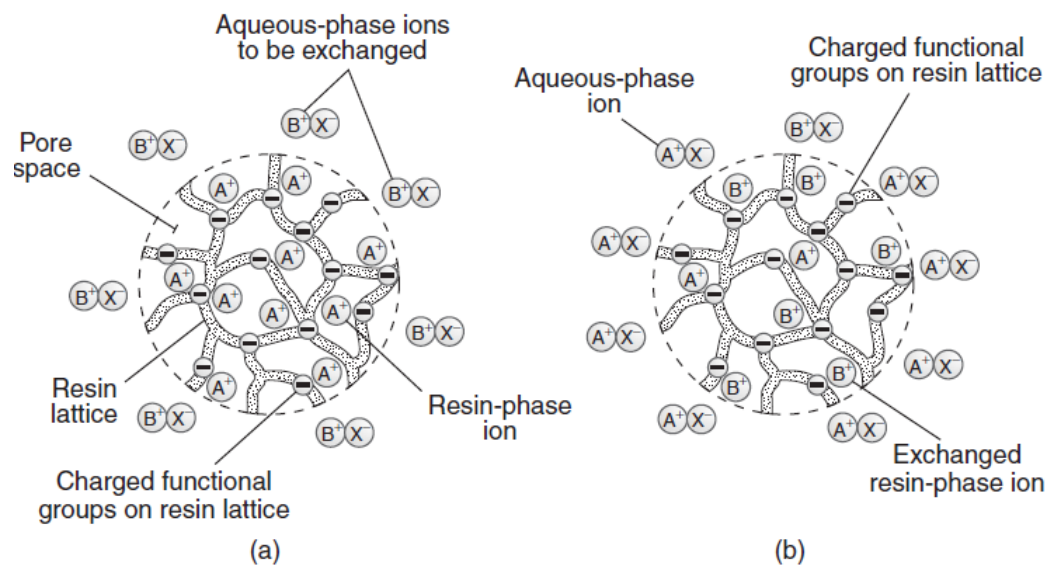


Figure 4.7 Schematic framework of functional cation exchange resin: (a) resin initially immersed in an aqueous solution containing B^+ cations and X^- anions and (b) cation exchange resin in equilibrium with an aqueous solution of B^+ cations and X^- anions.⁸

According to the functional groups attached to the structure of the resin, exchange resins are classified into four general types, which are: (1) strong acid cation (SAC), (2) weak acid cation (WAC), (3) strong base anion (SBA) and (4) weak base anion (WBA).^{8,15} Their differences are based on the pKa of their functional groups, in Table 4.5 we find a summary of their main characteristics and properties in their application in water treatment.

Although ion exchange is presented as a cheaper-based methodology and as a low-cost alternative for treating high alkalinity water,¹⁶ its application in municipal systems has been limited. The ion exchange process for water treatment is considered an unconventional process

since it is not widely used in large-scale plants due to its lack of selectivity and high sensitivity to the pH of the solution. Therefore, several companies choose to use RO, then adding the necessary salts to obtain the equilibrium composition.^{8,16}

Table 4.5 Characteristics of ion exchange resins used in water treatment processes.⁸

| Resin Type | Acronym | Fundamental Reaction ^a | Regenerant Ions (X) | pK | Exchange capacity meq/mL | Constituents removed |
|----------------------------|--------------------|---|------------------------------------|---------|--------------------------|---|
| Strong-acid cation | SAC | $n[RSO_3^-]X^+ + M^{n+} \rightleftharpoons [nRSO_3^-]M^{n+} + nX^+$ | H ⁺ or Na ⁺ | < 0 | 1.7-2.1 | H ⁺ form: any cation; Na ⁺ form: divalent cations |
| Weak-acid cation | WAK | $n[R(COO^-)]X^+ + M^{n+} \rightleftharpoons [nR(COO^-)]M^{n+} + nX^+$ | H ⁺ | 4-5 | 4-4.5 | Divalent cations first, then monovalent cations until alkalinity is consumed |
| Strong-base anion (type 1) | SBA-1 ^b | $n[R(CH_3)_3N^+]X^- + A^{n-} \rightleftharpoons [nR(CH_3)_3N^+]A^{n-} + nX^-$ | OH ⁻ or Cl ⁻ | > 13 | 1-1.4 | OH ⁻ form: any anion; Cl ⁻ form: sulfate, nitrate, perchlorate, etc. |
| ng-base anion (type 2) | SBA-2 ^c | $n[R(CH_3)_2(CH_3CH_2OH)N^+]X^- + A^{n-} \rightleftharpoons [nR(CH_3)_2(CH_3CH_2OH)N^+]A^{n-} + nX^-$ | OH ⁻ or Cl ⁻ | > 13 | 2-2.5 | OH ⁻ form: any anion; Cl ⁻ form: sulfate, nitrate, perchlorate, etc. |
| Weak-base anion | WBA | $n[R(CH_3)_2N]HX + HA \rightleftharpoons [nR(CH_3)_2N]HA + HX$ | Cl ⁻ | 5.7-7.3 | 2-3 | Divalent anions first, then monovalent anions until strong acid is consumed |

^aTerm within brackets represents the solid phase of the resin.

^bGreater regeneration efficiency and capacity than SBA-2.

^cGreater chemical stability than SBA-1.

4.3.3.4 Advanced Oxidation

Some water supplies, besides containing high amounts of alkalinity and hardness, may contain toxic synthetic organic compounds (SOC) that must be removed to protect public health. These chemicals include agricultural pesticides, herbicides, fuels, solvents, human and veterinary drugs, and other potential endocrine disruptors.⁸

Given the uncertainty of the toxicity of chemical oxidation by-products, any oxidation process used to remove these compounds must completely oxidize SOCs to carbon dioxide, water, and mineral acids. Three types of oxidation processes are used in water treatment to help solve the SOC problem:⁸

- 1) Conventional chemical oxidation
- 2) Oxidation processes carried out at high temperatures and/or pressures
- 3) Advanced oxidation processes (AOPs)

Conventional chemical oxidation processes use oxidants such as chlorine, chlorine dioxide, and potassium permanganate, these processes do not produce highly reactive species such as the hydroxyl radical (HO•), which is produced in the other two types of oxidation processes. The "dot" written as part of the hydroxyl and other radical species indicates that the outer orbital has an unpaired electron. Hydroxyl radicals are reactive electrophiles that readily react with most organic compounds by double bond addition reactions or by extracting hydrogen atoms from organic compounds.^{8,17}

Reaction rates of conventional oxidants are slower and selective than the ones involving HO•, in terms of the types of organic molecules they oxidize. Oxidation processes carried out at high temperatures and/or pressures such as wet oxidation, supercritical oxidation, gas-phase combustion, and catalytic oxidation processes can oxidize organic matter by free radical reactions involving HO•. In advanced oxidation processes (AOP), HO• radicals are generated at room temperature and atmospheric pressure.

AOPs have some inherent advantages over other processes such as:⁸

- (i) Contaminants can be completely destroyed
- (ii) Contaminants that are not adsorbable, or volatile can be wrecked
- (iii) Unlike mass transfer processes (like adsorption or extraction), that only transfer the contaminant to another phase, they don't often require additional treatment

The above-mentioned makes AOPs efficient methods for water treatment that allow the total or partial elimination of compounds resistant to conventional treatments, the reduction of toxicity, or the destruction of pathogenic microorganisms.¹⁷

HO• formed in AOP react mainly through hydrogen abstraction (equation 1), electrophilic addition to π -systems (equation 2), and electron transfer reactions (equation 3):¹⁷



Other reactive oxygen species (ROS) such as HO•, O₂•⁻/HO²•, H₂O₂ are also formed contributing to redox. Depending on the physicochemical process that leads to the formation of these species, AOPs can be classified as non-photochemical and photochemical processes, where photochemical processes are widely used.¹⁷ The most common AOPs of these classifications are listed in Table 4.6.

Table 4.6 Advanced non-photochemical and photochemical oxidation processes.¹⁷

| Non-Photochemical Processes | Photochemical Processes | |
|---|--|-------------------------------------|
| | Type of Process | Irradiation Wavelength Range (λ/nm) |
| Alkaline ozonation (O ₃ /HO ⁻) | Water photolysis in vacuum ultraviolet (VUV) | <190 |
| Ozonation with hydrogen peroxide (O ₃ /H ₂ O ₂) | UV/hydrogen peroxide (UV/H ₂ O ₂) | < 280 |
| Fenton and related processes (Fe ²⁺ /H ₂ O ₂) | UV/ozone (UV/O ₃) | 280-315 |
| Electrochemical oxidation | Photo-Fenton (PF) and related processes | UV-Vis up to 450 |
| γ-Radiolysis and electron-beam treatment | Zerovalent iron plus UV light | Rango UV |
| Non-thermal plasma (surface corona discharge) | Heterogeneous photocatalysis (HP) using TiO ₂ | UV: up to 380-400 |
| Electrohydraulic discharge-ultrasound (US, cavitation) | | |
| Wet air oxidation | | |
| Supercritical water oxidation | | |
| Zerovalent iron (ZVI) | | |
| Ferrate | | |

Another way to classify AOPs is on the type of wastewater in which it is used and the target compounds within each one. Fenton and Assisted Fenton processes are applied in the industrial wastewater from different sectors to remove dyes, reduce chemical oxygen demand (COD), and various persistent organic pollutants. Among radiation-based AOPs, heterogeneous photocatalysis (TiO₂) has been studied extensively for industrial wastewater treatment. Although, hydrogen peroxide-based treatments such as photo-Fenton and H₂O/UVC attracted attention in municipal wastewater applications to remove micropollutants and disinfection of water and wastewater.¹⁷ The aforementioned is listed in detail in Table 4.7.

Table 4.7 Summary of different advanced oxidation processes (AOP) associated with wastewater and target compounds.¹⁸

| AOP Treatments | Wastewater | Targets |
|---|---|---|
| Ozone, ozone/UV, TiO ₂ | Hospital, olive mill, petroleum refinery | Pharmaceuticals, bacteria |
| Electrochemical, H ₂ O ₂ /UV, heterogeneous photocatalysis, TiO ₂ | Textile industrial, paper industrial | Bisphenol a, formaldehyde, lignin, pharmaceuticals, pesticides, antibiotic resistant bacteria, endocrine disruptors |
| Fenton | Coking, textile, paper industrial, oil refinery, winery | Endocrine disruptors, acetaminophen, colors, COD |
| Electro-Fenton, anodic oxidation, sonoelectrochemistry | Industrial textile, petrochemical | Organic pollutants, organic matter, dyes |
| TiO ₂ , Fenton, photo-Fenton, UV | Livestock, winery, textile | Persistent organic pollutants |
| Electrolysis, Fenton, ozone, peroxy and peroxymonodisulfate, UV/persulfate, UV/H ₂ O ₂ , UV/TiO ₂ , Zero-valente ion | Saline | COD, 1,4-dioxane, atrazine, dyes |
| Electro Fenton, Fenton, microwave, ozonization, UV radiation, wet air oxidation | Dyeing | Phenols, heavy metals |
| Cavitation, ionizing radiation | Oily | Emerging contaminants, azo dyes |
| H ₂ O ₂ , photo-Fenton, UV, | Slaughterhouse, urban | E. coli, pharmaceuticals, COD |
| Ozonation, UV/Fenton | Municipal | Pharmaceuticals |
| H ₂ O ₂ , UV, UV/H ₂ O ₂ | Textile | Pesticides, nitrate, nitrite, dyes |
| Ultrasound, hydrodynamic cavitation, Fenton, photo-Fenton, TiO ₂ | Pharmaceutical | Paracetamol, phenol |
| Fenton, sonolysis, ultrasonic radiation | Papermaking | Herbicides, organic pollutant, COD |
| Solar irradiation | Drinking, tannery | COD, dyes |
| Ozonation | Drinking, tannery | Phenol, COD |

On some occasions, more than one AOP can be used for one type of wastewater, but only some of the commercially available AOPs can be considered for large-scale water treatment, such as: (1) ozone and hydrogen peroxide, (2) UV light and ozone, (3) UV light and hydrogen peroxide, (4) UV light and titanium dioxide, and (5) combinations of the aforementioned technologies.¹⁸

Another unwanted side-effect with AOP's (and processes that use ozone) is the production of brominated and bromate by-products in waters that contain bromide ions. In addition, another issue with AOP's is that they present two common reactions of HO • with organic compounds. These are addition reactions with double bonds and extraction of hydrogen atoms, where the addition of double bonds is much faster than the abstraction of hydrogen. Both reactions produce reactive organic radicals that rapidly undergo subsequent oxidation and combine with dissolved

oxygen to form peroxy organic radicals (ROO •). The organic peroxy radicals bear radical chain reactions producing a variety of unwanted oxygenated by-products. The general oxidation pathway for AOPs is as follows: Organic contaminant → aldehydes → carboxylic acids → carbon dioxide and mineral acids.⁸

4.3.4 Opportunities for nanotechnology in water treatment

New treatment technologies are still in development to remove a wide range of challenging contaminants from wastewater and RW successfully. As the world deals with shrinking water resources, nanotechnology can be used and tailored to enhance various water treatment processes and recover water resources for all the possible reuses.

Examples include designing nanostructured photocatalysts with surface chemistries with bandgaps that enable selective binding and degradation of targeted contaminants, modify the morphology and surface area of electrodes using nanotube arrays or three-dimensional macroporous structures to improve kinetics and mass transfer in electrochemical oxidation; and controlling the size of magnetic nanoparticles to increase superparamagnetism for low-energy separation and recovery with magnet.¹⁹

Nanotechnology offers new opportunities to improve both basic and advanced water treatment processes. The incorporation of selective nanoadsorbents in conventional adsorption media (using small quantities) could enhance performance and extend the range of contaminants removed. Photocatalytic oxidation of priority organic pollutants can be strengthened by nanotechnology by engineering nanoparticles with high-index crystal facets or through surface modification. Additionally, membrane separation processes for water purification and desalination using nanoparticles can also modify the surface wettability of membranes, altering the surface energy and enabling new applications.¹⁹

Enhancing water reuse may require unprecedented versatility to tap unconventional sources of varying water quality and flow rate, as well as the flexibility to accommodate diverse treatment objectives for different intended uses. Several nanomaterials and technologies could be available for integration in adaptive modules, including selective adsorbents, rapid magnetic separation of heavy metals, and other inorganic pollutants using superparamagnetic

nanoparticles, among many others.¹⁹ Within this panorama, water treatment using magnetite nanoparticles will be addressed below.

4.3.4.1 Iron-oxide magnetic nanoparticles in water treatment

In recent years the interest in magnetic nanomaterials for water treatment purposes has been increasing. These nanomaterials are basically composed of a magnetic core of iron oxide coupled with organic compounds, carbon materials, etc. The usage of magnetic nanoparticles is advantageous since magnetism is a unique physical property that independently helps in water purification by influencing the physical properties of contaminants, making the separation of solid from liquid more efficient. Thus, adsorption procedures combined with magnetic separation have extensive applications in water treatment and environmental cleanup.^{20,21}

MNPs are promising for industrial-scale water treatment, due to their following advantages:^{20,21}

- ❖ Low cost
- ❖ Strong adsorption capacity
- ❖ Easy separation and enhanced stability
- ❖ Small size and thus high surface to volume ratio
- ❖ Solid/liquid separation through magnetic filtration is selective
- ❖ Faster than centrifugation and filtration techniques
- ❖ Reusability
- ❖ Biocompatibility
- ❖ Magnetic separation

MNP applications in contaminated water treatment can be divided into two categories:²⁰

- a) MNP as nano-adsorbent or immobilization carrier for improving removal efficiency (adsorptive/immobilization technologies)
- b) MNP as photocatalysts to break down/convert contaminants into a less toxic form (i.e. photocatalytic technologies).

However, some technologies may utilize both processes.

4.3.4.2 MNP as nano-adsorbents

Adsorption is a well-known separation process and has been widely applied to remove chemical pollutants from water (see section 4.3.3.1 Adsorption). As mentioned before, adsorption has numerous advantages in terms of cost, flexibility, simplicity of design/operation, and insensitivity to toxic pollutants. Therefore, an effective and low-cost adsorbent with high adsorption capacity for a wide range of pollutants removal is desirable. MNPs are being explored for contaminant adsorption, particularly for the efficient treatment of large-volume water samples and fast separation via employing a strong external magnetic field.²⁰

Currently, Magnetic nanoparticles are used as an adsorbent for the removal of various types of contaminants, since heavy metals, organic contaminants, dyes, ionic and anionic species, pharmaceutical products, and pathogens.²⁰⁻²²

The adsorption of contaminants takes place via surface exchange reactions until the surface functional sites are fully occupied, and thereafter contaminants could diffuse into adsorbent for further interactions with functional groups. Therefore, the modification and chemical treatment of MNP is essential to enhance the target adsorption capability, since modified MNP can not only improve their dispersed stability in solution but also decrease the irreversible adsorption of analytes, overcoming the desorption problem that carbon materials present.^{20,22} The use of functionalized MNP in water treatment for heavy metal removal is illustrated in Figure 4.8, but this work principle can be transferred to the removal of several contaminants-type mentioned above.

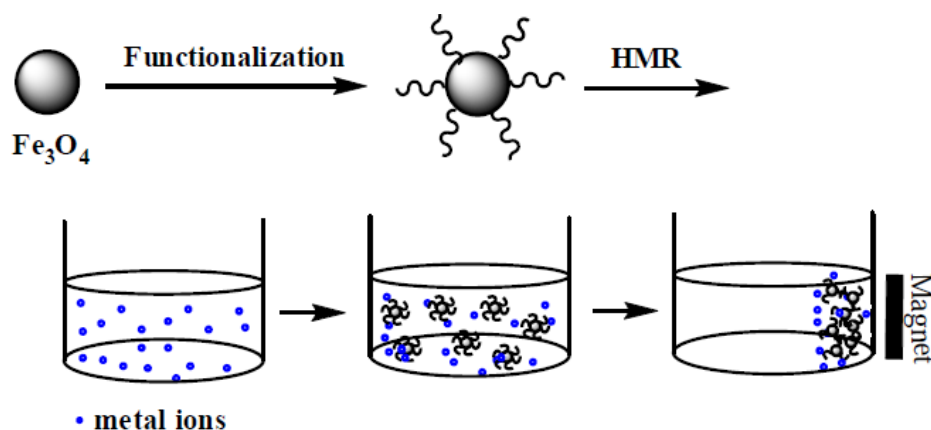


Figure 4.8 Scheme of the simplified process of magnetic nanoparticles used for heavy metal ions removal (HMR) in water treatment.²³

Adsorption mechanisms of contaminants from wastewater by modified MNP include electrostatic interaction, magnetic selective adsorption, surface site binding, and modified ligands combination. The addition of novel modification mechanisms to MNP can achieve high efficiency.²⁰

To summarize, a combination of the superior adsorption performance and magnetic properties of MNP is a promising approach to handle a variety of environmental problems. Advances in MNP will provide opportunities in developing next-generation adsorption systems with high capacity, easy separation, and extended lifecycles, and thus generate efficient and cost-effective remediation approaches in comparison with conventional technologies.^{20,21}

4.3.5 Hypothesis:

- ❖ The usage of magnetite-base nanoparticles will improve the quality of the RW (in terms of alkalinity and hardness)
- ❖ Functionalized MNP (MND, MCH, and MCCH) will show a better performance in RW conditioning than raw MNP.

4.4 Experimental and methods

4.4.1 Materials and reagents

- ❖ Sodium hydroxide (ACS reactive, $\geq 97.0\%$)
- ❖ Hydrochloric acid (ACS reactive, 37%)
- ❖ Alkalinity test kit, Hach
- ❖ Total hardness test kit, Hach

4.4.2 Equipment

- ❖ Analytical balance brand OHAUS model AV264
- ❖ Anton Paar Litesizer 500
- ❖ Horiba Laqua PC1100 Dual Channel pH/Ion Meter
- ❖ Shimadzu FT-IR, IRSpirit with ATR mode
- ❖ Optical microscope Chiron coupled to an Axio Vision webcam

4.4.3 Methodology

The RW was treated with iron-oxide magnetic nanoparticles and their modifications to study the improvement of the water quality in terms of alkalinity and hardness removal. This study was performed with RW at pH 7, 8, and 9. Briefly, magnetite or modified magnetite (MNP, MND, MCH, MCCH) was weighed and then placed into the RW sample at the pH previously adjusted (0.01 M of NaOH and HCl) in a dosage of 30 mg of magnetic material per liter of water. The solution was sonicated for 5 minutes, then settled into an orbital shaker for 10 minutes at 360 rpm. After this time, the nanoparticles were recovered using magnetic decantation. The water sample recovered was used to measure DLS and ζ -potential to know the new characteristics of the water. At the same time, alkalinity and hardness tests were performed to measure the percentage of removal of those parameters. Finally, the recovered magnetic nanoparticles were dried, weighed, and used to perform FT-IR analysis and to obtain optical microscope images, to corroborate the entrapment of calcium carbonate.

4.4.3.1 DLS characterization of treated RW

DLS was performed in an Anton Paar (Litesizer 500) to analyze the size of suspended particles present in the water samples from pH 7 to 9. The pH was adjusted with 0.1 M HCl to pH = 2 and 0.1 M NaOH .

4.4.3.2 ζ -potential characterization of treated RW

The physicochemical performance of treated RW was determined by Zeta Potential and pH measurements (7, 8, and 9) in an Anton Paar (Litesizer 500). The pH was adjusted with 0.1 M HCl and 0.1 M NaOH from pH 2 to pH 12.

4.4.3.3 Transmittance characterization of treated RW

Transmittance measurements were performed in different types of water (deionized, distilled, reclaimed, and treated reclaimed) in an Anton Paar (Litesizer 500) at pH 7.

4.4.3.4 Alkalinity test procedure for RW

Hach commercial kit was used to determine the alkalinity of the samples (treated RW) at three different pH values: 7, 8, and 9, following the standard titration procedure as described:

For the test, with a 50 mL sample of RW, we used H₂SO₄ 0.020 N as a titrant. A 25 mL burette was filled to the zero mark with the titrant. The sample was poured into a 250 mL Erlenmeyer flask, and the content of one phenolphthalein indicator powder pillow was added to the sample and swirled to mix. Since no change of color was observed, the content of one bromocresol green-methyl green indicator powder pillow was also added and swirled to mix. The flask was placed under the burette adding titrant swirling the flask until a change of color was observed from green to a light pink color. Finally, we multiplied the mL of titrant used by 20 to calculate the concentration in mg/L as CaCO₃ total alkalinity.

4.4.3.5 Total hardness test procedure for RW

Hach commercial kit was also used to determine the total hardness of treated RW at the pH values: 7, 8, and 9, following the standard titration procedure as follow:

The test was carried with a 50 mL sample of RW using EDTA 0.020 N as the titrant. A 25 mL burette was filled to the zero mark with the titrant. The sample was poured into a 250 mL Erlenmeyer flask, adding 1 mL of KOH 1 N (standard solution), and swirled to mix. The

content of one CalVer 2 calcium indicator powder pillow was added to the sample and swirled to mix. The flask was placed under the burette adding titrant swirling the flask until a change of color was observed from red to a pure blue color. Finally, we multiplied the mL of titrant used by 20 to calculate the concentration in mg/L of Ca as CaCO₃.

4.4.3.6 Gravimetric analysis of recovered nano-softeners (MNP, MND, MCH, and MCCH)

The recovered nanomaterials were weighted in a microbalance OHAUS AV264 and compared against the original mass used for each water treatment experiment. A difference in the weight can lead to a prove of remotion effectiveness of the magnetite materials.

4.4.3.7 FT-IR analysis of recovered nano-softeners

The recovered nano-softeners (MNP, MND, MCH, and MCCH) were characterized by FT-IR using a Shimadzu FT-IR (IRSpirit) ATR mode, to compare the functional groups of each nanoparticle before and after their use in treating RW and determine if there was a change in the spectrums.

4.4.3.8 Optical microscope images of recovered nano-softeners

Recovered nano-softeners images were obtained using an optical microscope (Chiron) with a 10X magnification and recorded using Axio Vision camera and program (version 4.8), images of the magnetic nanomaterials before their usage in RW treatment were also performed to compare all the images.

4.5 Results and discussions

4.5.1 DLS and ζ -potential comparison of RW before and after treatment with magnetic nanomaterials (MNP, MND, MCH, and MCCH)

After recovering the nanomagnetic materials and separating the treated RW samples, a DLS study was performed to compare the sizes of the suspended solids before and after the treatment at pH 7, 8, and 9. Figure 4.9 display the comparison of particles suspended in the RW before the treatment with nanoparticles (a and b, from the chapter III sections 3.5.5 and 3.5.6) and after the treatment with each material (c and d).

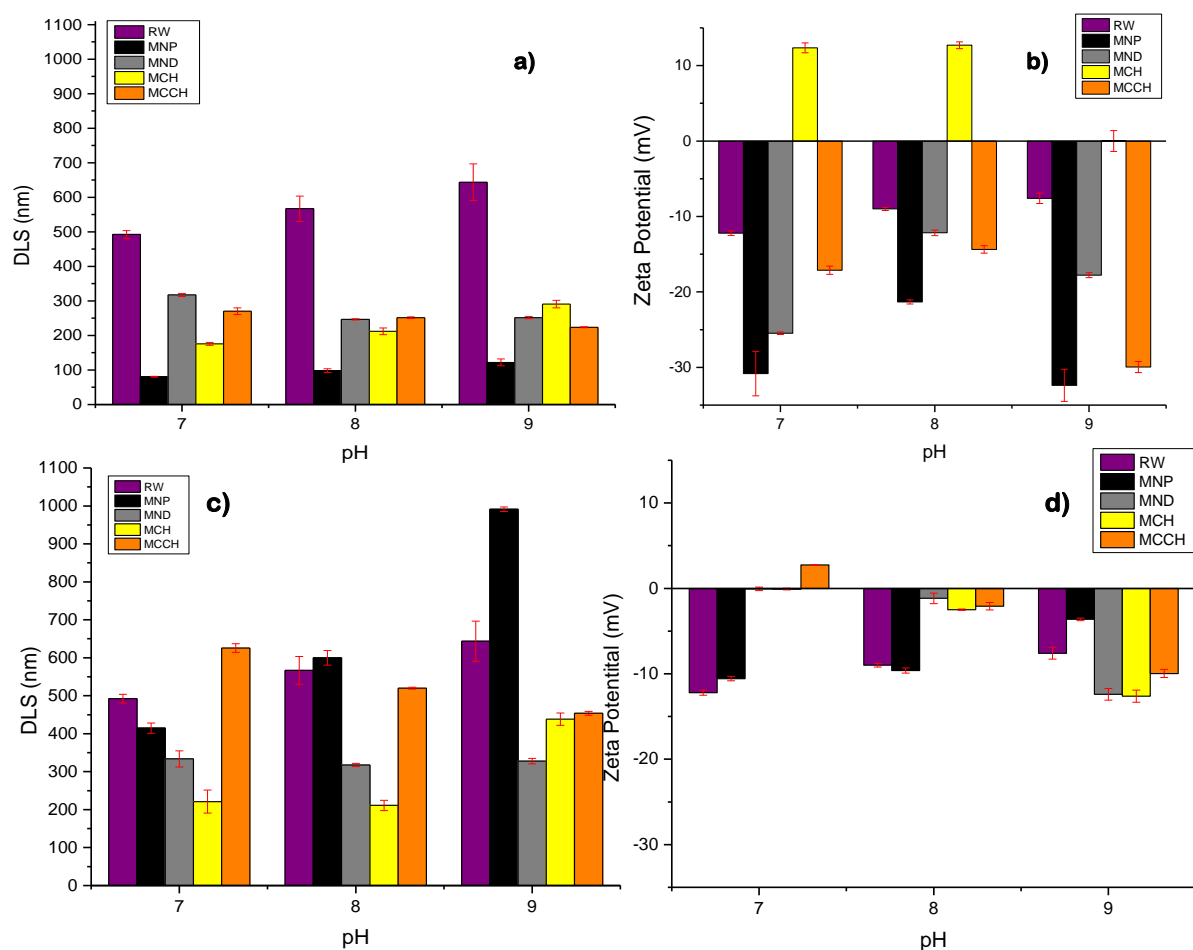


Figure 4.9 Comparison of measurements: a) and b) DLS and ζ -potential measurements, respectively, before RW treatment, nanoparticles are dispersed in deionized water, RW (purple), MNP (black), MND (gray), MCH (yellow), and MCCH (orange) at pH of 7, 8, and 9. C) and d) DLS and ζ -potential measurements, respectively, of untreated RW (purple) and RW treated with MNP (black), MND (gray), MCH (yellow), and MCCH (orange) at pH of 7, 8, and 9.

RW treated with MCH presents the smallest particle sizes, achieving a considerable size reduction at each pH, being more evident at pH 7 and 8 with sizes closer to 200 nm. MND also presents considerable and very stable size reductions at the three studied pHs, obtaining a particle size close to 300 nm for each case. MNP and MCCH only show size reductions in some pH values, and in others, these particle sizes increase.

The above is explained due to the change in its electric surface charges (Figure 4.9b and d). For water treated with MCCH at pH 7, its ζ -potential changes from a value close to -12 mV to +2 mV, while for the MNP-treated water it was reduced to -4 mV at pH 9. The other samples switch their potentials to more negative values (at pH 9), inducing the agglomeration of suspended particles.

On the other hand, for MCH and MND at pH 7, the values of their electric surface charges are reduced close to their IEP, while at pH 8 these values are reduced to values close to -3 and -1.5 mV, respectively. These changes in the particle surface charge and sizes can be attributed to the van der Waals interactions between the superficial charge of the magnetic materials and the cations (as Ca^{2+} and Mg^{2+}) contained in the RW.²⁴ DLS measurements after treatment (Figure 4.9c) may suggest that new salt seeds are present in water samples since the hydrodynamic diameter increased.

4.5.2 Alkalinity and hardness removal from RW

In water quality improvement processes, generally, it is desirable to minimize the suspended solids concentration, water turbidity, and color. Nevertheless, there are other concerns like hardness, alkalinity, microorganisms, and pH.²⁵ Therefore, RW quality parameter hardness and alkalinity were tested to evaluate the action of functionalized magnetic nanoparticles.

The graph in Figure 4.10 shows the removal percentages obtained after RW was treated with the different magnetite-base nanoparticles (as mg/L of CaCO_3). First, it is indispensable to point out that all the nanomaterials accomplish the removal of a certain percentage of alkalinity (Figure 4.10a), but the maximum removal is achieved due to the treatment with MCH and MCCH at pH 7 (23.5%), and MCH at pH 8 (22.3%). With these results, RW at pH 7 now fits

into the parameters of water quality suggested by the EPA, while at pH 8 there is an important reduction of this parameter which brings this value closer to this requirement.²⁶

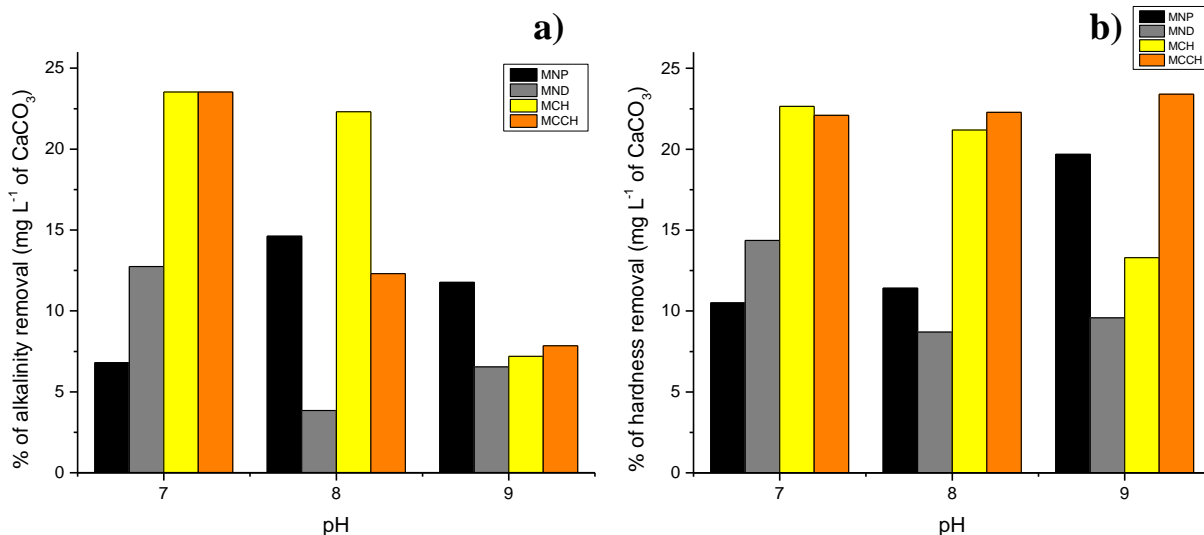


Figure 4.10 a) Comparison of the alkalinity removal of MNP (black), MND (gray), MCH (yellow), and MCCH (orange). b) Comparison of the hardness removal of MNP (black), MND (gray), MCH (yellow), and MCCH (orange). At pH of 7, 8, and 9, expressed as percentage in mg/L.

Regarding water hardness, as mentioned in the previous chapter, it is necessary to reduce the hardness of the waters to avoid scale formation and deposits in pipes. As we can notice in Figure 4.10b, and like for the alkalinity results, all nanomaterials achieved the removal of a certain level of hardness from RW. While at pH 7 and 8 MCCH obtained the highest levels of hardness removal with 22-23%, only slightly surpassed at pH 7 by MCH (22.4%), at pH 8 MCH also achieved a good level of hardness removal (21%). These results (% of removal of alkalinity and hardness) give evidence of the functionality of the synthesized nanomaterials to improve the quality of a RW. So these materials can be denominated now as magnetic nano-softeners.

4.5.3 Transmittance comparison of RW before and after treatment with magnetic nano-softeners (MNP, MND, MCH, and MCCH)

Light transmittance through transparent vials containing RW after being treated with the different nano-softeners at pH 7 was measured to evaluate water appearance and the absence of dispersed solids. Results are reported in Table 4.8 showing that in all cases transmittance was improved, where MCH and MND showed values closer to distilled water. This improvement in the transmittance means that dissolved species from RW were removed.

Table 4.8 Transmittance of different types of water and Reclaimed Water treated with the different magnetite-base materials at pH 7.

| Water | | Transmittance [%] |
|------------------------|------|-------------------|
| Deionized | | 90.54 |
| Distilled | | 90.37 |
| Reclaimed | | 88.01 |
| Reclaimed treated with | MNP | 89.38 |
| | MND | 89.9 |
| | MCH | 89.54 |
| | MCCH | 88.04 |

4.5.4 Gravimetric analysis of recovered nano-softeners

The solids were recovered after treat RW using Nd magnets dried and weighed to know their mass. The results are reported in Table 4.9.

As can be seen, the solid's recovered mass was greater than the initial magnetic nanoscavenger dosage, this weight gain points to the removal of calcium and magnesium carbonates from RW.

Table 4.9 Solids mass recovered after treating RW with magnetic nano-softeners (30 mg/L)

| Sample | Recovered mass (%) | | |
|--------|--------------------|-------|-------|
| | pH 7 | pH 8 | pH 9 |
| MNP | 224.2 | 245.5 | 224.2 |
| MND | 778.8 | 263.6 | 269.7 |
| MCH | 363.6 | 230.3 | 669.7 |
| MCCH | 181.8 | 187.9 | 157.6 |

4.5.5 FT-IR analysis of recovered nano-softeners

All the recovered nano-softeners were analyzed by FT-IR, all the resulting spectrums are showed in Figure 4.11. It can be noticed that all the materials still having the characteristic signal of magnetite 550 cm^{-1} related to the stretching of Fe-O bond, in Figure 4.11a and d this Fe-O

signal is more noticeable (greater extent), and in Figure 4.11b and c are barely noticeable. But this proves that all materials still have a certain degree of magnetism.

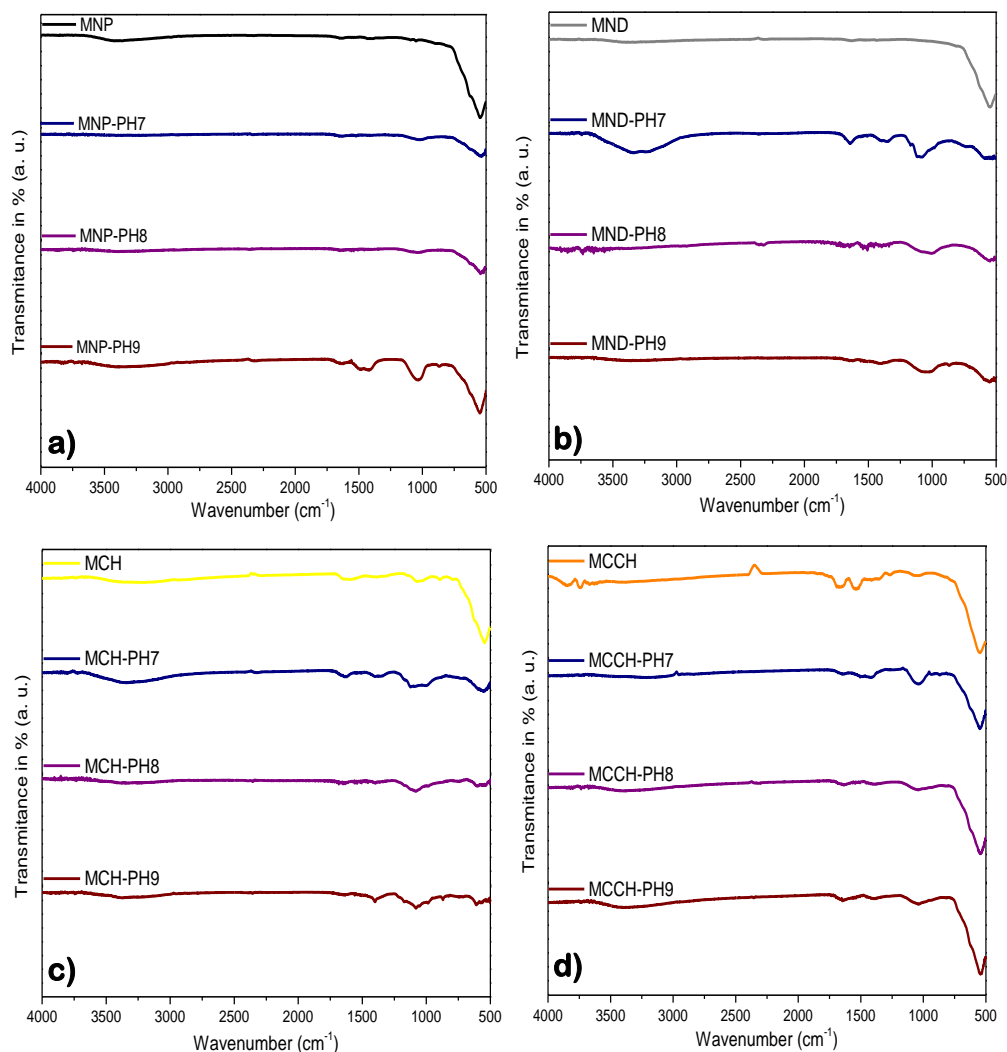


Figure 4.11 FT-IR a) MNP (black line) before and after use at pH 7 (blue line), pH 8 (purple line) and pH 9 (wine line). b) MND (gray line) before and after use at pH 7 (blue line), pH 8 (purple line) and pH 9 (wine line). c) MCH (yellow line) before and after use at pH 7 (blue line), pH 8 (purple line) and pH 9 (wine line). d) MCCH (orange line) before and after use at pH 7 (blue line), pH 8 (purple line) and pH 9 (wine line).

The most important changes concerning to the original spectra of the magnetic materials is the presence of new bands close to 1100 cm^{-1} and between 1440 and 1500 cm^{-1} are observed. Around 1100 cm^{-1} is due to the symmetric vibration of the CO_3^{2-} ion, where this vibration occurs closer to 1075 cm^{-1} for the samples with the highest Mg content and closer to 1090 cm^{-1} for those with the highest Calcium content.²⁷ The bands between 1440 and 1630 are characteristic

for calcite precipitates, due to the interaction between CO₂ and hydroxyl groups of the surface of MgO and CaO.^{27,28} This helps to corroborate the efficiency of the materials to remove Ca²⁺ and Mg²⁺ from the RW.

5.5.6 Optical microscope images of recovered nano-softeners

Finally, optic microscopies were obtained for the recovered solids to corroborate that salty crystals were trapped in the magnetic nano-softeners. Figure 4.12 displays a mosaic of different the four nano-softeners at the different pHs of RW treatment.

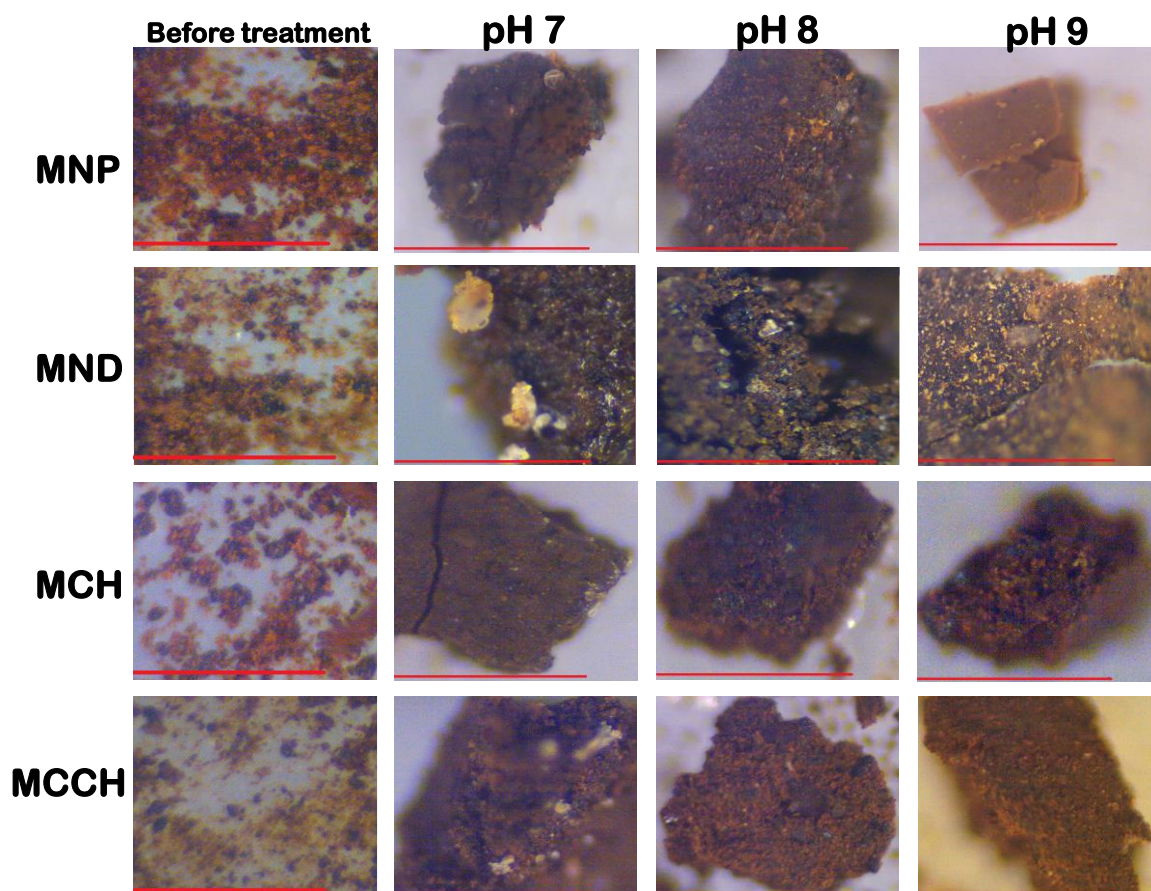


Figure 4.12 Light microscope images of the nano-softeners after they were recovered from the RW treatment. The red line represents a 1 mm scale bar.

Comparing the appearance of trapped crystals, MND at pH 7 showed larger crystals, while MCH trapped smaller crystals. For all nanoscavengers pH 9 show fewer crystals trapped matching with the alkalinity removal measurements.

5.5.7 Comparison of RW treated with the different magnetic nano-softeners at different pH values

From the result obtained Table 4.10 was elaborated to compare the different magnetic nano-softeners (functionalized magnetites) and choose one as the most promising material for water aesthetics improvement.

Even if all the materials have a certain degree of removal it is clear that MCH and MCCH achieved the bigger alkalinity and hardness removal. Although, a treatment with MCH showed smaller sizes of solids suspended in water and a more equal removal of hardness and alkalinity than MCCH. Therefore, MCH is more promising for aesthetics water improvement that can be used at pH 7 and 8. For this special application on the RW from the wastewater treatment plant “La Morita” since the natural pH of this water is 8 we recommend do not modify this pH for MCH use, since results are not far away from their best performance, allowing to save time and cost operations.

Table 4.10 Performances comparison of nano-softeners.

| RW treated with | pH | Size (DLS, nm) | ζ – potential (mV) | Alkalinity removal (%) | Hardness removal (%) |
|-----------------|----|----------------|--------------------------|------------------------|----------------------|
| MND | 7 | 333 | -0.1 | 12.8 | 14.4 |
| | 8 | 318 | -1.2 | 3.9 | 8.7 |
| | 9 | 328 | -12.4 | 6.6 | 9.6 |
| MCH | 7 | 221 | -0.1 | 23.5 | 22.7 |
| | 8 | 211 | -2.5 | 22.3 | 21.2 |
| | 9 | 438 | -12.6 | 7.2 | 13.3 |
| MCCH | 7 | 626 | 2.8 | 23.5 | 22.1 |
| | 8 | 520 | -2.1 | 12.3 | 22.3 |
| | 9 | 454 | -10 | 7.9 | 23.4 |

4.6 Conclusions

All magnetic nanomaterials demonstrated their effectiveness as alkalinity and hardness removal from real RW, therefore, they can be referred to as magnetic nano-softeners. These magnetic nano-softeners consist of a magnetic core (magnetite) superficially and chemically modified by eco-friendly organic materials (ND, CH, and CCH).

The results showed in this section proved the effectiveness of these magnetic nano-softeners to trap carbonates from reclaimed water, demonstrated by DLS, Zeta potential, light transmittance, and alkalinity and hardness tests, gravimetry, FT-IR and light microscope images.

Each magnetic nanomaterial demonstrated its potential application in water conditioning. MCH proved to be effective for removing alkalinity and hardness with percentages greater than 20% at pHs 7 and 8. MCCH turned out to be a good material to remove hardness at all studied pHs and effective for alkalinity at pH 7. MND is a very stable material in solution, with hardness removals of 10 to 15%, but the weight difference results showed that they are good removers of other contaminants present in recovered water, not studied in this work.

These new technologies allowed treating reclaimed water, finding that alkalinity and hardness removal are possible to improve reclaimed water quality. Finally, we also demonstrated that these materials can be easily recovered from water for further uses, reducing the cost of operation, resulting in environmentally friendly and sustainable nanomaterials.

4.7 References

- (1) Naturales, S. medio ambiente y recursos. *NOM-001-SEMARNAT-1996*; México, 1996; p 35.
- (2) Comisión Nacional del agua. *Estadísticas Del Agua En México, Edición 2018*; Secretaría de Medio Ambiente y Recursos Naturales: Ciudad de México, México, 2018.
- (3) Salgot, M.; Folch, M. Wastewater Treatment and Water Reuse. *Curr. Opin. Environ. Sci. Heal.* **2018**, 2, 64–74.
- (4) Garfí, M.; Cadena, E.; Sanchez-Ramos, D.; Ferrer, I. Life Cycle Assessment of Drinking Water: Comparing Conventional Water Treatment, Reverse Osmosis and Mineral Water in Glass and Plastic Bottles. *J. Clean. Prod.* **2016**, 137, 997–1003.
- (5) SEMARNAT. *Sistemas de Tratamientos de Aguas Residuales*; Secretaría de Medio Ambiente y Recursos Naturales: Ciudad de México, México, 2018.
- (6) Huang, X. Microbial Pathogen Detection and Removal in Water Reuse Practices, Ph.D. Thesis UC Irvine, Cañifornia, USA, 2015, pp 3-11
- (7) National Research Council. *Water Reuse: Potential for Expanding the Nation's Water Supply Through Reuse of Municipal Wastewater*; The National Academies Press: Washington, DC, 2012.
- (8) Crittenden, J. C.; Trussell, R. R.; Hand, D. W.; Howe, K. J.; Tchobanoglous, G. *MWH's Water Treatment: Principles and Design*; John Wiley & Sons, 2012, pp 21-99
- (9) e medical prep. Adsorption <https://www.emedicalprep.com/study-material/chemistry/surface-chemistry/adsorption/> (accessed May 9, 2021).
- (10) Mujeriego, R.; Asano, T. The Role of Advanced Treatment in Wastewater Reclamation and Reuse. *Water Sci. Technol.* **1999**, 40, 1–9.
- (11) Solis Vázquez-Mellado, M. *Sistema de Tratamiento de Aguas Mediante Osmosis Inversa*; Ph.D. Thesis, Mexico City, 2017, pp 6-18.

-
- (12) Membracon. Reverse osmosis systems in industrial processes
<https://smartwatermagazine.com/news/membracon/reverse-osmosis-systems-industrial-processes> (accessed May 10, 2021).
- (13) Carbotecnia. ¿Qué es la ósmosis inversa?
<https://www.carbotecnia.info/aprendizaje/osmosis-inversa/que-es-la-osmosis-inversa/>
(accessed Sep 20, 2020).
- (14) Barakat, M. A. New Trends in Removing Heavy Metals from Industrial Wastewater. *Arab. J. Chem.* **2011**, *4*, 361–377.
- (15) Carbotecnia. Intercambio iónico
<https://www.carbotecnia.info/aprendizaje/suavizadores-y-desmineralizadores/que-es-el-intercambio-ionico-y-tipos-de-resinas/> (accessed May 10, 2021).
- (16) Cortijo-Herrera, D. Desalcalinización Del Agua Mediante Intercambio Iónico. *Ing. Ind.* **2013**, *0*, 221–238.
- (17) Litter, M.; Quici, N. Advanced Oxidation Processes for Water and Wastewater Treatment. *Recent Patents Eng.* **2010**, *4*, 217–241.
- (18) Garrido-Cárdenas, J.; Esteban-García, B.; Agüera, A.; Sánchez Pérez, J. A.; Manzano-Agugliaro, F. Wastewater Treatment by Advanced Oxidation Process and Their Worldwide Research Trends. *Int. J. Environ. Res. Public Health* **2019**, *17*, 170.
- (19) Alvarez, P. J. J.; Chan, C. K.; Elimelech, M.; Halas, N. J.; Villagrán, D. Emerging Opportunities for Nanotechnology to Enhance Water Security. *Nat. Nanotechnol.* **2018**, *13*, 634–641.
- (20) Xu, P.; Zeng, G. M.; Huang, D. L.; Feng, C. L.; Hu, S.; Zhao, M. H.; Lai, C.; Wei, Z.; Huang, C.; Xie, G. X.; et al. c. *Sci Total Environ.* **2012**, *424*, 1–10.
- (21) Soloneski, S.; Larramendy, M. *Emerging Pollutants - Some Strategies for the Quality Preservation of Our Environment*; Intech Open; London, United Kingdom, 2018, pp 61-71

-
- (22) Mehta, D.; Mazumdar, S.; Singh, S. K. Magnetic Adsorbents for the Treatment of Water/Wastewater—A Review. *J. Water Process Eng.* **2015**, *7*, 244–265.
- (23) Li, X.-M.; Xu, G.; Liu, Y. Magnetic Fe₃O₄ Nanoparticles: Synthesis and Application in Water Treatment. *Nanosci. Nanotechnology-Asia* **2011**, *1*, 14–24.
- (24) Zuki, N. M.; Ismail, N.; Omar, F. M.; Chieh, D. C. J. Evaluation of Zeta Potential and Particle Size Measurements of Multiple Coagulants in Semiconductor Wastewater. *AIP Conf. Proc.* **2019**, *2124*, 20036-20046.
- (25) The world bank. *Water Resources and Environment Technical Note F.3*; DAVIS, R., HIRJI, R., Eds.; The International Bank for Reconstruction and Development/The world bank, 2003, pp 8-19
- (26) U.S. Environmental Protection Agency. *2012 Guidelines for Water Reuse*; Washington, D.C., 2012, pp 37-251
- (27) Schaeffer, A. G.; Coral, M. C.; Borja, N. A. Síntesis y caracterización del sistema cao - MgO. *Rev. Peru. Química e Ing. Química* **1998**, *1*.
- (28) Montoya, C.; Márquez, M.; López, J. M.; Cuervo, C. Caracterización de Cristales de Calcita Bioprecipitada Por Un Aislamiento Nativo de Bacillus Subtilis. *Rev. Colomb. Biotecnol.* **2005**, *7*, 19–25.

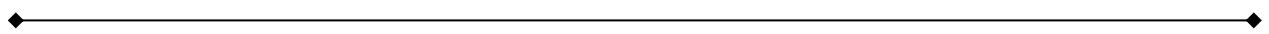
General conclusions

In this thesis work, we developed three new magnetic nanomaterials as part of a new technology for water treatment, and we can make the following conclusions:

1. We synthesized magnetite nanoparticles functionalized with different organic and biocompatible molecules (ND, CH, and CCH, this last one was also synthesized in this thesis) obtaining magnetic nanodiamond (MND), magnetic chitosan (MCH) and magnetic carbamoyl chitosan (MCCH). The synthesis was carried out using the coprecipitation method adding an extra step for an in-situ functionalization. All these magnetic solids served as adsorption sites for specific metal ions (hardness and alkalinity removal)
2. We corroborate the correct modification of the magnetic nanomaterials by using different characterization techniques such as TEM, EDX, FT-IR, TGA, BET surface area analysis, VSM, DLS, and ζ -potential. All this information allowed to corroborate the intrinsic properties of the synthesized materials. For example the correlation between: (i) FT-IT and TGA, (ii) magnetism and particle size, (iii) ζ -potential and pH, and, (iv) DLS and pH.
3. The size obtained from TEM for raw magnetite (MNP) is close to 16 nm, meanwhile sizes close to 13, 10.4 and 12.4 nm for MND, MCH, and MCCH, respectively. It's important to point that the modifiers provide better stabilization and less agglomeration effect to the magnetite. With this technique we ensure that the synthesized materials are on the nano scale.
4. We found out that all the synthesized materials have a superparamagnetic where the modification of the magnetite surface led to an increase of their magnetic properties due to a reduction in their sizes. The magnetization moments observed were 50.5, 60.5, 72, and 60.9 emu/g for MNP, MND, MCH and MCCH, respectively. These results match

with the correlation with the particle size described above (listed on number 3): the magnetism increase when the particle size decrease.

5. BET analysis showed that the adsorption and desorption are in a range of 0.7, 0.6, 0.5, and 0.6, to 1 P/Po, for MNP, MND, MCH and MCCH, indicating the presence of mesopores in the magnetite-base nanoparticles. This analysis helped to probe that the modified materials have potential adsorption capacities for 2+ metal ions such as Ca^{2+} and Mg^{2+} as Salazar-Camacho and Villalobos-Peñalosa (reference 62, chapter II).
6. We characterized reclaimed water obtained from the wastewater treatment plant “La Morita” (Tijuana, Baja California, México), finding values around 200-300 mg/L and 350 mg/L for alkalinity and hardness, respectively. Those parameters are acceptable for most irrigation urban reuses, but they are not acceptable for some industrial applications and water recharge or potable uses, and barely accomplish the Mexican regulation. Therefore, this water needs further treatment for other reuses and to avoid scale and corrosion on pipelines and other machinery.
7. Each magnetic nanomaterial demonstrated its potential application in water conditioning since all of them removed a certain percentage of alkalinity and hardness. From all the materials, MCH proved to be effective for removing alkalinity and hardness with percentages greater than 20% at pHs 7 and 8. MCCH turned out to be a good material to remove hardness at all studied pHs and effective for alkalinity at pH 7. MND is a very stable material in solution, with hardness removals of 10 to 15%, but the weight difference results showed that they are good removers of other contaminants as well.
8. Finally, we demonstrated that all the synthesized magnetic nanomaterials can be easily recovered from water using magnetic decantation, reducing the cost of operation.



Therefore, we have been proved that the developed materials act as nano-softeners in reclaimed water, improving this water aesthetics (alkalinity and hardness), resulting in environmentally friendly and sustainable nanomaterials.

Annexes

2.3.2.A Scanning electron microscopy

SEM differs from conventional light microscopes as they use light waves to create a magnified image. In SEM, when the electron beam strikes the specimen surface, it interacts with the surface. Moreover, SEM uses a fundamentally different process to form an image than that of TEM (Transmission electron microscopy), where instead of transmitting the electron beam through a thin sample, the beam rasters across the sample surface and collects electrons after they have interacted with the sample and builds an image pixel by pixel. SEM is able to retain the 3D topography of the sample due to having a much wider depth of field than TEM.^{1,2}

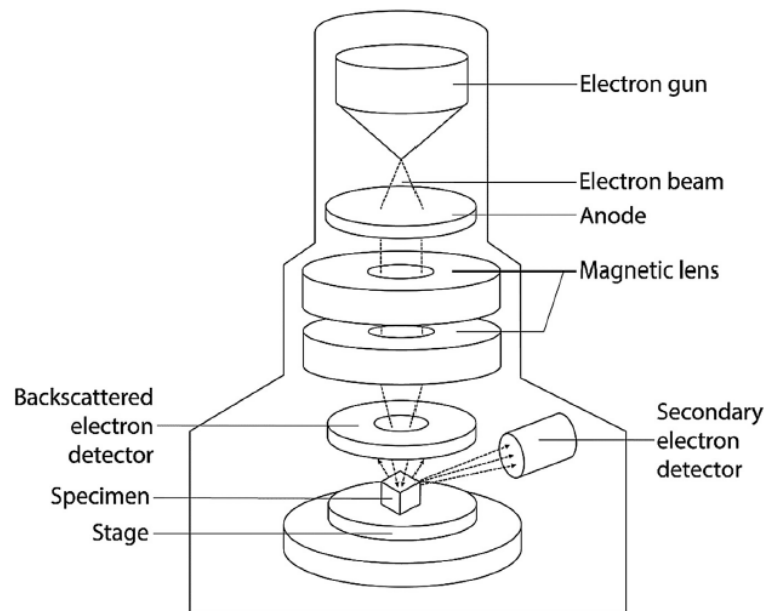


Figure A1. Outline of magnetic lens, beam path, and sample arrangement within a SEM.¹

A schematic diagram on the working of SEM is shown in Figure A1. When the incident beam of electrons hits the specimen, X-rays and three types of electrons are emitted: backscattered (or primary) electrons, secondary electrons, and Auger electrons. SEM makes use of the primary, and the secondary electrons. The highest resolution images are built by collecting secondary electrons that are emitted from very near the surface of the sample producing images with a maximum resolution of around 1–5 nm. For identifying elemental compositions, X-rays

are used by a technique known as EDX. The backscattered electrons are also used to form the image in this technique.^{1,2}

In the particular case of MNP, they tend to agglomerate so sample preparation is essential to get quality images. The use of SEM can help to understand the external structure and morphologies of the magnetite and their modifications.³

2.3.2.A1 SEM for MNP characterization

In the particular case of magnetic nanoparticles (MNP) they tend to agglomerate, therefore a good sample preparation is essential to get quality images. The use of SEM can help to understand the external structure of the magnetite and their modifications.³

SEM technique is one of the first characterization performed, since it's a relatively easy-access technique and help to confirm the morphology of the magnetite, revealing if the samples consisted of nanosized particles.⁴ For example, Porroy et al. used SEM to investigate the morphology with overall views on a wide area of a variety of prepared magnetite powders, also allowing them to check that no large particles were produced.⁵ In another study, Predoi *et al.* demonstrated, via SEM analysis, that they synthesized MNP with an spherical shape.⁶ Figure A2 shows a typical SEM image for raw magnetite nanoparticles (powder).

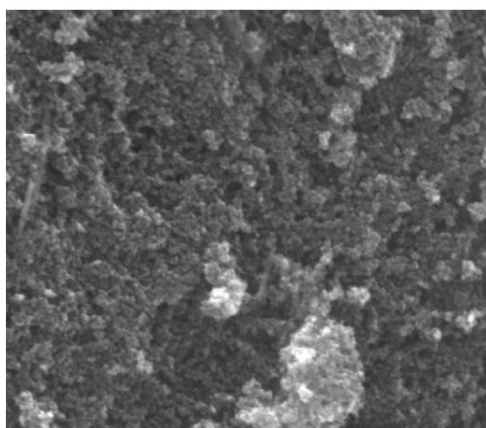


Figure A2. SEM image of raw magnetite nanoparticles.⁶

Some authors usually accompany SEM with transmission electron microscopy (TEM) due the resolution of this technique that allows observing the particles closer giving an approximation more accurate about their size.^{4,5,7}

2.3.2.B Scanning Transmission Electron Microscopy (STEM)

TEM and STEM are exceptionally powerful techniques for providing direct characterization of a number of critical features of the irradiation-induced microstructure.⁸

A STEM consists of a modified electron microscope, where the electron beam is focused to a fine spot that is then scanned over the sample in a raster, unlike conventional TEM. The rastering of the beam across the sample makes STEM appropriate for techniques as Z-contrast annular dark-field imaging and spectroscopic mapping by energy dispersive X-ray spectroscopy (EDX) or electron energy loss spectroscopy (EELS). Using EDX or EELS spectroscopy in the STEM it is possible to obtain elemental maps that show features down to the atomic scale.^{8,9}

Dedicated STEMs are equipped with high brightness field emission sources (field emission gun—FEG), which allow probes down to 1.5 nm or less to be formed. The fine probe can be stopped in selected positions and the X-ray signal generated by the interaction of the electron beam and the specimen is collected and analyzed.⁹

2.3.2.B1 STEM for MNP characterization

STEM is routinely employed to examine the internal microstructure in irradiated materials, minor and major elements to internal sinks and characterization of second phase particles.^{8,9}

STEM primary difference over conventional SEM imaging is the signal obtained through transmission of the electron beam through the sample, while conventional SEM signal corresponds to secondary electrons given information on the sample topography.

The usage of STEM at proper magnification can retrieve the size distribution directly by simply counting the particles with different sizes.¹⁰ In the particular case of magnetite nanoparticles, STEM allows inquiring more precisely about its shape and detail of the surface of the MNP by using high-angle annular dark-field (HAADF) or annular dark-field (BF/DF). An example of the above mentioned is the work of Plascencia-Villa *et al*, the authors performed a high-resolution analytical imaging of MNP where approximations of the size and shape of the materials were performed, in Figure A3 we can observe the STEM images they obtained for iron-oxide magnetic nanoparticles.¹¹

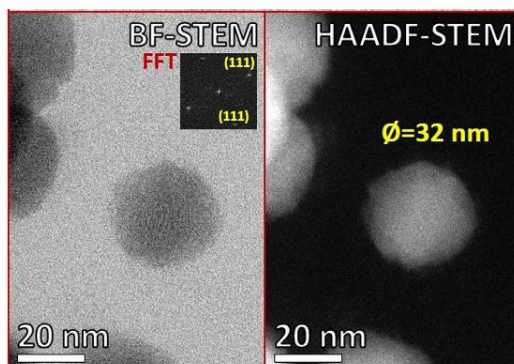


Figure A3. High magnification BF/HAADF-STEM of individual particles of 32 nm Fe₃O₄.¹¹

2.3.2.B2 Limitation of SEM and STEM technique

Imaging techniques as SEM, FE-SEM and STEM are useful to have an approximation of the shape, size and topography of magnetite nanoparticles, but these techniques are limited where it comes to determine directly a surface modification of magnetites since they don't show any information about the sample composition.

Although, a change in the size, shape, or aggregation of the sample can contribute to determine a surface modification indirectly. The assumption of the surface modification of magnetite with imaging techniques is often accompanied by alternative characterization techniques such as FT-IR, EDS, VSM, XDR etc.¹²⁻¹⁴

Rahbar *et al.* presented a study of magnetite and magnetic chitosan comparing both materials using FE-SEM where no change in the morphology is observed (Figure A4) but a variation on the size between the raw material and magnetic chitosan is enough to suggest a coating layer of chitosan on the magnetite, this suggestion is also confirmed using infra-red spectroscopy.¹⁵

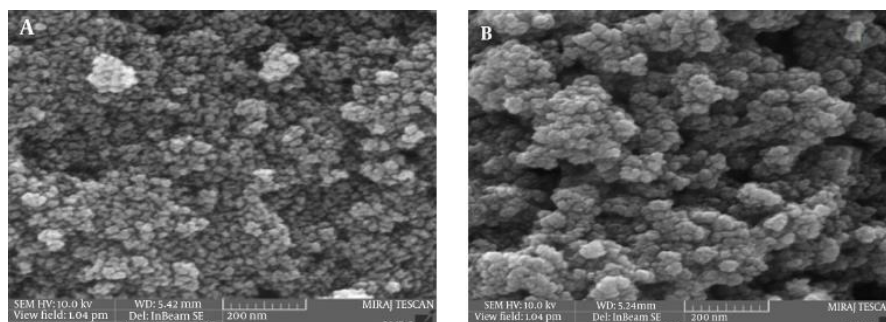


Figure A4. A) Magnetite nanoparticles; B) magnetic chitosan nanoparticles.¹⁵

The application of the STEM-based technique allows to analyze a broad range of particle sizes, as one would wish. STEM is routinely employed to examine the internal microstructure [cavities, dislocation lines, dislocation loops, solute redistribution (segregation and precipitation)] in irradiated materials, minor and major elements to internal sinks such as grain boundaries and characterization of second phase particles.^{8,9}

2.3.2.1 Transmission electron microscopy

Transmission electron microscopy (TEM) is a form of microscopy similar to SEM with the exception that the beam passes through the sample then interacts with the specimen when a highly focused electron beam (80-200 keV) is passed through a thin solid sample (100-200 nm in thickness). Electrons undergo coherent scattering or diffraction from lattice planes in the crystalline phase of materials, resulting in phase identification, the obtention of the images is explained in Figure A5.^{16,17}

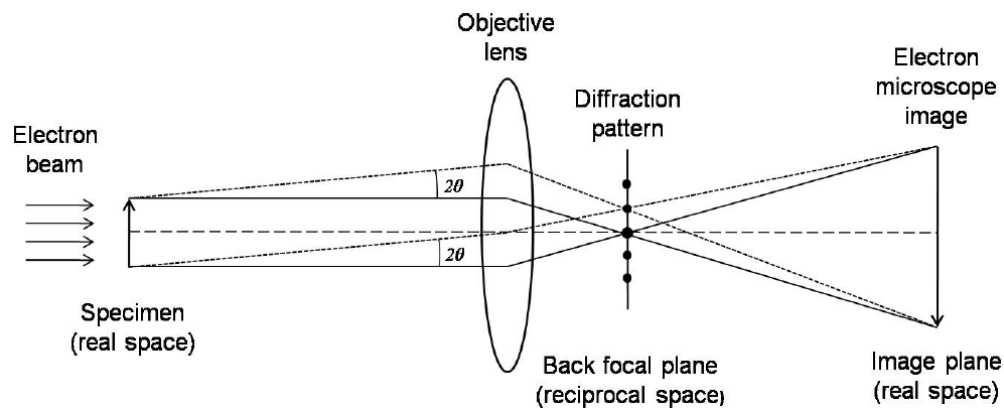


Figure A5. The optical electron beam diagram of TEM¹⁷

TEMs provide images with significantly higher resolution than visible-light microscopes (VLMs) do because of the smaller de Broglie wavelength of electrons. TEM images can be used to estimate finer details (strain field of small precipitates, defect clusters, and dislocation loops and lines), since the images are several thousand times higher than the highest resolution in a VLM (visibility limit close to 1–2 nm)⁸. Nevertheless, the magnification provides in a TEM image is in contrast to the absorption of the electrons in the material, which is primarily due to the thickness or composition of the material.^{8,17}

When a crystal lattice spacing (d) is investigated with electrons with wavelength λ , diffracted waves will be formed at specific angles 2θ , satisfying the Bragg condition:^{1,17}

$$2d\sin\theta = \lambda$$

The above equation estimates ability to distinguish between two separate objects next to each other is tied directly to the wavelength of the light being used to make the observation. If the distance between the structures is less than half the wavelength of the light being used, the two objects cannot be resolved and will appear as a single structure.¹ It is important to point out that this technique has a particular drawback is that a single TEM image has no depth sensitivity.¹⁷

2.3.2.2 Energy dispersive X-ray analysis (EDX)

EDX is used in conjunction with SEM, FE-SEM and STEM. An electron beam with energy of 10–20 keV strikes the conducting sample's surface, causing X-rays to emit from the material, and the energy of the emitted X-rays depends on the material under examination.²

Characteristic X-rays are produced when the electron beam interacts with an inner shell electron kicking it out and allowing an electron from a higher shell to drop down and fill the vacancy releasing in the process. These X-rays provide detailed information about the elemental makeup of the sample and are examined through energy-dispersive X-ray spectroscopy (EDX). While EDX is a powerful technique, it is generally used for elemental and spatial analysis across samples forming maps of elemental distribution on a sample. The resolution limit of SEM renders the use of EDX for analysis of nanoparticles limited in scope. While some samples may lend themselves toward EDX analysis, the resolution of SEM instruments tends to limit their applications.^{1,2}

The composition or amount of nanoparticles near and at the surface can be estimated using the EDX, provided they contain some heavy metal ions. For instance, nanoparticles like silver, gold, and palladium on the surface can be easily identified using EDX. Elements of low atomic number are difficult to detect by EDX.¹

2.3.3.1 Fourier transform infrared spectroscopy (FT-IR)

FT-IR is a technique based on the measurement of the absorption of electromagnetic radiation with wavelengths within the mid-infrared region ($4000\text{-}400\text{ cm}^{-1}$). FT-IR analysis is used for the identification of a broad of organic, inorganic, and polymeric materials utilizing infrared light for scanning the samples.^{2,9}

If a molecule absorbs infrared (IR) radiation the dipole moment is somehow modified, and the molecule becomes IR active. A recorded spectrum gives the position of bands related to the strength and nature of bonds, and specific functional groups, providing information concerning molecular structures and interactions. Besides, alterations in the characteristic pattern of absorption bands can easily indicate a change in the material composition when this has been modified.^{2,9}

A typical FT-IR spectrometer includes a source, sample cell, detector, amplifier, Analog-to-digital (A/D) converter, and computer. Radiation from the sources reaches the detector after it passes through the interferometer. The signal is amplified and converted to a digital signal by the A/D converter and amplifier, after which the signal is transferred to the computer where the Fourier transform is carried out. Figure A6 shows the schematic diagram of a FT-IR spectrometer. The resultant signal obtained at the detector is a spectrum (generally from 4000 to 400 cm^{-1}), which represents the samples' molecular fingerprint. Every molecule has a unique fingerprint, which makes FT-IR an invaluable tool for chemical identification.²

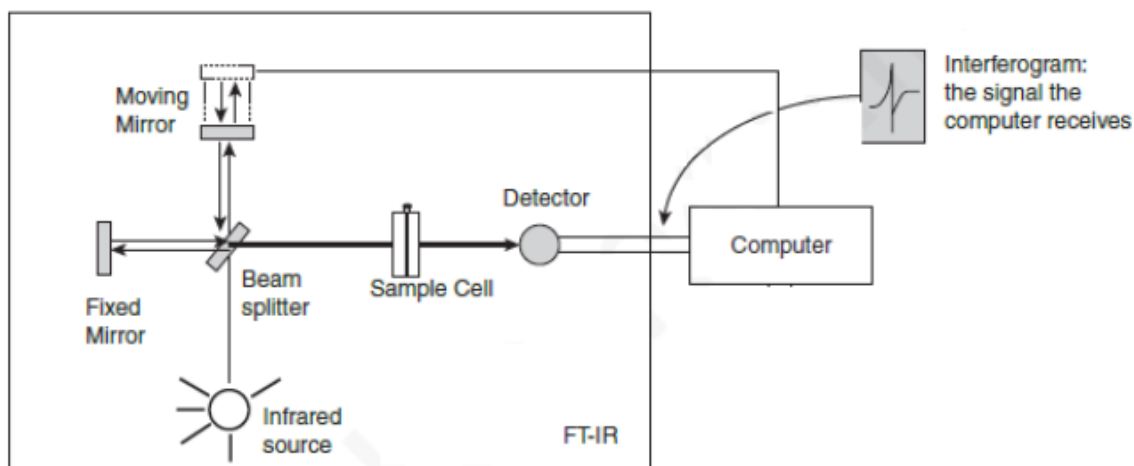


Figure A6. Schematic diagram of typical FT-IR spectrophotometer.¹⁸

Attenuated total reflection (ATR) method in FT-IR equipment is able to measure powder samples directly meanwhile other methods used to measure the infrared spectrum for powder samples need to be mixed in a medium such as KBr or liquid paraffin. ATR method involves pressing the sample against a high-refractive-index prism and measuring the infrared spectrum using infrared light that is totally internally reflected in the prism. A zinc selenide (ZnSe) or germanium (Ge) prism is used in the ATR accessory. ATR method is an excellent method for obtaining infrared information for the powder sample surface. ATR mode makes the FT-IR utilization easier since most samples will no need longer preparation to be measured.¹⁹

FT-IR was adopted as a reliable technique for differentiating the main iron oxide phases and it properly applies to explore transmission bands of bimetallic magnetic systems. Additionally, with this technique is facile to identify new bands after the modification of the magnetite with different coatings (like polymers and carboxylic groups, metals) and for core-shell MNP.^{9,20}

2.3.4.1 X-ray powder diffraction (XRD)

X-ray powder diffraction is a non-destructive technique widely used for the characterization of nanocrystalline crystals.²¹

XRD provides information regarding the crystalline structure, the nature of the phase, lattice parameters and crystalline grain size, and has been applied for phase identification, quantitative analysis, and determination of structure imperfections. Besides, XDR has the advantage of being commonly performed in samples in powder form, usually after drying their corresponding colloidal solutions, resulting in a statistically representative, volume-averaged values. The composition of the particles can be determined by comparing the position and the intensity of the peaks with the references patterns available at the International Centre for Diffraction Data (ICDD) or the Crystallography Open Database (COD).^{9,21}

The X-rays are produced when electrically charged particles with sufficient energy are decelerated. A high voltage is maintained between the electrodes, which attracts electrons toward the metal target. At the impact point, X-rays are generated and radiates in every direction. These generated X-rays are collimated and directed to a sample (in form of a finely ground

powder). X-rays are detected by the detector, and the signals are processed with a microprocessor or done electronically. In Figure A7 is shown the set-up of the technique.²

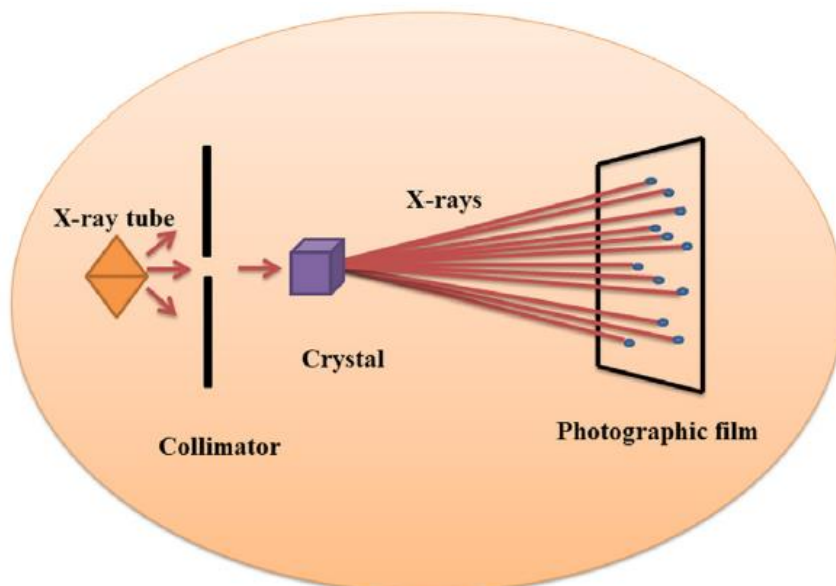


Figure A7. X-ray diffraction set-up.²

Each crystalline material has a distinctive atomic structure and thereby diffracts the X-rays in a unique pattern. Bragg's equation is used for measuring the angle of diffraction which is given by:

$$2d \sin\theta = n\lambda$$

where d denotes the spacing between the planes, θ denotes the angle of incidence, n denotes an integer, and λ denotes the beam wavelength (Figure A8).²

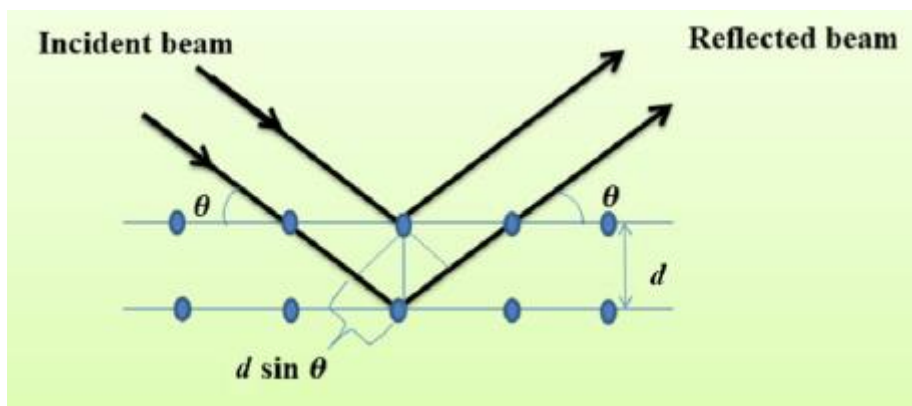


Figure A8. X-ray diffraction.²

It is important to point that XRD is not an accurate method to discern between both magnetite (Fe_3O_4) and maghemite ($\gamma\text{-Fe}_2\text{O}_3$) since they are inverse spinel structures, which results in nearly identical XDR spectrums, then, XRD is not an accurate method to discern between the two species. Anyhow, XRD allows determining information respecting to the crystalline ordering of the atoms in the magnetic core since the crystalline core is responsible for the magnetic response of these materials, hence, understanding the atomic ordering is critical to the success of most applications.²²

In addition to the above mentioned, from the XDR pattern it can be determined the degree of purity of the obtained magnetite and indicate the nanocrystalline nature of magnetite.²⁰

XDR for MNP characterization

It is important to point that XRD is not an accurate method to discern between both magnetite (Fe_3O_4) and maghemite ($\gamma\text{-Fe}_2\text{O}_3$) since they are inverse spinel structures, which results in nearly identical XDR spectrums, then, XRD is not an accurate method to discern between the two species. Anyhow, XRD allows determining information respecting to the crystalline ordering of the atoms in the magnetic core since the crystalline core is responsible for the magnetic response of these materials.²²

In addition, from the XDR pattern it can be determined the degree of purity of the obtained magnetite and indicate the crystalline nature of the nanoparticle.²⁰

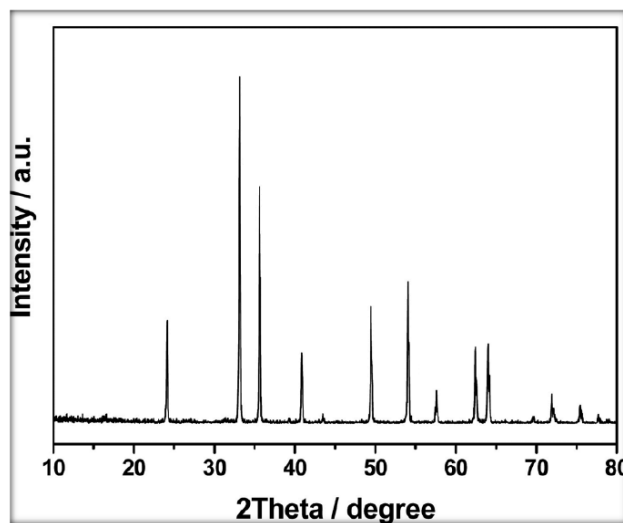


Figure A 9. XRD pattern of iron oxide nanoparticles.²³

Atif *et al* produced MNP and modified them with chitosan to obtain a potentiometric urea biosensor, in their study they show a representative XRD pattern (Figure A 9) with all diffraction peaks of MNP presenting a cubic spinel Fe_3O_4 and having the lattice parameter $a = 8.072 \text{ \AA}$. Besides, the authors mark that they synthesized iron-oxide nanoparticles with high purity and good crystal quality, confirmed by the small particle size and high crystalline nature of the material.²³

When a MNP has been functionalized with an organic molecule the XDR will not show change on the crystalline phase of the magnetite, but it will show a deformation of the crystalline structure. The above-mentioned is exemplified by the work of Shukla *et al*. The authors synthesized MNP and MNP coated with chitosan for in vitro toxicity assessment. In this study, the authors performed XDR to obtain the diffraction peaks of the materials (Figure A10). Firstly, the broad reflection planes on the magnetite nanoparticles were attributed to the nanosized. Secondly, on the iron oxide nanoparticle coated with chitosan, no change was observed on the crystalline phase of Fe_3O_4 . The authors confirmed the chitosan coating by the presence of the new peaks on the XDR spectra, coming from the CH.²⁴

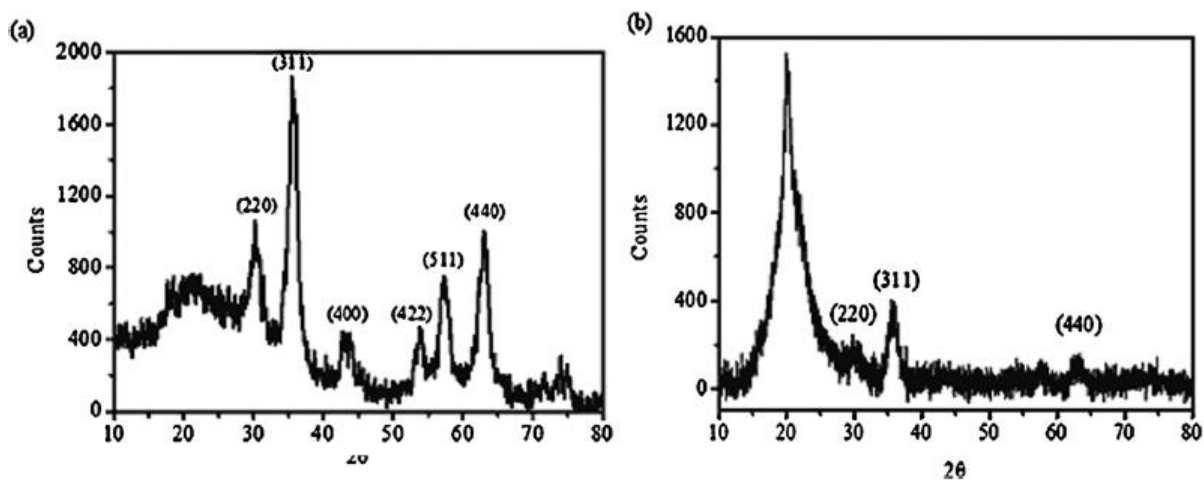


Figure A10. (a) XRD pattern of iron oxide nanoparticles, (b) XRD pattern of chitosan coated iron oxide nanoparticles.²⁴

2.3.5.1 Thermogravimetric analysis (TGA)

TGA analysis is a method in which the variation mass of a sample is measured over time with changes in temperature in a specified trend. Thermogravimetric analysis (TGA) measures changes in physical properties (phase transitions, including vaporization, sublimation, absorption, adsorption, desorption) and chemical properties (chemisorption, decomposition, and solid-gas reactions) by increasing temperature as a function of time. TGA can also determine either mass loss or gain due to decomposition or oxidation and its possible to evaluate the thermal stability of a material. Therefore, in a specific temperature range, if a material is thermally stable, no mass change will be observed.^{18,25,26}

The main principle of TGA includes a mass change for a sample that is studied under programmed conditions. Hence, TGA is mainly used for understanding certain thermal physical and chemical events mentioned above. In addition, TGA can be utilized for the evaluation of volatile or gaseous products lost during such chemical reactions for samples such as nanomaterials, polymers, polymer nanocomposites, fibers, paints, coatings, and films. And along with the prediction of thermal stability for samples, it is also possible to study the kinetics of chemical reactions under various conditions using TGA. To study the kinetics its necessary to optimize the factors which influence the mass change for samples during the experimental period. These factors include (i) weight and volume of sample, (ii) physical form of sample, (iii) shape and nature of sample holder, (iv) type of atmosphere under the performance of the analysis, (v) pressure of the atmosphere maintained in the sample chamber during the analysis, and (vi) rate of heating or cooling conditions.²⁷

Commercial TGA is capable of >1000 °C, 0.1 µg balance sensitivity, and a variable controlled heat-up rate under an atmosphere of air or another gas. The heat-up rate capability of TGA can vary from 0.1°C to 200°C/min. The heating element is made of platinum (reliable up to 1000 °C). An external furnace with a heating element made of an alloy of platinum and 30% rhodium can extend the temperature range to 1500 °C and is equipped with a micro-furnace that can be rapidly cooled.¹⁶

Thermogravimetry deals with the branch of thermal analysis which investigates the change in weight for a substance as a function of time or temperature. The weight change profile

is recorded when the sample is subjected to a heating or cooling environment in a controlled manner. When the weight change is recorded as a function of time, then it is termed as “isothermal mode”. In case of scanning mode, the weight change is recorded as a function of temperature.²⁷ A scheme of the setup of a TGA equipment is shown in Figure A11.

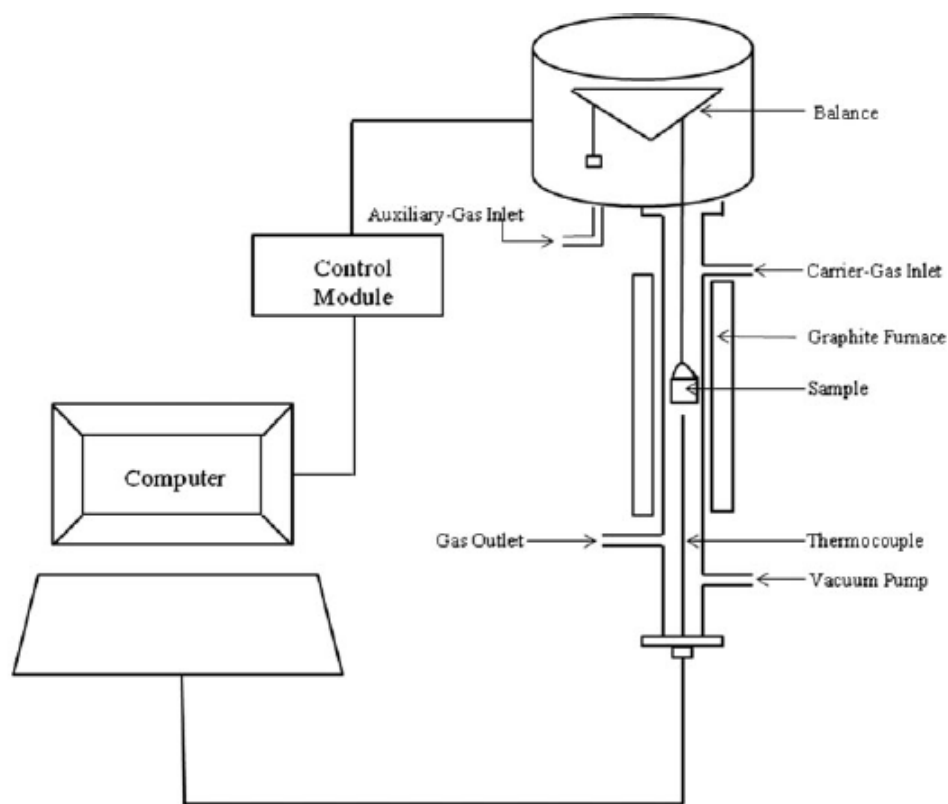


Figure A11. Schematic diagram of the TGA setup.²⁸

The TGA is a simple and direct technique and as another advantage, no special treatment is need for sample preparation, apart from having the sample in a dry state and only a few milligrams of the nanomaterial sample are required.⁹

When having a modified nanoparticle, FT-IR offers information about the interaction and conformation between a NP and the stabilizer type but does not give insights on the extent of surface coverage or the mass-to-mass ratio of NP to stabilizer. TGA gives information concerning the mass and composition of the stabilizers. In a TGA analysis, a nanomaterial sample is heated and components with different degradation temperatures decompose and vaporize, and a change of mass is recorded. The temperature and the loss of mass are recorded

by the TGA device and, considering the starting sample mass, the type and quantity of NP-organic ligands are determined.⁹

Magnetite NPs with many types of molecules and polymers adsorbed on their surface are being investigated with a TGA, and it is common to notice slight discrepancies between results from TGA and XRD experiments on the exact composition of the iron oxides that might originate from the formation of oxidized residue between these two different measurements.^{9,29}

2.3.5.2 Dynamic light scattering (DLS)

Characterization of colloidal solutions and nanoparticles is carried out with DLS. Light scattered from a laser, which travels through the colloidal solution, is measured by DLS.²

DLS is a widely employed technique to find the size of NPs in colloidal suspensions in the nano- and sub micrometer ranges. NPs dispersed in a colloidal solution are in continuous Brownian motion. DLS measures the light scattering as a function of time, which combined with the Stokes-Einstein assumption are used to determine the NP hydrodynamic diameter in solution.^{2,9}

DLS is noninvasive, and thus the sample can be reused for other purposes after the analysis. In addition, no specific modification is needed (except dilution), and a small sample volume (1–1.5 mL) is sufficient for the analysis.³⁰

The success of the technique is based on the fact that it provides estimates of the average particle size and size distribution within a few minutes, and that user-friendly commercial instruments are available. Several methods are being developed for DLS, in these methods can be classified in: (i) by the difference in raw data acquisition (autocorrelation, cross-correlation and frequency analysis), (ii) by the difference in optical setup (homodyne versus heterodyne mode), (iii) by the angle of observation.³¹

DLS typically can provide four different outputs: Z-average diameter ($\propto r^6$), intensity-weighted diameter ($\propto r^6$), volume-weighted diameter ($\propto r^3$), and number-weighted diameter ($\propto r^1$). The intensity weighted diameter is the raw data from the scattering intensity of each particle fraction, the number and volume are deduced from the intensity weighted, and the Z-

average is the “cumulant mean”. The Z-average is the most popular way to report the diameter measured by DLS, because of the reliance of the technique on least-squares fitting and insensitivity to noise, but it is very sensitive to agglomerates of particles. Some investigators are often tempted to report only number-average results, because typically show the smallest size and distribution in an effort to claim monodisperse particle distributions, but this form of selection bias should be avoided by reporting the various fits of the data.²²

DLS sizing can be conducted through a simple three: step 1, insert sample into the instrument; step 2, allocate proper setting on the software; and step 3, press START button to begin the measurement. After that, the user just needs to wait for the measurement results. These simplified steps have greatly reduced the proper technical training required to conduct DLS measurement, leading to the high popularity of this technique, but at the same time making DLS a “black-box” technique since any prior knowledge on scattering theory is needed to conduct the measurement or even getting “good” results. However, challenge arose from the correct interpretation of the obtained data.³⁰

The optical configuration of a typical experimental setup for dynamic light scattering measurement can be seen in Figure A12. The detector, which is usually a photomultiplier tube, measures the intensity of the scattered light in the form of rate modulated pulse train. These pulses are then passed through an electronic module called an amplifier-discriminator before entering to the correlator. The amplifier-discriminator is used to amplify the weak signals appearing from the detector output, suppress the background noise, and standardize the pulses making them suitable for processing by a correlator. The correlator performs autocorrelation of the rate modulated pulse trains by comparing the scattering intensity for a given period of time t_k in discrete steps Δt .³⁰

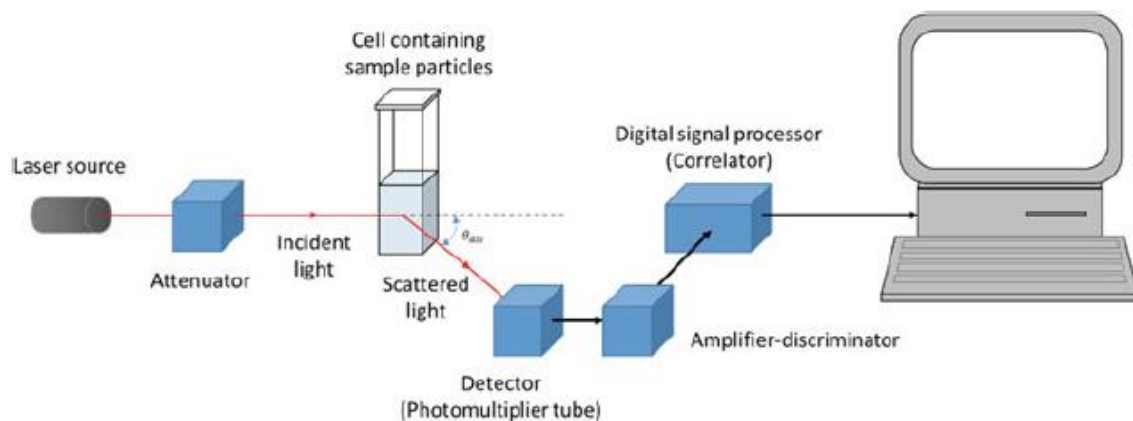


Figure A12. Scheme of a dynamic light scattering spectrometer.³⁰

One important parameter in DLS measurements is the polydispersity index (PDI). From a physical perspective, PDI represents the degree of heterogeneity in the hydrodynamic diameter of the particles within a particular system. The greater PDI value indicates the more significant non-uniformity in the particles' hydrodynamic diameter and higher polydispersity of the particle system. Table A1 demonstrates the description of particle systems according to their range of PDI value. It should be emphasized that PDI value is only representative for monomodal particle system (particle distribution with only one peak) as similar to Z-average. For multimodal particle system, PDI value lost its significance as the measure of particle dispersion and additional analysis should be conducted to obtain an accurate picture on the dispersity of the particle sample.³⁰

Table A1. Description of particle system with different range of PDI value.³⁰

| PDI | Description |
|---------|---|
| 0 | Uniform (or monodispersed) particle system. All particles are having the same size |
| 0–0.1 | Nearly monodispersed particle system. The dispersion are narrow and still can be considered as “monodispersed” throughout result analysis |
| 0.1–0.4 | Polydispersed particle system. Particle distribution should be considered in data analysis |
| > 0.4 | Highly polydispersed particle system. Particle distribution might be multimodal and multiple particle species might present |

Measurement of particle size is an essential step in research dealing MNP. This necessity is ascribed to the unique features of MNP, such as magnetism and magnetic responsiveness, which change with respect to its size. For instance, the saturation magnetization, M_s , and the

coercivity, H_c , of MNPs change as a function of the particle size. More importantly, extra care should be allocated when interpreting the DLS data for strongly interacting nanoparticles, such as MNP, which tend to agglomerate into clusters form.³⁰

It is important to consider concentration when measuring size based on DLS using MNP samples. With too low concentration there may not be enough scattering of the light occurring to accurately measure the sample. However, with too concentrated of a sample multiple scattering occurrences may appear leading to inaccurate results. A good reference is ISO 22412:2017(E), which provides a comprehensive view of sample preparation and analysis. Additionally, it is necessary to consider the dispersing media for DLS measurements for assessing the colloidal stability of these materials.²²

2.3.5.3 Zeta Potential (ζ -potential)

Nanoparticles or colloidal particles will have a surface charge in suspension. When an electric field is applied a particle starts moving due to the interaction between the electric field and the charged particle. The velocity and the direction of motion are a function of the electric field, charge, and the suspending medium. The velocity of the particle is measured by observing the Doppler shift in the scattered light, and the velocity proportional to the electrical potential of the particle at the shear plane is called the Zeta potential (ζ -potential).²

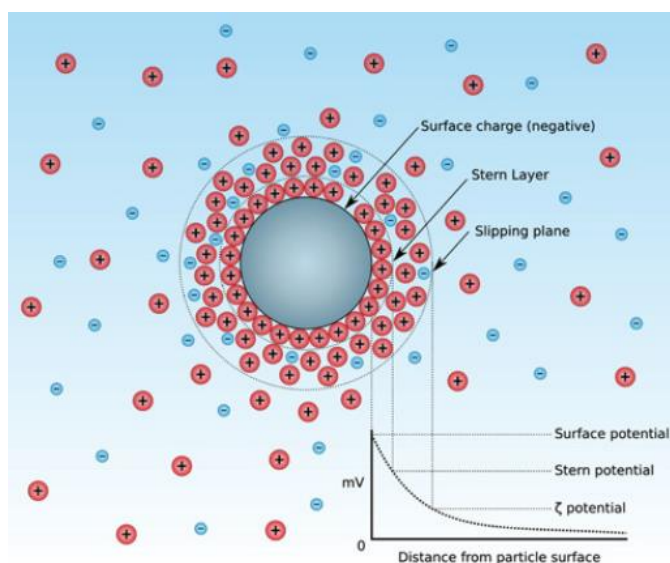


Figure A13. Schematic representation of the ionic concentration and potential difference as a function of distance from the charged surface of a particle suspended in a dispersion medium.³²

Under an electric field, the optical measurement of the particle's motion can be used to determine the ζ -potential, therefore, the ζ -potential is the electrical potential in the interfacial double layer at the location of the slipping plane, between the outer region of the particles charge cloud and the solvent it is suspended, and it should not be confused with the electric surface potential or the Stern potential. Figure A13 illustrates the basic concept of ζ -potential.^{1,2}

The relationship between zeta potential and colloidal stability is often the most broadly discussed since measures the magnitude of electrostatic repulsion/attraction between particles and thus, it has become one of the fundamental parameters known to affect stability of colloidal particles.¹

Highly positively or negatively charged particles tend to repel each other, resulting in more stability and a minor trend to agglomerate. Such highly charged particles are related to pH values which are far from the so-called 'isoelectric point' (IEP) of a solution, which refers to the pH value at which the zeta potential is zero. Contrarily, at low ζ -potential values in a colloidal NP dispersion causes the flocculation of the colloids and it corresponds to values closer to the IEP of the system. This property can be tuned by modifying the surface chemistry, where the stabilization of the colloidal suspension is obtained via electrostatic repulsion, influenced by the concentration of suspension, composition of solvent and other additives. So long as the repulsive forces overcome the attractive van der Waals component stability can be maintained.^{1,9}

The magnitude of the ζ -potential provides information about the particle stability. The higher magnitude represents increased stability due to increased electrostatic repulsion:²

- ❖ Particles tend to aggregate in the range of 0 to ± 5 mV.
- ❖ Minimally stable particles are in the range of ± 5 to ± 20 mV.
- ❖ Moderately stable particles are in the range of ± 20 to ± 40 mV.
- ❖ Highly stable particles are in the range of ± 40 mV.

Careful attention must be made to ensure that the materials remain fully in suspension during the entire measurement, including control over the pH and specific ion concentration of the suspending media, and precaution to ensure the effects of sample dilution do not alter the surface charge of the particles.²²

Nowadays, ζ -potential analysis and measurements have a lot of real-world applications. In the field of water purification and treatment ζ -potential analysis has established optimum coagulation conditions for removal of particulate matter and organic dyestuffs from aqueous waste products.³²

2.3.5.4 Brunauer-Emmett-Teller (BET) surface area analysis of nanoparticles

Named by the initials of the surnames of its developers, Brunauer, Emmett and Teller, BET technique is often used for the characterization of nanoscale materials. It is based on the principle of physical adsorption of a gas on a solid surface, and it is widely used for the determination of the surface area of nanostructures being a relatively accurate, rapid and simple method for this purpose.⁹

The theory is an extension to the Langmuir theory and assumes gas molecules adsorb onto the surface of the material and form infinitely thick stacks of monolayers of absorbed gases that only interact with their adjacent layers. The absorption process is driven by van der Waals forces between the gas and the material surface and is monitored by a continuous gas flow procedure or a volumetric analysis.¹

BET is a useful tool to determine how a nanomaterial will perform with other materials, since many of the properties of these materials are surface area limited. Frequently, BET analysis is performed using nitrogen on powder samples. The surface is heated under vacuum to remove all other adsorbed species and then the adsorbing analysis gas is admitted when temperature is constant. As the adsorption takes place, the pressure of the adsorbing gas decreases according to the BET isotherm. Relative pressures less than atmospheric pressure are achieved by creating conditions of partial vacuum. After the saturation pressure, no more adsorption occurs regardless of any further increase in pressure.^{1,33,34}

The data collected is displayed in the form of a BET isotherm, which plots the amount of gas adsorbed as a function of the relative pressure. There are five types of adsorption isotherms possible:

- ❖ Type I Isotherm: is a pseudo-Langmuir isotherm because it depicts monolayer adsorption (Figure A14a). This isotherm is obtained when $P/P < 1$ and $c > 1$ in the BET equation, where P/P is the partial pressure value and c is the BET constant, which is related to the adsorption energy of the first monolayer and varies from solid to solid. Materials with pore diameters less than 2 nm, gives this type of isotherm.
- ❖ Type II Isotherm: is very different than the Langmuir model. The flatter region in the middle represents the formation of a monolayer (Figure A14b). This isotherm is obtained when $c > 1$ in the BET equation. This is the most common isotherm obtained when using the BET technique. At very low pressures, the micropores fill with nitrogen gas. At the knee, monolayer formation is beginning, and multilayer formation occurs at medium pressure. At higher pressures, capillary condensation occurs.

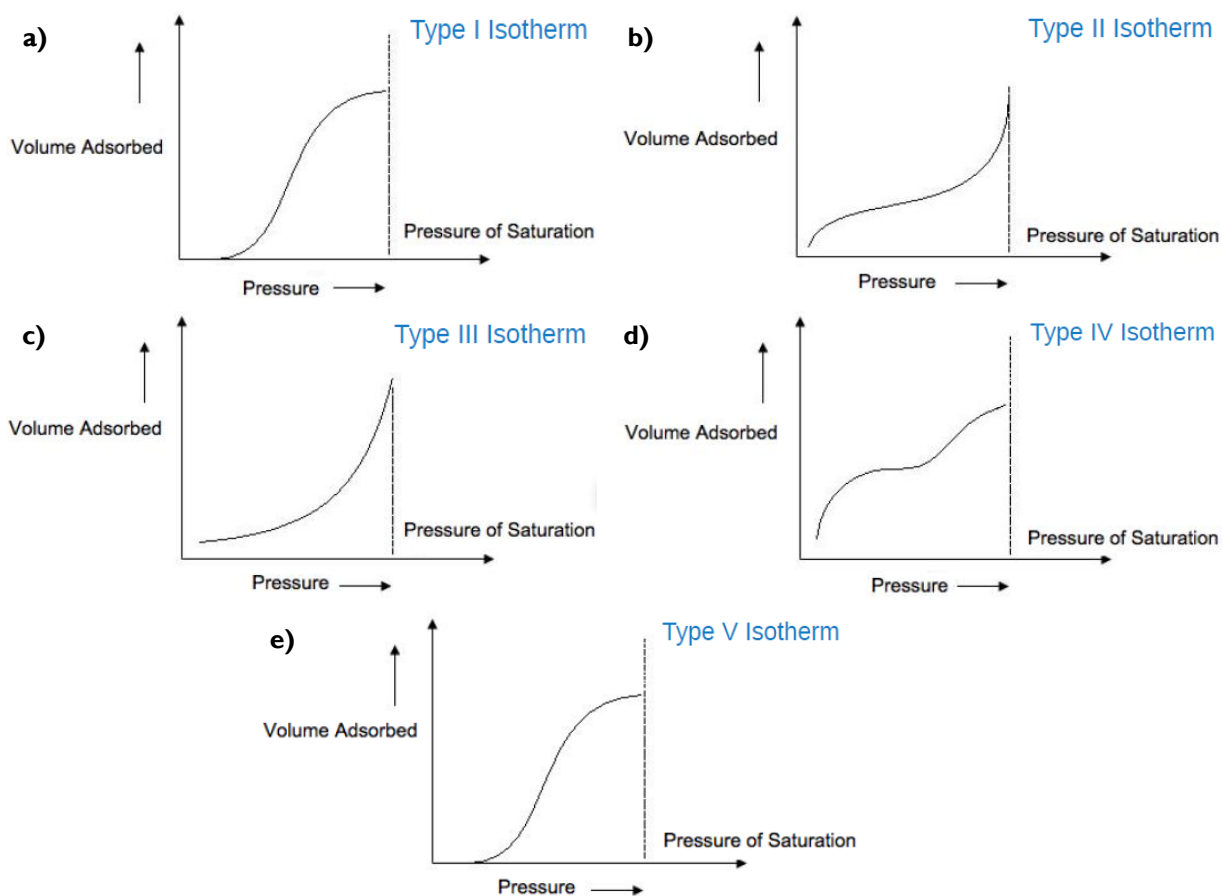


Figure A14. Isotherm plots with the volume of gas adsorbed onto the surface of the sample as pressure increases.³³

-
- ❖ A type III isotherm: this isotherm (Figure A14c) is obtained when the $c < 1$ and shows the formation of a multilayer. Because there is no asymptote in the curve, no monolayer is formed, and BET is not applicable.
 - ❖ Type IV isotherms: this (Figure A14d) occur when capillary condensation occurs. Gases condense in the tiny capillary pores of the solid at pressures below the saturation pressure of the gas. At the lower pressure regions, it shows the formation of a monolayer followed by a formation of multilayers. BET surface area characterization of mesoporous materials, which are materials with pore diameters between 2-50 nm, gives this type of isotherm.
 - ❖ Type V Isotherm: these isotherms (Figure A14e) are very similar to type IV isotherms and are not applicable to BET.

This technique works best with solid particles such as metals that will not alter morphology while undergoing the drying/freezing process of the measurement cycle. The accuracy of BET is ponderously related to the mass of material being measured, the more the sample mass, the greater the accuracy. Sample masses of less than 0.1 g are considered poor quality, and masses of 0.2 g and up are typically considered enough ss for a measurement with acceptable error. For some nanoparticle samples, this mass of material can be difficult to produce; however, this is a nondestructive technique, so sample is not lost after measurement.¹

2.3.5.5 Vibrating sample magnetometry (VSM)

The magnetic response of materials to an external magnetic field is influenced by the electronic configuration of its constituent elements, the way they combine chemically, and temperature.³⁵

One of the most common ways to describe magnetic behavior of a material is using direct current (dc) magnetometry techniques. In dc measurements, the field is uniform and constant, thus the samples must be physically moving in order to produce a change in the magnetic field. One way to measure the moment by force is using a vibrating-sample magnetometer (VSM).²²

VSM systems are used to measure the magnetic properties of materials as a function of magnetic field, temperature, and time. Powders, solids, liquids, single crystals, and thin films

are all readily accommodated in a VSM. The operating principle bases on the exhibition of a magnetic moment m by a magnetic sample placed within a uniform magnetic field H . By mechanically vibrating the sample within suitably placed sensing coils, a voltage is induced along the sensing coils. The measurement of the induced voltage can be related to the magnetic moment of the sample. The magnetic field may be generated by an electromagnet, or a superconducting magnet while variable temperatures may be achieved using either cryostats or furnace assemblies.³⁶ The essential features of a VSM are shown in Figure A15.

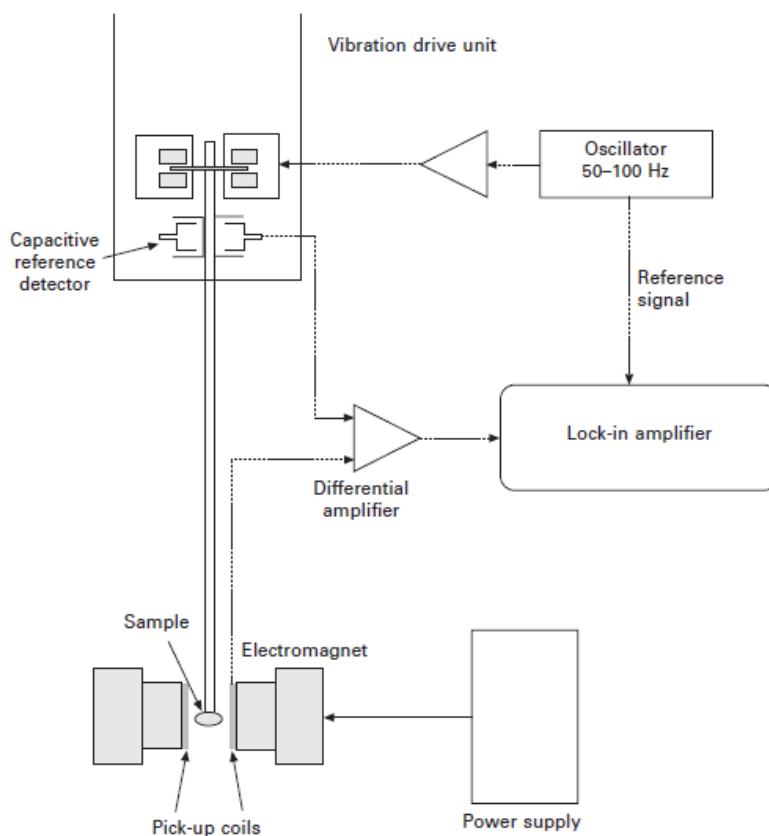


Figure A15. Schematic diagram of the essential features of a vibrating sample magnetometer.

VSM is a simple and relatively inexpensive technique, it is reliable and provide information about the magnetic moment of a material as a function of temperature, field, and crystal orientation. In preparing samples for this measurement, it is important to prevent unintended particle rotation.²²

Some common types of magnetic materials are listed below and an illustration of their magnetization curves are shown in Figure A16:^{22,35}

- ❖ **Diamagnets:** In a diamagnetic material, all the electron spins in the material are paired, and they display the weakest type of magnetic behavior. Inert gases, most nonmetals, and organic compounds are common diamagnets, and their response is weakly dependent on temperature.
- ❖ **Paramagnets:** Paramagnetic materials are those in which individual atoms have uncompensated spins that are randomly aligned. In the presence of an external magnetic field, the uncompensated spin moments tend to align in the direction of the field, and they have a positive magnetic susceptibility.

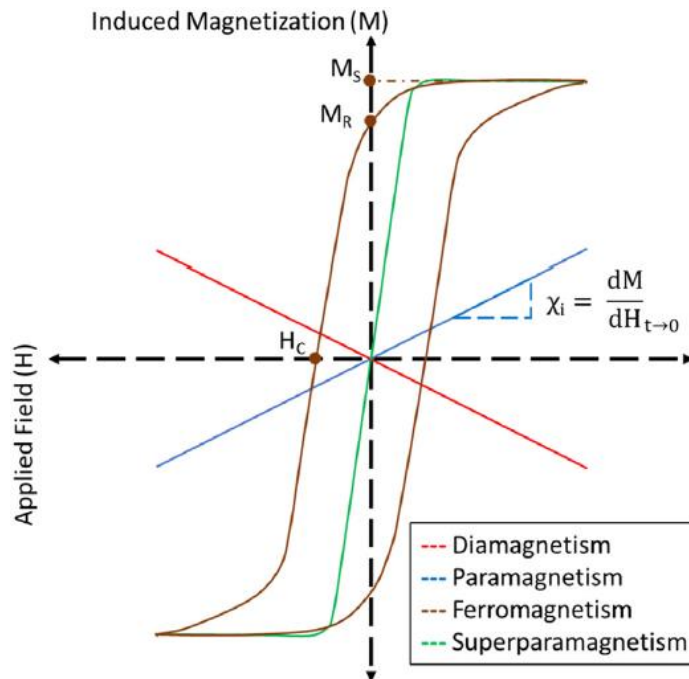


Figure A16. Illustration of magnetization curves for ferromagnetic, paramagnetic, diamagnetic, and superparamagnetic materials. M_S , M_R , H_C , and χ_i are the saturation magnetization, remanent magnetization, coercive field threshold, and the initial susceptibility of the material.³⁵

- ❖ **Ferromagnets:** The magnetic moments in each domain of a ferromagnet are oriented along an easy axis of magnetization, corresponding to a low-energy state. Uncompensated electrons in individual atoms tend to interact, resulting in coupling of spins in a preferred orientation. Unlike paramagnets, when the applied field is removed,

they may retain a component of magnetization in the direction of the applied field causing them to be “permanently” magnetized and their response is an open curve showing hysteresis. The net magnetization of ferrimagnets is greater than for antiferromagnets. Ferromagnetism is mostly seen in metals like iron, nickel, cobalt, and manganese.

- ❖ Superparamagnetism: Superparamagnetic nanoparticles only possess a single domain; they do not exhibit a hysteresis loop as ferromagnetic and ferromagnetic materials do, since they lose their magnetism in the absence of a field. Small ferromagnetic nanoparticles tend to behave as superparamagnets.

Hysteresis loops are magnetization curves that represent a materials magnetic behavior of the multiple domains as can be seen in Figure A17. When all the domains do not return to their original orientations after the magnetic saturation (M_s) is reached and the field is decreased, there is remnant magnetization (M_R). M_R can be removed by applying a magnetic field in the opposite direction to the originally applied field, which is defined as the coercive field (H_c).

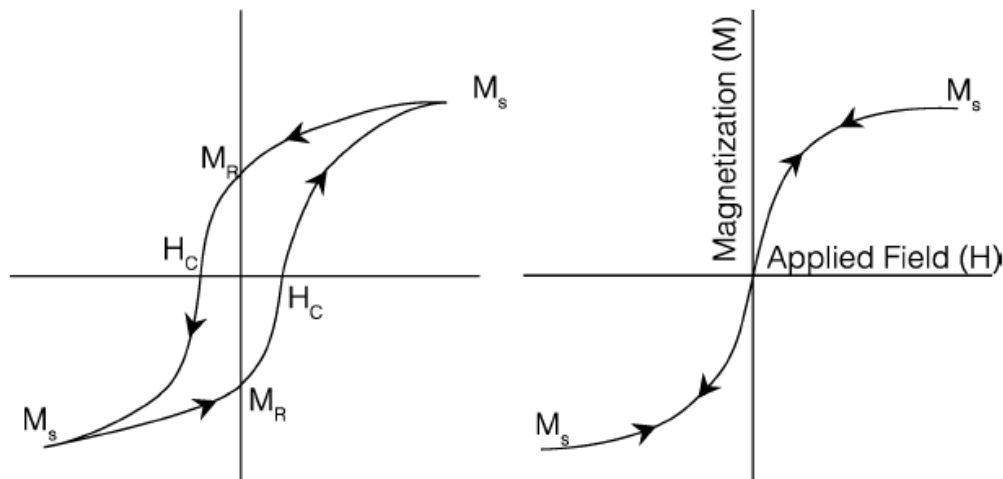


Figure A17. Representative M–H loops of (left) magnetic nanoparticles exhibiting hysteresis and (right) where no hysteresis is observed.²²

Since magnetite (Fe_3O_4) is the most magnetic naturally occurring mineral and is a ferrimagnetic material that can exhibit superparamagnetism at the nanoscale (with a reported upper limit for single domain), it becomes essential use VSM to characterize the material.³⁵

2.8.1 FT-IR of raw MNP and each of the modifier

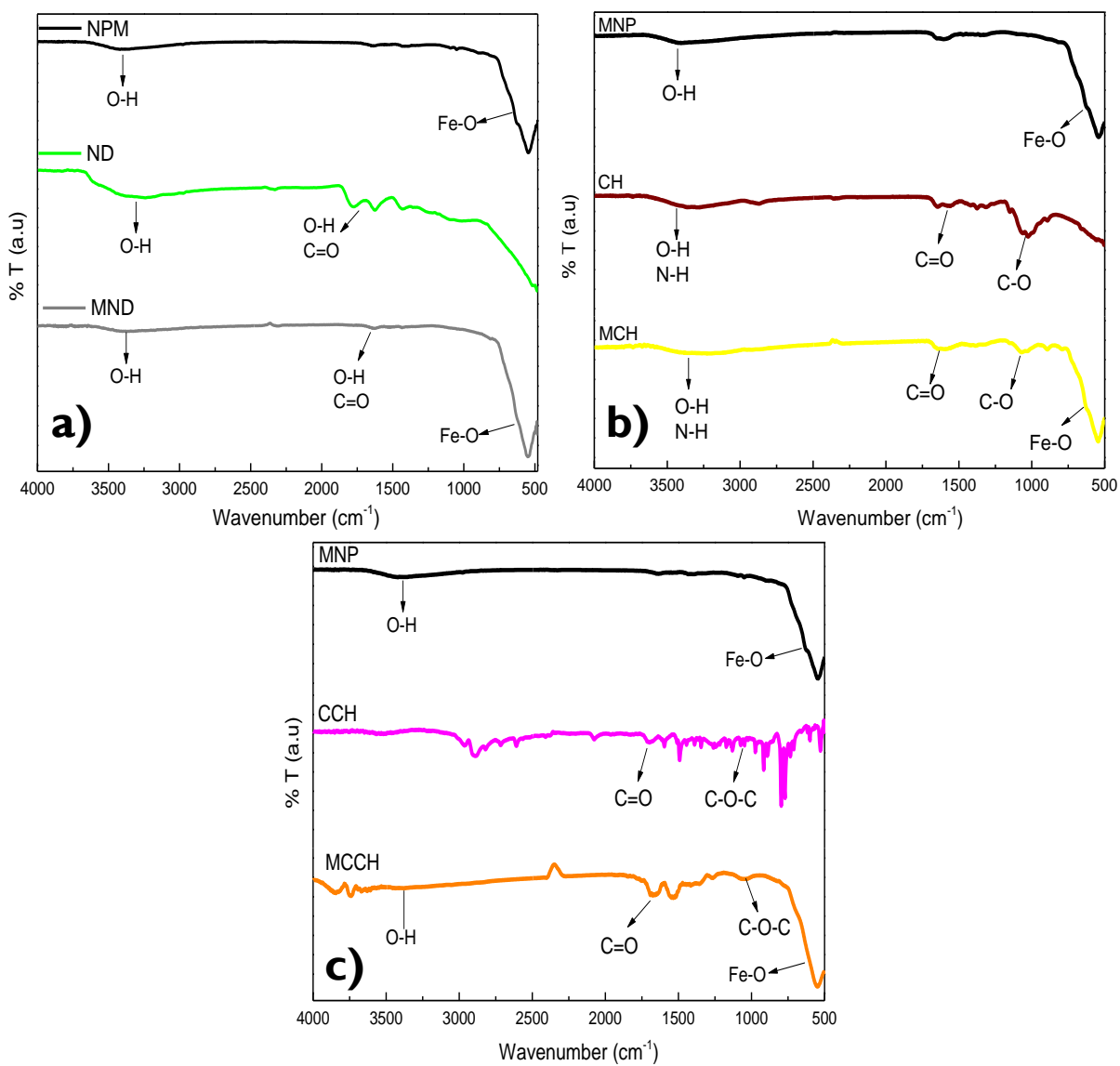


Figure A18. FT-IR's of a) MNP (black line), ND (green line), and MND (grey line). b) MNP (black line), CH (wine line) and MCH (yellow line). c) MNP (black line), CCH (pink line), and MCCH (orange line).

2.8.2 TGA of raw MNP and each of the modifier

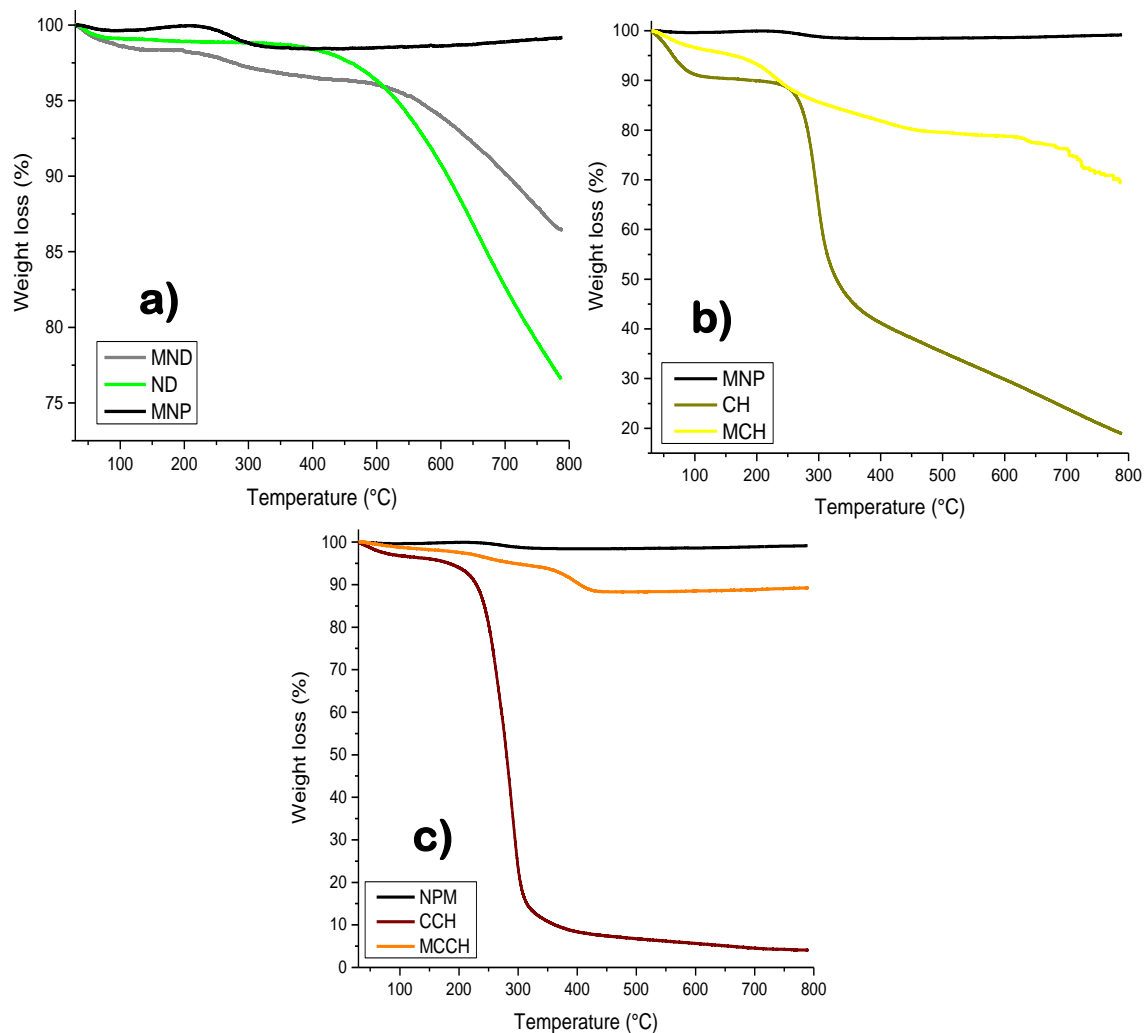


Figure A19. TGA's of a) MNP (black line), ND (green line), and MND (grey line). b) MNP (black line), CH (dark yellow line) and MCH (yellow line). c) MNP (black line), CCH (wine line), and MCCH (orange line).

2.8.3A STEM/SEM characterization of MNP, MND, MCH and MCCH

The morphology analysis of magnetic nanoscavengers were approached by SEM and STEM images. Figure A20a corresponds to the SEM image of MNP showing their agglomeration effect and giving an overview of their surface area. This fact allows us to verify that real nanometric particles have been produced despite the aggregation of the particles as a result of Van der Waals forces among particles.³⁷ At the same time, looking at the distribution analysis on Figure A21a we can inquire that the size of the material is less than 20 nm (~16 nm).

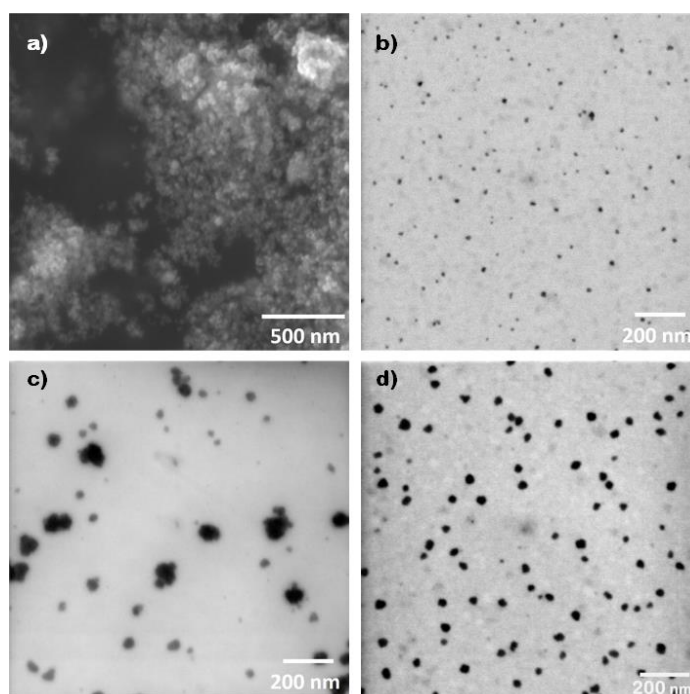


Figure A20. a) SEM image of MNP powder and STEM images of dried drop of aqueous dispersion of b) MND, c) MCH, and d) MCCH.

STEM images of the magnetic nanoscavengers were obtained after drying a drop of aqueous dispersed material. Figure A20b, c, and d, displays all prepared nanoscavengers and along with the distribution analysis on Figure A21b, c and d, we can observe that the particle sizes are around 18nm, 35, and 26 nm for MND, MCH, and MCCH, respectively. A better dispersion of the material, with fewer agglomerates, is noticed for the MND (Figure A20b), which lead to a smaller size than the other functionalized materials. The opposite effect is observed for the MCH, where the formation of clusters was detected and subsequently, they have a bigger size. This effect is certainly related to a higher degree of modification of the

material, as seen in TGA analysis and stronger electrostatic and Van der Waals interactions between particles (Figure A20c). MCCH particles are less agglomerated than MCH, certainly due to the coating of CCH, being a larger molecule with greater steric impediment (Figure A20 d), which is the reason for presenting a smaller size than MCH. This result was also suggested by the TGA analysis of CH and CCH.

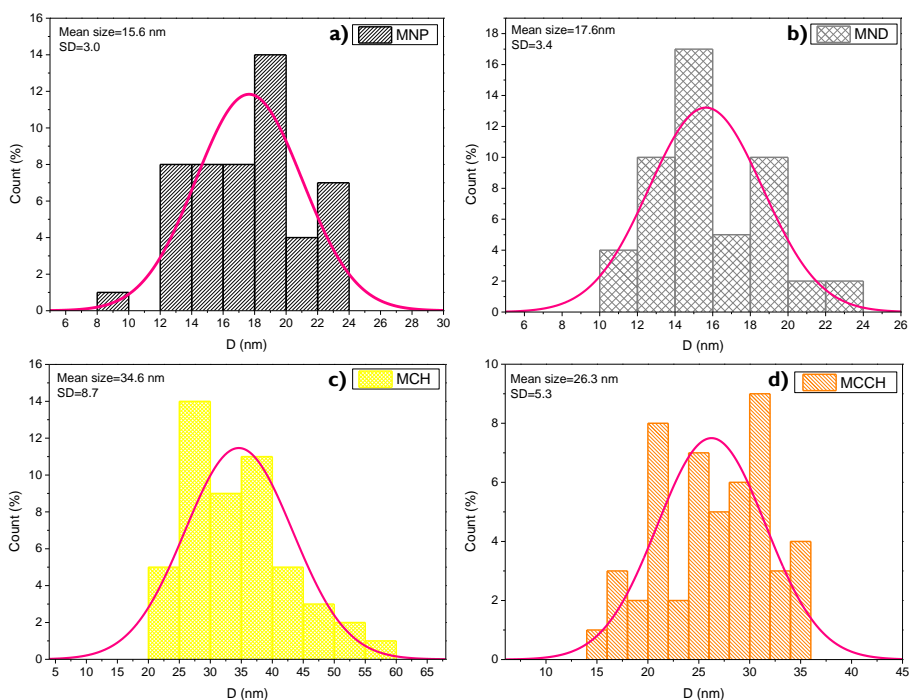


Figure A21. Size distribution of a) MNP, b) MND, c) MCH, and d) MCCH.

2.8.3B EDX tables for MNP, MND, MCH, and MCCH

Table A2. EDX table for MNP

| Element | Atomic N° | Series | Unn. (wt.%) | C Norm. (wt.%) | C Atom. (at.%) | C Error (1 σ , wt.%) |
|---------|-----------|----------|-------------|----------------|----------------|-----------------------------|
| Fe | 26 | K-series | 57.87 | 50.96 | 21.03 | 2.72 |
| O | 8 | K-series | 35.91 | 31.62 | 45.54 | 4.40 |
| C | 6 | K-series | 19.79 | 17.43 | 33.44 | 2.78 |
| | | Total: | 113.57 | 100.00 | 100.00 | |

Table A3. EDX table for MND

| Element | Atomic N° | Series | Unn. (wt.%) | C Norm. (wt.%) | C Atom. (at.%) | C Error (1 σ , wt.%) |
|---------|-----------|----------|-------------|----------------|----------------|-----------------------------|
| Fe | 26 | K-series | 48.62 | 43.68 | 16.45 | 1.70 |
| O | 8 | K-series | 38.46 | 34.56 | 45.44 | 5.20 |
| C | 6 | K-series | 24.22 | 21.76 | 38.11 | 3.85 |
| | | Total: | 113.30 | 100.00 | 100.00 | |

Table A4. EDX table for MCH

| Element | Atomic N° | Series | Unn. (wt.%) | C Norm. (wt.%) | C Atom. (at.%) | C Error (1 σ , wt.%) |
|---------|-----------|----------|-------------|----------------|----------------|-----------------------------|
| Fe | 26 | K-series | 62.35 | 59.03 | 28.41 | 2.08 |
| O | 8 | K-series | 38.04 | 36.01 | 60.50 | 4.66 |
| C | 6 | K-series | 5.24 | 4.96 | 11.10 | 1.07 |
| | | Total: | 105.64 | 100.00 | 100.00 | |

Table A5. EDX table for MCCH.

| Element | Atomic N° | Series | Unn. (wt.%) | C Norm. (wt.%) | C Atom. (at.%) | C Error (1 σ , wt.%) |
|---------|-----------|----------|-------------|----------------|----------------|-----------------------------|
| Fe | 26 | K-series | 56.34 | 52.37 | 22.21 | 1.88 |
| O | 8 | K-series | 35.36 | 32.86 | 48.66 | 4.36 |
| C | 6 | K-series | 15.89 | 14.77 | 29.12 | 2.41 |
| | | Total: | 107.59 | 100.00 | 100.00 | |

3.8.1 Urban reuse extensive water quality parameters

Table A6. Water quality required for urban reuse, extended.³⁸

| Parameter | Restricted | | | | Not restricted | | | |
|------------------------------------|-------------|-----------------------|---------|-----------------------|----------------|-----------------------|---------|-----------------------|
| | EPA | NOM-001-SEMARNAT-1996 | | NOM-003-SEMARNAT-1996 | EPA | NOM-001-SEMARNAT-1996 | | NOM-003-SEMARNAT-1996 |
| | 1992 | B | C | | 1992 | B | C | |
| pH | 6 – 9 | 5 - 10 | 5 – 10 | ----- | 6 – 9 | 5 - 10 | 5 – 10 | ----- |
| DBO ₅ | < 30 | 75 | 30 | ----- | < 10 | 75 | 30 | 20 |
| Turbidity (NTU) | ----- | ----- | ----- | ----- | < 2 | ----- | ----- | ----- |
| Settleable solids | ----- | 1 | 1 | ----- | ----- | 1 | 1 | ----- |
| Fecal coliforms (organisms/100 mL) | < 200 | < 1,000 | < 1,000 | 1,000 | not detectable | < 1,000 | < 1,000 | 240 |
| Helminth eggs | ----- | 5 | 5 | 5 | ----- | 1 | 1 | 1 |
| Residual chlorine (mg/L) | 1 | ----- | ----- | ----- | 1 | ----- | ----- | ----- |
| Fats and oils | ----- | 15 | 15 | ----- | ----- | 15 | 15 | ----- |
| Temperature (°C) | ----- | 40 | 40 | ----- | ----- | 40 | 40 | ----- |
| Floating matter | ----- | Absent | Absent | Absent | ----- | Absent | Absent | Absent |
| Total suspended solids | < 30 | 75 | 40 | ----- | ----- | 75 | 40 | 20 |
| Total Nitrogen | ----- | 40 | 15 | ----- | ----- | 40 | 15 | ----- |
| Total phosphorus | ----- | 20 | 5 | ----- | ----- | 20 | 5 | ----- |
| Arsenic | 0.1 | 0.1 | 0.1 | 0.1 | 0.1 | 0.1 | 0.1 | 0.1 |
| Cadmium | 0.1 | 0.1 | 0.1 | 0.1 | 0.01 | 0.1 | 0.1 | 0.1 |
| Cyanide | ----- | 1 | 1 | 1 | ----- | 1 | 1 | 1 |
| Copper | 0.2 | 4 | 4 | 4 | 0.2 | 4 | 4 | 4 |
| Chrome | 0.1 | 0.5 | 0.5 | 0.5 | 0.1 | 0.5 | 0.5 | 0.5 |
| Mercury | ----- | 0.005 | 0.005 | 0.005 | ----- | 0.005 | 0.005 | 0.005 |
| Nickel | 0.2 | 2 | 2 | 2 | 0.2 | 2 | 2 | 2 |
| Lead | 5.0 | 0.2 | 0.2 | 0.2 | 5.0 | 0.2 | 0.2 | 0.2 |
| Zinc | 2 | 10 | 10 | 10 | 2 | 10 | 10 | 10 |
| Total dissolved solids | 500 – 2,000 | ----- | ----- | ----- | 500 – 2,000 | ----- | ----- | ----- |
| Aluminum | 5 | ----- | ----- | ----- | 5 | ----- | ----- | ----- |
| Beryllium | 0.1 | ----- | ----- | ----- | 0.1 | ----- | ----- | ----- |
| Boron | 0.75 | ----- | ----- | ----- | 0.75 | ----- | ----- | ----- |
| Cobalt | 0.05 | ----- | ----- | ----- | 0.05 | ----- | ----- | ----- |
| Fluoride | 1.0 | ----- | ----- | ----- | 1.0 | ----- | ----- | ----- |
| Iron | 5 | ----- | ----- | ----- | 5 | ----- | ----- | ----- |
| Lithium | 2.5 | ----- | ----- | ----- | 2.5 | ----- | ----- | ----- |
| Manganese | 0.2 | ----- | ----- | ----- | 0.2 | ----- | ----- | ----- |
| Molybdenum | 0.01 | ----- | ----- | ----- | 0.01 | ----- | ----- | ----- |
| Selenium | 0.02 | ----- | ----- | ----- | 0.02 | ----- | ----- | ----- |
| Vanadium | 0.1 | ----- | ----- | ----- | 0.1 | ----- | ----- | ----- |

*All parameters in mg/L, except pH and those indicated
B and C are receptor water body types

3.8.2 Agricultural reuse extensive water quality parameters

Table A 7. Water quality required for agricultural reuse, extended parameters.³⁸

| Parameter | Not restricted | | | Restricted | | |
|-------------------------------|-------------------------------|-----------------------|------------|-------------|-----------------------|------------|
| | EPA | NOM-001-SEMARNAT-1996 | DGCOH 1987 | EPA | NOM-001-SEMARNAT-1996 | DGCOH 1987 |
| pH | 6 – 9 | 5 – 10 | 7 – 8 | 6 – 9 | 5 – 10 | 7 – 8 |
| DBO ₅ (mg/L) | < 10 | ----- | 20 | < 30 | ----- | 50 |
| Turbidity (NTU) | < 2 | ----- | 10 | ----- | ----- | 20 |
| Suspended solids (mg/L) | ----- | ----- | 100 | < 30 | ----- | 100 |
| Fecal coliforms (org/100 mL) | No detectable | < 1,000 | 1,000 | < 200 | < 1,000 | 10,000 |
| Standard account (Col/mL) | ----- | ----- | 200 | ----- | ----- | 200 |
| Helminth eggs | ----- | 1 | 1 | ----- | 5 | 1 |
| Residual chlorine (mg/L) | 1 | ----- | 0.2 | 1 | ----- | 0.2 |
| Oils and fats (mg/L) | ----- | 15 | V.F.* | ----- | 15 | V.F.* |
| Floating matter | ----- | Absent | ----- | ----- | Absent | ----- |
| Total dissolved solids (mg/L) | 500 – 2,000 | ----- | 2,000 | 500 – 2,000 | ----- | 2,000 |
| Parameter | Restricted and not restricted | | | | | |
| Aluminum | 5.0 | | ----- | 5.0 | | |
| Arsenic | 0.10 | | 0.2 | 0.10 | | |
| Beryllium | 0.10 | | ----- | ----- | | |
| Boron | 0.75 | | ----- | 1.0 | | |
| Cadmium | 0.01 | | 0.05 | 0.01 | | |
| Chlorine | 0.1 | | ----- | ----- | | |
| Cyanide | ----- | | 2.0 | 0.1 | | |
| Cobalt | 0.05 | | ----- | ----- | | |
| Copper | 0.2 | | 4.0 | 0.2 | | |
| Chromium | ----- | | 0.5 | 0.1 | | |
| Fluoride | 1.0 | | ----- | 1.0 | | |
| Iron | 5.0 | | ----- | 5.0 | | |
| Lead | 5.0 | | 5.0 | 5.0 | | |
| Lithium | 2.5 | | ----- | ----- | | |
| Manganese | 0.2 | | ----- | 0.2 | | |
| Mercury | ----- | | 0.005 | 0.002 | | |
| Molybdenum | 0.01 | | ----- | ----- | | |
| Nickel | 0.2 | | 2.0 | 0.2 | | |
| Selenium | 0.02 | | ----- | 0.02 | | |
| Vanadium | 0.1 | | ----- | ----- | | |
| Zinc | 2.0 | | 10.0 | 2.0 | | |

DGCOH= Dirección General de Construcción y Operación Hidráulicas (DGCOH)

*V.F. = virtually free

ANNEX REFERENCES

- (1) Campbell, J.; Burkitt, S.; Dong, N.; Zavaleta, C. Chapter 9 - Nanoparticle Characterization Techniques. In *Micro and Nano Technologies*; Chung, E. J., Leon, L., Rinaldi, C. B. T.-N. for B. A., Eds.; Elsevier, 2020; pp 129–144.
- (2) Titus, D.; James Jebaseelan Samuel, E.; Roopan, S. M. Chapter 12 - Nanoparticle Characterization Techniques. In *Micro and Nano Technologies*; Shukla, A. K., Iravani Characterization and Applications of Nanoparticles, S. B. T.-G. S., Eds.; Elsevier: Vellore, India, 2019; pp 303–319.
- (3) Kumar, N.; Sinha Ray, S. Synthesis and Functionalization of Nanomaterials: Introduction. In *Springer Series in Materials Science*; Springer Nature: Switzerland, 2018; pp 15–55.
- (4) Neamtu, M.; Nadejde, C.; Hodoroaba, V.-D.; Schneider, R. J.; Verestiuc, L.; Panne, U. Functionalized Magnetic Nanoparticles: Synthesis, Characterization, Catalytic Application and Assessment of Toxicity. *Sci. Rep.* **2018**, *8*, 6278.
- (5) Santoyo Salazar, J.; Perez, L.; de Abril, O.; Truong Phuoc, L.; Ihiawakrim, D.; Vazquez, M.; Greneche, J.-M.; Begin-Colin, S.; Pourroy, G. Magnetic Iron Oxide Nanoparticles in 10–40 Nm Range: Composition in Terms of Magnetite/Maghemite Ratio and Effect on the Magnetic Properties. *Chem. Mater.* **2011**, *23*, 1379–1386.
- (6) Prodan, A. M.; Iconaru, S. L.; Ciobanu, C. S.; Chifiriuc, M. C.; Stoicea, M.; Predoi, D. Iron Oxide Magnetic Nanoparticles: Characterization and Toxicity Evaluation by *In Vitro* and *In Vivo* Assays. *J. Nanomater.* **2013**, *2013*, 587021.
- (7) Lu, A.; Salabas, E. L.; Schüth, F. Magnetic Nanoparticles: Synthesis, Protection, Functionalization, and Application. *Angew. Chemie Int. Ed.* **2007**, *46*, 1222–1244.
- (8) English, C. A.; Hyde, J. M.; Odette, G. R.; Lucas, G. E.; Tan, L. Chapter 4 - Research Tools: Microstructure, Mechanical Properties, and Computational Thermodynamics; Eds.; Elsevier: Boston, 2019; pp 103–161.

-
- (9) Mourdikoudis, S.; Pallares, R.; Thanh, N. Characterization Techniques for Nanoparticles: Comparison and Complementarity upon Studying Nanoparticle Properties. *Nanoscale* **2018**, *10*, 12871-12934
- (10) Su, D. Advanced Electron Microscopy Characterization of Nanomaterials for Catalysis. *Green Energy Environ.* **2017**, *2*, 70–83.
- (11) Plascencia-Villa, G.; Ponce, A.; Collingwood, J. F.; Arellano-Jiménez, J.; Zhu, X.; Rogers, J. T.; Betancourt, I.; José-Yacamán, M.; Perry, G. High-Resolution Analytical Imaging and Electron Holography of Magnetite Particles in Amyloid Cores of Alzheimer's Disease. *Sci. Rep.* **2016**, *6*, 24873.
- (12) Yilmaz, E.; Ulusoy, H. İ.; Demir, Ö.; Soylak, M. A New Magnetic Nanodiamond/Graphene Oxide Hybrid (Fe₃O₄@ND@GO) Material for Pre-Concentration and Sensitive Determination of Sildenafil in Alleged Herbal Aphrodisiacs by HPLC-DAD System. *J. Chromatogr. B* **2018**, *1084*, 113–121.
- (13) Ulusoy, H.; Gülle, S.; Yilmaz, E.; Soylak, M. Trace Determination of Vitamin B12 in Food Samples by Using Fe₃O₄ Magnetic Particles Including Multi-Walled Carbon Nanotube and Nano Diamond. *Anal. Methods* **2019**, *11*, 5108–5117.
- (14) Pecova, M.; Sebel, M.; Marková, Z.; Polakova, K.; Cuda, J.; Safářová, K.; Zboril, R. Thermostable Trypsin Conjugates Immobilized to Biogenic Magnetite Show a High Operational Stability and Remarkable Reusability for Protein Digestion. *Nanotechnology* **2013**, *24*, 125102.
- (15) Rahbar, N.; Ramezani, Z.; Mashhadizadeh, Z. One Step In-Situ Formed Magnetic Chitosan Nanoparticles as an Efficient Sorbent for Removal of Mercury Ions From Petrochemical Waste Water: Batch and Column Study. *Jundishapur J. Heal. Sci.* **2015**, *7*, 13–19.
- (16) Ebnesajjad, S. Chapter 4 - Surface and Material Characterization Techniques; Ebnesajjad, S. B. T.-S. T. of M. for A. B. (Second E., Ed.; William Andrew Publishing: Oxford, 2014; pp 39–75.

-
- (17) Barron, A. R. *Physical Methods in Chemistry and Nano Science*. **2015**.
- (18) Jalvandi, J. *Novel Chemical and Physical Approaches for Sustainable Drug Release from Biodegradable Electrospun Nanofibres*, 2016.
- (19) Shimadzu Corporation. *Measurement Methods for Powder Samples* <https://www.shimadzu.com/an/service-support/technical-support/analysis-basics/ftirtalk/talk8.html> (accessed May 25, 2021).
- (20) Bertolucci, E.; Galletti, A. M. R.; Antonetti, C.; Marracci, M.; Tellini, B.; Piccinelli, F.; Visone, C. *Chemical and Magnetic Properties Characterization of Magnetic Nanoparticles*. In *2015 IEEE International Instrumentation and Measurement Technology Conference (I2MTC) Proceedings*; 2015; pp 1492–1496.
- (21) Louër, D. *Powder X-Ray Diffraction, Applications*; Lindon, J. C. B. T.-E. of S. and S., Ed.; Elsevier: Oxford, 1999; pp 1865–1875.
- (22) Sandler, S. E.; Fellows, B.; Mefford, O. T. *Best Practices for Characterization of Magnetic Nanoparticles for Biomedical Applications*. *Anal. Chem.* **2019**, *91*, 14159–14169.
- (23) Ali, A.; AlSalhi, M.; Atif, M.; Ansari, A.; Qadir, M. I.; Sadaf, J.; Ahmed, E.; Nur, O.; Willander, M. *Potentiometric Urea Biosensor Utilizing Nanobiocomposite of Chitosan-Iron Oxide Magnetic Nanoparticles*. *J. Phys. Conf. Ser.* **2013**, *414*, 2024.
- (24) Shukla, S.; Jadaun, A.; Arora, V.; Sinha, R.; Biyani, N.; Jain, V. *In Vitro Toxicity Assessment of Chitosan Oligosaccharide Coated Iron Oxide Nanoparticles*. *Toxicol. Reports* **2014**, *2*, 27–39.
- (25) Mishra, D.; Arora Soni, R.; Lahiri, S.; Amritphale, S.; Chandra, N. *Synthesis and Characterization of Iron Oxide Nanoparticles by Solvothermal Method*. *Prot. Met. Phys. Chem. Surfaces* **2014**, *50*, 628–631.
- (26) Hashemifard, S. A.; Khosravi, A.; Abdollahi, F.; Alihemati, Z.; Rezaee, M. *Chapter 11 - Synthetic Polymeric Membranes for Gas and Vapor Separations*; Ismail, A. F., Salleh,

-
- W. N. W., Yusof Gas Separation, and Energy Sustainability, Eds.; Elsevier: Bushehr, Iran, 2020; pp 217–272.
- (27) Loganathan, S.; Ravi babu, V.; Mishra, R.; Pugazhenti, G.; Thomas, S. Thermogravimetry Analysis for Characterization of Nanomaterials; 2017.
- (28) Yang, Y.; Teng, L.; Seetharaman, S. Kinetic Studies on Evaporation of Liquid Vanadium Oxide, VO_x (Where $x = 4$ or 5). *Metall. Mater. Trans. B* **2012**, *43*.
- (29) Díaz-Hernández, A.; Gracida, J.; García-Almendárez, B. E.; Regalado, C.; Núñez, R.; Amaro-Reyes, A. Characterization of Magnetic Nanoparticles Coated with Chitosan: A Potential Approach for Enzyme Immobilization. *J. Nanomater.* **2018**, *2018*, 1–11.
- (30) Leong, S. S.; Ng, W. M.; Lim, J.; Yeap, S. P. Dynamic Light Scattering: Effective Sizing Technique for Characterization of Magnetic Nanoparticles BT - Handbook of Materials Characterization; Sharma, S. K., Ed.; Springer International Publishing: Cham, 2018; pp 77–111.
- (31) International Organization for Standardization. *ISO 22412:2017(En)*; Switzerland, 2017; p 33.
- (32) Raja, P. M. V; Barron, A. R. Zeta Potential Analysis. April 25, 2021.
- (33) Raja, P. M. V; Barron, A. R. BET Surface Area Analysis of Nanoparticles. April 25, 2021.
- (34) Shanks, R. A. Chapter 2 - Characterization of Nanostructured Materials; Thomas, S., Shanks, R., Chandrasekharakurup, S. B. T.-N. P. B., Eds.; William Andrew Publishing: Oxford, 2014; pp 15–31.
- (35) Savliwala, S.; Chiu-Lam, A.; Unni, M.; Rivera-Rodriguez, A.; Fuller, E.; Sen, K.; Threadcraft, M.; Rinaldi, C. Chapter 13 - Magnetic Nanoparticles. In *Micro and Nano Technologies*; Chung, E. J., Leon, L., Rinaldi, C. B. T.-N. for B. A., Eds.; Elsevier, 2020; pp 195–221.
- (36) Galletti, A.; Bertolucci, E.; Marracci, M.; Tellini, B.; Visone, C. Characterization of

Magnetite Nanoparticles. In *Conference Record - IEEE Instrumentation and Measurement Technology Conference*; 2014; pp 464–467.

- (37) Hussein-Al-Ali, S. H.; El Zowalaty, M. E.; Hussein, M. Z.; Geilich, B. M.; Webster, T. J. Synthesis, Characterization, and Antimicrobial Activity of an Ampicillin-Conjugated Magnetic Nanoantibiotic for Medical Applications. *Int. J. Nanomedicine* **2014**, *9*, 3801–3814.
- (38) Escalante Estrada, V. E. *Reúso Del Agua Residual En México*, Curso inte.; Instituto Mexicano de Tecnología del Agua: Morelos: Morelos, México, 2004.